GROUT-FILLED BUCKLING RESTRAINED BRACES: INTERNAL CORE BEHAVIOUR AND FEASIBILITY OF ALTERNATIVE PVC CASING

A thesis submitted to the University of Manchester for the degree of

MPhil(Master of Philosophy)

in the Faculty of Science and Engineering

May 2022

Manuel Alejandro Calzeta Valdes

Department of Mechanical Aerospace and Civil Engineering

Contents

Word Count: 25035

List of figures

List of tables

Abstract

Buckling Restrained Braces (BRBs) are an innovative and popular seismic retrofitting solution with broad research on the behaviour of BRB-equipped structures. BRBs have been successfully used in buildings to resist earthquake actions. The device casing is traditionally made of steel, however, it is unclear whether other materials are a feasible alternative. Lighter and more economical casings may potentially benefit developing communities in earthquake-prone areas, moreover, durable and aesthetically preferred materials could also result in the fulfilment of architectural project requirements. Therefore, this thesis explores the possibility to use PVC/uPVC casing as an alternative to conventional steel casing through conducting both numerical and experimental studies.

Dedicated 3D numerical BRB models are developed for this study. The specimen from published literature is first modelled to validate the finite element model through comparing the numerical and experimental results. A series of numerical investigations are conducted to simulate cyclical loading actions on BRBs and reveals the behaviour of the core yielding portion and quantify the lateral thrust exerted on the grout. The simulation provides an insight into the deformation and stress of cores subjected to cyclic loading.

It is observed from the 3D modelling that the cores with a rectangular cross-section deforms independently in the two perpendicular directions when subjected to cyclic loading. This provides a basis to propose a 2D model to simulate the behaviour of BRBs, i.e. a full 3D model can be replaced by using two 2D models in the two perpendicular directions. The comparison between the results from the 3D and 2D models shows a good agreement. The use of the 2D model highly reduces the computational time of the modelling.

Then numerical modelling and experimental studies of BRBs with PVC casing are conducted. The findings suggest that PVC can be a feasible and practical alternative to steel casings in situations where the inter-story drift is of reduced magnitude e.g. in low to medium rise structures. In demonstrating the feasibility of a relatively low-cost material such as PVC, the work also paves the way for investigation of other alternative casing products in the future.

Declaration of originality

I hereby confirm that no portion of the work referred to in the thesis has been submitted in support of an application for another degree or qualification of this or any other university or other institute of learning.

Copyright statement

i The author of this thesis (including any appendices and/or schedules to this thesis) owns certain copyright or related rights in it (the "Copyright") and he has given The University of Manchester certain rights to use such Copyright, including for administrative purposes.

ii Copies of this thesis, either in full or in extracts and whether in hard or electronic copy, may be made *only* in accordance with the Copyright, Designs and Patents Act 1988 (as amended) and regulations issued under it or, where appropriate, in accordance with licensing agreements which the University has from time to time. This page must form part of any such copies made.

iii The ownership of certain Copyright, patents, designs, trademarks and other intellectual property (the "Intellectual Property") and any reproductions of copyright works in the thesis, for example graphs and tables ("Reproductions"), which may be described in this thesis, may not be owned by the author and may be owned by third parties. Such Intellectual Property and Reproductions cannot and must not be made available for use without the prior written permission of the owner(s) of the relevant Intellectual Property and/or Reproductions.

iv Further information on the conditions under which disclosure, publication and commercialisation of this thesis, the Copyright and any Intellectual Property and/or Reproductions described in it may take place is available in the University IP Policy (see `http://documents.manchester.ac.uk/DocuInfo.aspx?DocID=24420`), in any relevant Thesis restriction declarations deposited in the University Library, The University Library's regulations (see `http://www.library.manchester.ac.uk/about/regulations/`) and in The University's policy on Presentation of Theses.

Acknowledgements

I wish to express my very great appreciation to Dr. Tianjian Ji and Dr. Lee Cunningham for their valuable advice and guidance on my work.

Finally, I wish to thank my parents, friends and partner for their unconditional support and encouragement.

Chapter 1

Introduction

Buckling-Restrained Braces (**BRBs**) are energy dissipation devices, often known as structural fuses that form part of mitigation techniques or Seismic Protection Systems (SPS) used to preserve structural integrity in a seismic event (**Figures 1.1, 1.2 and 1.3**). For communities living in seismic prone areas, damage due to earthquakes has shown throughout the years to be a major concern and a challenge for structural design as it represents an important hazard to human beings at various levels; from the loss of built assets and loss of life to plain important economic losses that highly impact communities in both the developed and developing world. Moreover, structural damage ranging from minor crack propagation to the total collapse, also affects the functionality of infrastructure that is highly needed after a seismic event such as hospitals and other contingency services.

BRBs have been a popular method to retrofit frames in a seismic scenario. In conjunction, frame and bracing synergise as a whole form a ductile Buckling Restrained Braced Frame (**BRBF**) where any degree of damage can be first absorbed by the bracing, therefore, it is

Figure 1.1: *Vancouver City Hall, steel moment frame built in 1975 and retrofitted with 16 BRBs for earthquake demands in 2016. Image from: CoreBrace (2016)*

Figure 1.2: *a)UVU Student Life Centre, steel frame built retrofitted with 132 BRBs, some in chevron arrangement.b)Stratford School, external braces connected to the same plate Image from: CoreBrace (2021)*

possible to design the frame for gravitational loads while the bracing takes the lateral loads in form of displacement demand. This technique has shown to be effective for trusses and moment and non moment resisting frames.

However, while Buckling Restrained Braced Frames (BRBFs) have been studied thoroughly in structural response and dynamic behaviour, BRBs do not have yet a substantial basis of design, this results in an inconsistent application of BRBFs since for BRBFs to meet the target performance, BRBs are also required to meet their target performance as ambiguous as it may be. This implies firstly that the casing must be adequate to provide the stability required and secondly that all the components can withstand both ductility and force demand. In general, although BRBs are an innovative class of Seismic Protection System(SPS) they are also relatively recent in research and deployment which leads to the need to revising in depth the current state of the art surrounding BRBs.

Broadly speaking, Seismic Protection Systems(SPSs) have been substantially researched and deployed in recent years as a "technology to mitigate seismic risk" (Medel-Vera and Ji 2015), however, relevant design provisions such as SEAOC-AISC (2001) and American In-

Figure 1.3: *10-storey gymnasium application at Chinese Culture University, Taipei from Lin et al. (2012)*

stitute of Steel Construction (2005) only address the target performance of the global structure equipped with the protection system in question, this strongly suggests that target performance at a component level remains in an under developed stage since design guidance is often not offered by codes or other literature resources. The lack of such development results critical to understand failure modes and subsequently define well understood Ultimate Limit States(ULS).

During the last 150 years, Structural Engineering has developed significantly, and the use of steel allowed changing the design criteria that rule the industry from elastic to ductile. Hence, the study of geometrical and material non-linearities is a necessity to establish adequate codes and design recommendations. This refers particularly to structures equipped with Structural Fuses in which functionality is delimited within the ductile range.

Although the limit state of structures varies according to different codes, ductile design implies that damage is acceptable at moderate levels in structural elements that can meet the target performance and robustness considerations. However, this conventional approach implies that even though damage can be monitored and predicted, it is not controlled. Structural fuses represent a solution to this by dissipating energy as damage; allowing the structural frame to maintain its integrity and allowing the BRB to be easily replaced following the seismic event.

1.1 Background

Buckling-Restrained Braces are considered structural fuses that allow concentrating the ductile response of Buckling-Restrained Braced Frames (BRBFs) on a slender bracing element with a small cross-sectional area that yields at relatively small drift values, thus dissipating energy (Guerrero, Escobar, and Gómez 2017).
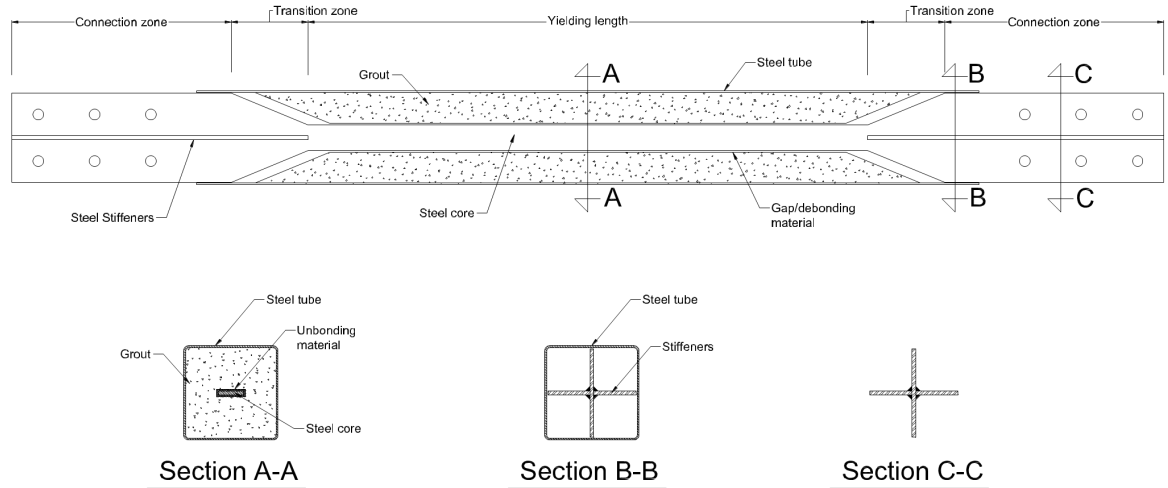
Figure 1.4: *Grout filled Buckling Restrained Brace and components adapted from Uang and Nakashima (2003)*

BRBs comprise a steel core divided into three portions with different cross-sectional area: a yielding portion, connections to a BRBF and a transition between them. Since the core is slender, the yielding portion is encased with a tubular structure generally a concrete or grout infilled steel tube with the purpose of preventing Buckling under axial reverse loading conditions. Likewise, the core is coated with a debonding layer, preventing direct surface to surface contact between steel and filler material **Figure 1.4**. Whilst the aforementioned is the most common form of BRB, all-steel systems have also been used.

Even though Structural fuses may not be applicable to every structure, BRBFs have shown important benefits in comparison with conventional frames in particular cases such as low-rise buildings where the dynamic response can be represented as a Generalised Single Degree of Freedom System(GSDOFs) with accuracy.

Guerrero, Ji, et al. (2018) conducted an experiment with a scaled model with precast con-

crete frames where BRBs have performed satisfactorily by dissipating the energy of the response under a real Earthquake loading, reproduced on a shaking table.

Nonetheless, a predominant feature of BRBs is that the tubular structure generally comprises a steel tube. The general aim of this thesis is to assess the feasibility of an alternative casing material to restrain buckling and satisfactorily meet the target performance resulting in a lightweight, easy to fabricate and economically effective casing as an option for seismic protection in developing countries. Likewise, the method can also be used to modify the casing for architectural reasons as in applications it is often exposed as part of the façade. According to Sabelli (2004), a BRB performs satisfactorily when no failure mode occurs under a cyclic loading equivalent to twice as much the frame design drift, both in tension and compression. Such recommendations were later introduced in American Institute of Steel Construction (2005) and codes from China, Japan, New Zealand, Canada, Chile and Taiwan.

From this derives two broad improvement opportunities for implementation of BRB type retrofit system yield in terms of the *design* of the BRB itself and its *fabrication*. This implicitly involves a wide series of studies that range from the design criteria of the assembled parts to the quality control of the manufactured device.

From the angle of design criteria, should component failure be closely investigated, criteria other than global stability could be implemented, therefore, extrapolation of the current target performance would transition to more complete criteria of acceptance leading to a consistent understanding of this type of SPS. As a consequence of the latter action, it would be possible to fabricate other types of BRBs which can be better suited to meet architectural requirements. On the other hand, considering that the filler material is often a major part of the weight, BRBs could be lighter devices, thus making it possible to avoid assembling the parts on-site due to crane lifting capacity constraints.

A second point to address is the fabrication since it is at this stage when quality control is conducted and rule if the target performance is met. Testing as described in **Chapter 2** is conducted in a sub-assemblage type, therefore, the device is connected to a frame and re-
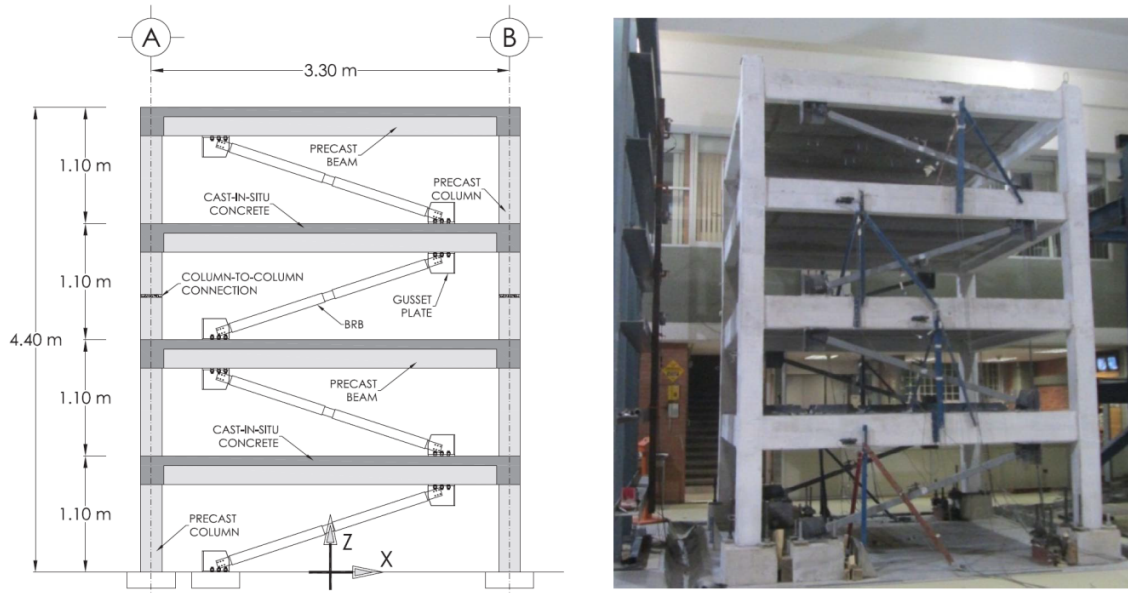
Figure 1.5: *BRBF considered for testing on shaking table from Guerrero, Ji, et al. (2018)*

versal loading is applied horizontally on the frame accounting for connection performance, however, there is not an established criterion to rule local failure based on the current practice. This impacts the consistency of BRB design since parts are not necessarily required to pass a quality check. Moreover, these devices excel at dissipating energy due to the core yielding at very low drift values which raises uncertainty in terms of durability, hence the necessity to quantify stress and strain states within the assembled parts.

1.2 Aims and Objectives

The motivation of the present work is based on the conducted literature review presented in the next chapter where it was observed that the current understanding of the interaction of the GFBRB components is not sufficient to estimate with accuracy the limiting factors that influence the structural performance of the GFBRB in terms of stability and durability. Likewise, the conducted review revealed that the mechanisms of failure where steel cases are used are generally well understood, however, clarity is needed on the limitations of the GFBRB knowledge framework when proposing innovative casings comprised by a tubular structure with a lower modulus of elasticity E or with non-linear material properties. Moreover, the present work focal points have been delimited to the study of the interaction between the core yielding portion and the infilled tubular structure as well as the global stability criteria.

The benefits of understanding such behaviour and casing demand are, as described before, producing an updated version of design provisions that include the design requirements for BRBs allowing the designer to consider more options to cover architectural, light-weight and cost-effective needs. Furthermore, it opens the possibility of further research for cases where large braces are needed as a macro bracing or long truss element.

The general aim is to assess the feasibility of an alternative durable economically-effective casing that is easy to fabricate and is suitable for application in developing countries, then the methodology can be applied to satisfy architectural requirements. In order to arrive at suitable alternative casing materials, the behaviour of the BRB components and system must first be understood in detail. Towards this goal, non-linear 3d finite element modelling will be undertaken using the commercially available software ABAQUS (2013). See **Table 1.1**.

In chapter 2 a systematic review is conducted on the current state of the art knowledge of BRB behaviour and design. From the literature review, it was identified that no design guidance is delivered for target performance at the component level, however, 3D modelling of BRBs is computationally costly using the 2 integration methods available in the commercial software ABAQUS (Dynamic Explicit and Dynamic Implicit), where the Dynamic Explicit complexity grows linearly with the problem and Dynamic Implicit grows faster since it implies an iterative procedure at every time step ABAQUS (ibid.). Therefore, experimental work is needed with new methods to measure parameters that corroborate the FEM other than the axial response, hence, understanding the BRB local and global behaviour is highly dependent on FEM and experimental data for validation purposes.

In chapter 3 substantial FE model validations are undertaken by simulating experiments from the literature and quantifying the results that cannot be obtained experimentally, such as the lateral thrust exerted by the core. Although it has been an intermediate step to answer the central research question of this thesis, it is where most time spent of the programme concentrates. The analyses include the case of study of an All-Steel BRB (ASBRB) and two Grout-Filled BRBs (GFBRBs), it demonstrates the ability to model BRBs by correctly

predicting global failure and by characterising identified parameters that affect the hysteretic response of the device. This chapter reveals the behaviour of the BRB and identifies modelling challenges that have not been addressed in great depth in the reviewed literature. Also, a parametric analysis is conducted, aiming to examine the effect of key variables including friction, buckling wave formation and failure.

Based on the observations made within the validations conducted, a new technique to simplify a 3D model of a Grout-Filled Buckling Restrained Brace(GFBRB) into 2 equivalent 2D problems is presented. This technique has been used to dramatically increase the efficiency of computational analysis normally used for 3D analysis in order to assess the global structural stability of the GFBRB. Furthermore, the lateral thrust exerted on the grout has been quantified, thus revealing the behaviour of the yielding portion of the core at a significantly reduced computational cost. Such reduction has shown to be as much as 95% less of the equivalent 3D model .

In chapter 4 relevant experimental work of a BRB with a PVC casing is used to study numerically the feasibility of PVC as a material that can potentially replace steel, 4 samples of PVC BRBs were prepared and tested under compressive monotonic loading and compared with the numerical analysis; findings from the experimental work are discussed and presented as milestones to the question whether PVC is feasible as innovative casing material, likewise, the observed performance of the samples, failure modes and the observed effects of increasing the gap are presented. In addition, challenges of the fabrication of samples is introduced and discussed.

Finally, chapter 5 includes a discussion of the findings from previous chapters and recommendations for further work are given with final conclusions.

Table 1.1: Aims and Objectives

Aim	Investigate the feasibility of PVC as a tubular structure for Grout-Filled BRBs
Objectives	
	• Identify gaps in research though a literature review
	• Investigate numerical techniques to model BRBs covering the wide variety of types of casings as a focal point of research
	• Conduct substantial numerical analysis and calibrate model against existing experimental data
	• Obtain information from the modelling allowing to create a solid basis for the experimental investigation of PVC
	• Design BRB samples with PVC casing
	• Sample, test and characterise PVC for use in numerical model in experimental chapter
	• Conduct testing of PVC casings using the experimental design and numerical analysis
	• Propose numerical methodology to conduct research of Grout-Filled BRBs more effectively based on own work

Bibliography

ABAQUS (2013). "Abaqus user's manual". In: *Version 6.13* USA, Dassault Systems.

American Institute of Steel Construction (2005). "Seismic Provisions for Structural Steel Buildings". In: *Seismic Provisions for Structural Steel Buildings* 1, p. 402.

CoreBrace (2016). *Vancouver City Hall - 4-story steel moment frame building built in 1975 and seismically upgraded in 2016*.

– (2021). *Retrofit of Milpitas Preschool and Elementary School Campus involving the use of externally mounted BRB outrigger frames connecting to a common node*.

Guerrero, Hector, J. Alberto Escobar, and Roberto Gómez (2017). "A Study of the Damping Provided by Buckling-Restrained Braces (BRBs) within Their Linear-Elastic Response". In: *ASCE Journal of Structural Engineering* Structures Congress 2017, pp. 558–565. DOI: 10.1080/15391523.2007.10782485.

Guerrero, Hector, Tianjian Ji, et al. (2018). "Effects of Buckling-Restrained Braces on reinforced concrete precast models subjected to shaking table excitation". In: *Engineering Structures* 163.February, pp. 294–310. ISSN: 18737323. DOI: 10.1016/j.engstruct.2018.02.055.

Lin, S. L. et al. (2012). "Development and implementation of buckling restrained braces in Taiwan". In: *2012 New Zealand Society for Earthquake Engineering (NZSEE) Annual Technical Conference* 094.

Medel-Vera, Carlos and Tianjian Ji (2015). "Seismic protection technology for nuclear power plants: A systematic review". In: *Journal of Nuclear Science and Technology* 52.5, pp. 607–632. ISSN: 00223131. DOI: 10.1080/00223131.2014.980347.

Sabelli, Rafael (2004). "Recommended Provisions for Buckling-Restrained Braced Frames".

In: *Engineering Journal* 41, pp. 155–175.

SEAOC-AISC (2001). "Recommended Provisions for Buckling-Restrained Braced Frames

(draft)". In: *SEAOC and AISC*.

Uang, Chia-Ming and Masayoshi Nakashima (2003). "Steel buckling-restrained braced

frames". In: *Earthquake engineering: Recent advances and applications*, Chapter 16.

Chapter 2

Literature Review

2.1 Overview of Existing BRB Research

Research of Buckling-Restrained Braces (**BRBs**) has achieved a gradually improved understanding of the function of the different components, physical behaviour and failure modes of the device using steel as a common denominator in terms of material for the restraining element, however, as component failure can be observed from the current performance-based design approach, there are important gaps in knowledge and questions that require attention.

Numerous efforts have been made by a vast number of authors explaining the potential limitations of the casing by elaborating Finite Element Models and conducting exhaustive experimental work. The difficulty of observing and measuring the behaviour and mechanism of the internal section of the yielding core has added challenges to understanding how these devices can be further improved, however, important achievements have been done experimentally conducting testing of the type of Buckling-Restrained Braced Frames (**BRBFs**) and isolated **BRBs** mounted on Universal Testing Machines (**UTM**). Furthermore, analytical solutions have been developed to estimate transfer forces between steel core and casing which are pointed out critically in this section.

These actions have allowed researchers to develop further the design methods used for the casing taking into consideration the corresponding geometrical and material non-linearities, thus achieving a state of the art of Buckling Restrained Braces of a wide range of different types ranging from all-steel casing **(ASBRBs)** to infilled tubular structures which can
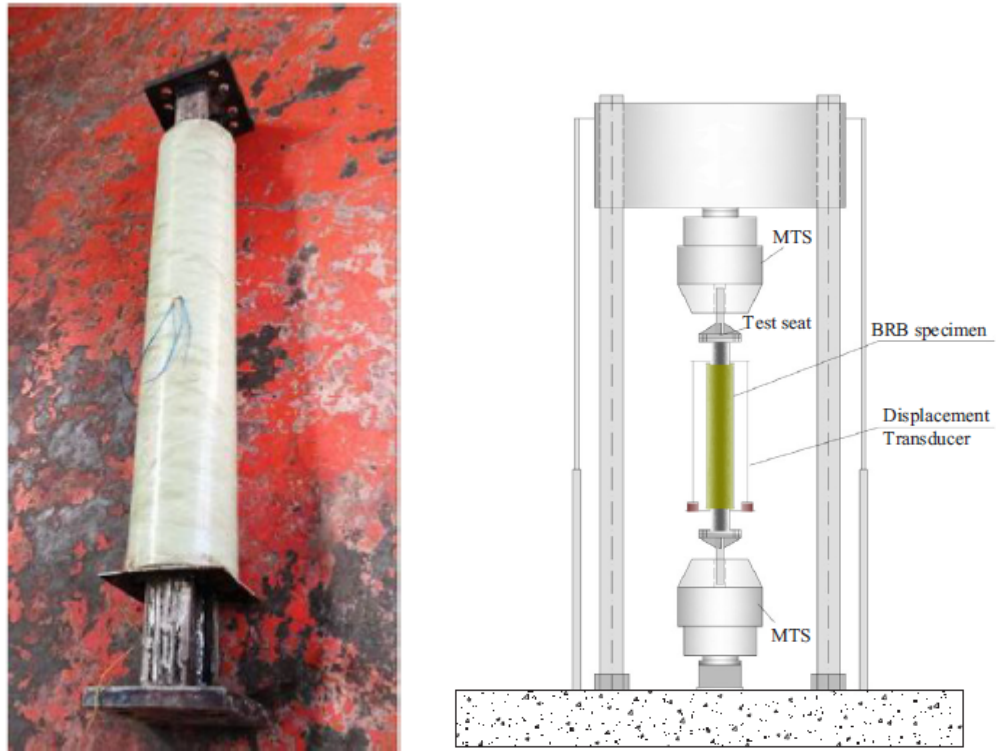
Figure 2.1: BRB specimens with GFRP casing from H. Sun et al. (2019)

be made either from steel (traditionally), Glass Fibre Reinforced Polymer **(GFRP)** (J. Sun, Pan, and H. Wang 2018; H. Sun et al. 2019) or Carbon Fibre Reinforced Polymer **(CFRP)**(Jia et al. 2017).

Generally speaking, one of the central research core question has been the sizing of the casing which has been a line of research followed by many authors to determine safely the limiting compressive force or displacement before the stability of the system is compromised. This chapter aims at justifying the relevance of the research questions that are treated in later chapters as a core of the work and intends to provide evidence of originality in the study of alternative casings such as PVC. Likewise, focal points are highlighted in a discussion at the end of the chapter and literature resources are critically reviewed, scrutinised and reported in a structural context; these intend to provide supporting reasons of the considered relevant work to be conducted to further develop improvements in the understanding of **BRBs**. This literature review is based in the latest findings up to 2020, hence, it provides a reasonably accurate and updated overview of the state of the art of Buckling Restrained Braces.

It is also intended that the present Literature Review provides a clear picture to the reader

of the vast numerical, analytical and experimental work by summarising the research in a table for each subsection. In addition, the format of the work is presented in a systematic way, following the 5 steps of a systematic review (Higgins and Green 2006) to the best extent: 1)Framing questions, 2)Identifying relevant literature, 3) Assessing the quality of literature, 4) Summarising the evidence, 5) Interpreting the findings.

Furthermore, this section is intended to discuss the research questions that, as well as highlighting the most impacting research that provide a breakthrough to understanding the behaviour of and mechanism of **BRBs** using tubular infilled structures as buckling restraining component.

Likewise, the research questions are discussed in a logical sequence to provide a critical review of the revised literature to present the corresponding Analytical, Numerical and Experimental investigation and a meticulous interpretation on the achievements in research. Gaps are identified, and challenges and opportunities are discussed. Finally, the research questions that are the motive of this chapter are: 1) Why is steel prioritised as material for the design of **BRBs**? 2) What are the challenges to overcome when studying the mechanism and behaviour of **BRBs**?, 3) How can we better understand BRB behaviour so that we can produce efficient, economic designs, using traditional or alternative materials ? Such research questions are discussed in the following paragraphs to identify and discuss the gaps in research.

2.2 BRBFs current practice

Deployment of **BRBs** as core components of **BRBFs** have been widely researched in literature, in numerous studies the behaviour of multi-storeys **BRBFs** has been treated, finding satisfactory performance in the system that has been also termed dual, since it comprises the non-linear behavioural response of the bracing and the idealised linear behaviour of the retrofitted frame structure. However, studies are in their majority based or the assumption that this non-linear response can be simplified and therefore predicted.

Table 2.1: Summary of updated database on BRB reviewed literature

Author (year)	*Focal point*
H. Sun et al. (2019) and J. Sun, Pan, and H. Wang (2018)	Investigation of constraint ratio using concrete infilled **GFRP** tubes as alternative casing system
Rahnavard et al. (2018)	Investigation of modelling approaches of **BRBs** using Finite Element Method (**FEM**) (ABAQUS) aiming improvement in the computing time
Jia et al. (2017)	Investigation of modular casing for Assembled **BRBs** (**ABRBs**), using 2 assembled concrete-filled steel channel sections wrapped with carbon or basalt fibre
Dehghani and Tremblay (2017)	Proposition of analytical estimates of lateral forces exerted by the core on **ASBRBs** buckling restraining systems with bolted connections
Jiang, Dou, et al. (2017) and Jiang, C., et al. (2017)	Analytical study on design methods for pinned connections of **BRBs**
AlHamaydeh, Abed, and Mustapha (2016)	Study of the key parameters of the mechanism of **GFBRBs** by conducting sensitivity analysis
Judd et al. (2016)	Experimental investigation of the hysteretic behaviour of **ABRBs**, termed Web-Restrained **BRBs** subjected to combined axial and rotational demands by conducting sub-assemblage testing type
Metelli, Bregoli, and Genna (2016a) and Metelli, Bregoli, and Genna (2016b)	Experimental study on the lateral thrust generated by core buckling in bolted-**BRBs**
Tremblay et al. (2016)	Comparison of seismic design provisions for **BRBFs** in Canada, Chile, New Zealand and the United States
J. Wang, Shi, and Y. Wang (2016)	Constitutive Model of Low-Yield Point Steel and Its Application in Numerical Simulation of Buckling-Restrained Braces
Deng et al. (2015a) and Deng et al. (2015b)	Study of **GFRP** Steel Buckling Restraint Braces
Mirtaheri et al. (2011a) and Mirtaheri et al. (2011b)	Experimental optimisation studies on steel core lengths in buckling restrained braces

BRBFs experimental research has shown that the frame can experience global failure when the casing is not sized adequately. This has been primarily evidenced in cases when the bracing is subjected to sub assemblage testing which has brought more close attention to the detailing and design of Buckling Restriction Component.

A rather general definition of **BRBFs** failure can be ambiguously put as the loss of energy dissipating features due to component failure; however, this is a general description only to state the target performance is not met. From this previous statement it can be appreciated that local behaviour and component performance is not included in the current definition

of failure, which has important implications in the progression and further development of not only **BRBs** but also other structural fuses formed with sub-assembled components. Therefore a more specific definition of failure is needed to understand better the conditions of loss of energy dissipation features at a component level.

Such definition has been a common focal point in research following the issue of design provisions for **BRBFs** (SEAOC-AISC 2001; American Institute of Steel Construction 2005) where performance of **BRBs** at component level is paramount to understand the ultimate limit state and serviceability conditions. AlHamaydeh, Abed, and Mustapha (2016) shows important findings on the effects of key parameters that influence the hysteretic response and identifies associated failure modes. The study strongly suggests the need to study the components in more depth to define reasonable Limit States.

Moreover, examined experimental sub-assemblages have provided supporting grounds to pursue this line of research since during testing different local component failure govern the design of **BRBFs**, hence the necessity of further thoroughly studying associated failure mechanisms.

2.3 Development, testing and types of BRBs

It is considered relevant to provide a brief road map showing how Buckling Restrained Braces have evolved from an innovative attempt to make masonry panels ductile to the devices that occupy the market as one of the most demanded (and rising) seismic protection systems in Earthquake prone areas.

BRBs were first introduced as a structural fuse for Pre-Cast Concrete (PCC) panels (**Figure 2.2**) as it can be found in Wakabayashi, Nakamura, Katagihara, et al. (1973) and Wakabayashi, Nakamura, Kashibara, et al. (1973) followed by Watanabe et al. (1988) who extrapolated the idea to the traditional bracing encased in a Grout infilled tubular structure.

From the basic understanding on BRB performance followed that the development of these

a)   b)
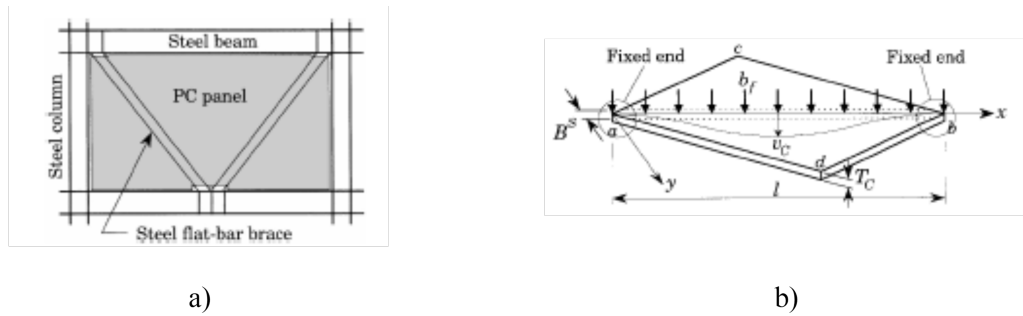
Figure 2.2: *a) Precursor structure of BRB;b)loading on concrete panel restraining core from Inoue, Sawaizumi, and Higashibata (2001)*

a)   b)
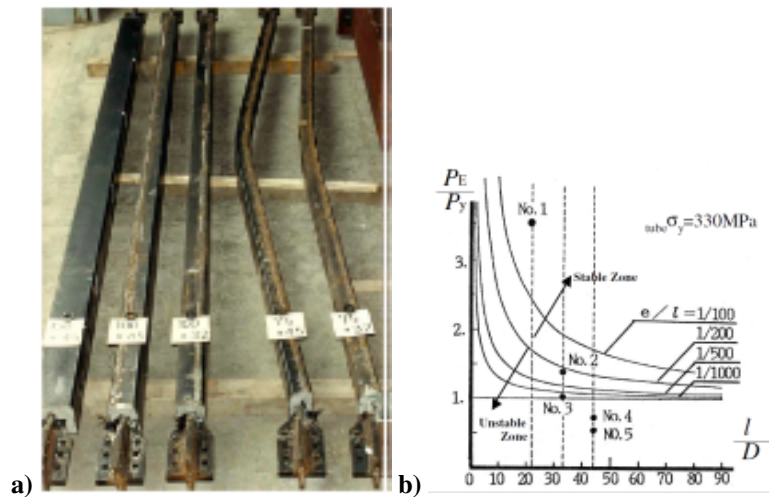
Figure 2.3: *a) Experimental set of **BRBs** with different size of braces; b) Stability chart from Wada and Nakashima (2004), Akira Wada and Nakashima (2004), and Watanabe et al. (1988)*

devices was strongly guided by the need of overcoming global types of failure, hence the the subsequent buckling restraining methods consisted of grout infilled steel hollow core and tubular sections. Substantial testing was conducted in Watanabe et al. (1988), **Figure 2.3** shows a replication of this work in Wada and Nakashima (2004) and Akira Wada and Nakashima (2004) 5 **GFBRBs** with identical core dimensions, material properties, constant debonding layer thickness and the corresponding global failure mechanisms.

The study consisted in testing a BRBF retrofitted with a BRB, the same frame was tested with 5 different specimens of different cross-sectional area of the casing and constant core thickness to identify a stability boundary based on the ratio P_e/P_y, also termed constraint ratio, where P_y is the axial yielding load at strain ε_y of the core and P_e is the Euler load of the grout-infilled steel hollow core section.

The BRBF was designed for seismic loading which was induced in a displacement-controlled sub assemblage testing series. From the study, it was observed that for that group of speci-
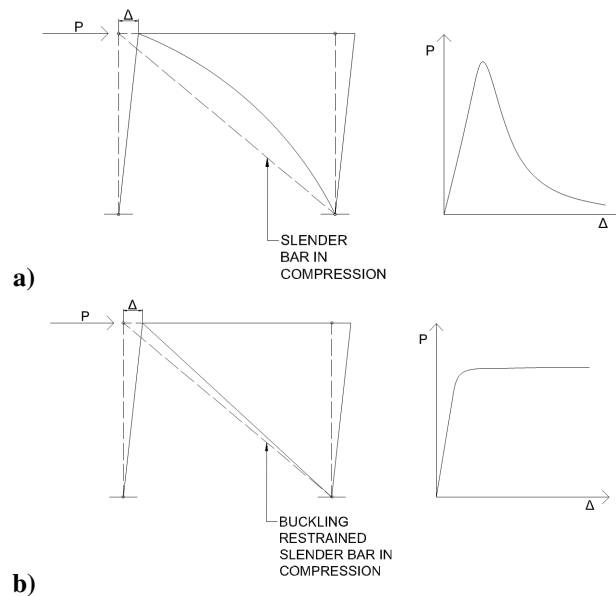
Figure 2.4: *Differences in terms of performance between (a) conventional braces (global buckling) and (b) **BRBs** (ductile frame) adapted from Xie (2005a) and Xie (2005b)*

mens buckling lateral restriction showed to be sufficient when the P_e/P_y ratio was greater than 1. In contrast, global buckling **Figure 2.4** occurred at ratios lower than 1. Although the accuracy of this ratio remains unclear, this experiment signified a basis to the study of the device's global stability and a clear link between axial load and flexural strength.

Following research has studied the effects of parameters such as size of the gap, debonding layer material, core geometry, casing material and connections. Likewise, design guidance has been provided and numerical modelling practice has been undertaken as a major resource to understand component failure as described in the subsections below.

BRBs were first studied and research discovered a feasible way to prevent buckling in a compressed strut by restraining the displacements perpendicular to the axis along the full length of the slender component. It was observed that if such restriction is ensured, then both yielding in compression and tension was feasible.

The ductile Pre-Cast Concrete (PCC) panel was re examined later in Inoue, Sawaizumi, and Higashibata (2001), Ding, Zhang, and Zhao (2009a), and Ding, Zhang, and Zhao (2009b) in **Figure 2.2**, in both cases the steel core was encased between 2 reinforced concrete panels, however, the system rose concern before the occurrence of punching failure due to lateral thrust of the steel core.

Owing to the fact that a BRB is ductile, yielding of the brace is ensured by material mechanical properties only. Currently, steel is the only material used for the core. Given the mechanical properties of the material the resultant cross sectional area that ensures yielding at small displacements, making the brace slender which is vulnerable to buckle before yield where no restriction to the buckling is provided. A first solution for this main issue was proposed by Wakabayashi, Nakamura, Katagihara, et al. (1973) who investigated the behaviour of a steel slender bar as previously described that was buckle-restrained by reinforced concrete panels. Since the steel bar is the only axial load carrying unit, debonding the steel bar from the buckling restraining element was a second issue to be considered; as a result elastomeric material was used to coat the core and provide some extent of sliding between the two interfaces.

The outcome of this study was a clear ductile behaviour of the core both in tension and compression obtaining a force - displacement plot showing hysteretic semi symmetric loops thus suggesting stability. However, the observations of this eventually led to other feasible ductile devices without further investigation of the specimen tested.

The experiment of Wakabayashi, Nakamura, Katagihara, et al. (ibid.) was followed by Watanabe et al. (1988) who proposed the first Grout- Filled Buckling Restrained Brace (**GFBRB**) based on the observations of the former study, where a core with the same characteristics was tested by inducing axial cyclic displacements at the tip this time substituting the restraining element for a steel tube filled with grout in order to investigate the cross section properties needed to prevent ductile patterns in the casing. The experiment consisted in testing five specimens with a determined core cross section and variable size of steel tube. The outcome of the study showed a discrete transition (as only five different sections were tested) from instability to stability in a force-displacement plot where unstable behaviour could be physically observed in the steel tube surface with the formation of ductile patterns.

In late stages, research has been remarkably oriented on the proposal of new types of **BRBs** where a second variant of **BRBs** is identified and can be addressed as all-steel **BRBs** (**ASBRBs**), which differ from the **GFBRBs** in terms of the buckling restraining system. In the Table 2.2
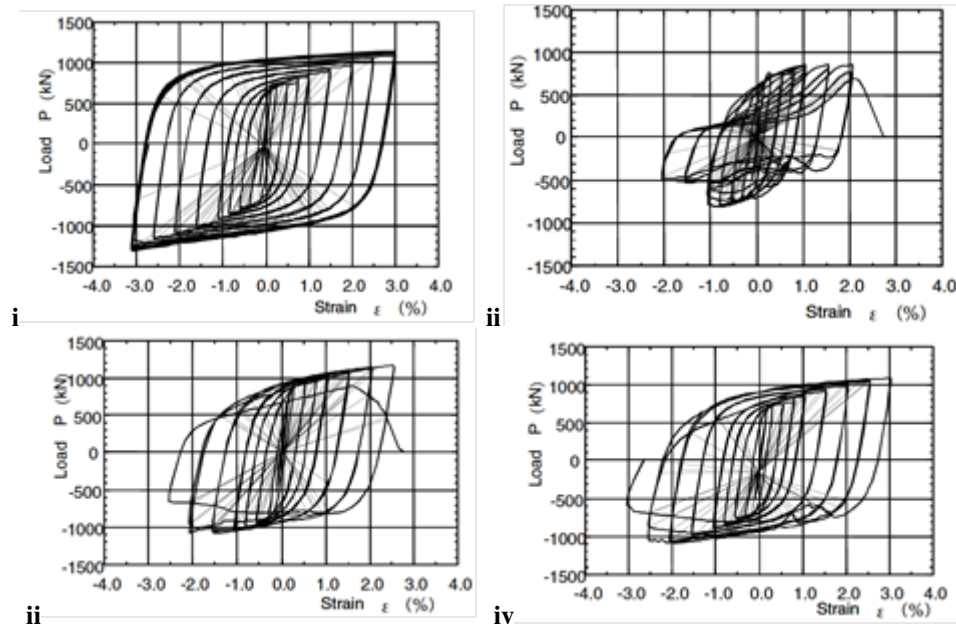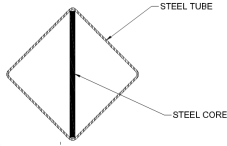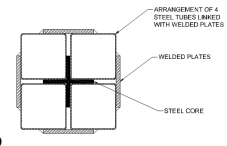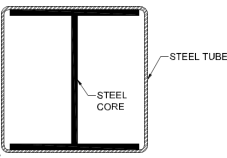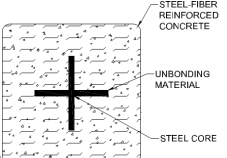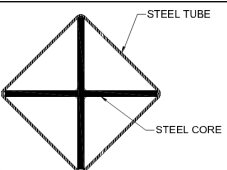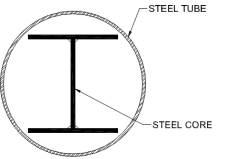
Figure 2.5: Hysteretic curves of specimens i) GFBRB ii) ASBRB (Table 2.2a) iii) ASBRB (Table 2.2j) iv) ASBRB (Table 2.2c) from Iwata (2004)
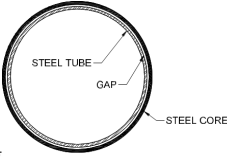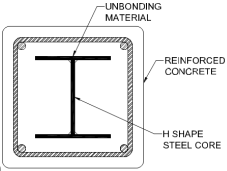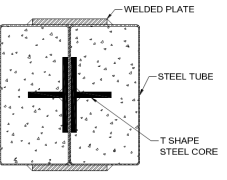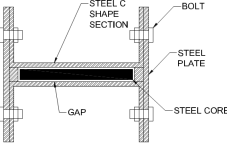
is shown a range of variations of cross-sections of **BRBs** that has been tested, nonetheless, it is to be remarked that **GFBRBs** are the only type being used in industry thus far, the reason is that the cross section of **GFBRB** has qualitatively shown to behave in a rather stable and predictable way as the casing filled with grout is stockier than All- steel **BRBs**. In general, AS**BRBs** have been proposed as an attempt to find a lighter weight and more economically efficient BRB.

The study of other types of **BRBs** in terms of performance remains qualitative (and so the justification of usage of GF**BRBs** only), as an example, Iwata (2004b) studied experimentally the behaviour of 4 different sections in total with one specimen of GF**BRBs** and 3 different AS**BRBs** (cross sections: a, c and j in Table 2.2), from this study the four different force-displacement response shown in Figure 2.5 were obtained. The study consisted in testing comparable specimens by making the core cross sectional area constant and varying the Buckling-Restraining Units (BRU). Qualitatively, it is noticeable that meanwhile stable conditions are conserved in all cases; however the energy dissipated by **GFBRB** suggests that this BRU makes energy dissipation features more effective than the AS**BRBs** specimens tested, although comparison with other AS**BRBs** is required to obtain a more objective conclusion.

Table 2.2: ABRB Research Cross Sections

Type of section	Author	Description
a	(Manabe, Simokawa, et al. 1996) (Manabe, Kamiya, et al. 1997) (Iwata 2004)	BRU: Squared steel tube without grout Core: steel plate Debonding material: gap
b	(Narihara, Koetaka, and Tsujita 2000b; Narihara, Koetaka, and Tsujita 2000a)	BRU: 4 squared steel tubes arranged around the core fixed with welded plates without grout Core: 3 welded steel plates arranged in a cruciform form Debonding material: gap
c	(Usami and Kaneko 2001; Usami, Kaneko, and Ono 2002; Iwata 2004)	BRU: Squared steel tube without grout Core: I section formed by 3 welded plates Debonding material: gap
d	(Mase and Yabe 1995)	BRU: steel-fibre reinforced concrete without the presence of a steel tube Core: 3 welded steel plates arranged in a cruciform form Debonding material: unspecified material
e	(Shimizu et al. 1997)	BRU: Squared steel tube without grout Core: 3 welded steel plates arranged in a cruciform form Debonding material: gap
f	(Suzuki, Kono, et al. 1994; Suzuki, Kaneko, et al. 1995)	BRU: Circular steel tube without grout Core: I section formed by 3 welded plates Debonding material: gap

Table 2.3: ABRB Research Cross Sections(Continued)

Type of section	Author	Description
g	(Kuwahara et al. 1993b; Kuwahara et al. 1993a)	BRU: Inner circular steel tube without grout Core: outer circular steel tube Debonding material: gap
h	(Nagao, Mikuriya, Matsumoto, et al. 1988; Nagao, Mikuriya, Yuki, et al. 1989; Nagao and Takahashi 1990; Nagao and Takahashi 1991; Nagao, Sera, et al. 1992)	BRU: Reinforced concrete section Core: I section formed by 3 welded plates Debonding material: unspecified material
i	(K. C. Tsai et al. 2013; K C Tsai and Y. C. Huang 2002; K C Tsai and Weng 2002; K C Tsai and J. W. Lai 2001; K C Tsai, J.-w. Lai, et al. 2003)	BRU: Double composite steel tube filled with grout and fixed with 2 welded plates Core: Two symmetric T sections formed with 2 welded plates each Debonding material: Unspecified material
j	(Isoda et al. 2001; Iwata 2004)	BRU: 2 Symmetric U channel steel sections bolted to a steel plate Core: Steel plate Debonding material: gap

2.4 Buckling Restrained Braced Frames within design codes and testing methods

Strength considerations for **Buckling Restrained Braced Frames** (**BRBFs**) first appeared in SEAOC-AISC (2001) where the global performance of the structure is to meet a list of requirements in order to be qualified as satisfactory under a performance based assessment approach. In order to do so, parameters describing the main features of the hysteretic curve were created to conduct a quantitative analysis. The recommendations SEAOC-AISC (ibid.) were introduced to the codes American Institute of Steel Construction (2005) where an acceptation criteria for **Buckling Restrained Braced Frames (BRBFs)** were provided. The general requirements for the performance of a BRBF to be satisfactory are based on two features: ductility capacity and buckling resistance which will be assessed by means of testing.

a) Ductility capacity – The core shall be capable to withstand a ductility equivalent to twice the design story drift as a minimum

b) Buckling Resistance – The Buckling Restraining Unit shall inhibit local and global buckling corresponding to a displacement of twice the design story drift

The definition of Buckling Restrained Braces has been briefly introduced in some European codes such as EN15129 (2009) and BSEN1998-3:2005 (2005) where the device is termed as Unbonded Brace. Likewise, more consideration on the detailing and rationale of **BRBFs** and target performance is provided in FEMA (2003a) and FEMA (2003b) and a similar design approach is shown in the codes of New Zealand, Canada, China, Japan and Chile (M. L. Huang, Fu, and Bao 2014; J. H. Huang et al. 2014; Tremblay et al. 2016).

The deployment of **BRBs** in frames has implied establishing standards of target performance by means of design provisions. Some design considerations can be found in Sabelli (2004) and Sabelli and Aiken (2004); in order to assess the two aforementioned requirements, two types of testing are to be undertaken accounting for different types of displacement induced to the bracing so as to simulate real life conditions. The two testing types
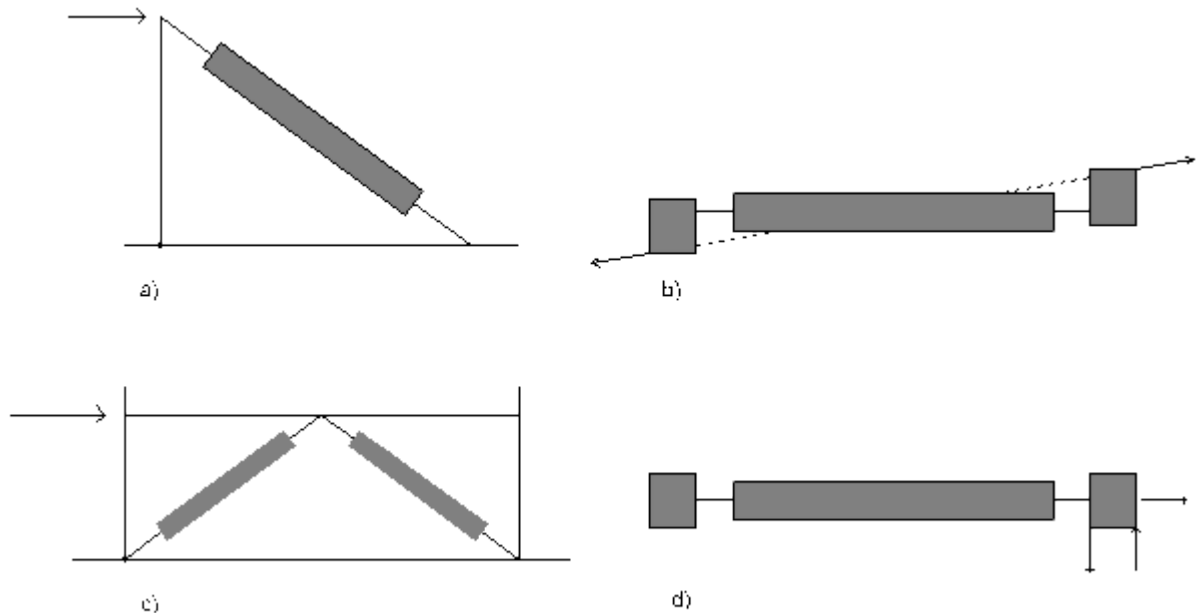
Figure 2.6: Possible sub-assemblage tests: a) Loading of brace and column b) Eccentric loading of brace c) Loading of BRBF d) Loading of brace with constant imposed rotation; adapted from (American Institute of Steel Construction 2005)

account for story drift (sub-assemblage testing) and uni-axial displacement. In the sub-assemblage testing, the specimen is positioned in the same direction as when installed in the frame; the nature of the displacement is rotational combined with axial (Figure 2.6). The first outcome of such devices is a stable hysteretic curve as it implies a successful restraint to buckling or enough buckling resistance. Secondly the test allows observing the performance at a component level where it is possible to observe failure at a component level diagnosed in the hysteretic response.

The parameters that were created to describe the hysteresis obtained from the test are listed in Table 2.4 which describes key points in the curve. The relevance of these parameters is that they are associated to the maximum values of forces and displacements which allow having a reference to quantify the maximum strength boundary (adjusted brace strength) so as to design the connections with the frame (Gusset plates); likewise, the Cumulative Deformation Capacity (CDC) can be quantified in the number of cycles before the core reaches fracture. The values of the maximum forces are determined by testing; Figure 2.7 shows the idealised bi-linear curve from a BRBF.

According to American Institute of Steel Construction (2005), the design provisions were elaborated for a value of β≤3 stating that currently available braces should be able to satisfy

this requirement. In addition, for a BRB to be accepted it must show a CDC of 200 times the yield story drift value Δ_{by}.

Table 2.4: Adjusted brace strength parameters (descriptors of backbone curve)

Notation	Name	Expression
β	Compression over strength factor (often called compression correction factor)	$\beta = \dfrac{P_{max}}{T_{max}}$
ω	Strain hardening factor	$\omega = \dfrac{T_{max}}{F_{ysc}A}$
μ	Ductility	$\mu = \dfrac{2\Delta_{bm}}{\Delta_{by}}$
P_{max}	Maximum compression force at maximum displacement amplitude	–
T_{max}	Maximum tension force at maximum displacement amplitude	–
Δ_{bm}	Design story drift	–
Δ_{by}	Yield story drift	–
CDC	Cumulative deformation capacity	$\sum |Inelastic\ deformations|$

Testing of **BRBs** consists of inducing a cyclic axial displacement history at the tip of the core. A recommended loading protocol is given in the provisions in order to ensure the requirements are met, however such protocol considers a semi-static loading protocol due to the cost increase implied. According to the provisions, the engineer will determine the time of application of the load so as to ignore the dynamic effects.

Table 2.5: Load protocol recommended in American Institute of Steel Construction (2005)

Step	Number of cycles	Deformation
1	2	Δ_{by}
2	2	$\mathbf{0.5}\Delta_{bm}$
3	2	Δ_{bm}
4	2	$\mathbf{1.5}\Delta_{bm}$
5	2	$\mathbf{2}\Delta_{bm}$
6	Additional cycles to complete CDC requirement	$\mathbf{1.5}\Delta_{bm}$

There is a well-established target performance in the available provisions for **BRBFs**, however, there is also a necessity to further expand the current provisions to account for local effects in the device itself by establishing a target performance at a component level based
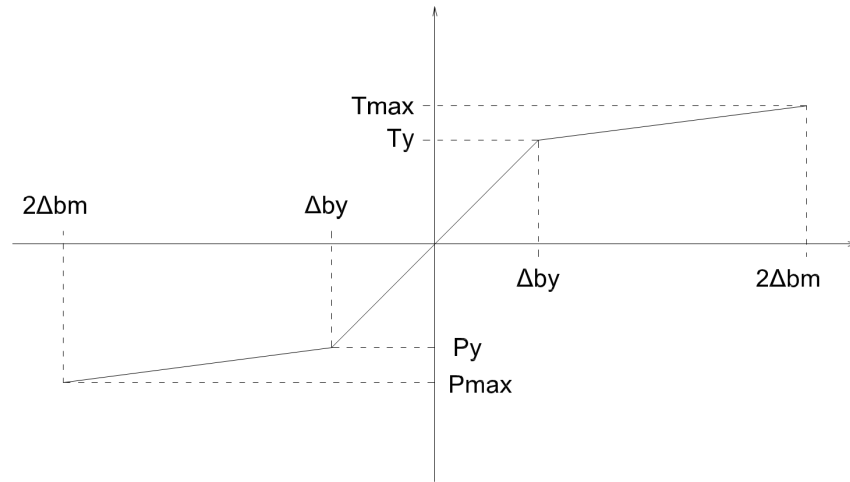
Figure 2.7: Diagram of brace force displacement backbone curve adapted from AISC (2005)

on the failure modes that are described in the following pages. In addition, some ideas of what testing can be done based on experimental work conducted by others are outlined in the discussion section of this chapter.

2.5 Global mechanism and stability criteria

Mechanism of **BRBs** has been studied by different authors; nonetheless, the existing mechanism corresponding to the Ultimate Limit State(ULS) has been deduced from observing failure patterns in tested specimens and no globally accepted theory is available nowadays. Currently, the theory supporting BRB design leads to a general explanation of overall stability and therefore no detailed validated analytic method to assess internal forces has yet been investigated.

Further research has led to add components in order to avoid observed failure patterns as experiments of **GFBRBs** listed in Table 2.9 where the justification of these components is highly attached to the failure patterns observed. From the observations and acquiring of knowledge, a basic set of 5 components for a BRB to withstand the effects of sub-assemblage testing are: core yielding portion, core transition portion, core connection portion, debonding material and buckling restraining unit. For the case of Grout-Filled Buckling Restrained Braces (**GFBRBs**) the above mentioned set of components can be expanded to 6, where the

Buckling Restraining Unit is composed by a steel tube and grout. To further explore the target performance of BRB component pairs, their primary function can be described.

Buckling Restrained Braces' global functionality is to dissipate energy by means of a ductile core that yields when an axial displacement of magnitude Δ_y is induced at the tip at low displacement values. As the core incurs in the plastic range, this occurs in ductile stable behaviour. Some parameters that have been often investigated are the correlation between material E, second moment of area I and maximum axial load at yield P_y assuming elasto-plastic material.

Core and debonding material/air gap - It has been mentioned that the size of the gap and imperfections causes the core forming into a high order buckling mode shape, thus squeezing the debonding material against the grout and slipping from it once the shear stress on the surface of the grout, in this interface the axial load is isolated to the core (i.e. the casing only acts laterally) resembling to a bilaterally restrained column separated by a gap.

The problem of a bilaterally restrained column (**Figure 2.8**) was addressed in Chai (1998) who conducted experimental work and proposed mathematical expressions for a vertical steel plate separated to the restraining wall by a small distance (gap). It was observed that when the plate was subjected to a steady compressive displacement, the plate corrugates into higher buckling shape modes (**Figure 2.9**). In addition, the results showed that sudden steps of force decay could be observed as the load increased. What is more, there was a direct correlation between wave mode formation increase and axial force sudden decays. This evidence strongly suggests that these occur at the same time. From this experiment was observed that the column deformed shape evolved to a high number of buckling modes at an increasing loading. Such a phenomenon has been approached by different studies by making use of the Finite Element Method (B. Wu and Mei 2015).

Grout as a restraining surface - Based on the experiment of a bilaterally restrained column, a reaction is induced on the opposite side of the debonding material (lateral thrust). The grout is initially cast in order to fill the voids between the steel tube and debonding material, however, the aforementioned lateral forces imply that the grout is an important part

a) Specimen from Chai (1998)   b) Testing
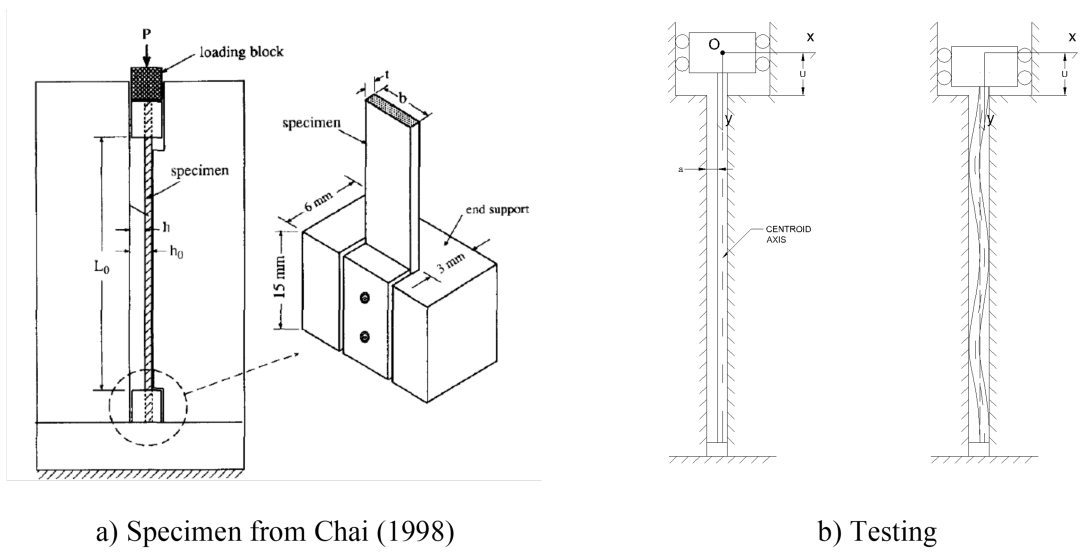
Figure 2.8: Bi-laterally constrained column and formation of higher modes

a)   b)

c)
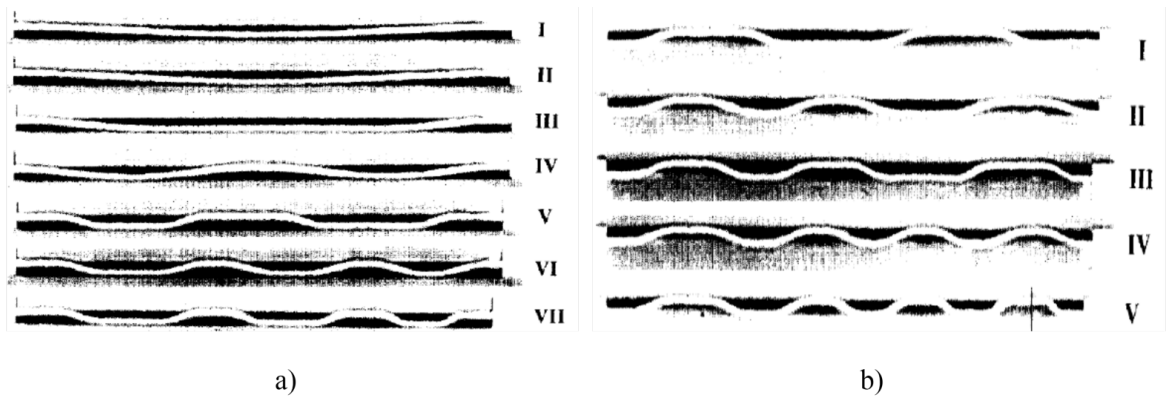
Figure 2.9: Experiment from Chai(1998)

of the load path.

Studies have shown that the filler material in the casing also functions as a medium to transmit forces by means of lateral thrust. Lateral thrust has also been identified as key to understand the mechanism of a BRB as this force acts on the surface of the grout becoming a demand for the casing which is the component that makes possible restraining buckling and avoid global instability issues, however difficulties have been found to measure it experimentally. Studies like Chai (1998) and B. Wu and Mei (2015) propose analytical expressions to estimate them, nonetheless given the lack of experimental data, this interface has been measured predominantly with the help of Finite Element software.

Genna and Gelfi (2012a) studied the effects of lateral thrust which provides a method to quantify these lateral forces for All-Steel **BRBs** (**ASBRBs**). The experimental study was conducted on bolted **BRBs** based and consisted in the assembly of 7 casings comprised by two parts attached with 4 instrumented bolts (Figure 2.10) to measure the tensile strain when compressive axial loading is applied.

The experiment showed that it is possible to quantify the resulting forces acting laterally, however the bigger challenge was to understand the phenomena locally. For this reason, a second study followed as a continuation of this investigation (Genna and Gelfi 2012b) where a similar specimen was tested, however, the inner steel surface was instrumented with pressure sensors.Genna and Gelfi (2012a) and Genna and Gelfi (2012b) showed the difficulty of quantifying lateral thrust and the necessity and relevance of conducting numerical analysis.

Steel tube/casing - Sizing correctly the infilled tubular structure has been a major addressed question and concern in the current state of the art of **BRBs**. The casing is aimed at containing the filler material, provide sufficient flexural stiffness to prevent global buckling and transfer the bending moment to the connection at the same time of providing rotational restriction through 2 point contact. Zhao, B. Wu, and Ou (2012) proposed analytically a stability boundary by using an amplified moment method for the design of the connections determining a limit eccentricity to avoid local failure (Zhao, B. Wu, and Ou 2013) see **Fig.**
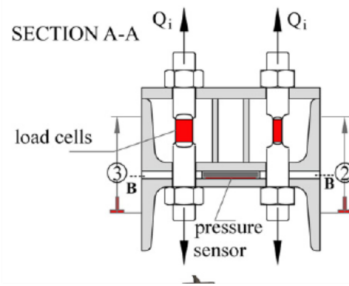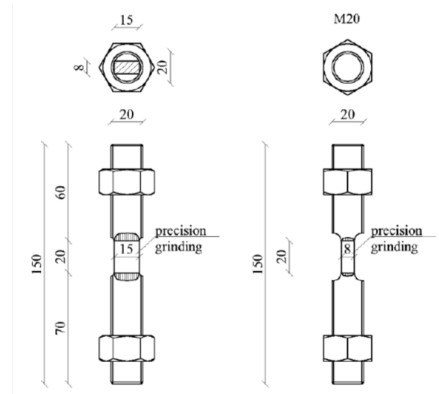
a) Cross-section　　　　　　　　　　　　　b) Grinded and instrumented bolts
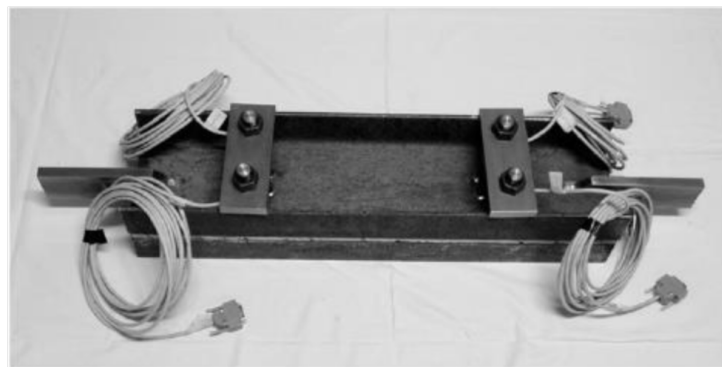
c)Specimen

Figure 2.10: Bolted reduced length ABRB from Genna and Gelfi (2012)
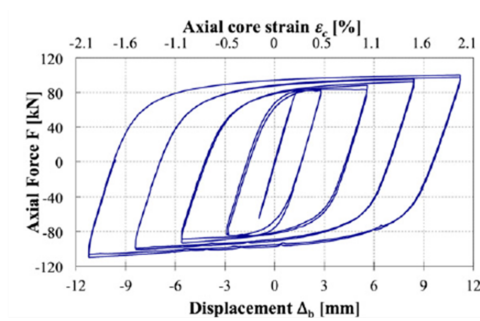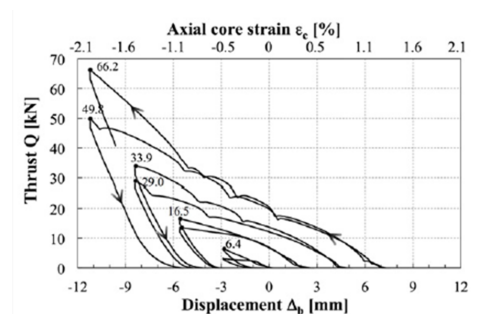
a) Hysteretic response　　　　　　　　　　　b) Lateral thrust

Figure 2.11: Axial and lateral hysteretical behaviour of a BRB from Metelli et al. (2016)
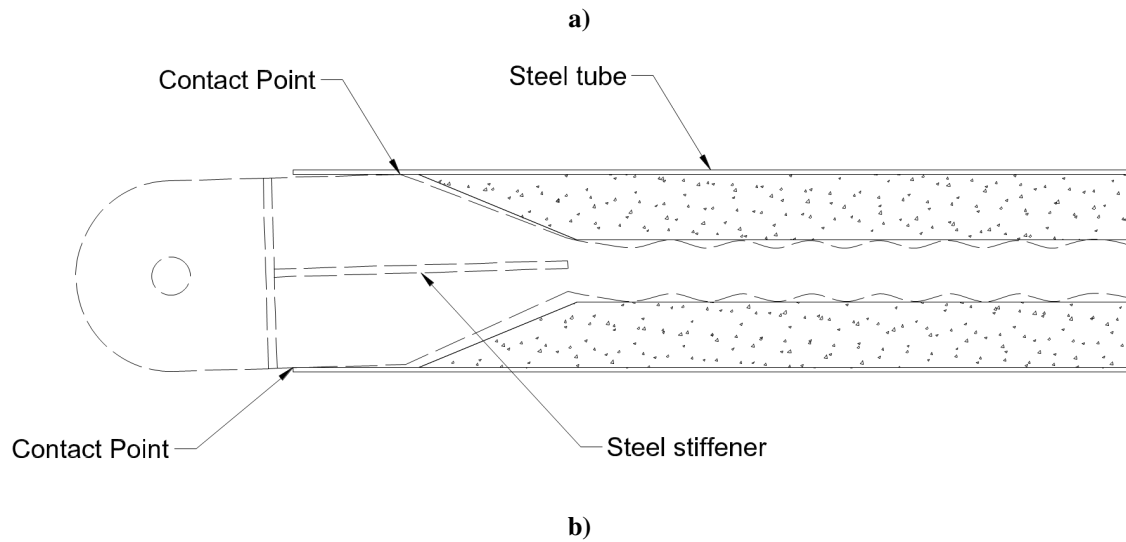
Figure 2.12: *(a) 2 point contact mechanism and (b) failed specimen with collar ends from Zhao, B. Wu, and Ou (2012) and Zhao, B. Wu, and Ou (2013)*

2.12. In addition, Zhao, B. Wu, and Ou (2014) also analysed the possibility of using end collars as alternative for moment transfer.

2.6 Global stability criterion

Owing to the fact that buckling is implied in the mechanism of a BRB regardless the type, a first concern arises in terms of global stability or the capability to withstand the axial displacements, which implies a sufficient lateral restriction so as to inhibit buckling. According to Black et al. (2002) the BRB global stability can be explained with the ratio P_e/P_y (where P_e is the critical load of the steel tube and P_y is the yield load of the core) and this comes from studying a beam on an elastic foundation under the following assumptions:

- The displacement perpendicular to the centroid axis of the steel core is the same in both the core and the casing

- The core material is elasto-plastic
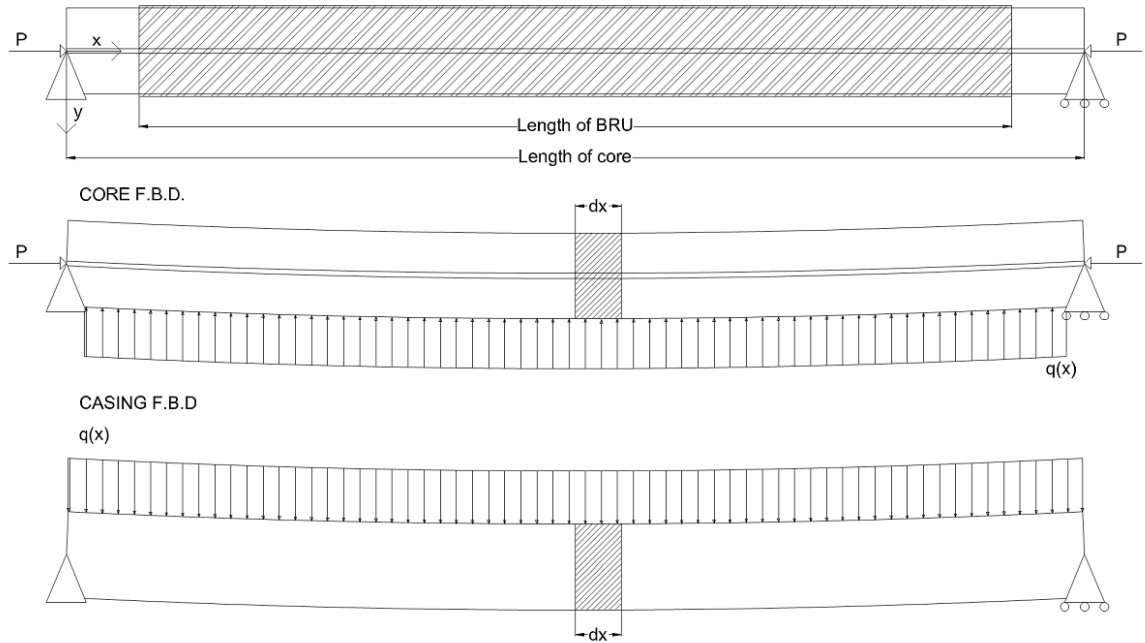
Figure 2.13: Core-Buckling Restraining Unit System (adapted from (Black, Makris, and Aiken 2002))

- The size of the gap or clearance between core and grout is negligible

- The length of the core and Buckling Restraining Unit (infilled casing) are the same

- No axial displacement takes place before the critical load of the system

- The flexural stiffness of the core is negligible in comparison with the flexural stiffness of the casing

- The system is linear-elastic

Under the above mentioned assumptions, the system graphically explained in Figure 2.13 can be mathematically analysed (as shown in Black et al. (2002)) if the Free Body Diagram (FBD) of a differential portion of the core is considered (Figure 2.14).

From the FBD of the core, the governing equation of a beam on elastic foundation can be derived by computing the summation of moment about n and deriving twice, resulting in the expression 2.1

$$E_i I_i \frac{d^4 y(x)}{dx^4} + P_{cr} \frac{d^2 y(x)}{dx^2} = -q(x) \tag{2.1}$$

Where $E_i I_i$ is the flexural stiffness of the core; $q(x)$ the reaction of elastic foundation; P_{cr} the critical load of the core and $y(x)$ the vertical displacement. Likewise from the *FBD*
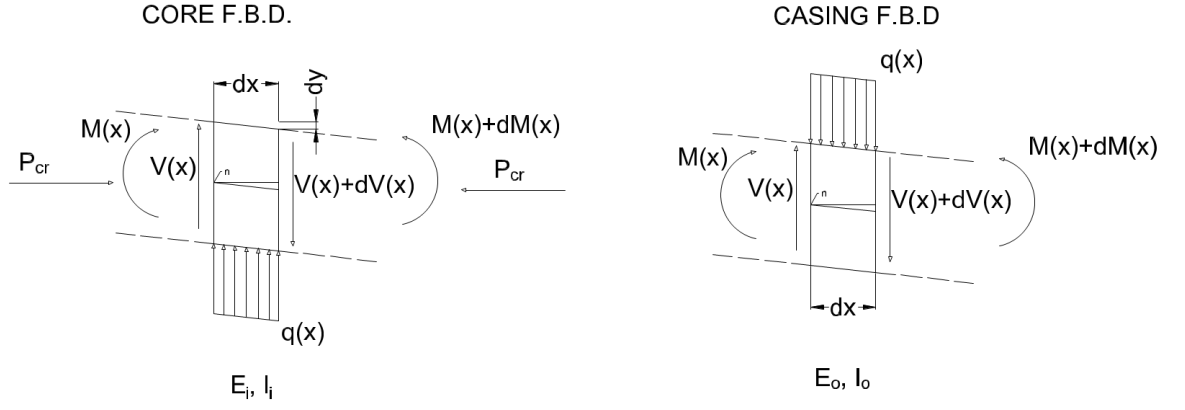
Figure 2.14: F.B.D. of a deformed differential segment of the core and casing (adapted from Timoshenko and Gere (1961), p.3)

of the casing shown in Figure 2.14 is not difficult to deduce that the condition for vertical equilibrium leads to equation 2.2

$$E_o I_o \frac{d^4 y\,(x)}{dx^4} = q\,(x) \tag{2.2}$$

Where $E_o I_o$ is the flexural stiffness of the infilled casing. Thus, the governing equation of the system can be obtained by substituting 2.2 in 2.1 as shown in 2.3

$$E_i I_i \frac{d^4 y\,(x)}{dx^4} + P_{cr} \frac{d^2 y\,(x)}{dx^2} = -E_o I_o \frac{d^4 y\,(x)}{dx^4} \tag{2.3}$$

$$\frac{d^4 y\,(x)}{dx^4} + \frac{P_{cr}}{E_i I_i + E_o I_o} \frac{d^2 y\,(x)}{dx^2} = 0 \tag{2.4}$$

$$P_{cr} = \frac{\pi^2 \left(E_i I_i + E_o I_o \right)}{L^2} \tag{2.5}$$

Simplifying the form of the equation in (4) the critical load value corresponding to the first mode is expressed in (5) where the first remark is to be made; whenever the flexural stiffness of the core $E_i I_i$ is comparatively smaller than the summation $E_i I_i + E_o I_o$, this can be neglected resulting in the simplified expression (6) which equals to the critical load of the infilled casing P_e.

$$P_{cr} = P_e \approx \frac{\pi^2 E_o I_o}{L^2} \tag{2.6}$$

Under the debonding condition assumption and perfect elasto-plastic properties of the core the criterion for overall stable equilibrium of the BRB is that the ratio P_e/P_y is greater than 1, where P_e is the critical load of the casing and P_y is the yield load of the steel core.

Assuming that the flexural stiffness of the core is negligible in comparison with the casing the critical load value corresponds to the casing only. If we consider the core material as bilinear then ensuring that the maximum load P_y is under the critical value is the condition for stability, experimental results agree with the derived formula (Table 2.6),. Even though efforts of measuring the accuracy of this model have been made with experimental work (Watanabe et al. 1988), it the limitations remain unclear.

Table 2.6: P_e/P_y ratios from Watanabe et al. (1988) in Uang and Nakashima (2003)

Specimen No	P_e/P_y	Observations
1	3.53	These specimens showed stable behaviour as ductility could be observed from a force-displacement plot
2	1.39	
3	1.03	
4	0.72	These specimens revealed overall instability condition with the formation of plastic hinges in the longitudinal direction of the casing.
5	0.55	

The analysis described in Black, Makris, and Aiken (2002) explains the stability of the 3 stockiest casings and the failure of the pair of most slender specimens of Watanabe et al. (1988) as BRBs with a P_e/P_y ratio greater than 1 were stable. However, the outcome of such an experiment showed a different feature form the assumed elasto-plastic condition. The hysteretic behaviour shows a non-perfect elasto-plastic ductile curve which develops an increase in the force applied as displacement occurs after yield both in tension and compression. Figure 2.16 is the hysteresis plot of one of the mentioned specimens; it illustrates the behaviour of the ductile zone showing an increment in P_{max} of about 30% of P_y.

The implications of this differential force are that the infilled casing is subjected to an increased demand and even though overall stability is ensured before yield with the mentioned criterion, instability may be an issue during the post buckling stage of the core, however the adopted criteria has shown satisfactory results in global terms as experimental studies like those shown in Table 2.7 use this criteria for specimen design.

Moreover, experimental studies like those conducted by (A.-C. Wu et al. 2013; B. Wu and

Figure 2.15: Tested specimens from (Watanabe et al. 1988) in (Wada and Nakashima 2004)
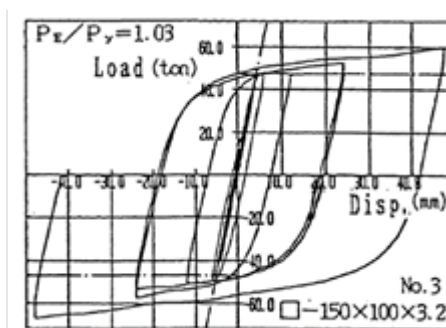
Figure 2.16: Hysteretic behaviour of specimen no. 3 from (Watanabe et al. 1988)

Mei 2015) and (Palazzo et al. 2009) present evidence of a high ductile buckling modes pattern occurring when the core has been extracted after having been tested in both All-Steel BRBs (ASBRBs) and GFBRBs respectively. Wu et al. (2014) conducted experimental research with a steel core encased in two pieces of steel work reporting the formation of waves along the core with a wavelength of about 12 times the core plate thickness; likewise, Palazzo et al. (2009) reports that "the core is bent; it is shaped roughly like a warped sinusoidal wave whose wavelength ranges between 100 and 200 mm and whose amplitude reaches 2 mm" this suggest that buckling does occur at a component level, however it is controlled by the restraining mechanism. Likewise, the formation of such waves also implies non-uniformly distributed strain along the core.

The formation of such a buckling mode number implies that the vertical displacements of the core and the bracing (alluding to Figure 2.12) are no equal in reality and that the formulation presented as a first criterion for overall stability is not valid for a post buckling anal-

ysis of the core where two main studies have been conducted. Black et al. (2002) analyses the problem by assuming the reaction force of the casing $q(x)$ as proportional to the vertical displacement $y(x)$, thus $q(x) = \beta y(x)$ where β is an elastic spring constant with units $[FL^{-2}]$. The resulting equation is expressed as in equation 2.7

$$E_i I_i \frac{d^4 y(x)}{dx^4} + P_{cr} \frac{d^2 y(x)}{dx^2} + \beta y(x) = 0 \tag{2.7}$$

Solving the differential equation, it can be seen that the critical load is given by equation (8) where β, according to the author, can be obtained from the assumption that the only contribution to this spring constant is the filling material which lateral compression modulus (E_c) under confined conditions is obtained by equation (9).

$$P_{cr} = 2\sqrt{\beta E_i I_i} \tag{2.8}$$

$$\beta = E_c \frac{1 - \nu}{(1 + \nu)(1 - 2\nu)} \tag{2.9}$$

The main implication for this analysis being accurate is that the filling material of traditional GFBRBs can be modified as long as the ratio P_{cr}/P_y is greater than 1 (Black, Makris, and Aiken 2002). Hence, equation (10) is the criterion for core stability for GFBRBs only, where the restraining unit is a tube filled with an isotropic material.

$$\beta \geq \frac{\sigma_y^2 A_i^2}{4 E_i I_i} \tag{2.10}$$

According to Zhao et al. (2014) experiments have shown that the conservativeness of this method remains unclear since the gap, initial deflection of the casing at the time of fabrication and imperfection of the core are not considered. The strength based method in contrast proposed by Shimizu et al. (1997), considers the same idealisation of the structure however this time a gap between the core and the casing is considered. The criterion consists in comparing the bending moment at the centre of the casing with its ultimate resisting moment or limit state. The bending moment at the middle of the casing (maximum bending moment in the first buckling mode formation) and criterion can expressed as

$$M_b = \frac{P(\delta_0 + 2c)}{1 - \frac{P}{P_{eb}}} < M_{yb} \qquad (2.11)$$

Where P is the maximum compressive force and P_{eb} the critical load of the casing, c is the size of the gap; δ_0 is the initial deflection and M_{yb} the ultimate resisting moment of the cross section of the casing. This criterion accounts for the presence of the gap and the flexural behaviour of the casing which is the mechanism that resists the lateral forces and provides stability.

With these methods a good approximation of casing size can be determined however, results of sub assemblage testing (Zhao et al. 2012b;Zhao et al. 2012a) show the need to account for moment transfer from the connection to the casing. With this purpose, Zhao et al. (2014) analyses the problem under a modified strength based criterion by introducing a moment value at the ends of the casing which is the result of a 2 point contact, also an amplification factor is introduced in order to estimate conservative values. An important advantage of this method is that the idealisation of the BRB is dimensionless as all the parameters involved are normalised.

2.7 Failure modes

Globally, failure of BRBs can be defined as the stage where the device loses its functionality. The primary function of a structural fuse is to dissipate energy so as to control lateral displacements; hence the failure stage is when it no longer has dissipation features. In experiments where global failure was observed, failure could be diagnosed from the sudden loss of force in the behaviour of the hysteretic loops (Figure 2.15).

On the other hand, locally, the global function described before can be understood as the product of the function of each component acting together, which allows understanding failure conditions as the loss of functionality of one or more components. Experimental evidence (see Table 2.7) reports component level failure during the induction of displacement cycles where not all the components developed such pathologies at the same time. The nature of failure type varies according to the working mechanism of each of these compo-

nents; however, the failure patterns predominate in the core and casing.

Specifically, the function of the core is to dissipate energy by yielding at relatively small axial displacements and providing a larger ductility than the considered for the protected structure without failure. In terms of structural behaviour this feature is relevant as it will eventually lead to fracture due to Low Cycle Fatigue (LCF). The function of the casing is to provide buckling resistance to the yielding core and ensure the uniaxial position of the yielding core permanently. From the literature, no failure patterns have been observed on the grout filling the tube whereas damage in the tube was visible in all cases.

The patterns observed in the axial load carrying unit can be addressed as: fracture and connection rotation. In the case of the restraining unit the failure types can be listed as: local buckling and formation of plastic hinges due to lateral forces induced from the core. In contrast with the global approach, there are studies available that propose a methodology to predict component failure by using the Finite Element Method mainly. Table 2.7 summarises the function and the typical failures observed from different studies.

Low Cycle Fatigue (LCF) – Being the displacement of the core cyclic in nature, where the component reaches yield in every incursion during testing, it is generally well acknowledged that at the microscopic structural level, steel crystals deform and restructure progressively in every cycle changing their arrangement until the formation of a crack is triggered, such a crack rapidly propagates along the cross section producing fracture. Unlike the most common type of fatigue which is driven by cyclic stress in the elastic range (High-Cycle Fatigue), Buckling Restrained Braces are driven by cyclic strain mostly in the plastic range, therefore the cycles required to fracture are significantly less than the former type of fatigue.

In addition to the nature of the displacement, experiments have shown that the strain distribution along the core is not even or constant, which suggests the concentration of strain in specific and not yet predicted locations along the core. In the Figure 2.17 it can be seen fracture occurring where a concentration of strain takes place.

Table 2.7: Component failure criteria according to the function and usual measures taken to overcome such patterns

Component	Function	Typical failures
Core (yielding portion)	Energy dissipation	Low Cycle Fatigue (necking)
Debonding material	Primary function: Reducing the magnitude of axial force induced to the casing Secondary function: Construction feasibility as it ensures no interaction occurs between core and grout when this latter is poured in the steel tube	No evidence of failure or decay of performance associated to debonding material rupture has been detected
Grout	Idealised as filling material to maintain the core in one position (parallel to the steel tube), however research suggests it also contributes to buckling resistance alongside the steel tube (composite action)	Generally, the grout is semi-confined in a steel tube working in composite action and grout failure is associated to bulging effect because of gap increase due to lateral thrust. System failure can be observed in the progressive degradation of the BRB hysteretic envelop.
Steel tube	Primary: Providing core buckling resistance Secondary: Manufacturing feasibility as it is a formwork for grout	Formation of global plastic hinges in the longitudinal direction due to overpassing the yield stress due to bending. Formation of local plastic hinges in the transverse direction due to induced normal loads by the core (bulging)
Connections	Transmitting displacements to yielding portion of the core ensuring energy dissipation features (ductility)	Formation of plastic hinges in the transition of the yielding portion and protrusion for connection
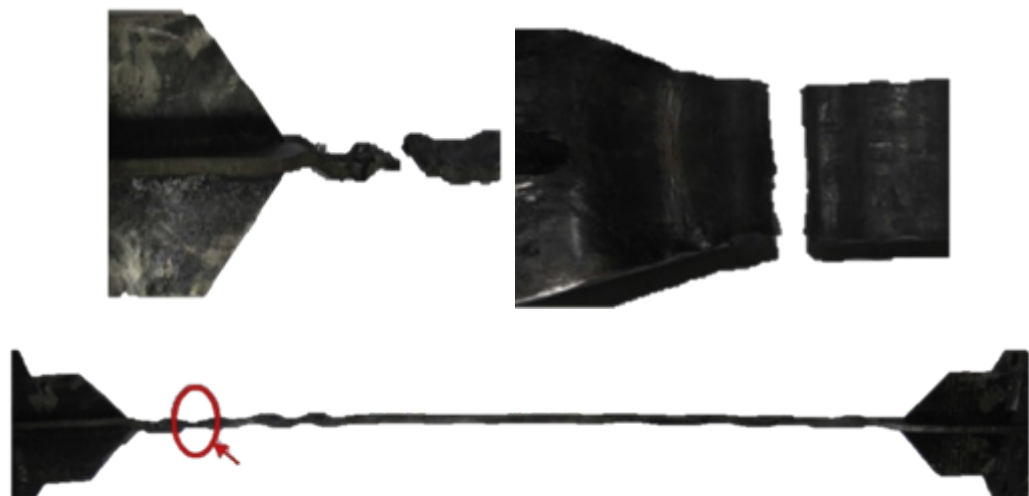
Figure 2.17: Low cycle fatigue fractured necking location adapted from Razavi Tabatabaei, Mirghaderi, and Hosseini (2014)

Low cycle fatigue has been approached by different authors to assess the fatigue life of different components of BRBs C.-L. L. Wang, Usami, and Funayama (2012), C.-L. Wang et al. (2013), and Usami, C. Wang, and Funayama (2011) and new types of devices. The effect on fatigue that some recent BRB detailing variants such as the usage of a stopper to avoid sliding, new materials such as nickel-titanium alloy and other type of devices such as self-centering BRBs have also been mentioned in the previous studies to a different degree, however, it is appreciated that the uncertainty to predict such phenomena prevails and more further studies are required.

To tackle such uncertainty, interesting statistical approaches to predict the number of cycles before necking based on the Cumulative Ductile Capacity (CDC) have been proposed by (Andrews, Fahnestock, and Song 2009c; Andrews, Fahnestock, and Song 2009a; Andrews, Fahnestock, and Song 2009b).

Table 2.8: Research related to Low Cycle Fatigue

Author	Achievement/Remark
Usami et al. (2011)	Conducted LCF analysis for an ASBRB with welded stiffening plate with and without grinded welding toe showing improvement for welded toe
Wang et al. (2012)	Observed improvement of LCF by using stoppers
Wang et al. (2013)	Based on experiments with extruded aluminium alloy BRBs recommends a formula for strain-based damage assessment
Andrews et al. (2009)	Proposed a Bayesian methodology for Ductility Capacity Models
Andrews et al. (2008)	Proposed a statistical method to predict the CDC with a reasonable accuracy
Takeuchi et al. (2008)	Proposes a method to predict CDC of a BRB based on past experiments

Connection rotation - The function of the connection is to transmit directly the loads (displacements) to the yielding core interacting with the structure by attaching to it with bolts or welding; as an example of this failure pattern experiments that have previously conducted sub-assemblage testing are shown Mahin et al. (2004) and Hikino et al. (2012), reporting unstable behaviour in the connection in this part of the core with the formation of plastic hinges at the ends (Figure 2.18).

Casing Global failure - From the parametric study of Watanabe et al. (1988) (Figure 2.15) the steel tube shows to work in bending. The results of the experiment reveal the plastic hinge is likely to occur whenever the flexural resistance of the restraining unit is overpassed.
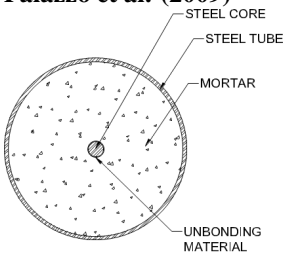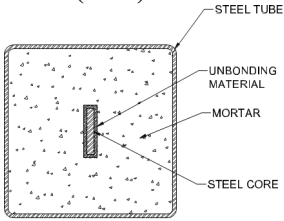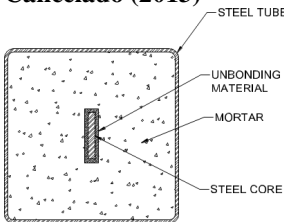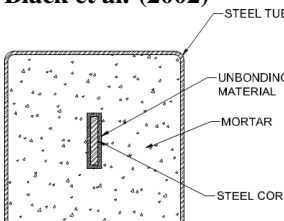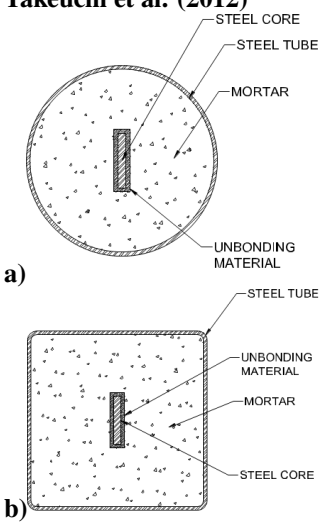
Bulging – A study from Takeuchi et al. (2012) shows the effects or a short clearance be-
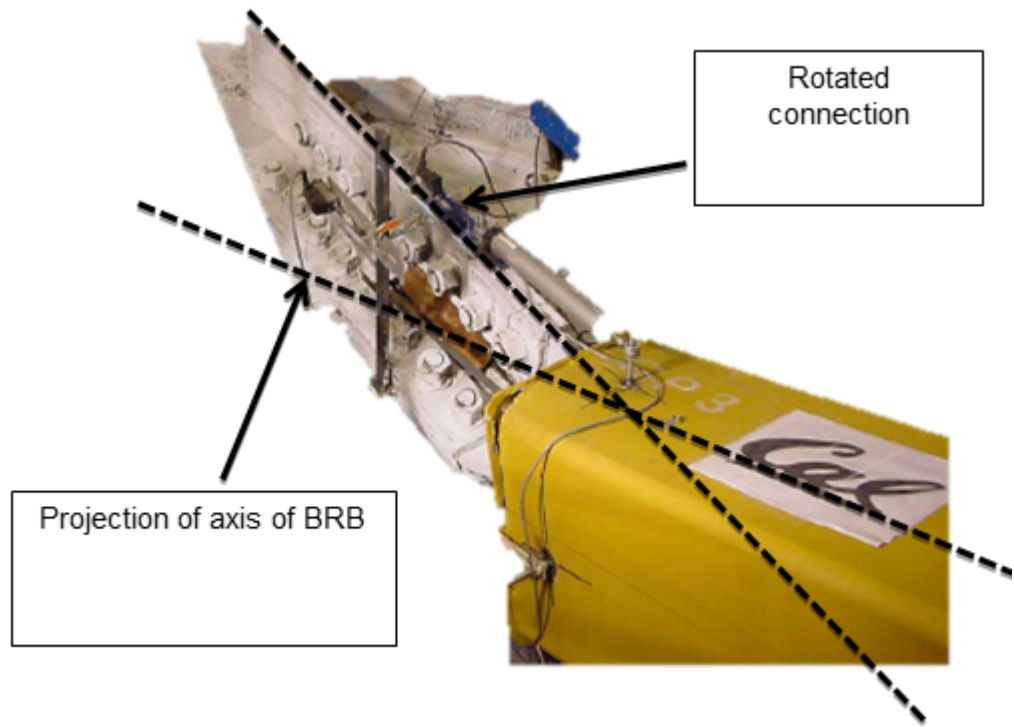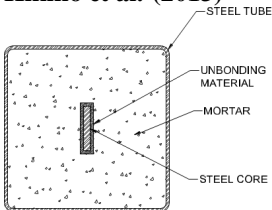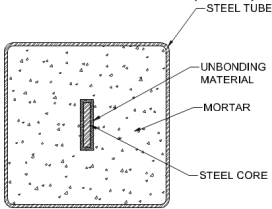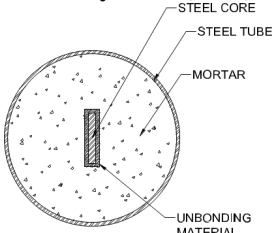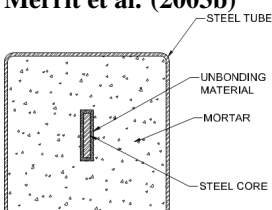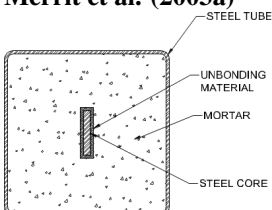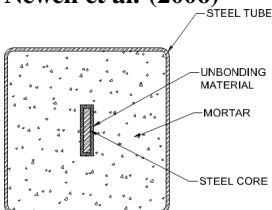
Figure 2.18: BRB end rotation Mahin et al. (2004)

tween core and steel casing when a mechanism forms pushing the grout against the sides of the tubular structure forming local failure (**Figure 2.19**). This study shows that when this distance is short, the higher mode formation of the core can produce tensions within the grout to produce local bulging effects on the steel tube. However, the same stusy showed that a practical and efficient solution to bulging is whether to increase the filler material or to use a circular tubular section as casing working forming a catenary in the direction of the loading.

Table 2.9: Cross section description of GFBRBs experimental research

Author	Specimen	Observations
Palazzo et al. (2009)	BRU: Cylindrical hollow steel-tube filled with grout Core: Circular core section coated Debonding layer: teflon, grease and 1.7mm thick rubber layer	4 specimens tested, 1 of them presented end buckling and the 3 others fracture in yielding portion.
Iwata (2004)	BRU: Rectangular hollow steel tube filled with grout Core: Steel plate coated with a Debonding layer: 1mm thick rubber layer	Buckling of unrestrained portion (connection)
Cancelado (2013)	BRU: Rectangular hollow steel tube filled with grout Core: steel plate coated with Teflon Debonding material: grease and 1.7mm thick rubber layer	No failure pattern observed
Black et al. (2002)	BRU: Rectangular hollow steel tube filled with grout Core: steel plate Debonding material: unspecified	Fracture within the yielding portion was observed in one specimen
Takeuchi et al. (2012)	a)Cylindrical steel tube filled with grout and core plate b) Rectangular hollow section filled with grout and core plate	a) No failure pattern observed b) Formation of plastic hinges within the steel tube

Table 2.10: Experimental studies conducted on GFBRBs (continued)

Author	Specimen	Observations
Hikino et al. (2013)	BRU: Rectangular hollow steel tube filled with grout Core: steel plate Debonding material: unspecified	Unrestrained portion rotation
Watanabe et al. (1988)	BRU: Rectangular hollow steel tube filled with grout Core: steel plate Debonding material: unspecified	Global buckling (bending of casing)
Tremblay et al. (2006)	BRU: Cylindrical steel tube filled with grout Core: steel plate	Fracture within the yielding portion was observed in one specimen
Merrit et al. (2003b)	BRU: Rectangular hollow steel tube filled with grout Core: steel plate Debonding material: Unspecified	Fracture within the yielding portion was observed in two specimens
Merrit et al. (2003a)	BRU: Rectangular hollow steel tube filled with grout Core: steel plate Debonding material: Unspecified	Fracture within the yielding portion was observed in all 6 specimens
Newell et al. (2006)	BRU: Rectangular hollow steel tube filled with grout Core: steel plate Debonding material: Unspecified	No failure pattern observed
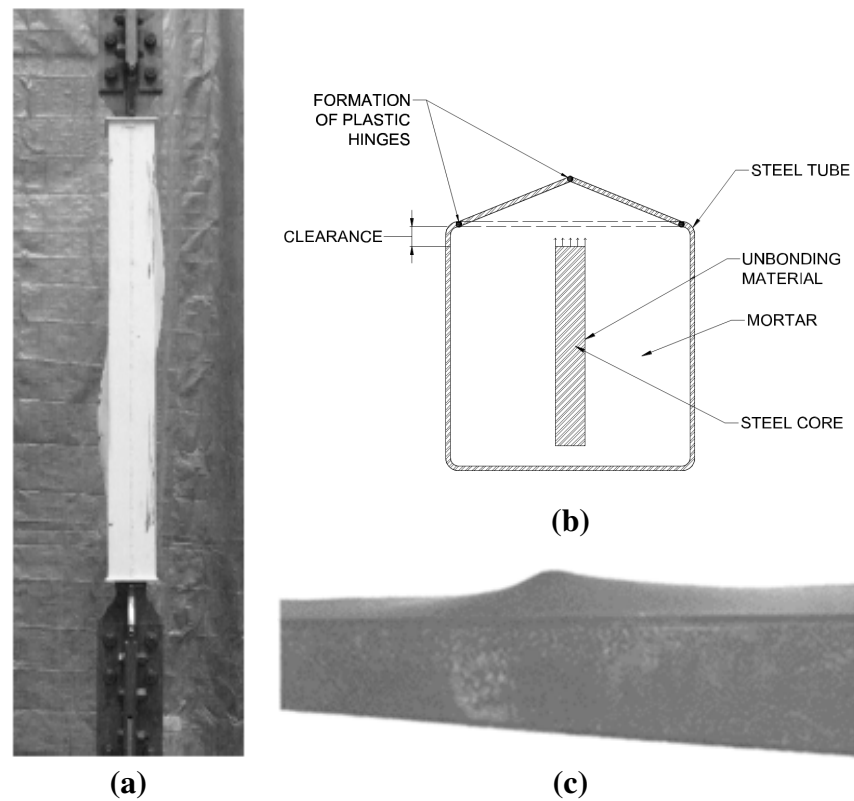
Figure 2.19: Bulging of steel casing a), b) adapted from (Takeuchi et al. 2012; Uang and Nakashima 2003)

2.8 Challenges and opportunities in BRB research

This literature review highlights the overall need to investigate BRB components including the casing. In spite of the casing material being a central research question for the present work, it is only one of the components that do not have a clear target performance defined. Some tangible examples that have been identified as gaps in research and therefore opportunities are listed below:

1. The load transfer from the connections load the casing with a two point contact mechanism, however, during testing gap-opening has been identified which has resulted in proposed end collars as a mean to retrofitting this portion. Given that the connection slides in reversal loading in and out of the casing, the possibility of using ball bearings should be analysed.

2. It is unclear what materials are suitable to compose the debonding layer. From discussions with professionals working in the BRB industry it was found that manufacturers have their own patents and these cannot be disclosed, however, it is fundamental to quantify the friction that this layer induces in the steel core, thus forming necking.

3. The grout-infilled tubular steel structure is not provided with shear connectors on the inside to transfer transverse shear and ensure composite action, this produces uncertainty in the function of the grout and challenges the structural efficiency of the filler material under lateral thrust.

So far, the findings in literature have been presented and a general picture of the research of BRBs can be appreciated, however, there are yet important particularities to be interpreted to provide a clearer picture of the conducted research in terms of trends, scope, limitations and critical discussion of what has been studied in the past 30 years.

To have a better understanding of the subtopics that require attention, it is important to know the limitations of conducting further work and highlight the effort made by previous researchers in attempting to answer fundamental research questions regarding Buckling Restrained Braces so as to manage expectations.

To present, Buckling Restrained Braces are still considered as an innovative system by different authors, this implies that fundamental questions that apply to a general BRB structure remain unanswered such as measuring the accuracy of the results obtained by FEM, computational cost and convergence, modelling techniques, assumptions that lack demonstration in real structures when conducting analytical derivations, limitations to measure important parameters other than axial displacement and force; these can include initial imperfections in the fabrication process, friction forces, real time monitoring of inner core, etc.

Due to the aforementioned reasons, there is still a long way to go until we can regard Buckling Restrained Braces, as well as other structural fuses, a mature area of knowledge, however significant effort and achievements have been made allowing to answer some of the questions regarding local effects and global stability considerations; there is a big challenge and patience is essential when conducting BRB research. From the analysed literature, gaps of knowledge and research opportunities can be listed in 3 categories: a) experimental b) numerical and c) analytical
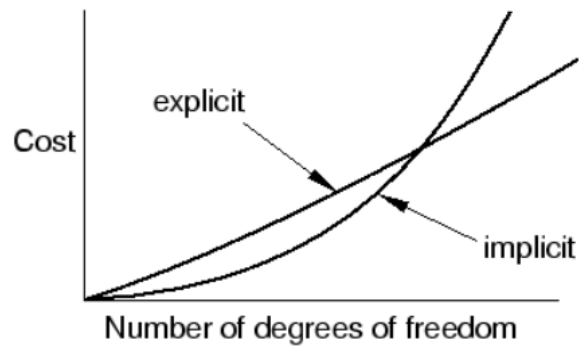
Figure 2.20: Computational cost vs number of elements from ABAQUS user's manual (SIMULIA, n.d.)

Experimental necessity - BRB target performance is ruled by available provisions that establish seismic requirements as it is described in the previous section. Testing of the devices under different loading protocols in both uniaxial and sub assemblage testing are essential so the specimen can be used safely.

Generally speaking it is not possible to observe the evolution of the core formation inside the casing as load is applied. This limitation is in fact one of the reasons why the behaviour of GFBRBs is not fully understood as it is not possible to associate the performance (hysteretic response) with the mechanism of the device (core evolution and formation of higher buckling shape modes).

Numerical analysis - BRB research is highly dependent on numerical analysis to obtain information that testing cannot measure, however, the lack of measurements in alternative directions to the axial load (code provisions requirements) imply that numerical validation is incomplete, therefore accuracy and further parameters to attest the modes are research opportunities to explore.

From the numerical studies revised, there is a consensual concern of computational cost and convergence problem, however, even though it cannot be significantly reduced, it can be mitigated by using different modelling techniques such as the Dynamic Explicit method(SIMULIA, n.d.)

Figure 2.20 shows that efficiency can be improved using the explicit method; a larger number of elements could be analysed in a shorter window of time without convergence issues

and an improved computational cost.

Bibliography

AlHamaydeh, Mohammad, Farid Abed, and Abdilwahhab Mustapha (2016). "Key parameters influencing performance and failure modes for BRBs using nonlinear FEA". In: *Journal of Constructional Steel Research* 116, pp. 1–18. ISSN: 0143974X. DOI: 10.1016/j.jcsr.2015.08.038.

American Institute of Steel Construction (2005). "Seismic Provisions for Structural Steel Buildings". In: *Seismic Provisions for Structural Steel Buildings* 1, p. 402.

Andrews, Blake M., Larry a. Fahnestock, and Junho Song (2009a). "Ductility capacity models for buckling-restrained braces". In: *Journal of Constructional Steel Research* 65.8-9, pp. 1712–1720. ISSN: 0143974X. DOI: 10.1016/j.jcsr.2009.02.007.

– (2009b). "Ductility capacity models for buckling-restrained braces". In: *Journal of Constructional Steel Research* 65.8-9, pp. 1712–1720. ISSN: 0143974X. DOI: 10.1016/j.jcsr.2009.02.007.

– (2009c). "Ductility capacity models for buckling-restrained braces using a Bayesian Methodology". In: *Journal of Constructional Steel Research* 65.1, pp. 1712–1720. ISSN: 0143974X. DOI: 10.1016/j.jcsr.2009.02.007.

Black, Cameron, Nicos Makris, and Ian Aiken (2002). *Component testing, stability analysis and characterization of buckling-restrained Unbonded Braces*. Tech. rep. September. Berkeley, CA.: Pacific Earthquake Engineering Research Center, Univ. of California, p. 100.

BSEN1998-3:2005 (2005). "Eurocode 8: Design of structures for earthquake resistance. Part 3: Assessment and retrofitting of buildings". In: *British Standard*.

Chai, Herzl (1998). "The post-buckling response of a bi-laterally constrained column". In: *Journal of the Mechanics and Physics of Solids* 46.7, pp. 1155–1181. ISSN: 00225096. DOI: 10.1016/S0022-5096(98)00004-0.

Dehghani, M. and R. Tremblay (2017). "An analytical model for estimating restrainer design forces in bolted buckling-restrained braces". In: *Journal of Constructional Steel Research* 138, pp. 608–620. ISSN: 0143974X. DOI: 10.1016/j.jcsr.2017.07.007.

Deng, Kailai et al. (2015a). "Study of GFRP Steel Buckling Restraint Braces". In: *Journal of Composites for Construction*, p. 4015009. ISSN: 1090-0268 1943-5614. DOI: 10.1061/(asce)cc.1943-5614.0000567.

– (2015b). "Study of GFRP Steel Buckling Restraint Braces". In: *Journal of Composites for Construction*, p. 4015009. DOI: 10.1061/(asce)cc.1943-5614.0000567.

Ding, Yukun, Yaochun Zhang, and Junxian Zhao (2009a). "Tests of hysteretic behavior for unbonded steel plate brace encased in reinforced concrete panel". In: *Journal of Constructional Steel Research* 65.5, pp. 1160–1170. ISSN: 0143974X. DOI: 10.1016/j.jcsr.2008.11.003.

– (2009b). "Tests of hysteretic behavior for unbonded steel plate brace encased in reinforced concrete panel". In: *Journal of Constructional Steel Research* 65.5, pp. 1160–1170. ISSN: 0143974X. DOI: 10.1016/j.jcsr.2008.11.003.

EN15129 (2009). "European Stardard of Anti-seismic devices". In: *EUROPEAN COMMITTEE FOR STANDARDIZATION*.

FEMA (2003a). "NEHRP Recommended Provisions for Seismic Regulations of Buildings and other Structures". In: *Federal Emergency Management Agency, Washington, D.C.*

– (2003b). "NEHRP Recommended Provisions for Seismic Regulations of Buildings and other Structures". In: *Federal Emergency Management Agency, Washington, D.C.*

Genna, Francesco and Piero Gelfi (2012a). "Analysis of the Lateral Thrust in Bolted Steel Buckling-Restrained Braces. I: Experimental and Numerical Results". In: *Journal of Struc-*

tural Engineering 138.10, pp. 1244–1254. ISSN: 0733-9445. DOI: 10.1061/(ASCE)ST. 1943-541X.0000564.

Genna, Francesco and Piero Gelfi (2012b). "Analysis of the Lateral Thrust in Bolted Steel Buckling-Restrained Braces. II: Engineering Analytical Estimates". In: *Journal of Structural Engineering* 138, pp. 1244–1254. ISSN: 0733-9445 1943-541X. DOI: 10.1061/(asce)st.1943-541x.0000564.

Higgins, J. and S. Green (2006). *Cochrane Handbook for Systematic Reviews of Interventions*. 4th ed. The Cochrane Library.

Hikino, Tsuyoshi et al. (2012). "Out-of-Plane Stability of Buckling-Restrained Braces Placed in a Chevron Arrangement". In: *Journal of Structural Engineering* 139.November, p. 121029070242 ISSN: 0733-9445. DOI: 10.1061/(ASCE)ST.1943-541X.0000767.

Huang, Jia Hao et al. (2014). "Comparative Investigation on the Seismic Performance of a Benchmark Steel Frame with Different Bracing Systems". In: *Applied Mechanics and Materials* 638-640, pp. 1917–1922. ISSN: 1662-7482. DOI: 10.4028/www.scientific. net/AMM.638-640.1917.

Huang, Mei Ling, Zhao Yu Fu, and En He Bao (2014). "Seismic Performances of Buckling-Restrained Braced Steel Frames in China, Japan and US". In: *Advanced Materials Research* 1065-1069, pp. 1106–1111. ISSN: 1662-8985. DOI: 10.4028/www.scientific. net/AMR.1065-1069.1106.

Inoue, Kazuo, Shinichi Sawaizumi, and Yasuo Higashibata (2001). "Stiffening Requirements for Unbonded Braces Encased in Concrete Panels". In: 2.June, pp. 712–719.

Isoda, K et al. (2001). "Development of unbonded brace damper restrained by channel section steel". In: *Summaries of technical papers of annual meeting, vol. III. Architectural Institute of Japan, Structural Engineering Section*, 663–8 [in Japanese] IN Xie(2004).

Iwata, Mamoru (2004). "Applications-design of buckling restrained braces in Japan". In: *13th World Conference on Earthquake Engineering* 3208.

Jia, Mingming et al. (2017). "Experimental research of assembled buckling-restrained braces wrapped with carbon or basalt fiber". In: *Journal of Constructional Steel Research* 131, pp. 144–161. ISSN: 0143974X. DOI: 10.1016/j.jcsr.2017.01.004.

Jiang, Z. Q., Dou C., et al. (2017). "Theoretical study on design methods for pinned assembled BRB with flat core". In: *Engineering Structures* 133, pp. 1–13. ISSN: 18737323. DOI: 10.1016/j.engstruct.2016.12.004.

Jiang, Z. Q., C. Dou, et al. (2017). "Theoretical study on design methods for pinned assembled BRB with flat core". In: *Engineering Structures* 133, pp. 1–13. ISSN: 18737323. DOI: 10.1016/j.engstruct.2016.12.004.

Judd, Johnn P. et al. (2016). "Cyclic tests of all-steel web-restrained buckling-restrained brace subassemblages". In: *Journal of Constructional Steel Research* 125, pp. 164–172. ISSN: 0143974X. DOI: 10.1016/j.jcsr.2016.06.007.

Kuwahara, S et al. (1993a). "A study on stiffening capacity of double-tube members". In: *Journal of Structural and Construction Engineering, Architectural Institute of Japan* 445:151–8.

– (1993b). "Horizontally loading test of the steel frame braced with double tube members". In: *Journal of Structural and Construction Engineering, Architectural Institute of Japan* 203–8 [in.

Mahin, Stephen et al. (2004). "Seismic Performance of Buckling Restrained Braced Systems". In: *13th World Conference on Earthquake Engineering; Vancouver, B.C., Canada.*

Manabe, N, M Kamiya, et al. (1997). "Elasto-plastic behavior of flat-bar brace stiffened by square steel tube". In: *Summaries of technical papers of annual meeting, vol. III. Architectural Institute of Japan* C1, Struct, 789–92 [in Japanese] IN Xie (2004).

Manabe, N, H Simokawa, et al. (1996). "Elasto-plastic behaviour of flat-bar brace stiffened by square steel tube". In: *Summaries of Technical Papers of Annual Meeting, Architectural Institute of Japan* C1, Struct, pp. 783–784.

Mase, S and Y Yabe (1995). "Elasto-plastic damper using unbonded brace of low yield-point steel (part 2 low cycle fatigue test)". In: *Summaries of technical papers of annual*

meeting, vol. III. Architectural Institute of Japan C1, Struct, 409–10 [In Japanese] IN Xie (2004).

Metelli, Giovanni, Guido Bregoli, and Francesco Genna (2016a). "Experimental study on the lateral thrust generated by core buckling in bolted-BRBs". In: *Journal of Constructional Steel Research* 122, pp. 409–420. ISSN: 0143974X. DOI: 10.1016/j.jcsr.2016.04.004.

– (2016b). "Experimental study on the lateral thrust generated by core buckling in bolted-BRBs". In: *Journal of Constructional Steel Research* 122, pp. 409–420. ISSN: 0143974X. DOI: 10.1016/j.jcsr.2016.04.004.

Mirtaheri, Masoud et al. (2011a). "Experimental optimization studies on steel core lengths in buckling restrained braces". In: *Journal of Constructional Steel Research* 67, pp. 1244–1253. ISSN: 0143974X. DOI: 10.1016/j.jcsr.2011.03.004.

– (2011b). "Experimental optimization studies on steel core lengths in buckling restrained braces". In: *Journal of Constructional Steel Research* 67.8, pp. 1244–1253. ISSN: 0143974X. DOI: 10.1016/j.jcsr.2011.03.004.

Nagao, T, K Mikuriya, Y Matsumoto, et al. (1988). "An experimental study on the elasto-plastic behavior of unbonded composite bracing (part 1–4)". In: *Summaries of technical papers of annual meeting, vol. II. Architectural Institute of Japan, Structural Engineering Section*, 1329–36 [in Japanese] IN Xie (2004).

Nagao, T, K Mikuriya, S Yuki, et al. (1989). "An experimental study on the elasto-plastic behavior of unbonded composite bracing (part 5–7)". In: *Summaries of technical papers of annual meeting, vol. II. Architectural Institute of Japan, Structural Engineering Section*, 1501–6 [in Japanese] IN Xie (2004).

Nagao, T, S Sera, et al. (1992). "A study on the RC encased H-section steel brace (part 1. general description, part 2 results and discussion)". In: *Summaries of technical papers of annual meeting, vol. II. Architectural Institute of Japan*, 1773–6 [in Japanese] IN Xie (2004).

Nagao, T and S Takahashi (1990). "A study on the elasto-plastic behavior of unbonded composite bracing (part 1 experiments on isolated members under cyclic loading)". In: *Journal of Structural and Construction Engineering, Architectural Institute of Japan*, 415:105–15 [in Japanese] IN Xie (2004).

– (1991). "A study on the elasto-plastic behavior of unbonded composite bracing (part 2 analytical studies)". In: *Journal of Structural and Construction Engineering, Architectural Institute of Japan*, 422:45–56 [in Japanese] IN Xie (2004).

Narihara, H, Y Koetaka, and O Tsujita (2000a). "The experimental study on BRBs: Parts 1 and 2". In: *Summaries of Technical Papers of Annual Meeting, Architectural Institute of Japan* 3, pp. 911–14.

– (2000b). "The experimental study on BRBs: Parts 3". In: *Summaries of Technical Papers of Annual Meeting, Architectural Institute of Japan* 3, pp. 651–2.

Palazzo, G. et al. (2009). "A low-tech dissipative buckling restrained brace. Design, analysis, production and testing". In: *Engineering Structures* 31, pp. 2152–2161. ISSN: 01410296. DOI: 10.1016/j.engstruct.2009.03.015.

Rahnavard, Rohola et al. (2018). "Investigating modeling approaches of buckling-restrained braces under cyclic loads". In: *Case Studies in Construction Materials* 8.December 2017, pp. 476–488. ISSN: 2214-5095. DOI: 10.1016/j.cscm.2018.04.002.

Razavi Tabatabaei, Seyyed Ali, Seyyed Rasoul Mirghaderi, and Abdollah Hosseini (2014). "Experimental and numerical developing of reduced length buckling-restrained braces". In: *Engineering Structures* 77, pp. 143–160. ISSN: 01410296. DOI: 10.1016/j.engstruct.2014.07.034.

Sabelli, Rafael (2004). "Recommended Provisions for Buckling-Restrained Braced Frames". In: *Engineering Journal* 41, pp. 155–175.

Sabelli, Rafael and Ian Aiken (2004). "U . S . BUILDING-CODE PROVISIONS FOR BUCKLING-RESTRAINED BRACED FRAMES : BASIS AND DEVELOPMENT". In: *13 th World Conference on Earthquake Engineering*. 1828. Vancouver, Canada.

SEAOC-AISC (2001). "Recommended Provisions for Buckling-Restrained Braced Frames (draft)". In: *SEAOC and AISC*.

Shimizu, T et al. (1997). "Design method to prevent buckling of low yield strength steel tube brace and fracturing of joints (part 1&2)". In: *Summaries of technical papers of annual meeting, vol. III. Architectural Institute of Japan* C1, Struct, 781–4 [in Japanese] IN Xie(2004).

Sun, Hongpeng et al. (2019). "Study of buckling-restrained braces with concrete infilled GFRP tubes". In: *Thin-Walled Structures* 136.December 2017, pp. 16–33. ISSN: 02638231. DOI: 10.1016/j.tws.2018.10.040.

Sun, Jiangbo, Peng Pan, and Haishen Wang (2018). "Development and experimental validation of an assembled steel double-stage yield buckling restrained brace". In: *Journal of Constructional Steel Research* 145, pp. 330–340. ISSN: 0143974X. DOI: 10.1016/j.jcsr.2018.03.003.

Suzuki, N, H Kaneko, et al. (1995). "Mechanical behavior of H-shape braces with flexural buckling stiffeners (part 1. fundamental characteristics of stiffeners". In: *Summaries of technical papers of annual meeting, vol. III. Architectural Institute of Japan* C1, Struct, 393–4 [in Japanese] IN Xie (2004).

Suzuki, N, R Kono, et al. (1994). "Experimental study on the H-section steel brace encased in RC or steel tube". In: *Summaries of technical papers of annual meeting, vol. II. Architectural Institute of Japan* C, Structu, 1621–2 [in Japanese] IN Xie (2004).

Takeuchi, T. et al. (2012). "Effect of local buckling core plate restraint in buckling restrained braces". In: *Engineering Structures* 44, pp. 304–311. ISSN: 01410296. DOI: 10.1016/j.engstruct.2012.05.026..

Timoshenko, Stephen and James Gere (1961). *Theory of Elastic Stability*. Ed. by McGraw-Hill. New York.

Tremblay, R. et al. (2016). "Comparison of seismic design provisions for buckling restrained braced frames in Canada, United States, Chile, and New Zealand". In: *Structures* 8, pp. 183–196. ISSN: 23520124. DOI: 10.1016/j.istruc.2016.06.004.

Tsai, K C and Y C Huang (2002). "Experimental responses of large scale BRB frames". In: *Center for Earthquake Engineering Research, National Taiwan University*, [In Chinese] IN Xie (2004).

Tsai, K C and J W Lai (2001). "A study of BRB frames". In: *Center for Earthquake Engineering Research, National Taiwan University*, [In Chinese] IN Xie (2004).

Tsai, K C, Jiun-wei Lai, et al. (2003). "Buckling Restrained Brace Research in National Taiwan University". In: *The Sixteenth KKCNN Symposium on Civil Engineering*. Korea, pp. 1–6.

Tsai, K C and C H Weng (2002). "Experimental responses of double-tube unbonded brace elements and connections". In: *Center for Earthquake Engineering Research, National Taiwan University*, [In Chinese] IN Xie (2004).

Tsai, K. C. et al. (2013). "Buckling Restrained Braces: research and implementation in Taiwan". In: *Steel Innovations Conference*. February. Christchurch, New Zealand.

Uang, Chia-Ming and Masayoshi Nakashima (2003). "Steel buckling-restrained braced frames". In: *Earthquake engineering: Recent advances and applications*, Chapter 16.

Usami, Tsutomu and H Kaneko (2001). "Strength of H-shaped brace constrained flexural buckling having unconstrained area at both ends: both ends simply supported". In: *Journal of Structural and Construction Engineering, Architectural Institute of Japan*, 211–8 [In Japanese] IN Xie (2004).

Usami, Tsutomu, H Kaneko, and T Ono (2002). "Strength of H-shaped brace constrained flexural buckling having unconstrained area at both ends: both ends simply supported". In: *Journal of Structural and Construction Engineering, Architectural Institute of Japan*, 211–8 [In Japanese] IN Xie (2004).

Usami, Tsutomu, Chunlin Wang, and Jyunki Funayama (2011). "Low-cycle fatigue tests of a type of Buckling Restrained Braces". In: *Procedia Engineering* 14, pp. 956–964. ISSN: 18777058. DOI: 10.1016/j.proeng.2011.07.120.

Wada, A and Masayoshi Nakashima (2004). "From infancy to maturity of buckling restrained braces research". In: *13th World Conference on Earthquake Engineering; Vancouver, B.C., Canada*.

Wada, Akira and Masayoshi Nakashima (2004). "From Infancy To Maturity of Buckling Restrained Brace Research". In: *13th World Conference on Earthquake Engineering* 1732, Paper No. 1732.

Wakabayashi, M, T Nakamura, A Kashibara, et al. (1973). "Experimental study of elasto-plastic properties of precast concrete wall panels with built-in insulating braces". In: *Summaries of Technical Papers of Annual Meeting, Architectural Institute of Japan* [in Japane.

Wakabayashi, M, T Nakamura, A Katagihara, et al. (1973). "Experimental study on the elastoplastic behavior of braces enclosed by precast concrete panels under horizontal cyclic loading (Parts 1 & 2)". In: *Summaries of technical papers of annual meeting. Structural Engineering Section. Architectural Institute of Japan*. Vol. 10, pp. 1041–4.

Wang, Chun-Lin et al. (2013). "Low-cycle fatigue testing of extruded aluminium alloy buckling-restrained braces". In: *Engineering Structures* 46, pp. 294–301. ISSN: 01410296. DOI: 10.1016/j.engstruct.2012.07.016.

Wang, Chun-Lin Lin, Tsutomu Usami, and Jyunki Funayama (2012). "Evaluating the influence of stoppers on the low-cycle fatigue properties of high-performance buckling-restrained braces". In: *Engineering Structures* 41, pp. 167–176. ISSN: 01410296. DOI: 10.1016/j.engstruct.2012.03.040.

Wang, Jiaojiao, Yongjiu Shi, and Yuanqing Wang (2016). "Constitutive Model of Low-Yield Point Steel and Its Application in Numerical Simulation of Buckling-Restrained Braces". In: *Journal of Materials in Civil Engineering* 28.3, p. 4015142. ISSN: 08991561. DOI: doi:10.1061/(ASCE)MT.1943-5533.0001416.

Watanabe, Atsushi et al. (1988). "Properties of brace encased in buckling-restraining concrete and steel tube". In: *9th World Conference on Earthquake Engineering* IV, pp. 719–724.

Wu, Bin and Yang Mei (2015). "Buckling mechanism of steel core of buckling-restrained braces". In: *Journal of Constructional Steel Research* 107, pp. 61–69. ISSN: 0143974X. DOI: 10.1016/j.jcsr.2015.01.012.

Wu, An-Chien et al. (2013). "High-mode buckling responses of buckling-restrained brace core plates". In: *Earthquake Engineering & Structural Dynamics* 41.August 2013, pp. 1549–1568. ISSN: 00988847. DOI: 10.1002/eqe.2349.

Xie, Qiang (2005a). "State of the art of buckling-restrained braces in Asia". In: *Journal of Constructional Steel Research* 61, pp. 727–748. ISSN: 0143974X. DOI: 10.1016/j.jcsr.2004.11.005.

– (2005b). "State of the art of buckling-restrained braces in Asia". In: *Journal of Constructional Steel Research* 61, pp. 727–748. DOI: 10.1016/j.jcsr.2004.11.005.

Zhao, Junxian, Bin Wu, and Jinping Ou (2012). "Flexural Demand on Pin-Connected Buckling-Restrained Braces and Design Recommendations". In: *Journal of Structural Engineering* 138, pp. 1398–1415. ISSN: 0733-9445 1943-541X. DOI: 10.1061/(asce)st.1943-541x.0000549.

– (2013). "Global stability design method of buckling-restrained braces considering end bending moment transfer: Discussion on pinned connections with collars". In: *Engineering Structures* 49, pp. 947–962. ISSN: 01410296. DOI: 10.1016/j.engstruct.2012.12.042.

– (2014). "A practical and unified global stability design method of buckling-restrained braces: Discussion on pinned connections". In: *Journal of Constructional Steel Research* 95, pp. 106–115. ISSN: 0143974X. DOI: 10.1016/j.jcsr.2013.12.001.

Chapter 3

Validation of Numerical Modelling of ASBRBs and GFBRBs

Numerical modelling of BRBs has shown to be a challenging part of their development and study due to the limited availability of experimental data, lack of techniques to obtain revealing component performance descriptors and the computational power at hand. These factors together result in BRBs requiring high complexity models that require a three dimensional approach where the Finite Element Method offers effective solutions.

One of the main caveats in quantitative and qualitative analysis of BRBs is the prevalence of uncertainty due to the difficulty (or even impossibility) to obtain measurements inside the casing which implies that only the stress state of accessible and visible components can be subject to direct observation and measurements. Therefore, components that are not accessible are highly reliant on numerical modelling to understand and predict their behaviour, hence the relevance of this chapter.

The objective of this chapter is to explore the modelling techniques used to replicate the data obtained in experimental studies by different authors. The studies were selected based on the observed mode of failure and different types of BRBs were analysed. Some of the main intended features to replicate are the observed wave formation of the yielding portion of the core and global buckling failure.

However, the complexity of the models required extensive sub validations to account for

imperfections, surface to surface contact, strain cyclic, kinematic hardening and Bauschinger effect (Mughrabi 1987). Likewise, friction and slip were modelled alongside with various sizes of mesh and types of element.

The mentioned sub validations were not included in this chapter as they were intermediate steps, however, a few important remarks are to be made in order to understand the time spent in the contents of this chapter and for the reader to consider should they conduct future BRB research. The large number of sources of both material and geometrical non-linearities result in a complex and high computational-costly analysis, the method of calculation was Dynamic Implicit which is an iterative method, however, it is not the correct method to use for parametric studies since convergence is an unsolved problem. For this reason, BRBs numerical modelling requires Explicit Integration.

It is hereby acknowledged that some questions about the modelling technique remain unresolved, however, given the agreement obtained with experimental observation and measurements, the value of including these in the present work is justified. Some of the questions that require further scrutiny are the mesh size, debonding material, the friction between the wave-like deformed core and the ultimate limit state of the bonding between the semi smooth casing surface and grout and the usage of explicit integration as a better calculation method.

In this chapter, 3 validations are presented and compared with experimental data, the first 2 correspond to experimental studies conducted by Razavi Tabatabaei, Mirghaderi, and Hosseini (2014) and Watanabe et al. (1988) where an All-steel Buckling Restrained Brace (AS-BRB) and a Grout –Filled Buckling Restrained Brace (GFBRB) are analysed respectively. Finally, a third model is presented proposing a simplified modelling technique adapted from Genna and Gelfi (2012a) and Genna and Gelfi (2012b) which consists in using the transformed section of a GFBRB specimen to produce a 2D model aiming at mitigating the computational cost.

3.1 Validation of an All- Steel BRB

In order to acquire the required knowledge to model the mechanism of a Buckling Restrained Brace (BRB) a problem was selected form the literature and split in different simple problems so as to assembly simple models into a complex model. As a starting point, this study aims to produce a BRB model against the experimental and numerical results produced by Razavi Tabatabaei, Mirghaderi, and Hosseini (2014) where the specimen was an All –Steel Buckling Restrained Brace (ASBRB) with the cross section shown in **Figure 3.1**.

The study of Buckling Restrained Braces requires the use of approximation methods as the Finite Element Method. A hysteretic curve depends on the interaction between the bracing and the restraining unit which implies the study of contact between these two and the progressive wave formation in the core. In order to gain understanding in the interaction of these, a validation of experimental and numerical data is intended.

The assembly of the core and casing required the use of a stopper (**Figure 3.2**) in order to avoid sliding at the mid length of the bracing. A layer of polyethylene was used to coat the core in order to reduce the friction produced in the contact interface.

In order to obtain the hysteretic curve, the specimen was placed in the equipment vertically, inducing axial displacements at one end. Figure 3.2 shows the top view of the specimen and the read displacement is expressed as Δ.

3.1.1 Material properties

Core - The steel properties for the core were determined with the conduction of two coupon tests. The outcome of the tests justified the specified values for nominal yield and ultimate strength which are 235 MPa and 365 MPa respectively; likewise, a Poisson's ratio of 0.3 was undertaken.

Casing - On the other hand the steel used for the casing (Buckling Restrained Unit) has a nominal yield and ultimate strength of 355 MPa and 510 MPa respectively.

Debonding material – In order to reduce the friction induced at this interface, a debonding system is used. On the core side, two layers of 0.5 mm polyethylene are taped to the
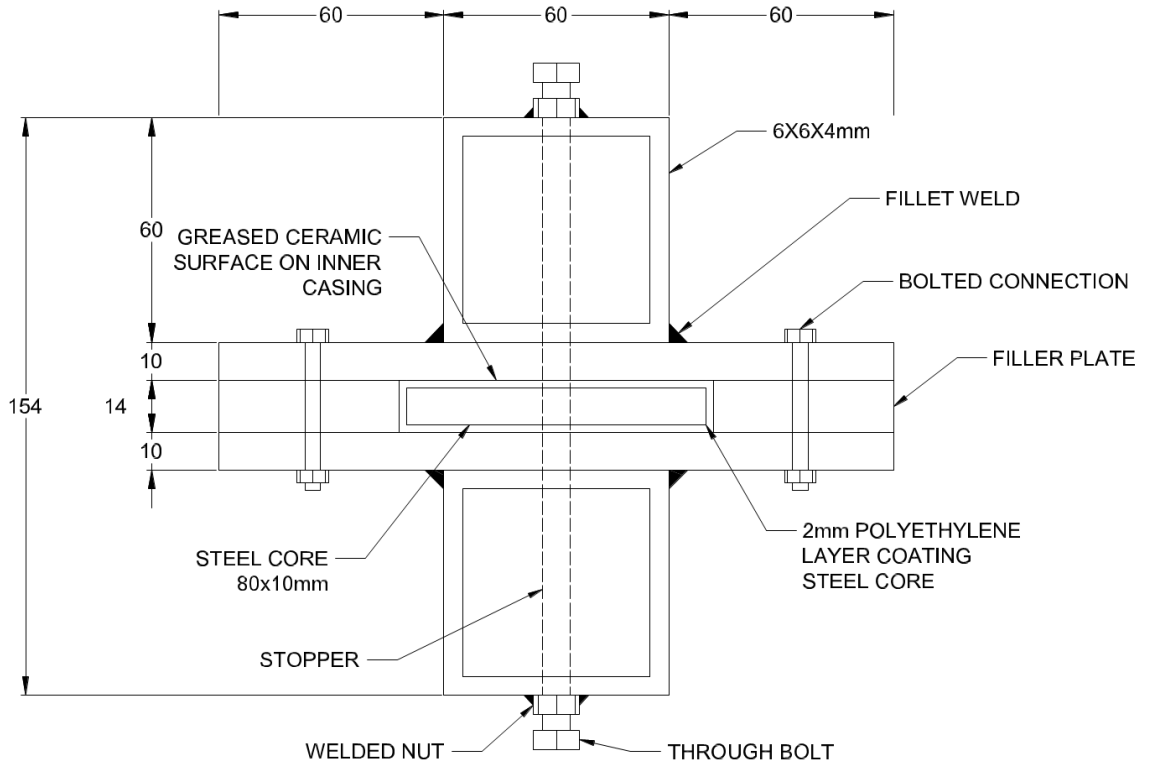
Figure 3.1: Cross section of specimen adapted from Razavi (2014)
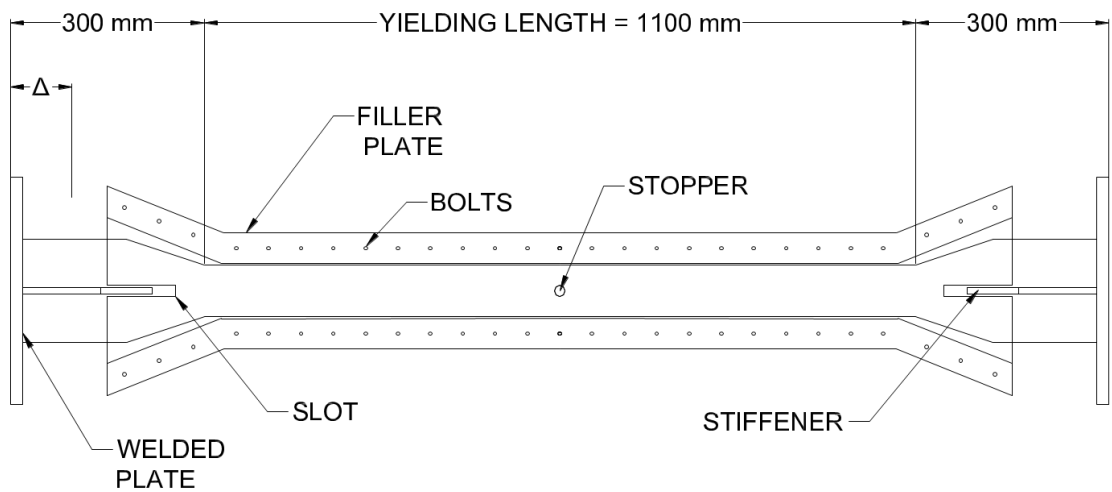
Figure 3.2: Top view of specimen adapted from Razavi (2014)

core; additionally, Razavi (2014) uses ceramic coating the inner side of the casing (as this component remains elastic which prevents the crushing of the material), furthermore the ceramic surface was greased in order to further inhibit the friction.

3.1.2 Loading protocol

The specimen was designed and tested under the American Institute of Steel Construction (2005) BRBF design provisions where the device was approached so as to ensure two main

78

features listed below:

- Ensure the dissipation capabilities (ductility capacity and cumulative ductility capacity)

- Avoid failure mechanisms (bulging, core end rotation, Low cycle fatigue and global buckling or casing failure)

The loading history according to American Institute of Steel Construction (2005) comprises of 2 cycles with 5 different amplitudes so as to start with the theoretical yielding displacement (denoted as Δby) as first amplitude and finishing with an amplitude equivalent to twice the drift of the structure in study, where the equivalent lateral displacement of the structure is denoted as Δbm. In Table 3.1 the corresponding amplitudes for each cycle is summarised; it is to be noticed that the displacements in step 5 exceed importantly the yield displacement Δby.

Table 3.1: Displacement controlled loading protocol

	Δby (Step 1)	0.5Δbm (Step 2)	Δbm (Step 3)	1.5Δbm (Step 4)	2Δbm (Step 5)
Number of cycles	2	2	2	2	2
BRB displacement or cycle amplitude (mm)	1.7	13.3	27.7	42.1	56.6
Time of application per cycle (s)	40	40	40	40	40

3.1.3 Experimental results

From the uniaxial test of the specimen it was observed satisfactory dissipative features. Two types of failure patterns presented including the yielding of the encasing in the zone of the connection due to the excessive increase of lateral force of the core inducing bulging and Low Cycle Fatigue (fracture).

The interpretation of the results is given by the parameters defined by AISC (2005) in order to quantify the main points within the hysteretic curve. It is of the first importance to notice the value of the parameter ω defined as hardening factor which is a ratio of the applied load vs yielding load (i.e. a value of ω greater than 1 implies yielding). Table 3.3 shows a

Table 3.2: Backbone curve descriptors

Factor	Formula
Hardening factor	$\omega = \dfrac{T_{max}}{T_y}$
Compression adjustment factor	$\beta = \dfrac{P_{max}}{T_{max}}$
Ductility	$\mu = \dfrac{d_{max}}{d_y}$
Tensile yield load	$T_y = R_y A_s f_y$ (R_y determined by coupon test)
Compressive load	$P_{max} = \beta \omega T_y$

variation of ductility μ, hardening factor ω and compressive strength adjustment factor β, likewise, and a preliminary strain value ϵ_y is shown.

From Table 3.3 it can be observed that the hardening adjustment factor ω overpasses the unit value at the first induced displacement where 1% above the yielding displacement is measured. This adjustment factor would increase in subsequent cycles until 68% which presented at the 7th cycle prior Low Cycle Fatigue Failure.

On the other hand the variation is slighter when it comes to the Compressive strength adjustment factor as it varies from 9% to 13% above the maximum tensile strength value of each cycle.

Table 3.3: Measured hysteretic parameters

Cycle	ϵ_y(%)	μ	ω	β
0.5Δbm	1.2	8	1.01	1.09
0.5Δbm	1.2	8	1.11	1.11
Δbm	2.1	14	1.28	1.12
Δbm	2.3	15	1.36	1.14
1.5Δbm	3.5	23	1.45	1.17
1.5Δbm	3.8	25	1.55	1.13
2Δbm	**5**	**33**	**1.68**	**LCF**
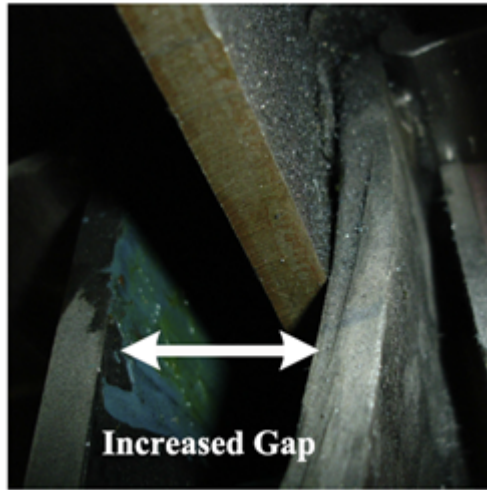
Figure 3.3: Gap increase and bulging at end of casing of specimen in Razavi Tabatabaei, Mirghaderi, and Hosseini (2014)

a)Major axis view

b)Minor axis view

c)   d)
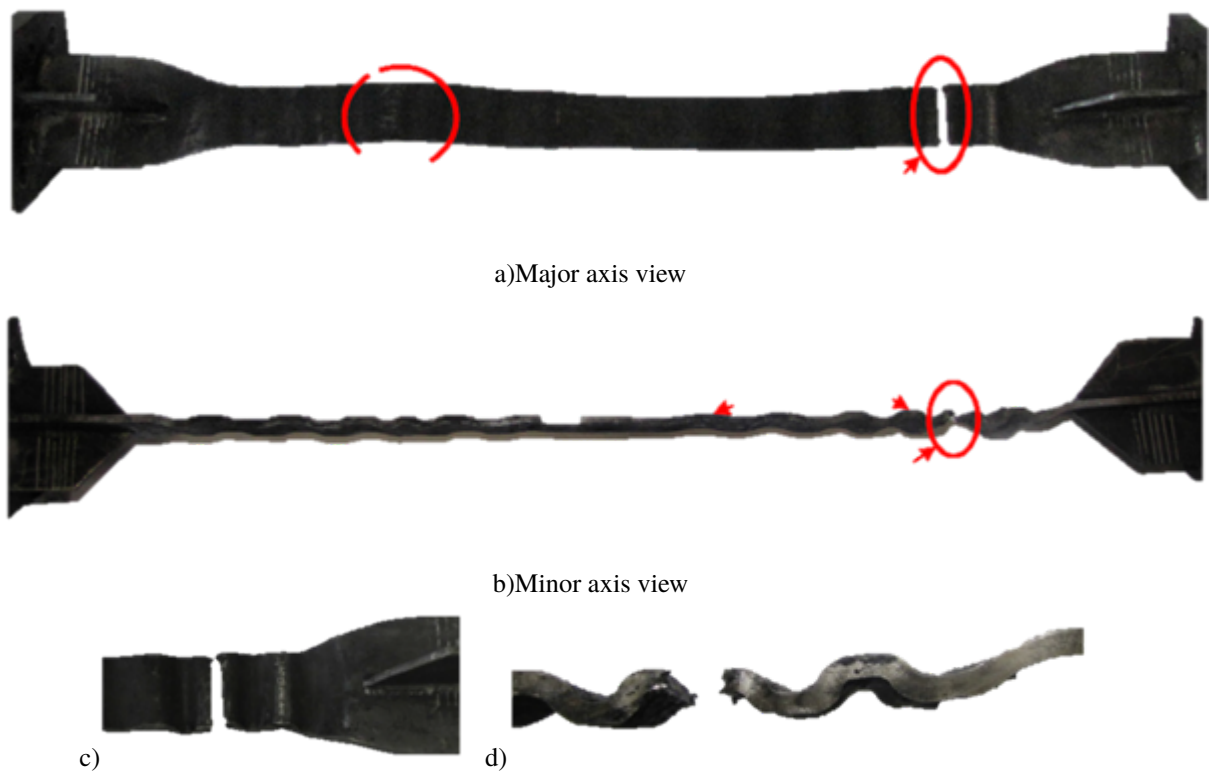
Figure 3.4: Final mode shape of extracted core and Low Cycle Fatigue failure

3.1.4 Idealisation of the structure and assumptions

Given the outcome of the testing (hysteretic curve and maximum force-displacement values) the specimen is conceptually simplified in order to focus on the numerical study of the behaviour of the core yielding zone and to reduce the computer time.

Table 3.4 shows differences between the specimen and the concept of the problem. In general, the problem represents a simplified model of the BRB in study however reasons are provided in order to justify such a validation. A brief discussion is provided in the next sec-
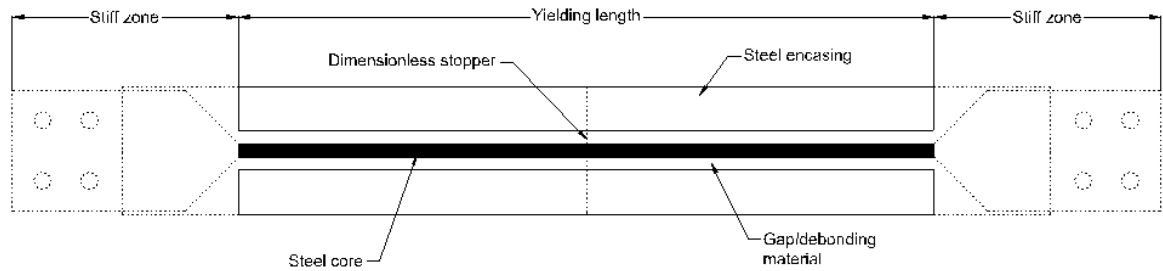
Figure 3.5: Idealisation of the specimen

tion.

The most important assumption made relates to the core initial conditions as the software considers this as the starting point for the iterative solution method of the problem. As it can be noticed in **Figure 3.5**, a perfectly straight core is never in contact with the surface of the casing because an axial displacement at the tip will result in a uniform stress distribution acting on the surface which leads to pure axial deformation. As a result, an imperfection needs to be made to produce bending, amplification of lateral displacements and finally contact between the surfaces of the core and the casing.

As mentioned in Table 3.4, the use of the stopper restraints the core preventing rotation about all axis but the axis of the stopper itself. Therefore, the stopper provides a boundary condition for the imperfection imposed where the rotation at the midpoint of the bracing must be zero. From eigenvalue analysis it is possible to determine a reasonable initial imperfection.

Casing - The boundary conditions for the casing were assumed to be restrained for rotation but free to displace axially at both ends faces (**Figure 3.5**); a justification for this assumption is that the connection zone of the bracing is also the zone where rotation of the casing is restrained. Originally the specimen has bolted connections which inhibit the rotation in the casing.

Stopper - The use of the stopper implies compatibility of rotational and unidirectional displacements at the mid length of both the core and the casing. In the experiment, a fastener was used which numerically was conceptualised by Razavi Tabatabaei et al. (2014) by assuming a rigid beam for numerical modelling.

Core – The connections were assumed axially infinitely stiff and rotation restrained due to the bolts; the ends of the core were restrained differently **Figure 3.7**. One of the tips was

Table 3.4: Differences between experiment and conceptualisation of the problem (assumptions)

Part	Experiment	Idealisation
Core	The core is coated by two layers of polyethylene which is greased on the surface. The use of the stopper requires a hole in the middle of the core length. The restrained length is shorter than the casing to avoid locking.	No layer of polyethylene is considered, however the effects of this material are modelled with the friction coefficient. The size of the holes and their effect on the global behaviour of the device are negligible. No holes are considered for the analysis.
Casing	The casing comprises of two symmetric encasings formed by welding a hollow core section and a plate. The two encasings are bolted together with a filler plate thicker than the core in order to allow space for the core and a clearance of 2mm (i.e. this clearance is only 1mm of air gap and 1mm of polyethylene) Holes spaced along the section of the plates are used for the bolted connection	The slip between the different parts of the encasing is negligible. Thus the casing comprises of one continuous cross section ignoring slip. No holes/bolts nor welding are included in the model. The casing is assumed to be the same length of the yielding zone (the actual restrained length is 30 mm shorter on each end, i.e. 1040 mm)
Stiffened section (connection zone)	The connection (including the transition zone) comprises of a widened section of the plate stiffened with perpendicular welded plates in order to avoid yielding and restrain rotation when interacting with the casing. Furthermore, the type of connection is bolted which inhibits the rotation.	The rotation of the connection and axial strain are negligible, therefore, the connection represents a boundary condition for the yielding part of the core.
Stopper	A through bolt (stopper) is used in order to condition the axial displacement of the core with the casing at the mid length (i.e. the relative displacement at this point is zero). The stopper also restraints the rotation about 2 axes, thus the only rotation allowed is about the stopper itself.	Since no holes or such modifications of the geometry are considered in this analysis, the stopper is modelled as a restriction of compatibility of axial and rotational displacements with an dimensionless infinitely rigid beam.

set as fixed (passive) and the other tip was restrained to rotation and out of plane displacements in order to allow axial displacement (active); the displacement history induced at the active end is shown in Table 3.1. Likewise the relative rotation at the mid length of the core must be zero due to the presence of the stopper which is a criterion to select an appropriate imperfection. As initial imperfection the 3rd buckling mode was imposed whereas Razavi Tabatabaei et al. (2014) considers the first mode.

3.1.5 Description and properties of the FE Model

Finally, the specimen above-mentioned is modelled with Finite Element software. A first reason to select this cross section as starting point is that the study contains information sufficient so as to reproduce the results by means of Finite Element software (ABAQUS).
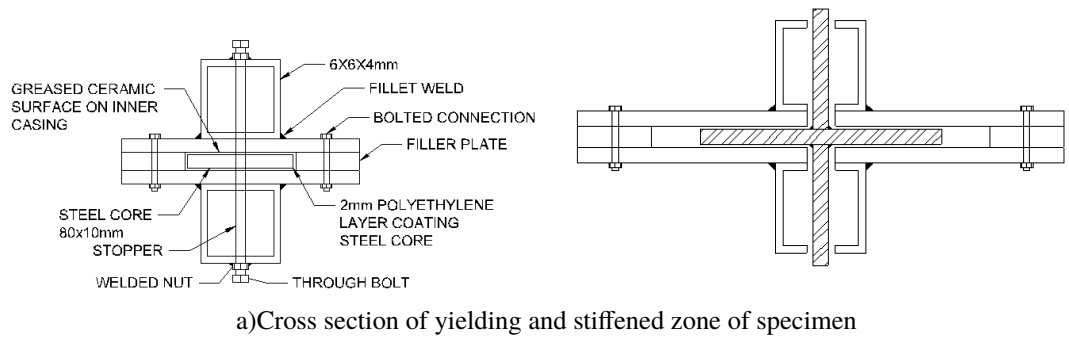
a)Cross section of yielding and stiffened zone of specimen
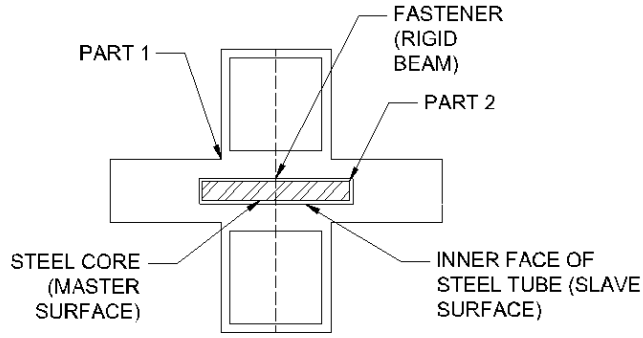
b) Cross section of present model
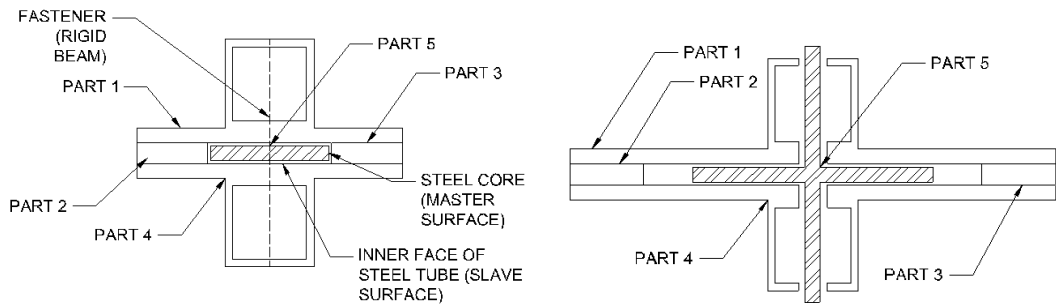
c)Cross section of yielding and stiffened zone from Razavi Tabatabaei et al. (2014)

Figure 3.6: Cross section of parts considered for the numerical analysis
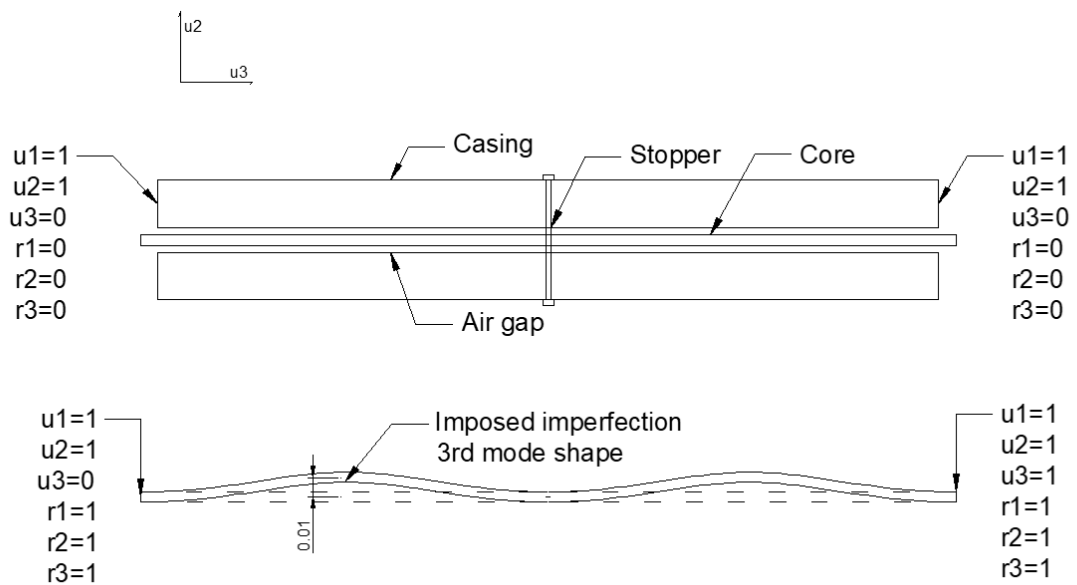
Figure 3.7: Node boundary conditions in global axes 1,2 and 3 (1 for restrained and 0 for unrestrained) and imperfection assumed for present model

A second reason is that no grout is involved in the device which simplifies the problem as the parts of the casing do not show to incursion in nonlinear behaviour.

The model conducted by Razavi Tabatabaei et al. (2014) aims at considering both the elastic and inelastic displacements so as to compare directly the data obtained from the experiment. The analysis was conducted using 3D elements as shown in **Figure 3.8**, where the device was modelled with all its components. In contrast, the present model considers a simplified conceptualisation of the specimen by making assumptions which will be further discussed in the results section.

It is to be remarked the particular interest in the reproduction of the hysteretic behaviour (Force-displacement) which resides in the yielding zone of the bracing mainly. The complexity of the model resides in the constant interaction of the core with the casing involving a contact problem

In Table 3.5 the material properties of the core and debonding material are summarised. For this analysis combined non-linearity model was adopted to model the behaviour of the material; Razavi Tabatabaei et al. (2014) reports material properties obtained from coupon testing where the yield stress was observed at 248 MPa being 235 MPa the nominal yield stress where the 2% strain offset method was used. However for modelling purposes a yield load value of 157 MPa alongside kinematic and isotropic hardening was found suitable to obtain a similar stress strain curve to the experimental.

3.1.6 Mesh size and type of elements

Two types of elements were considered for the analysis where three different meshes were studied in order to conduct a sensitivity analysis by varying the number of the elements of the core. The points of the hysteretic curve taken as a reference to verify convergence were the maximum and minimum forces of the last cycle. Only three different meshes were used for the analyses as the problem takes a relatively long time to solve it.

Figure 3.8 shows the combination used for sensitivity analysis where three cases were analysed, the number of elements used for the casing remained constant in all cases (896 elements) and the elements of the core were varied from a total of 110 elements to 880 elements. **Figure 3.11** shows the maximum compressive and tensile values obtained for the

Table 3.5: Characteristics of Finite Element Model conducted by Razavi Tabatabaei et al. (2014)

	Geometry	Material properties	Interaction
Core	Rectangular cross section 80X10mm Length: 1100mm	Elastic properties fy=157 MPa (coupon test) E=200 GPa ν= 0.3 Plastic properties Combined harden-ing (Kinematic and isotropic)	Surface of the core is greased in contact with debonding material. Contact properties for the interface are assumed to have hard contact and 0.15 as friction coefficient
Debonding mate-rial and interfaces	Comprises a layer of polyethylene of 0.5 mm tapped to the core. However only an air gap will be con-sidered as the behaviour of this interface is unknown.	–	Unknown- in the analysis the layer was merely assumed to modify the friction coefficient however it was not included in the model. The friction coefficient was modified so as to calibrate the model

Table 3.6: Strain Hardening characterisation properties considered in the 3D model

Kinematic hardening						Isotropic hardening	
Number of back-stresses	Yield stress at zero strain (MPa)	C1 (MPa)	C2 (MPa)	$\gamma1$	$\gamma2$	Qb (MPa)	b (MPa)
2	157	4600	98000	25	1000	110	4

three cases, from this figure it is unclear whether convergence has been achieved or not, however, the discrepancy between the values range between 365 MPa to above 369 MPa in tension and 514 MPa to 556 MPa in compression which suggests the need for another iteration with a larger amount of elements.

3.1.7 Interaction and initial imperfection analysis

For this model the core was modelled using different elements and validating with Euler's formula and obtaining the eigenvalues for different modes. The reason of conducting this analysis resides in the assumption of an air gap between steel core and steel casing; the core is assumed not to be in contact with the casing at time zero and bending is needed for contact condition. Moreover it is important to consider a reasonable seed of imperfection which allows a progressive deformation until the core makes contact with the casing. Fig-ure 3.12 shows the displacements corresponding to bifurcation points where the instability is triggered; this could be verified with a post buckling analysis using the Riks method us-
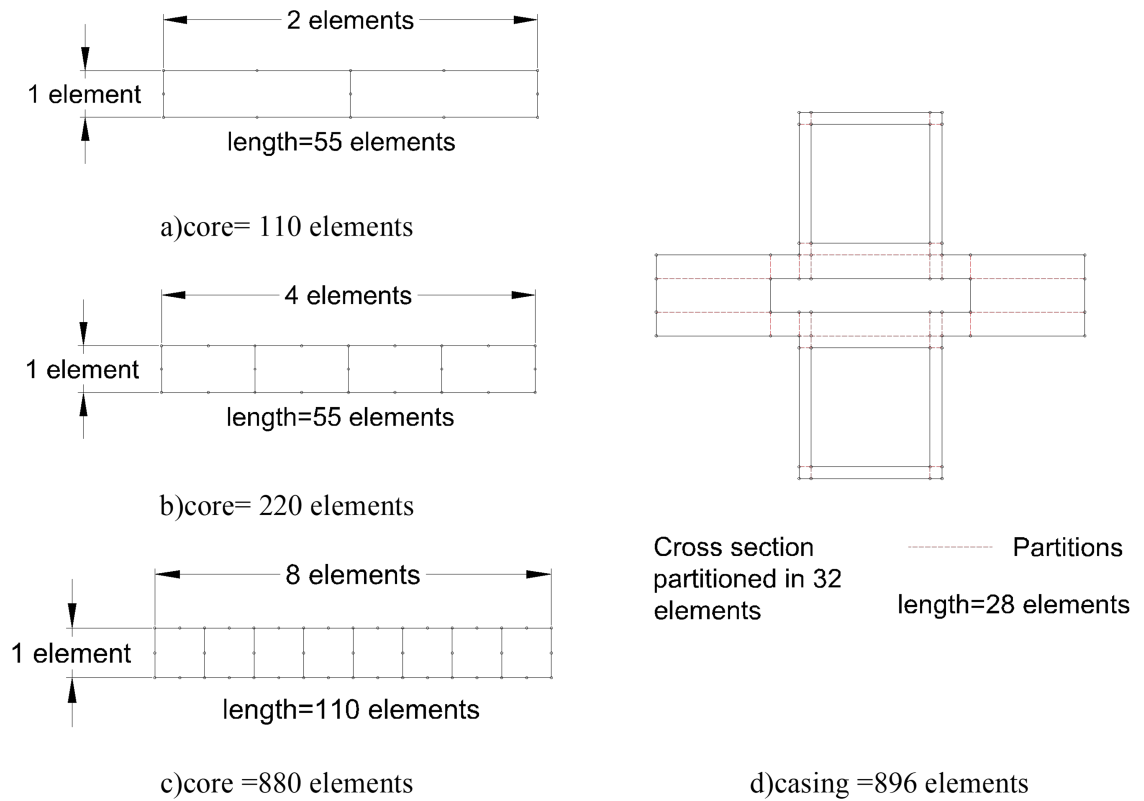
Figure 3.8: Mesh combinations considered for sensitivity analysis

ing the imperfection aforementioned.

Once the lateral displacement is large enough to overpass the limits of the air gap, contact between parts takes place. The contact was modelled in ABAQUS with surface to surface interaction (**Figure 3.10**) where the master surface was assigned to the core and the slave to the casing where the master surface is to be the more rigid however the material is the same in both cases; the penalty method is used. In the case of the stopper, a mesh independent fastener is considered at the point where corresponds where the connector section "beam" was selected.

Table 3.8 compares the geometry, material properties and modelling details between the specimen used in the experiment and the numerical models developed by Razavi Tabatabaei et al. (2014) and this study. This table summarises and compares when possible the data obtained from testing, numerical analysis conducted by the author and the numerical results of the present model.

Furthermore, table 3.7 shows the parameters used in the BRB model in Razavi Tabatabaei, Mirghaderi, and Hosseini (2014) where these values were provided to characterise the cyclic
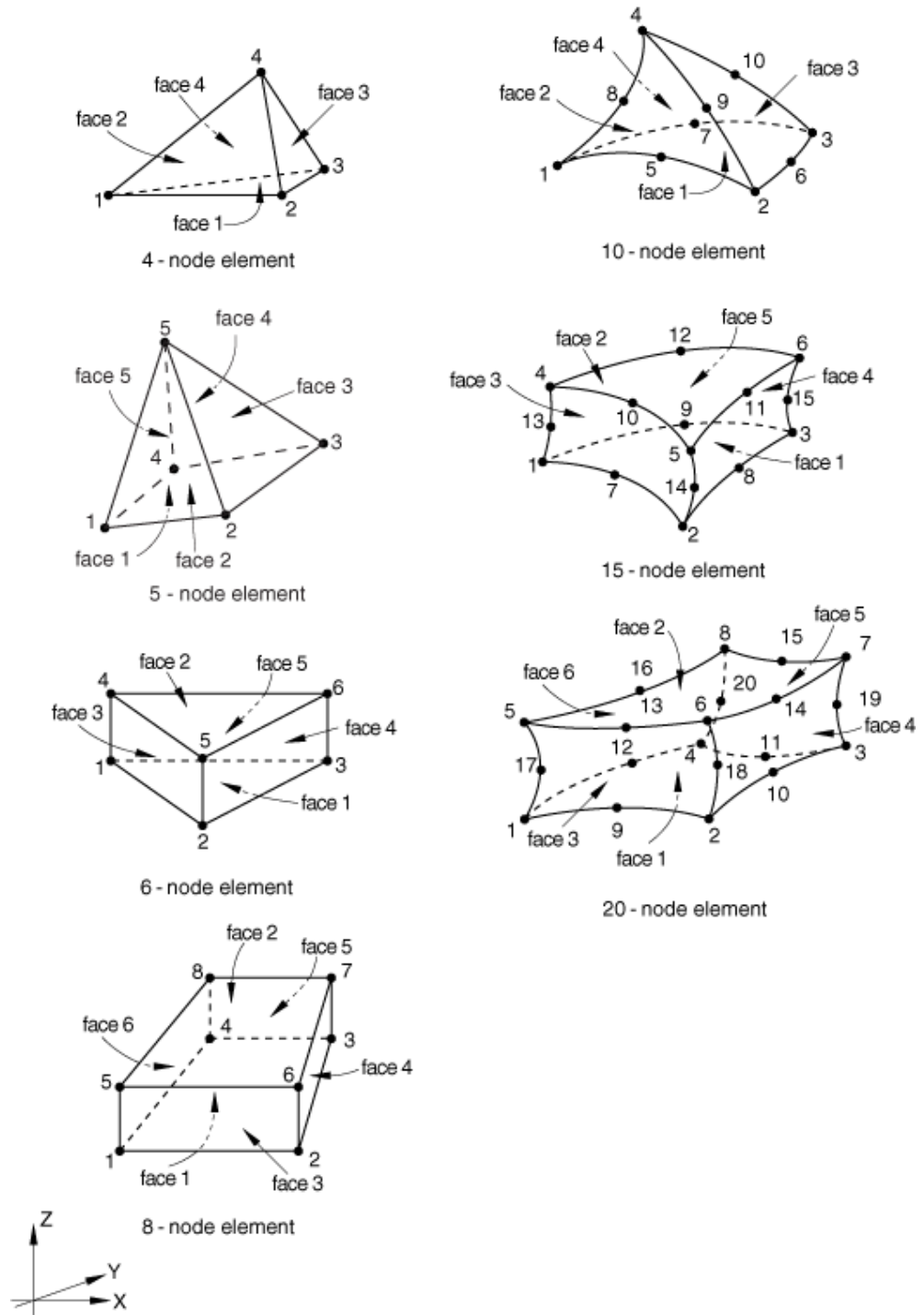
Figure 3.9: Elements available in ABAQUS 2013 from MIT (2017). 8-node elements (C3D8) were used for the casing and 20-node element (C3D20) were used for the core
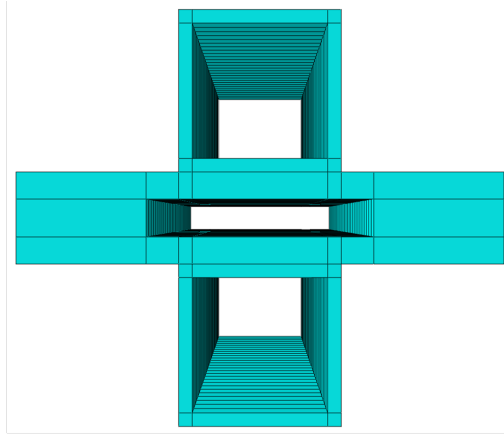
a)Casing mesh (896 C3D8R elements)
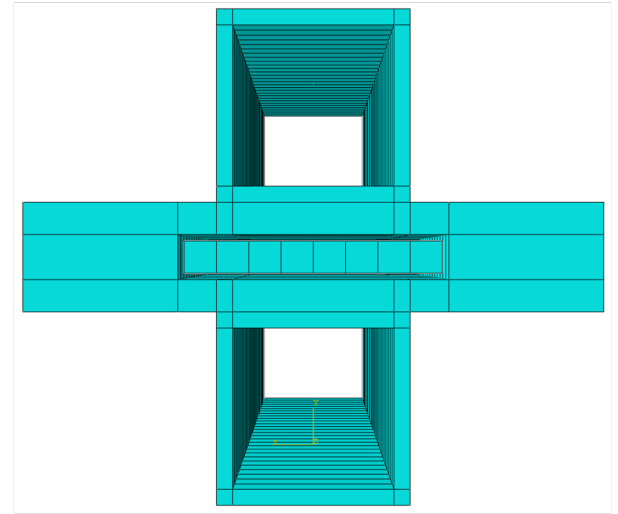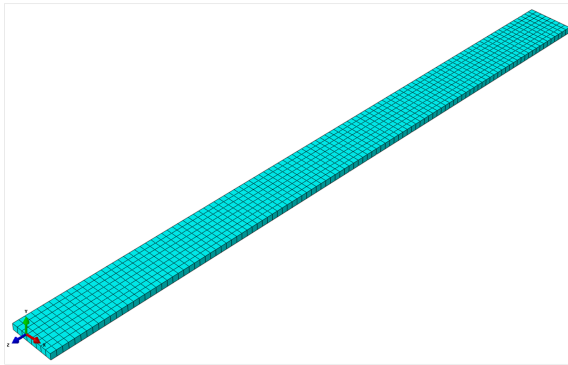
b)Core mesh (880 C3D20 elements)   c)Assembly

Figure 3.10: FE model meshed assembly
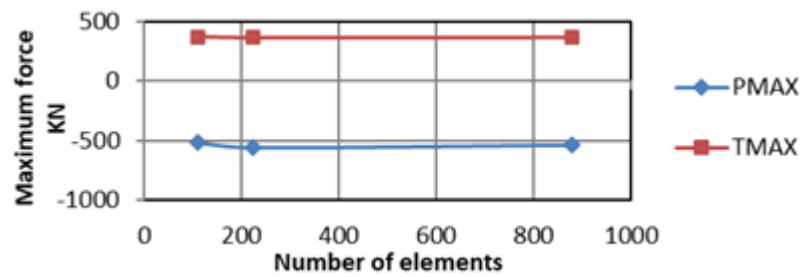
Figure 3.11: Sensitivity of maximum force with number of elements
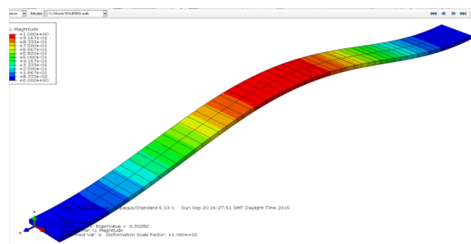
a)First mode (evalue=0.30282)   b)Third mode(evalue=1.2161)
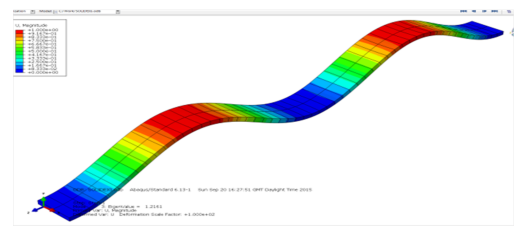
Figure 3.12: Assumed initial imperfections for core obtained from Eigen modes
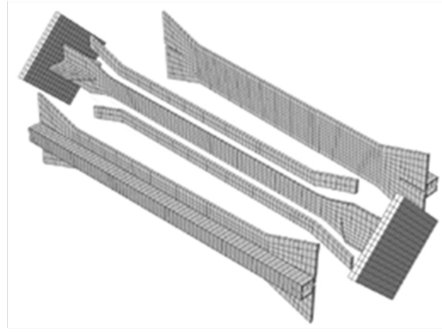
Model of Razavi (2014)
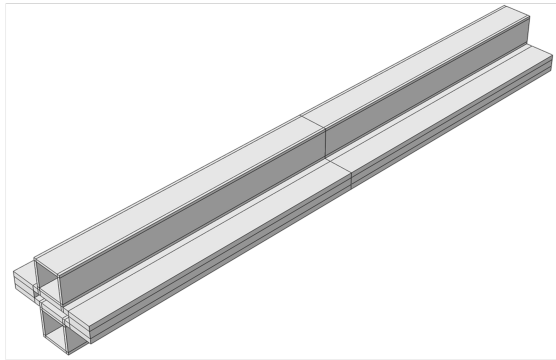
3D view of present FE model
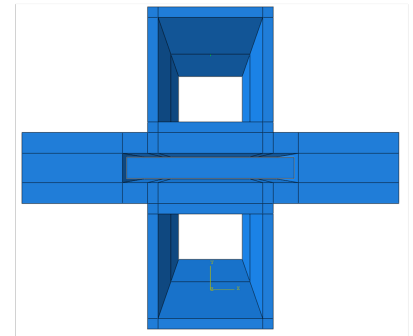
Cross section of present model

Figure 3.13: Finite element model

hardening properties of the core. However, although the core behaviour could be success-
fully replicated to further explore the complexity of the model and core behaviour, discrep-
ancies in the input values from those in the revised literature were obtained and herewith
presented.

Table 3.7: Experiment Razavi Tabatabaei et al. (2014)

Parameter	Experiment
Number of parts	Core: plate 800X10mm
	Casing: 2 Hollow core sections welded to a plate separated by 2 filler plates
Density [tonne/mm3]	ρ=7.80E-09
Elastic	E=200000 Mpa
Plastic	fy=248 Mpa
	fu=402MPa
Strain hardening	Maximum strain hardening adjustment factor measured ω=1.62
Debonding layer	A layer of Polyethylene is used to coat the core in order to reduce the friction. On the casing inner side, ceramic with grease is used.
Hardening factor (ω)	**ω=1.68**
Compressive strength adjustment factor (β)	**β=1.13 (fracture occurs before the maximum compressive strength)**

Table 3.8: Replication of numerical analysis in Razavi Tabatabaei, Mirghaderi, and Hosseini (2014)

Parameter	FE Model in Razavi Tabatabaei et al. (2014)	3D Model
Input		
Number of parts	5	2
Parts description (number of parts)	Core (1 part), filler plates (2 parts), casing (2)	Core (1 part) and casing (1 part)
Material properties		
Density [tonne/mm3]		
Elastic	v=0.3	
Plastic	f_y=157 MPa (Mild steel)	
Strain hardening	Isotropic and kinematic hardening	
	Isotropic	Kinematic
	Qb=110 Mpa	Backstresses= 2
	b=4	C1=4600 Mpa
		C2=98000 Mpa
		γ1=25
		γ2=1000
Assembly		
Interaction	Surface to surface	Surface to surface
Tangential contact	Friction coefficient 0.15	Friction coefficient 0.15
Normal contact	Penalty hard contact	Penalty hard contact
Surface 1	4 lateral faces of the core	4 lateral faces of the core
Surface 2	4 inner faces of the casing	4 inner faces of the casing
Fasteners	Used to simulate stopper	Used to simulate stopper
Boundary conditions		
Casing	Only restrained at the stopper	Restrained at the end and stopper.
Core	Boundary conditions applied on the connections with one end fixed and the other free only in one degree of freedom	Boundary conditions applied at the tips of the core with one end fixed and the other free only in one degree of freedom
Step		
Type of solver	–	Dynamic Implicit (quasi static)
Time increment	–	0.1 s
Loading history	–	Ramp
Time of load application	–	80 s
Mesh		
Number of elements for the core	1184	880
Type of element	C3D8 for casing, C3D20 for core	C3D8 for casing, C3D20 for core
Layers along thickness	2	1
Results		
Hardening factor (ω) and Compressive strength adjustment factor (β)	**ω not provided**	**ω=2.37**
	β=1.185	**β=1.72 for a friction factor of 0.15) (ω=2.406** **β=1.162 for a friction factor of 0.05)**

3.1.8 Results and sensitivity discussion

The deformed shape of the core changed throughout time as the displacement increased and developed into the formation in waves. Important points of the hysteresis curve obtained are shown in **Figure 3.14** where the maximum strain deformed core shapes are illustrated.

The behaviour of the core throughout time can be described in the curve as follows:

- First and second cycle (Δ_{by}) – In tension, the bracing starts yielding, the bracing remains straight and permanent deformation is barely visible in the hysteresis curve. When the direction of the displacement is negative (causing compression), the third mode buckling shape takes places as the imperfection is amplified by the axial displacement. The bracing is still in the elastic range

- Third and fourth cycle ($0.5\Delta_{bm}$) – In tension, the bracing yields to a ductility of half the drift of the Buckling Restrained Frame (BRBF) yielding after the point Δ_{by}. Once the displacement is reversed, the core recovers an elastic displacement equal Δ_{by} and from this point onwards waves start appearing alongside compressive force on the bracing. The waves start forming even though the point of zero displacement has not been reached.

- Fifth and subsequent cycles (Δ_{bm}, 1.5 Δ_{bm} and 2 Δ_{bm}) – The process of the previous couple of cycles is repeated, however the number of waves which the core is formed increase progressively. The mechanism by which the number of waves increased was studied analytically by Wu and Mei (2015) and experimentally by Chai (1998).

Δ_{by} F=153.9KN μ=1 waves=0		$-\Delta_{bm}$ F=-315.73KN μ=-16.3 waves=14	
$-\Delta_{by}$ F=-156.5KN μ=-1 waves=2		$1.5\Delta_{bm}$ F=337.253 μ=24.8 waves=	Permanent wave formation
$0.5\Delta_{bm}$ F= 237.38KN μ=7.8 waves=0		$\Delta_3=0$ F=-293.406 μ=-0.1 waves=14	
$\Delta_1=0$ F= -210.04KN μ=-0.1 waves=6		$-1.5\Delta_{bm}$ F=-380.051 μ=-24.8 waves=17	
$-0.5\Delta_{bm}$ F=-248.85KN μ=-7.8 waves=7		$2\Delta_{bm}$ F= 370.22KN μ=33.3 waves=	Permanent wave formation
Δ_{bm} F= 287.52KN μ=16.3 waves=	permanent wave formation	$\Delta_4=0$ F= -329.97KN μ=-0.1 waves=17	
$\Delta_2=0$ F=-254.27KN μ=-0.2 waves=7		$-2\Delta_{bm}$ F= -430.27KN μ=-33.3	

Figure 3.14: Higher-mode shape wave formation deformed shape of core (side view) with a frictional factor 0.05

The force displacement curve was obtained by extracting the nodal forces in the axial direction on the face of the tip where displacement history is induced and finally adding them. **Figure 3.15** shows the hysteretic curves of the present model against the experimental and numerical study conducted by Razavi Tabatabaei et al. (2014). This figure reveals that when
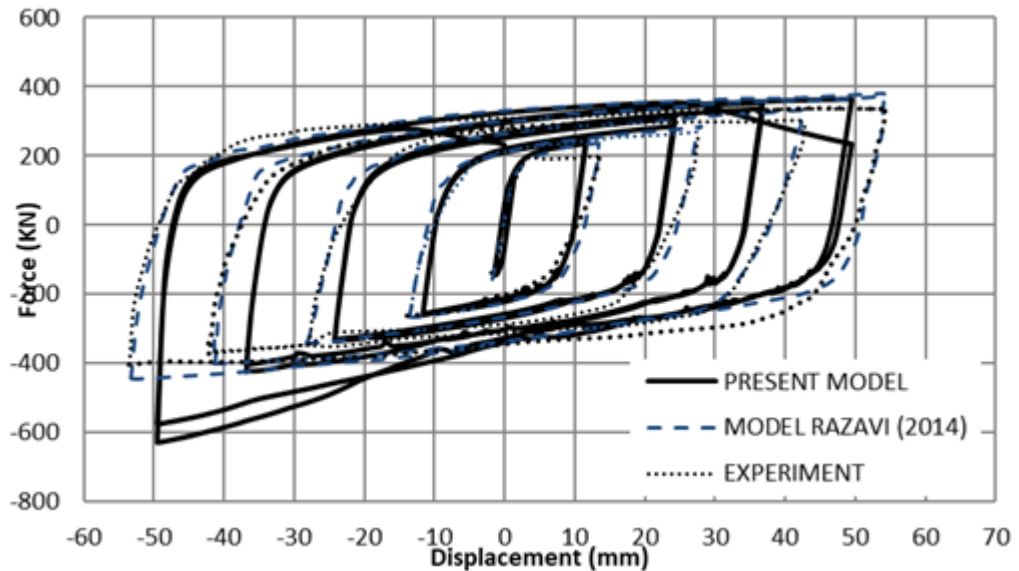
Figure 3.15: Comparison of force displacement response for a frictional coefficient of 0.15
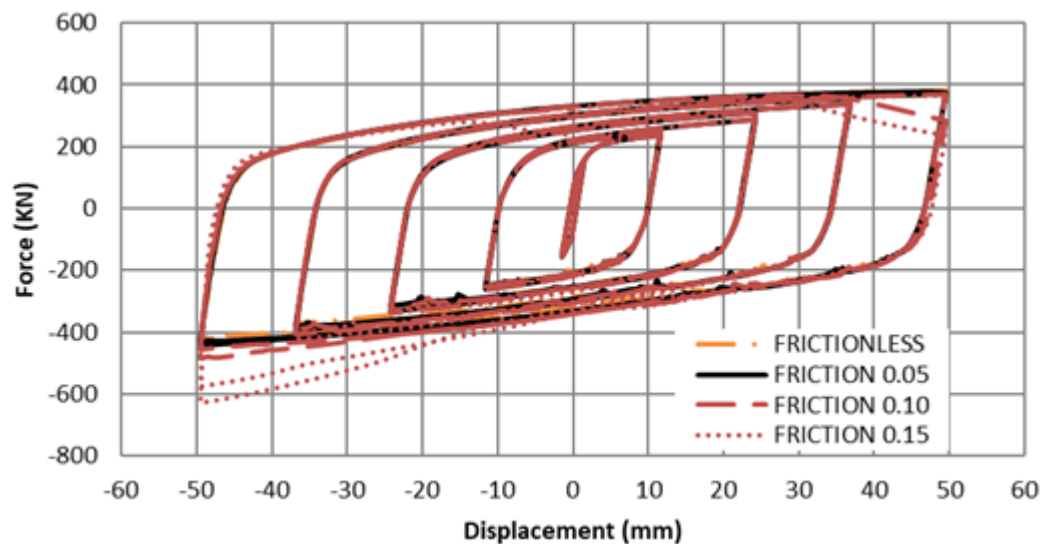
Figure 3.16: Effect of frictional coefficient on the hysteretic curve

a friction coefficient of 0.15 is undertaken, the maximum force in compression of the core increased over 172% of the experimental maximum tensile strength.

Figure 3.15 shows a parametric analysis conducted by varying the frictional coefficient; the interface with friction coefficient 0.05 of was by far closer to the values of the experiment which suggests that friction between interfaces may not be considerable in this specimen and with that gap size. Qualitatively the approximation to the experimental data is reasonable, however in order to increase accuracy a parametric study was conducted by varying the frictional coefficient between the two factors finding that a frictional coefficient of 0.05 or simply frictionless tangent interaction the model's hysteretic behaviour becomes more accurate to the reality.
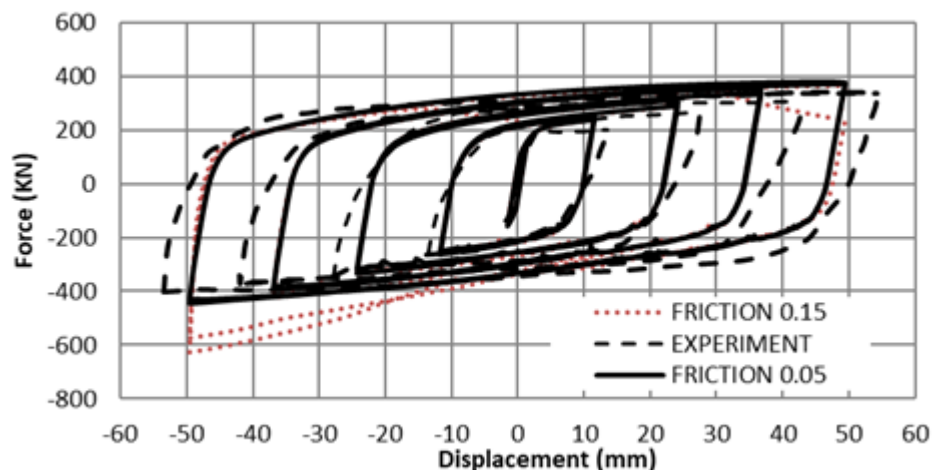
Figure 3.17: Calibration of friction factor in contact surfaces

3.1.9 Conclusions and remarks

From the present numerical analysis, it is observed that friction contributes importantly to the compressive strength of the device as important discrepancies in the value of β depend on this factor. Moreover the frictional coefficient kept constant accounts for an assumed undamaged layer of debonding material, however, it is acknowledged that a friction coefficient can potentially oversimplify the real effects of the wave formation combined with sliding in the pair interfaces of core-debonding layer and debonding layer-grout. The study of such interfaces require further detailed examination to understand the frictional effects of using different materials to debond the core from the grout.

Likewise, it is to be noticed that although a 3D modelling technique and comparison with experimental data have been used, there are still numerous assumed parameters involved to model a Buckling Restrained Brace and hysteretic response. For such a reason, the comparison of the global performance of a Buckling Restrained Brace with the experiment does not guarantee that all the parameters have been calibrated correctly or that the model represents the behaviour of unobserved components with accuracy. Moreover, very similar results can be reached by permuting and adjusting assumed values, hence the need to study the BRB at a component level.

The objective of this research is to pursue the meticulous examination of each of those parameters such as size of the gap, friction coefficient, introduction of debonding material to the model and contact properties with different methods (Lagrange or penalty method). However, during the BRB modelling exercise it has been found that other arisen research

Figure 3.18: Types of samples in Watanabe et al. (1988)

questions are sufficiently extensive to deviate the attention from the research focal point and scope therefore such interactions have been left as characterisations or 'educated assumptions', however, these are included and discussed in the chapter of recommended Further Research.

The aim of this validation is to reproduce the results, identify parameters that require characterisation and estimate reasonable material and contact values, this was accomplished throughout the process of modelling. Ultimately these are to be used in the modelling BRBs with atypical components such as a PVC casing included in the chapters that follow.

Discrepancies between the experimental and numerical hysteretic curves remain mainly in the compressive zone. Some possible reasons are discrepancies of gap size, friction coefficient values, differences between the specimen and model considered imperfections and characterisation of steel cyclic behaviour. Therefore, experimental data is ideally required for the modelling and characterisation of BRBs.

3.2 Validation of a GFBRB

A Grout-Filled Buckling Restrained Brace was validated according to the experiments conducted by Watanabe et al. (1988) where a set of 5 specimens was tested showing the transition from stability to global failure. A model of specimen 1 was validated against the hysteretic behaviour and a mesh sensitivity analysis was conducted in order to determine a mesh density sufficient to reproduce the experimental results with sufficient accuracy. For the aforementioned purpose two models were considered in order to validate against experimental data.
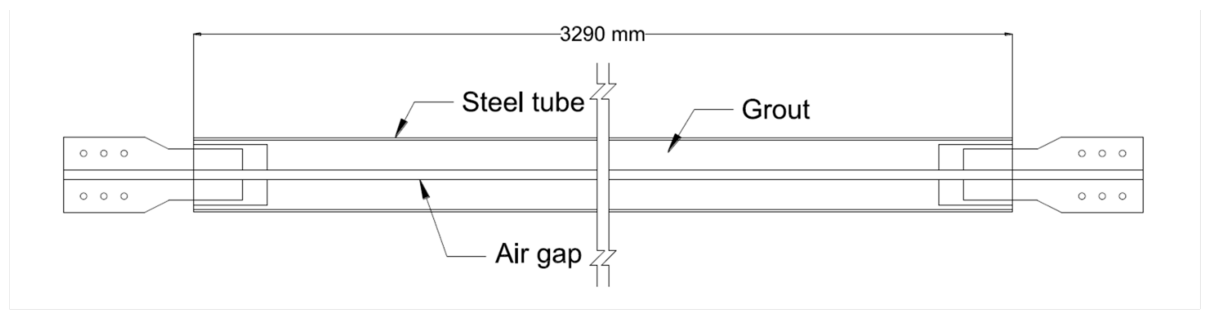
a)   Side view
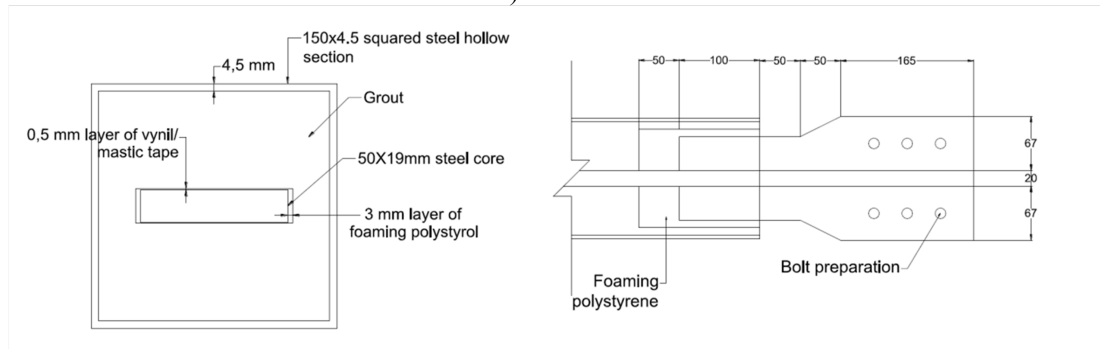
b)   Cross section and connection details

Figure 3.19: a) General composition of BRBs b) Specimen details of specimen 1 Watanabe et al. (1988) c) Connection details of all specimens

The experimental setup that consisted of 5 specimens from which only three showed to provide sufficient buckling restriction (specimens 1, 2 and 3) and two showed global failure (specimens 4 and 5). A model of specimens 1 and 4 were considered for validation purposes imposing the same level of displacement in both cases; the analysis shows that the complexity of the model is not sufficient and the assumptions should be modified so as to have a valid model. However this model is important for two reasons as firstly it was possible to identify the component most sensitive to meshing and secondly to design a mesh where the computing time is optimised.

It was found that the mesh of the core is where a major influence on the results can be observed, moreover a reduction of elements in the grout result in a significant reduction of time being able to analyse a refined mesh in the other components in only 15 hours using the Computational Shared Facility (CSF) from The University of Manchester.
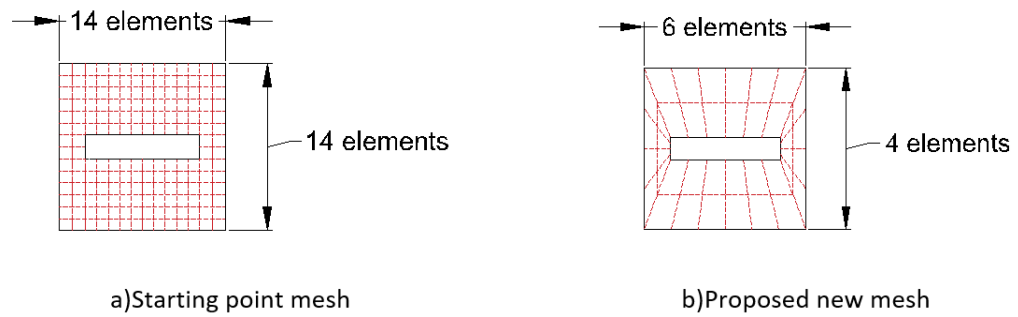
Figure 3.20: Mesh considered for analysis
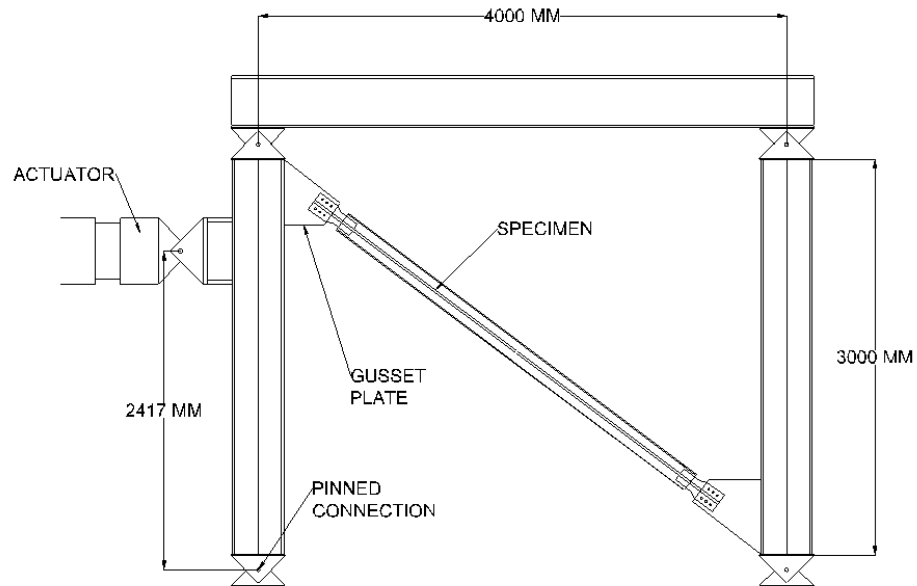
Figure 3.21: Testing apparatus

3.2.1 Idealisation of the structure and assumptions

The model consists of 3 parts (core, grout and steel tube) where the Buckling Restraining System was idealised as elastic and only the core reaches yield under the imposed displacements. The properties of the materials were set according to studies where a cyclic test of a coupon test

A mesh sensitivity analysis of a Buckling Restrained Brace is hereby conducted. The general objective of the study is to determine a number of elements per area where a reasonable degree of accuracy is achieved and identify possible features of a sensible mesh.

The concern on this study resides in the observation of time consumed during the analysis which varied from 10 to 120 hours. Hence the computing time must be reduced as much as it is possible and a strategy is proposed for such a reason. The strategy comprises of two

a)Cross section

b)Plan View
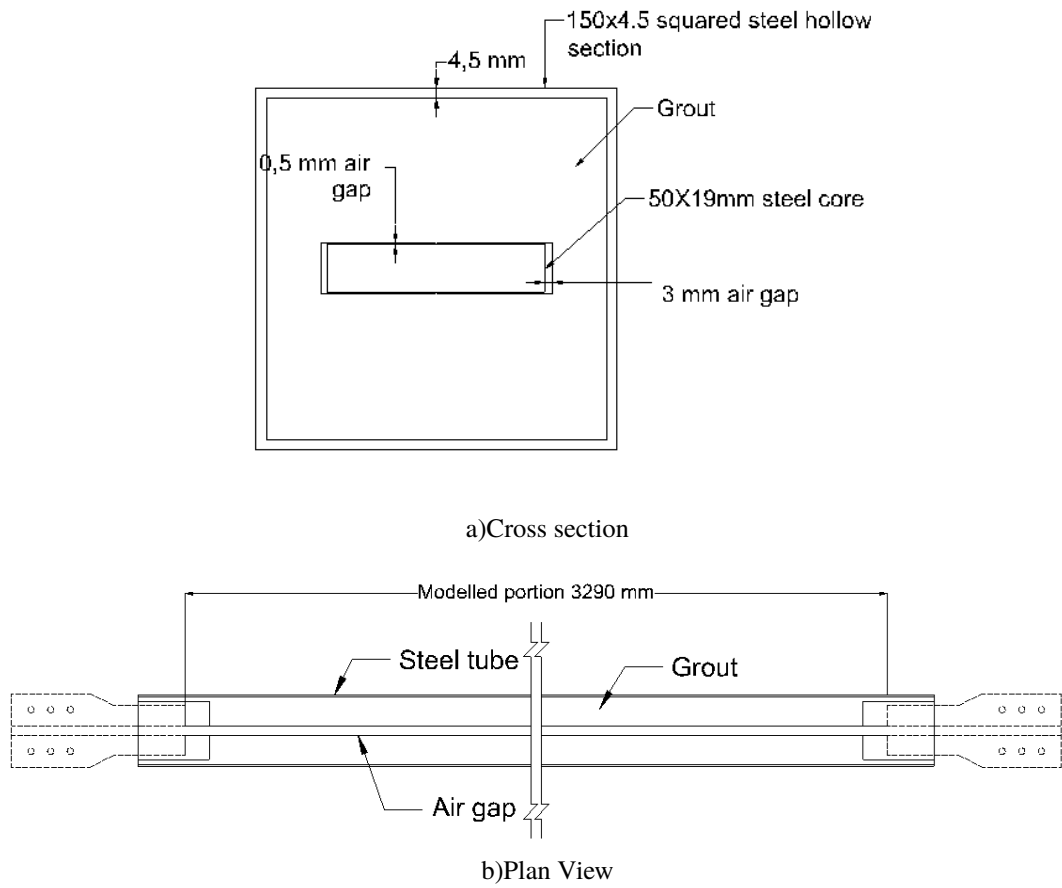
Figure 3.22: FE Model

a)Core

b)Casing
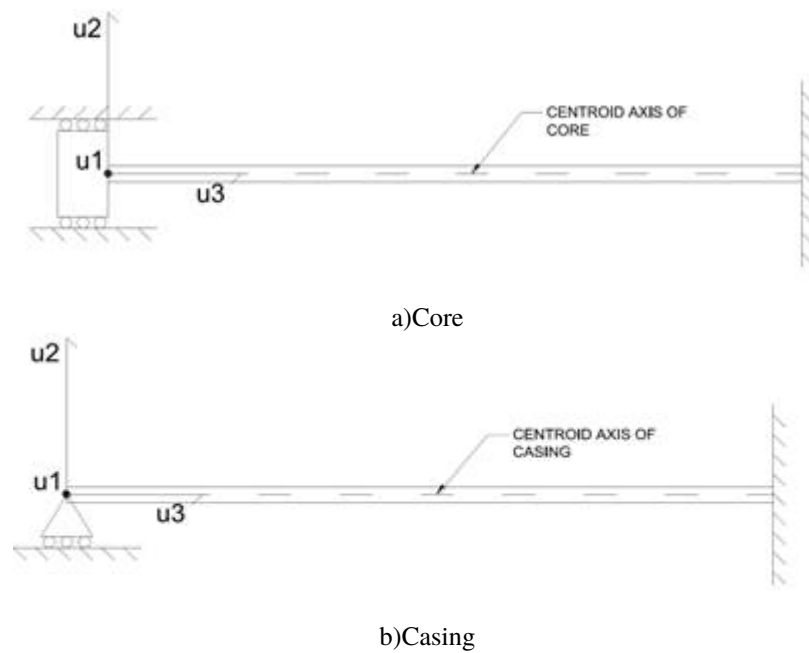
Figure 3.23: Idealisation of the structure
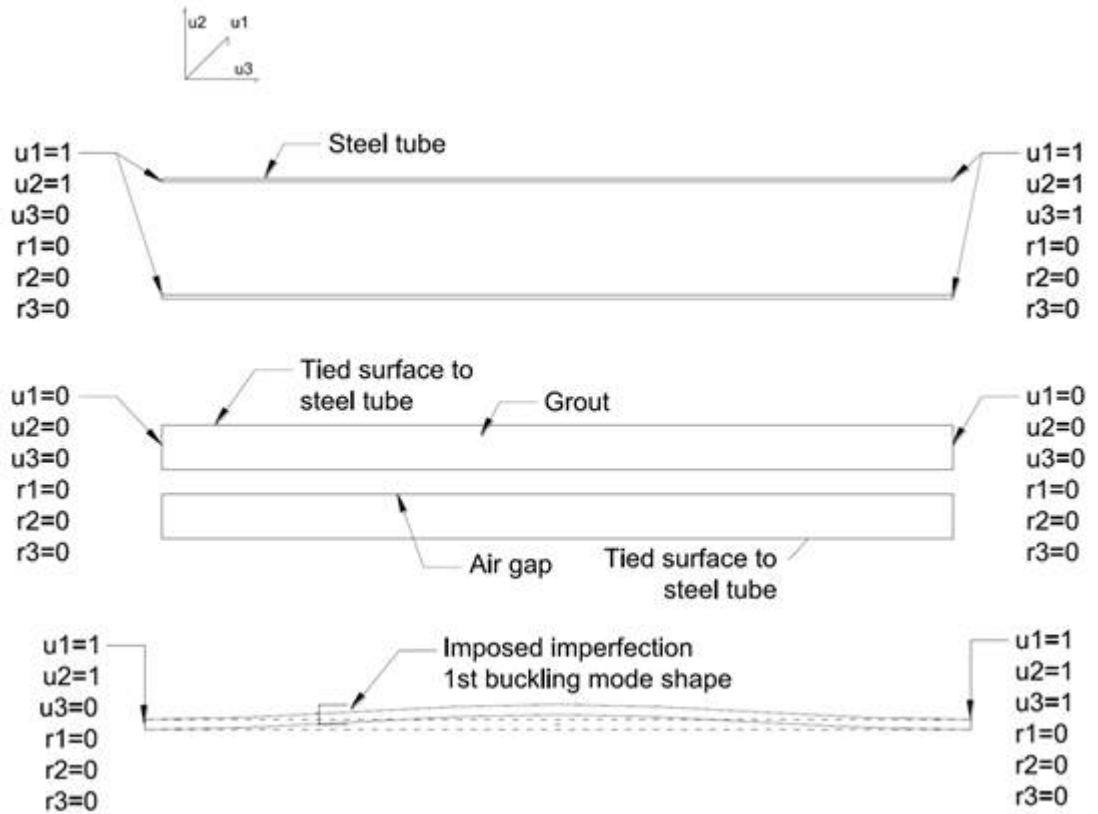
Figure 3.24: Boundary conditions

Table 3.9: Material Properties

Component	Assumption	Material properties
Core	The component was modelled with plastic properties comprising combined strain hardening (isotropic and kinematic) parameters	E=200GPa v=0.3 fy=282.4315 MPa
Grout	The component was modelled as linear elastic	E=20GPa v=0.15
Steel tube	The component was modelled as elasto plastic	E=200GPa v=0.3 fy=362.846 MPa

steps, each with different aims.

As a first step two mesh cases (coarse and refined) are proposed for every component and their combinations (8 cases) are analysed, the aim is to assess the effects of the variation the meshing size in each of the components of the model and identify the part of the Buckling Restrained Brace is most relevant for a sensitivity analysis.

As outcome it was shown that the variation of the mesh density on the core is more relevant to the model and that the number or elements of the grout increased considerably the time used. Likewise, it was noticed that the consistency of the mesh results in a more efficient
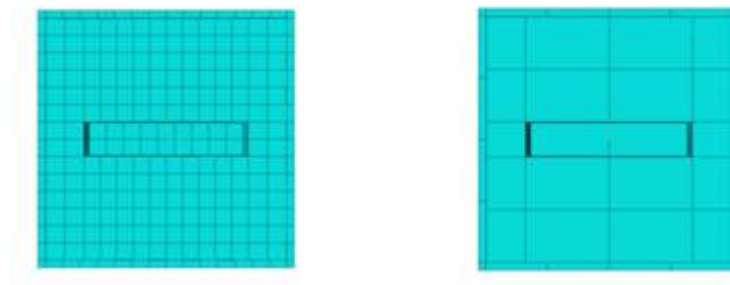
Figure 3.25: Coarse and refined mesh considered for sensitivity analysis

computing time, presumably for contact reasons. Finally the mesh density of the casing is where the least sensitivity was found under the assumptions undertaken.

A second step is to study further mesh variation of the core. The level of accuracy can be obtained in two different ways which can be found in the description however this analysis requires a complete different model so as to reproduce the stress level in the casing or the damage and failure patterns.

3.2.2 Validation methodology

The study is conducted by selecting two different mesh densities for each part and analyse all the possible combinations obtaining peaking principal stress values at relevant points and hysteresis of each case. The model comprises of three parts and their densities varied from coarse to a refined mesh (**Figure 3.25**). The combination of the 3 parts with 2 different mesh densities (Table 3.10) result in a total of 8 cases for analysis (Table 3.11).

The mesh sensitivity analysis currently limits to the analysis of variation of a set of relevant parameters and features due meshing size given the number of cases in regard. In order to notice convergence, the analysis of more than 2 meshing sizes is required, however an excessive amount of computing time reveal the need for narrowing down the cases by assessing the influence of varying the mesh density importantly in each part. The benefits of doing this analysis are that the computing time can be optimised by identifying the most consistent mesh for this problem and the number of cases for a full analysis can be reduced by varying the mesh of the part is more relevant to the model only.

Table 3.10 shows the proposed element distribution in each part of the model. The element density was proposed based on the simplest regular mesh possible and the study conducted

Table 3.10: Mesh distribution

	Case number	Element distribution			Approximate element size	Number of elements
		Thickness	Width	Length		
Core	1	1	2	82	40x40	164
	2	2	9	329	10x10	5922
Grout	1	18 elements cross section		82	40x40	1476
	2	176 elements cross section		329	10x10	57904
Hollow core section	1	20 elements cross section		82	40x40	1640
	2	60 elements cross section		329	10x10	19740

by Razavi Tabatabaei et al. (2014) where a good approximation to experimental data is obtained. The proposed meshes for the core included an additional layer along the thickness varying from 1 to 2 layers with a total of 164 and 5922 elements respectively. Likewise the number of elements used in the grout varied from 1476 to 57904 and in the case of the steel tube they ranged from 1640 to 19740. Table 3.11 shows the possible combination of cases and the results are presented in the next section with the corresponding mesh number. The overall maximum number of elements was 83566 and the minimum 3280.

Table 3.11: Mesh cases to analyse

Mesh number	Case number		
	Core	Grout	Hollow core section
1	1	1	1
2	1	1	2
3	1	2	1
4	1	2	2
5	2	1	1
6	2	1	2
7	2	2	1
8	2	2	2

3.2.3 Mesh sensitivity

In this section is presented the response of the device in terms of force displacement curve during the application of the displacement. Likewise, maximum principal stress values, contours of distribution and deformed shapes are given at the peaking compressive displacement where the maximum demand of buckling resistance is reached.
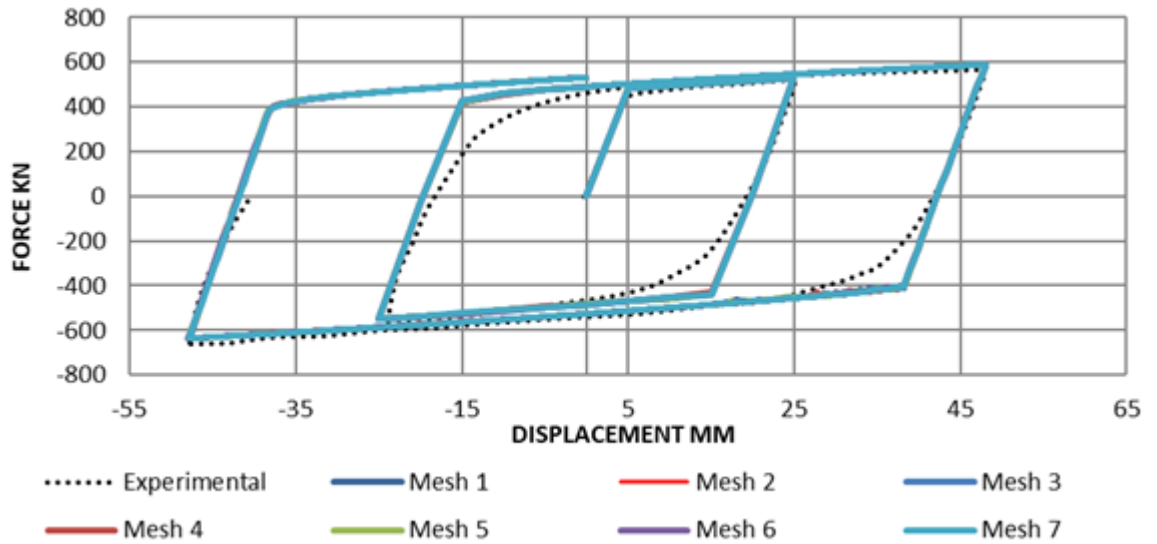
Figure 3.26: Influence of mesh in hysteresis in specimen 1
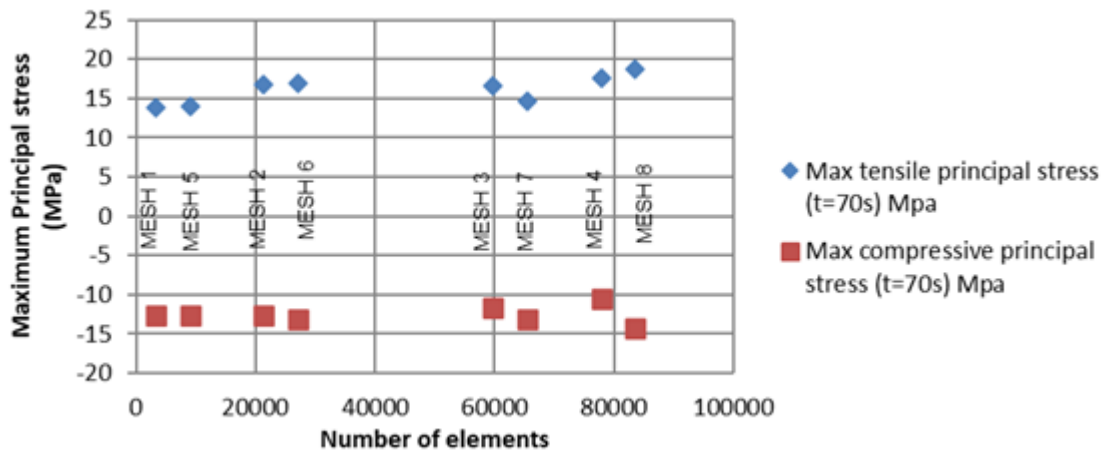
Figure 3.27: Variation of maximum principal stress and global number of elements

In the analysis, observations are made on a set of parameters and features such as localisation of maximum principal stress value, the magnitude, principal stress contours and core deformed shape. A value not analysed here is the contact pressure however it is highly linked to the stress in the casing.

In all cases, the force displacement response (Figure 3.26) resulted in the same hysteretic behaviour. Although a variation is expected due to the mesh sizes and element distribution, the reason for this similitude is that no friction is involved in the model at any contact interface and therefore the mesh density in both cross section of the core and longitudinal does not have implications in the hysteresis. The magnitude of the reaction forces can vary on the nodes of the core cross section, however the integration of these forces result in the same value.
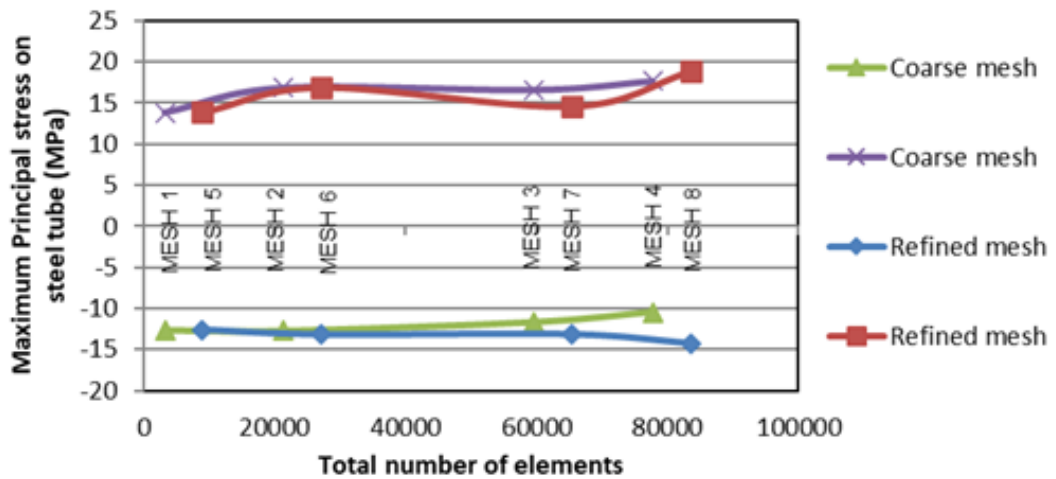
a)Maximum stress for two different core meshes
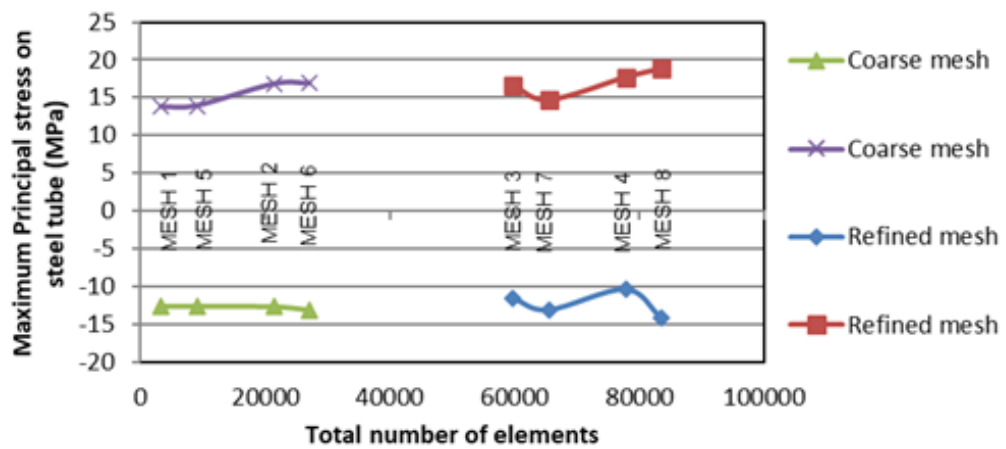
b)Maximum stress for two different grout meshes
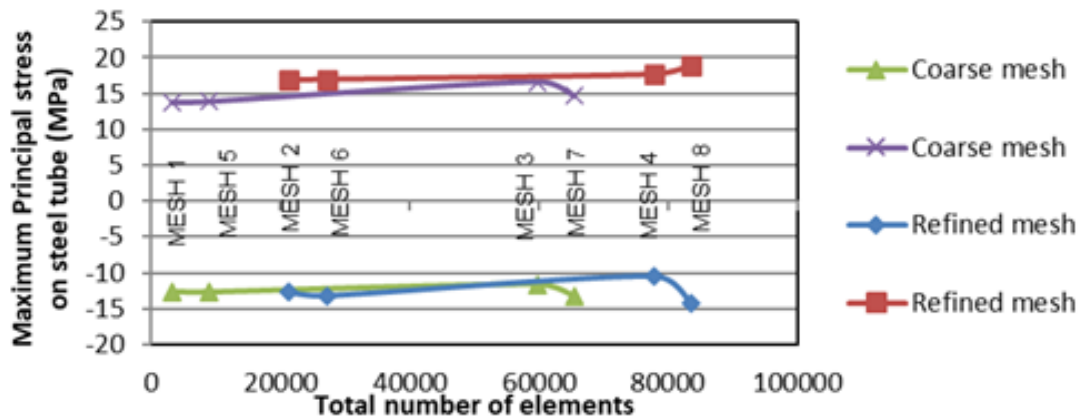
c)Maximum stress for two different steel tube meshes

Figure 3.28: variation of stress according the mesh density of each component

Figure 3.27 presents an overall variation of principal stress magnitude both compressive and tensile maximum values occurring at a maximum compressive core displacement. From the figure it can be seen that there is no direct correlation of number of elements and convergence as tensile stress varies significantly.

Figure 3.28 shows differences in the stress level of the steel tube using the possible combi-
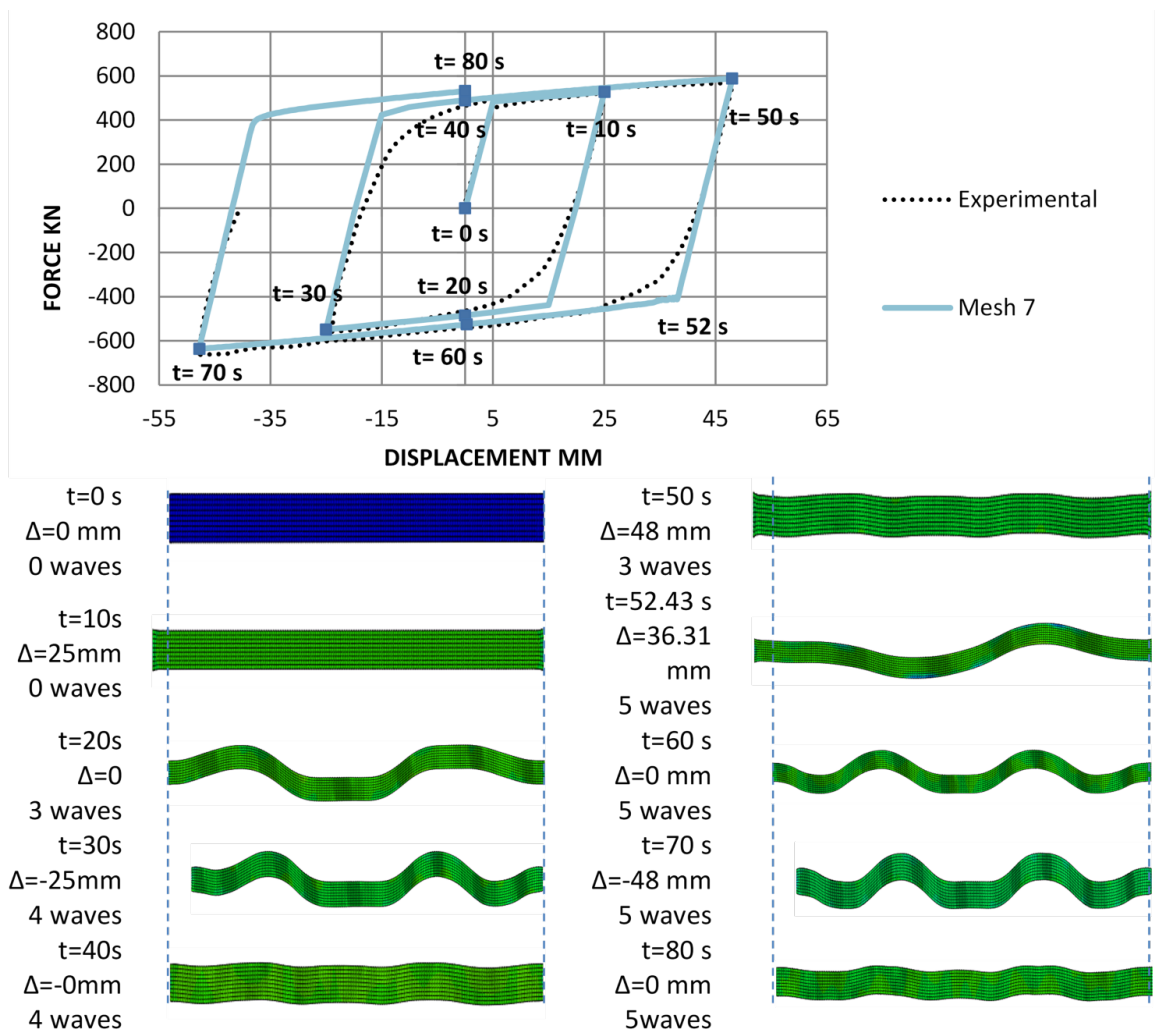
Figure 3.29: Buckling shape evolution of core with a refined mesh about the major axis

nations with a fixed mesh density for the three different components in order to quantify the isolated effect of changing the mesh size. The ratio maximum compressive stress-minimum compressive stress varied from 1.006 to 1.129 where the maximum ratio can be found when the mesh size of the core is changed. Similarly the ratio minimum tensile stress –maximum tensile stress varies from 1.006 to 1.352, this latter value corresponds to the variation of core mesh density.

Contours in sections observed and deformed shapes The analysis showed a large amount of computer time varying from 10 hours to 96 hours; however the study also reveals that the consistency of mesh density in the contact interfaces is crucial to reduce this time as it was observed that even though 96 hour is the longest, this does not correspond to the number of elements. The maximum number of elements corresponding to Mesh 8 (Table 3.12) is 83 566 elements where the mesh was set to have the same distribution on the contact surface; the analysis completed after 37 hours whereas Mesh 2 completed after 96 hours with 21380
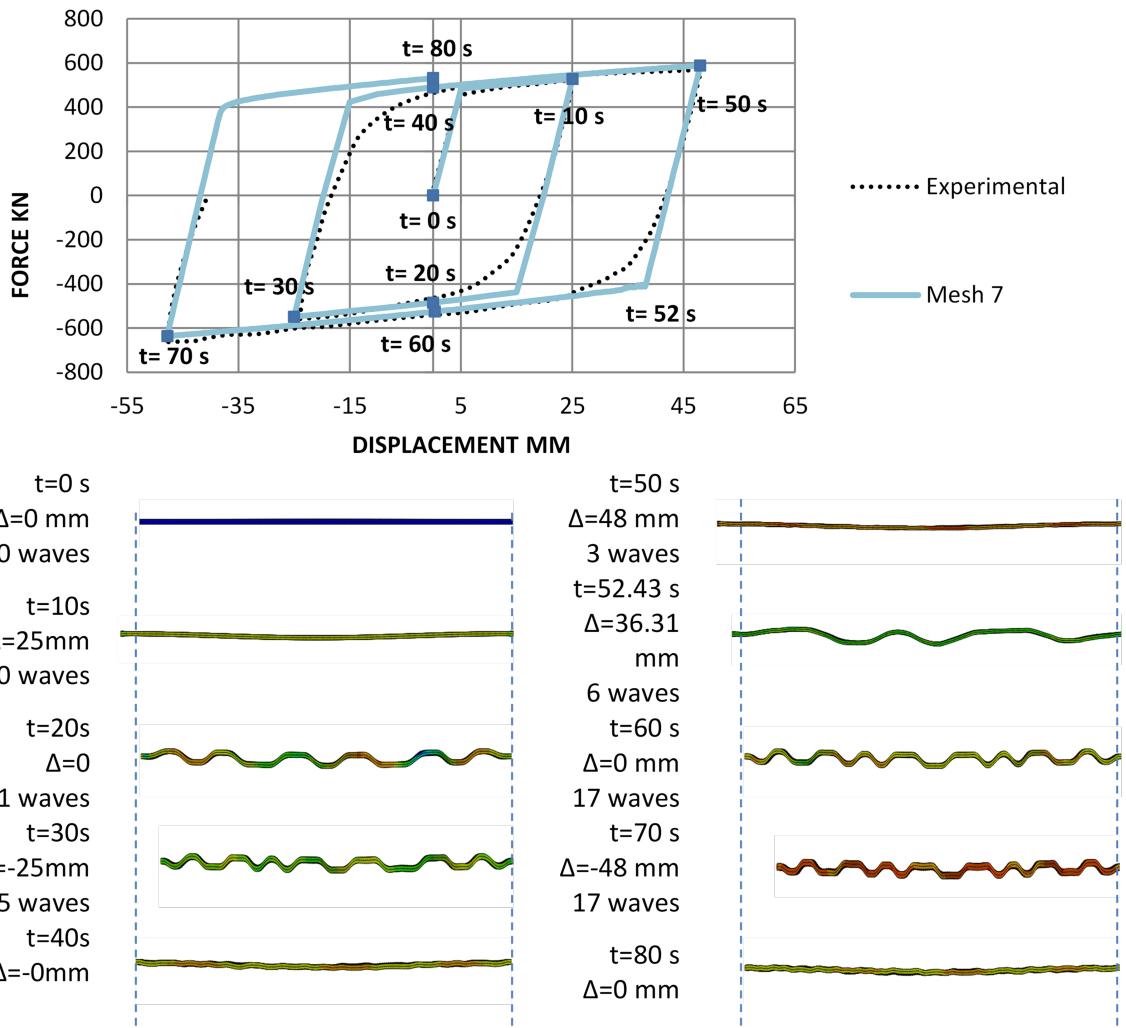
Figure 3.30: Buckling shape evolution of core with a refined mesh about the minor axis

elements which distribution consisted of a coarse mesh for the core and the grout and a re-

fined mesh for the steel tube.

Table 3.12: Computing time and Maximum Principal stress on steel tube

Mesh number	Running time (hrs)	Number of elements	Max tensile principal stress (t=70s) MPa	Max compressive principal stress (t=70s) MPa
1	10	3280	13.76	-12.61
2	96	21380	16.83	-12.69
3	84	59708	16.57	-11.65
4	120	77808	17.64	-10.47
5	35	9038	13.91	-12.64
6	28	27138	16.91	-13.21
7	29	65466	14.63	-13.2
8	37	83566	18.8	-14.27

Figure 3.31 and Figure 3.32 show the core deformed shape about the minor and major axis

respectively at a peaking compressive displacement; it can be seen that in the case the num-

ber of waves is not constant in the weak axis direction, hence a high mesh dependency can

Mesh 1	5 waves
Mesh 2	5 waves
Mesh 3	5 waves
Mesh 4	6 waves
Mesh 5	5 waves
Mesh 6	5 waves
Mesh 7	5 waves
Mesh 8	5 waves
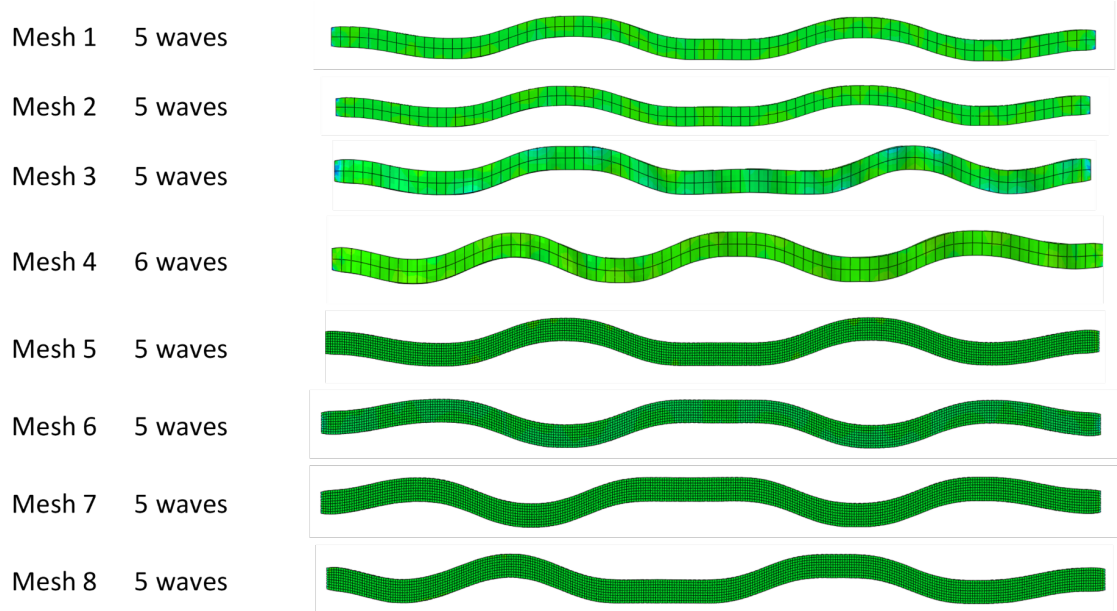
Figure 3.31: Influence of mesh in core deformed shape at peaking compressive displacement (major axis)

Mesh 1	21 waves
Mesh 2	22 waves
Mesh 3	19 waves
Mesh 4	21 waves
Mesh 5	17 waves
Mesh 6	17 waves
Mesh 7	18 waves
Mesh 8	19 waves
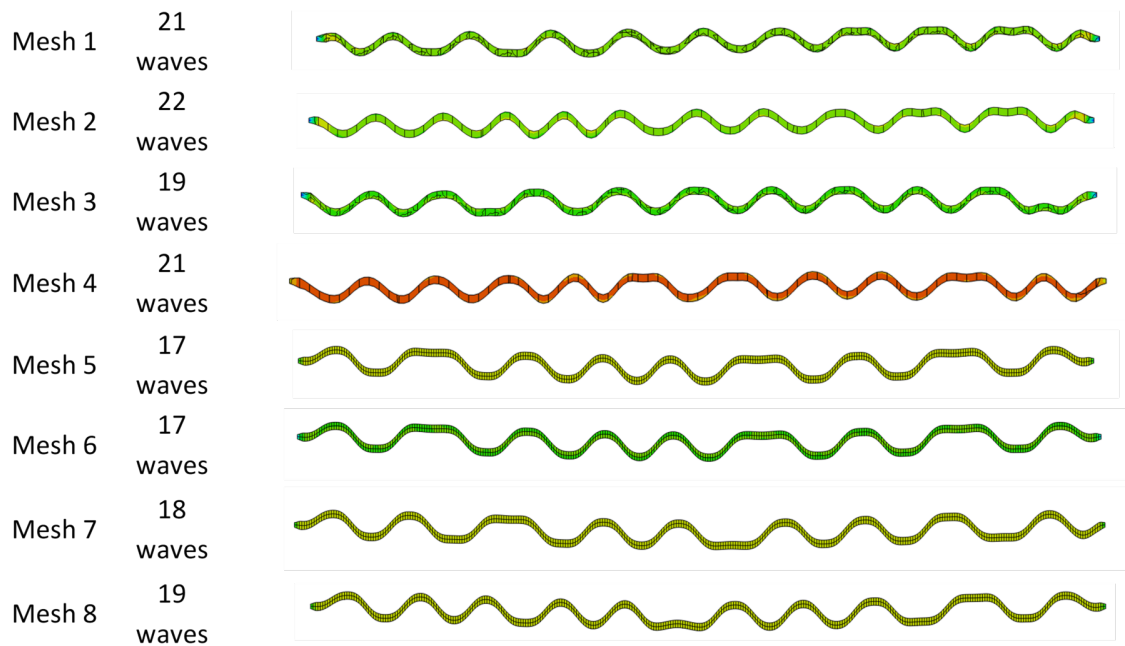
Figure 3.32: Influence of mesh in core deformed shape at peaking compressive displacement (minor axis)

be addressed. On the other hand, a rather predictable deformed shape can be appreciated in the strong axis, where the variation of the waves results similar in all cases

Figure 3.34 shows the contours of the principal stress distribution for the 8 Mesh cases generated. From the figure, it can be seen that qualitatively the distribution of stress does not vary importantly however, the maximum stress value points seem to alternate the sides of the casing. Moreover, it is noticeable that the strong axis of the core is the direction where largest stress is induced. This suggests that the reduced buckling mode shape rules the de-
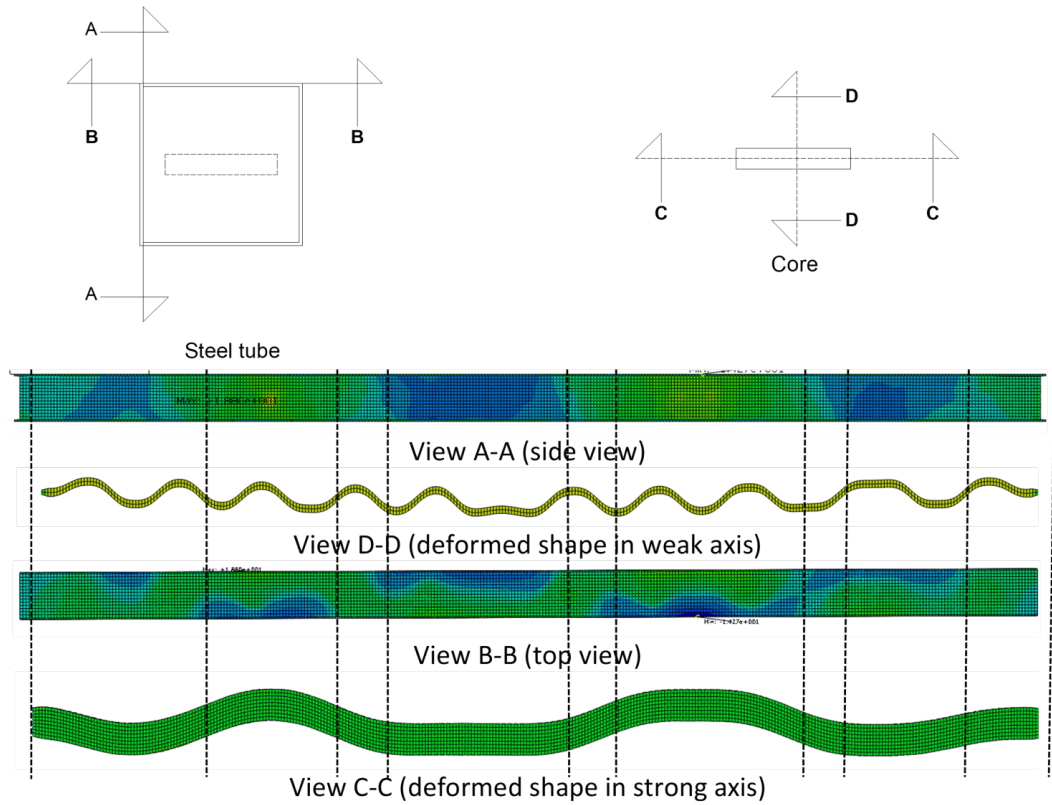
Figure 3.33: Principal stress contours on steel tube and core deformed shapes
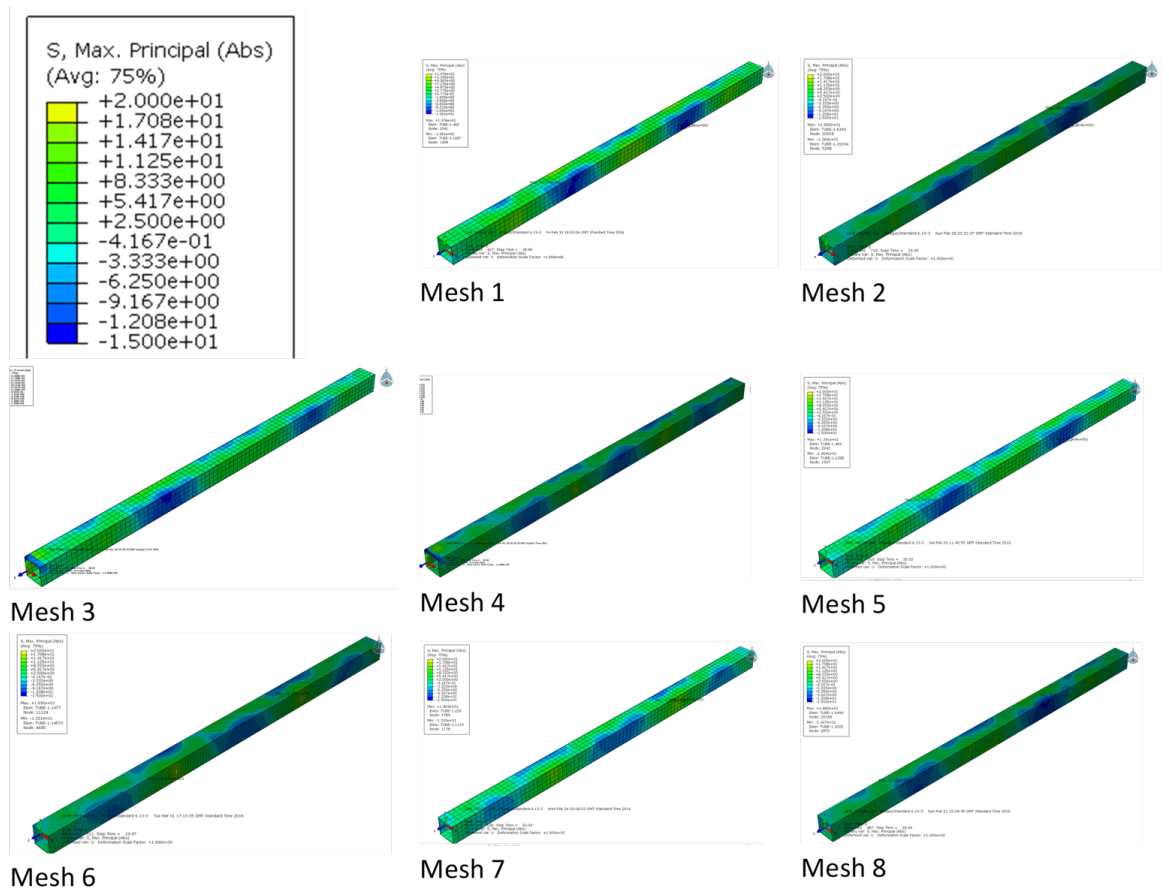
Figure 3.34: Distribution of principal stresses on Steel Hollow core section for 8 mesh cases
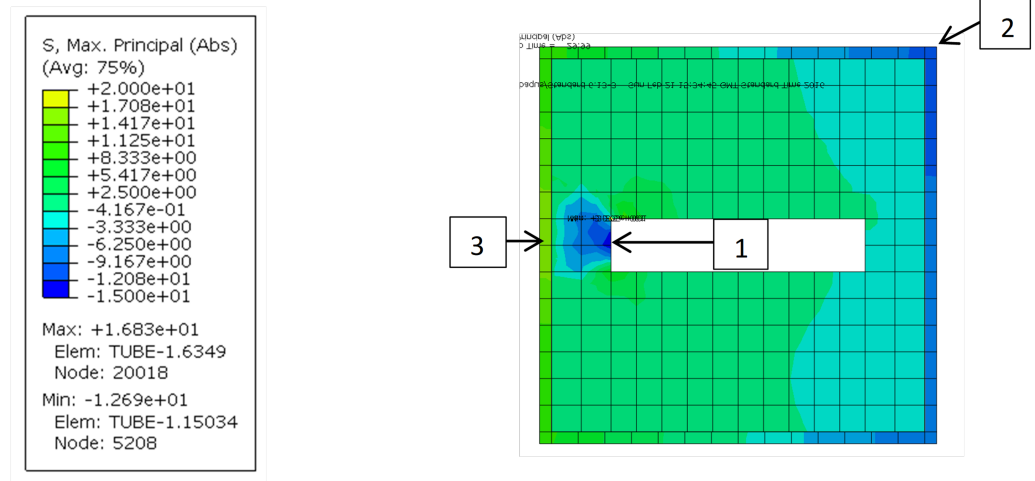
1. Maximum contact pressure on grout (15 MPa)
2. Maximum compressive stress on steel tube (12.69MPa)
3. Maximum tensile stress on steel tube(16.83 MPa)

Figure 3.35: Principal stress contour at maximum contact pressure point at peaking compressive displacement (t=70)

sign of the casing which is crucial in order to understand the mechanism of the device.

Figure 3.35 shows a contour of principal stresses ate the maximum pressure point from the core on the grout, the section shows a concentration of stress at the inner part of the grout, the loading path shows that such a stress is closely applied to the steel tube (as the clearance occupied by the grout in that direction is significantly thinner than in the weak axis) in such a way that concentration of stresses on the steel tube are induced as shown in Figure 3.36. Likewise, the contours in the steel tube reveal that this loading induces tension in the half where the pressure occurs and compressive stresses appear on the opposite half which suggests the induction of bending moment demand on the tube globally.

Figure 3.35 also shows a remarkable feature in the distribution of stress in the grout. The section of the casing in this model, shows to work as a composite due to the fully bonded interface between these two, however, and the distribution shows tensile stress acting on the grout which leads to cracking therefore it is important to increase the complexity of the model to consider the possible formation of cracks.

Figure 3.37 shows the localisation of the maximum stresses as a fraction of the length of the casing. The table shows three different lengths identifying key points as point of maximum principal stress, point of maximum contact pressure and the point of maximum tensile stress. The results showed that the maximum compressive point can be located at half the
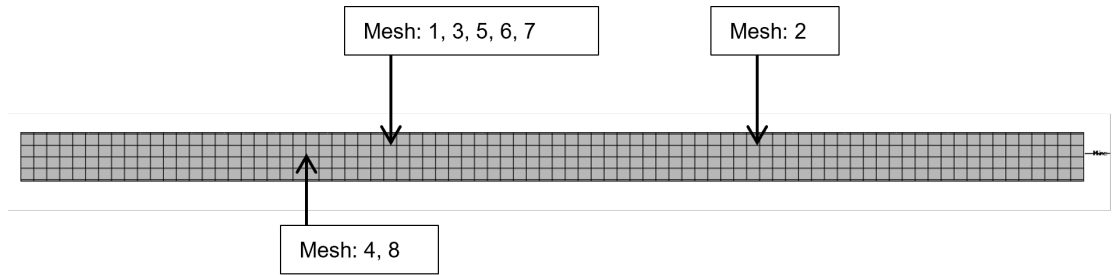
Figure 3.36: Maximum tensile stress on steel tube

height of the tube and 1/3 or 2/3 of the length of the casing from the top or bottom approximately. Also view A-A, shows how the load is transmitted to the casing since the contact is produced.

3.2.4 Remarks

The numerical analysis conducted gives a good idea of the mechanism of the device and level of stress as long as the device does not experience failure. However, even though this model can represent a reasonable approximation to reality for some cases, its validation is only based on the comparison with the real hysteretic behaviour and accuracy in terms of lateral thrust remains unknown and requires to be further investigated.

The mesh sensitivity conducted gives a good idea of the influence of affecting the number of elements in each component showing that the number of elements in the core is most influential in the results. The modelling solver (dynamic implicit) needed a day to complete the analysis; further work in the optimisation of the model is needed.

3.3 Global bending failure condition of Buckling Restrained Braces based on a numerical analysis

The mechanism of Buckling Restrained Braces (BRBs) is investigated so as to understand failure condition of the casing. The understanding on the casing mechanism and consequent understanding on effects of parameters (gap, grout strength, steel strength and size) is remarkably important in order to quantify actions and provide design guidance by determining a safety factor. In order to do so, numerical analysis has been undertaken to validate the case of one experiment comprising a failed specimen of a rectangular section BRBs

The legend:

S, Max. Principal (Abs)
(Avg: 75%)
+2.000e+01
+1.708e+01
+1.417e+01
+1.125e+01
+8.333e+00
+5.417e+00
+2.500e+00
-4.167e-01
-3.333e+00
-6.250e+00
-9.167e+00
-1.208e+01
-1.500e+01

Mesh	Z/L	Z1/L	Z2/L	A-A view
1	0.33	0.17	0.70	
2	0.71	0.16	0.70	
3	0.32	0.69	0.33	
4	0.25	0.75	0.25	
5	0.32	0.71	0.71	
6	0.32	0.71	0.71	
7	0.34	0.97	0.70	
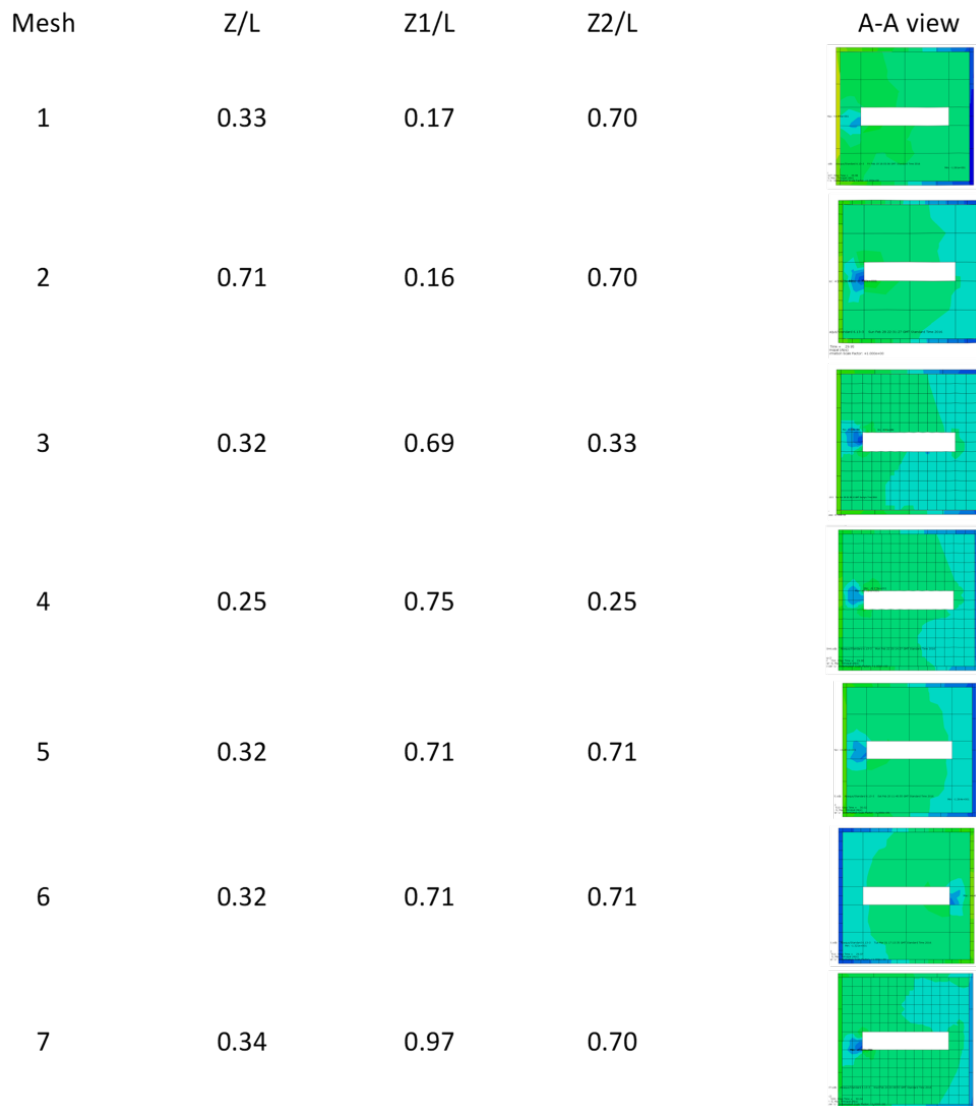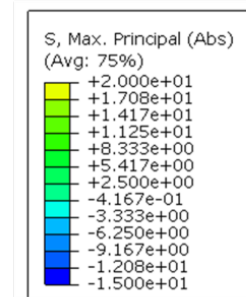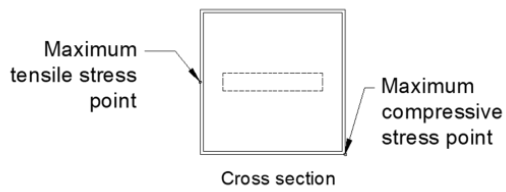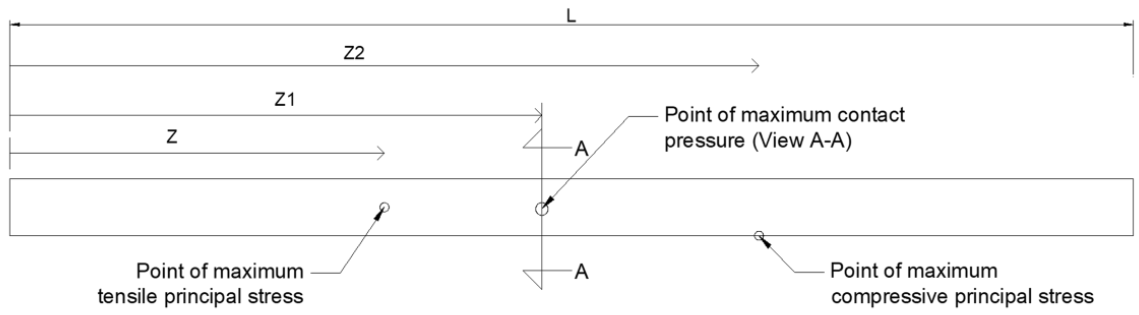
Figure 3.37: Localisation of maximum stresses and cross sections

tested in a frame (sub assemblage) by Watanabe et al. (1988) who observed the transition from stability to failure of different casings.

Generally the most relevant outcome of an experimental BRB programme is a force displacement curve; however it is to be noticed that these curves do not reveal information about the mechanism of the device, which is particularly relevant when studying the casing. To overcome this, a specimen where failure could be observed was modelled and validated against experimental available data. The magnitude and distribution of lateral thrust was investigated and the stress strain distribution of the casing is revealed.

The study on the casing highly relies on the analysis of forces transmitted by the core and the connections; therefore it is crucial to understand the variation of magnitude and distribution of these forces along time. In this study the evolution on the distribution of these forces and failure conditions are analysed. Likewise a parametric study is conducted and the effects of the material strength of the steel and grout are investigated.

The study reveals that the force distribution acting on the casing changes from a point contact to a line contact at the moment of failure. The deformed shape of the whole bracing corresponds to the first mode of buckling shape and remains like this as axial displacement is induced. Failure occurs even when the casing has not reached the yielding stress and bending stress in the core become important. After the core yields in tension, yield values are not reached under reversed loading in this component, however reduced dissipation capacity is still possible due to the ductile behaviour of the casing. Contact force increase is proportional to axial compressive displacement and is not proportional to axial compressive force.

3.3.1 Methodology

BRB design consists mainly in the design of a casing sufficiently big to ensure stability when the core is in compression. Pre dimensioning methods have been successfully proposed by previous research and the mechanism of the core in higher buckling mode formation has been studied, however there is a remarkable gap in understanding how forces are transmitted to the casing and how big they are.

Methods to quantify the lateral force induced by the core have been proposed; these are
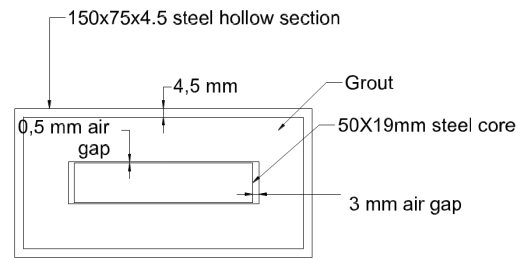
Figure 3.38: Cross section of specimen studied

based on different plane stress assumptions and provide a breakthrough towards understanding lateral thrust. However, experimental evidence has shown important inaccuracies from both numerical and analytical solutions. This former statement suggests that further studies under different approaches are required.

The improvement of accuracy of the calculation of lateral forces is needed in order to understand the boundaries of bending stability in terms of lateral thrust as the failure occurs due to bending. Likewise, lateral thrust can be correlated to axial displacement which is the nature of the loading.

Experimental data of a specimen over 3 m long was collected from Watanabe et al. (1988). Figure 3.43 show the testing configuration of the specimen which comprises a BRB installed in an isostatic frame. As a result from the experiment the force displacement curves under an imposed displacement history could be obtained. The experiment aims to determine the stability limits of a BRB with rectangular cross section. Therefore, a specimen was selected from these in order to understand the failure mechanism of the device by conducting the numerical analysis. The validation consists in comparing the force displacement curves of the experiment and the model where the model is a simplification of the test in order to study the yielding portion. The curves compared correspond to the test of a specimen that shows bending failure, Figure 3.39 shows the cross section of a BRB where global bending failure could be observed.

A three dimensional simplified model of BRB was analysed under a set of assumptions, sensitivity of boundary conditions was conducted. The simplification allows reducing computational cost and focusing on the part of the bracing where buckling was observed.

First, in order to analyse numerically the BRB it was necessary to study the boundary conditions that best suit the problem. In this section, a comparison of 3 boundary conditions

a)Side view

b)Cross section at mid length   c)Connection detail
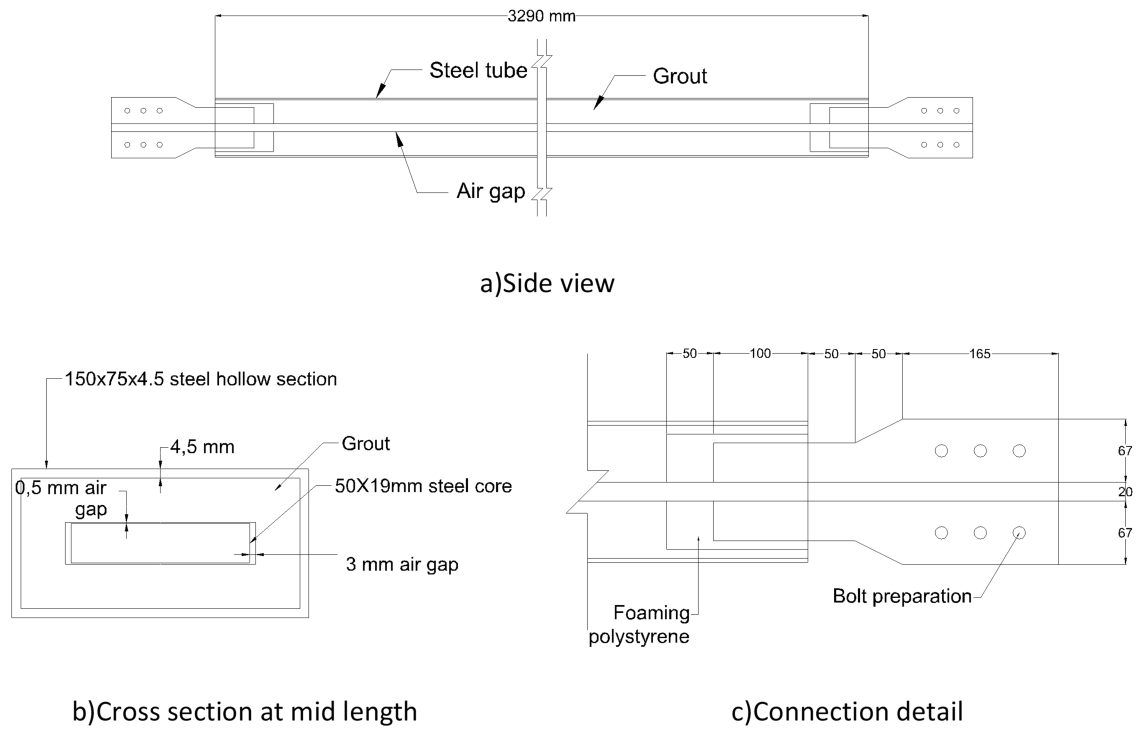
Figure 3.39: Specimen tested in Watanabe et al. (1988)

for two different casings was analysed. A boundary condition is selected as most suitable for the analysis of Buckling Restrained Braces based on a good agreement with experimental data.

Furthermore, a sensitivity analysis of the material properties of the grout is conducted as the results of the experimental programme involve failure. It is necessary to account for degradation of the material in order to understand the failure mechanism. A comparison of 2cases is conducted in order to quantify the effects of the strength of the grout in the force displacement response.

Finally, the results are shown in terms of stress peaking values on the casing and lateral thrust magnitude in one force in x and y direction. Although the study is conducted for one BRB in particular, this study also aims at providing a breakthrough in the study approach of future innovative BRBs.

The lateral thrust is analysed in two ways: in total magnitude for each direction and the distribution of these forces of the surface of the grout. Nodal forces can be obtained with the software ABAQUS by analysing the two interacting surfaces. Figure 3.40 shows the sets of the model; the advantage of calculating the forces on the 2 surfaces is that the magnitude of total thrust and distribution can be obtained.

Top set

Right set

Left set

Bottom set

Left

Top

Right

Bottom

a)Sets on casing

b)Sets on core
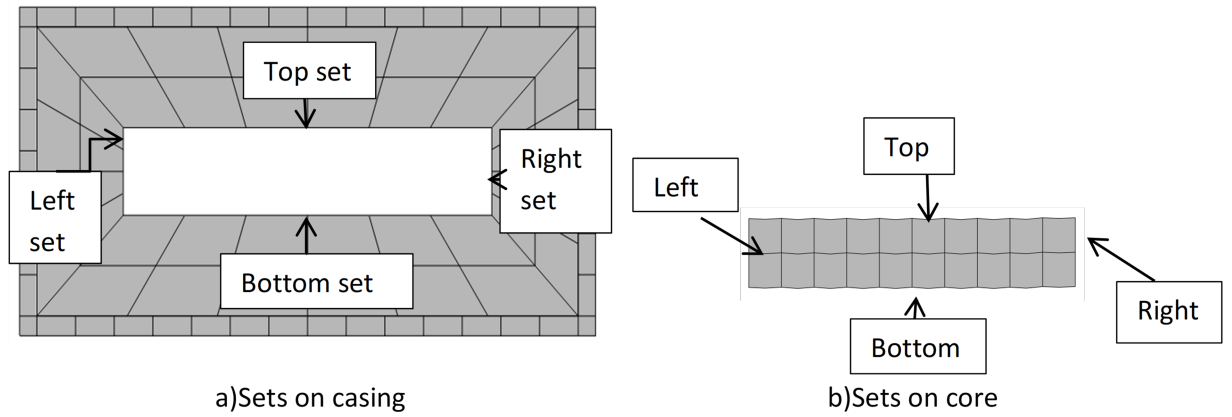
Figure 3.40: Surface sets on Finite elements model

CFN2

CFN1
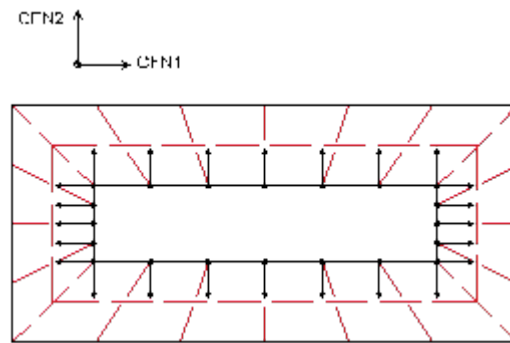
Figure 3.41: Horizontal and vertical forces analysed on grout

In order to analyse the lateral thrust in terms of magnitude, the integration of the forces on one face is needed. Figure 3.41 shows the direction of the forces analysed; the magnitude was obtained by adding up these forces at one same frame of time.

The distribution of forces was obtained by analysing the core deformed shape vertical forces at the time of failure. The waves of the core were analysed separately and the location of the centroid of the forces was identified. These values were used for validation with the analytical solution of a simply supported beam. The plastic values of the numerical and analytical solution were compared.

The test consisted of applying a lateral displacement on a frame by means of an actuator

U2,U1

U3
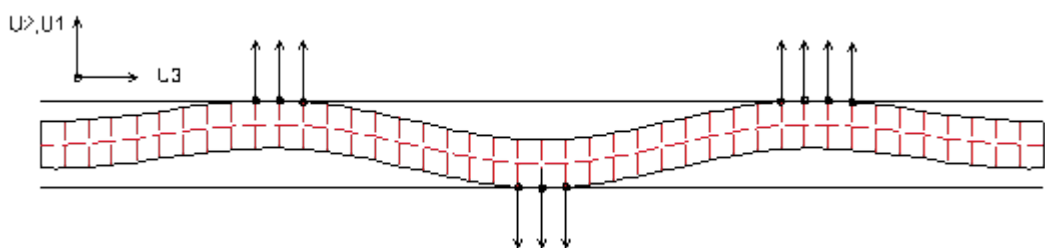
Figure 3.42: Horizontal forces analysed on core
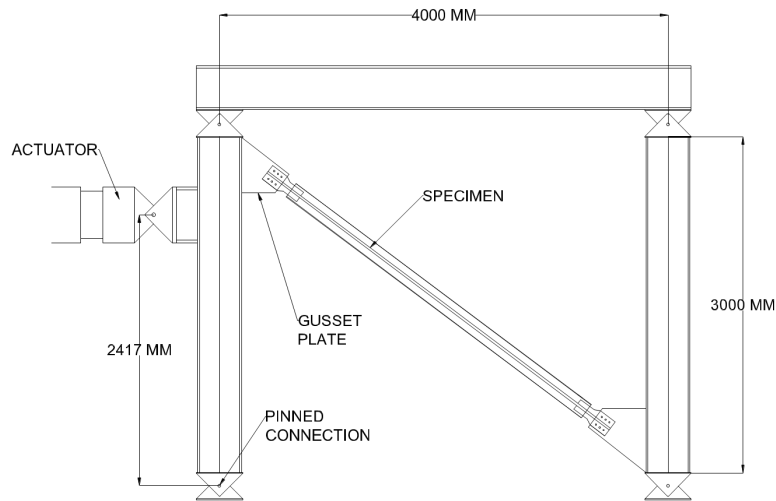
Figure 3.43: Testing configuration

Figure 3.43. The frame comprises of hinged connections and the beam-column elements can be considered rigid as the size of cross sections are importantly larger to the cross section of the bracing which implies no contribution of frame stiffness in the horizontal direction. Therefore lateral stability is provided by the bracing only.

In order to verify that the amplitude of displacement used for the model is correct, a geometrical analysis was conducted where frame elements were considered a rigid body and hinges at the base centres of rotation (Figure 3.44). Two control points were selected in the bracing ate the two ends of the yielding zone in order to measure the relative displacement between them and a rotation about the fixed hinges was induced. After the rotation the position of the two reference points was identified and the distance between them was measured from a scaled drawing.

The loading comprises of 2 cycles with different amplitudes; the amplitudes of the cycles are 12 mm and 24 mm respectively (Figure 3.45).

3.3.2 Numerical analysis

Numerical modelling reveals the evolution of contact forces in the casing. The three dimensional model (Figure 3.46) shows a reasonable agreement with the experimental outcome in terms of force-displacement response and final deformed shape of failed casing. From this validation, lateral forces acting on the grout were analysed and causes of failure were investigated.
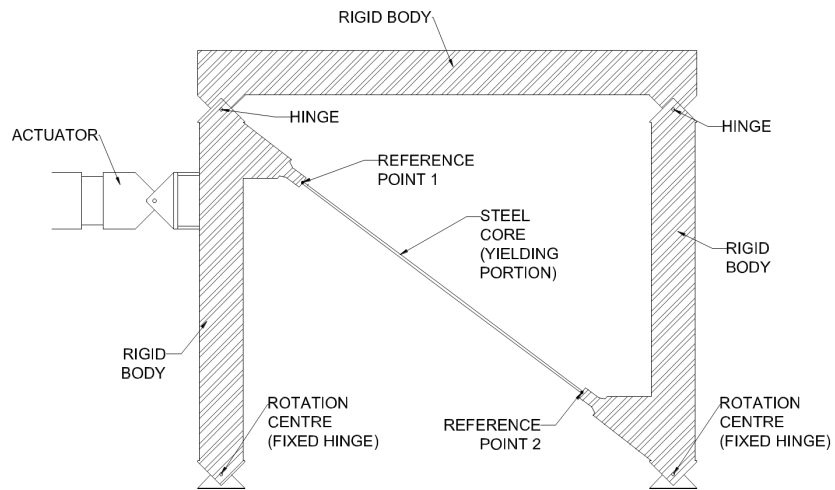
Idealisation of frame
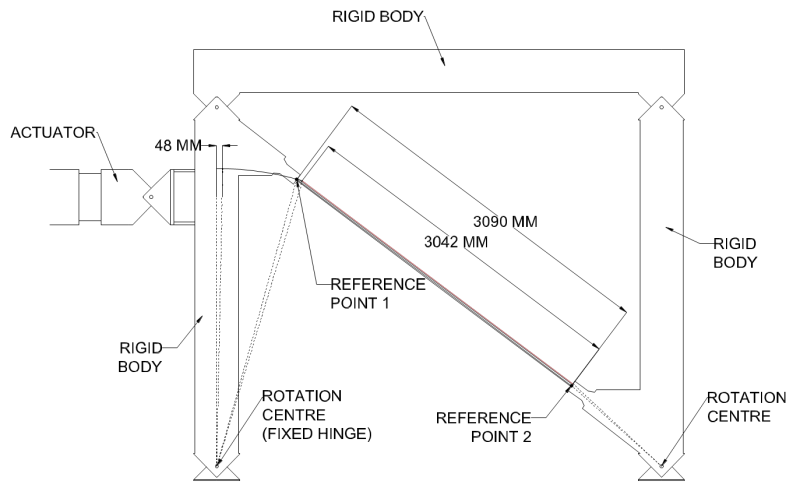
Frame after rotation

Figure 3.44: Analysis of frame equivalent displacement
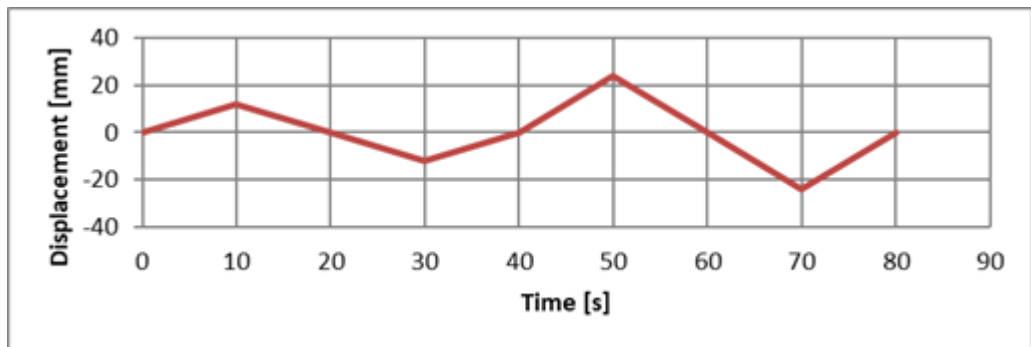
Figure 3.45: Imposed displacements

a)3D FEM   b)Cross section and meshing
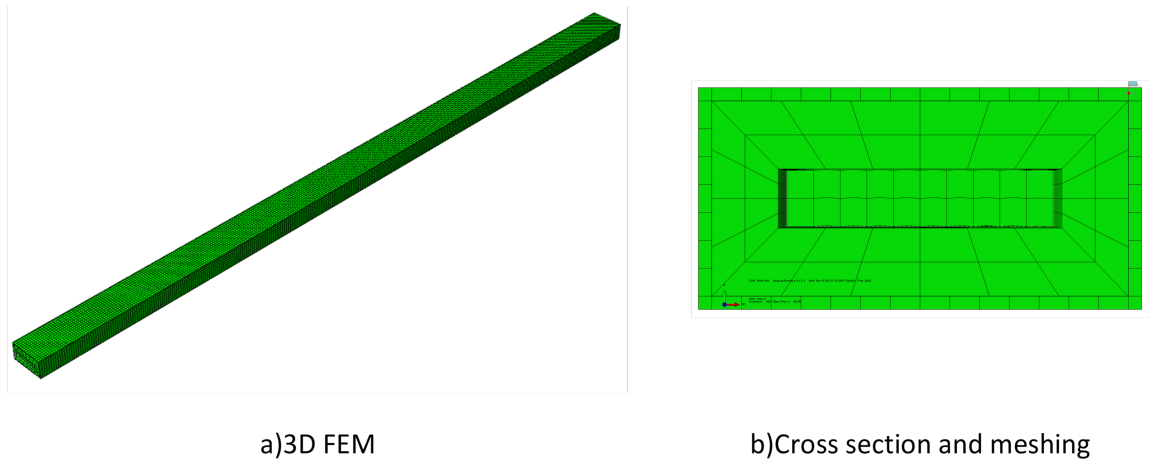
Figure 3.46: Finite element model
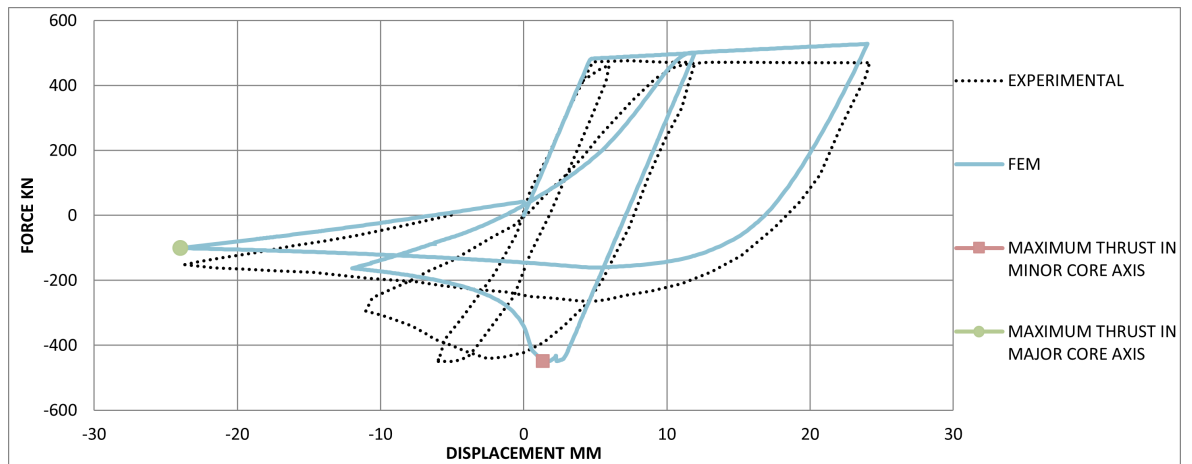
Figure 3.47: Validation of FEM

Figure 3.47 shows the validated model against experimental available data. In this figure, discrepancies can be observed from comparing the two hysteresis curves; however even though this discrepancy is larger in terms of displacement, the model has shown to have a reasonable accuracy in terms of forces. Likewise, in the figure it can be observed the point selected to extract the data, being this point the maximum force reached before failure. The contact points after contact suggest that the casing works as a simply supported beam. Furthermore, lateral thrust increases alongside axial displacement however axial force does not behave proportional to the lateral thrust.

3.3.3 Assumptions

The large amount of computational time shows the need for a simplified model of BRB which can be done undertaking a set of assumptions. The assumptions to be discussed are 4: material properties, boundary conditions for the 2 cases in study, contact properties and

loading.

Table 3.13 summarises the assumptions considered for each component, the idealisation of the structure consists in 3 parts; core, grout and steel tube. The steel used in the experiment for the core and steel tube have a strength f_y=282.43MPa and f_y=362.84MPa respectively. The grout has a compressive and flexural strength of f_c=80MPa and f_t=11MPa respectively.

Table 3.13: Assumptions for the components of the model

Component	Material	Boundary conditions
Core	Steel with elastic range and strain Hardening (Isotropic, kinetic and cyclic)	Fixed-roller with no rotation Displacement applied on a surface of one end Surface to surface contact Initial imperfection corresponding to the scaled first buckling mode Displacement applied on a surface of one endInitial imperfection corresponding to the scaled first buckling mode
Grout	Damage plasticity model corresponding to a bilinear behaviour accounting for compressive and tensile strength (flexural strength)	Perfect bonding between grout and steel tube (surface nodes coupled). No additional boundary conditions are considered as composite action is assumed
Steel tube	Elastoplastic behaviour	Three different boundary conditions are analysed: fixed-roller, pinned-pinned and pinned in one end only (stability provided by contact with the core) Perfect bonding between grout and steel tube (surface nodes coupled)

Calibrated constitutive models were used for both concrete and steel. In the case of the steel core the model accounts for elastic and plastic behaviour, strain hardening is also defined and is modelled as a combination of kinematic and isotropic behaviour with cyclic hardening effects. For the steel tube bilinear elasto-plastic behaviour is assumed.

According to the experimental data the steel used for the core is S275 and S355 for the steel tube. The material properties of steel of the core were validated against the first tensile displacement as no interaction exists with the casing. A constitutive model found in Jia and Kuwamura (2014) was modified to meet the yield stress required as this model was developed for a steel S235, however, the values used appear to agree with reasonable accuracy to the desired behaviour. An elastic modulus of 200 GPa, Poisson's ration of 0.30 and density of 7.85E-009 Tonne/mm3 were considered (Table 3.14).

In order to model the grout part, a simplification of a damage plasticity model is used where no degradation of the stiffness is considered; this numerical analysis does not aim to ac-

Table 3.14: Strain hardening properties of steel

Component	Steel	σ_0 (MPa)	b	Q (MPa)	γ	C (MPa)
Core	S275	282.4315*	4	110	25	4600
					98000	1000
Casing	S355	362.846*	-	-	-	-
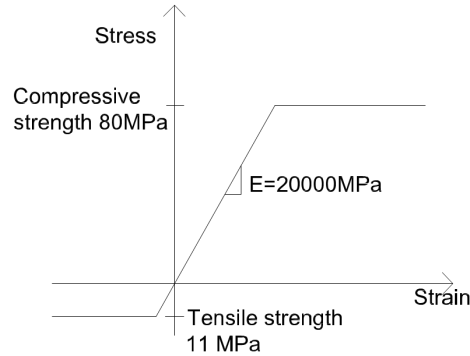
Figure 3.48: Stress strain curve assumed for grout

count for damage in concrete but for nonlinear behaviour. The importance of considering damage (with a more realistic behaviour and degradation of the Young's module) will be addressed within the parametric analysis by comparing a simplified model and a constitutive model. Default values for modelling concrete in ABAQUS were used for the analysis alongside the values shown in Figure 3.48.

Contact between components is modelled as surface to surface with normal hard contact and tangential frictionless properties. Current agreement with experimental data does not suggest it is necessary to consider friction for the study of the casing; however it is likely that this parameter has more relevance for the study of the core, such as fatigue. Also regarding future research plans, the dynamic analysis of the device under seismic conditions, friction is likely to become an important factor.

The axial displacement was applied as a boundary condition on the nodes on the face of the tip of the core where rotation is inhibited indirectly by doing so. On the right tip both vertical and horizontal displacements are constrained accounting for the interaction with the non-yielding portion of the core. Also, an imperfection corresponding to the first buckling mode scaled by a factor of 0.4 was introduced so as to start bending. The imperfect initial deformed shape is smaller than the size of the gap 0.4 mm where the gap is 0.5 mm thin. Figure 3.49 shows a diagram of the boundary conditions undertaken.

On the other hand, the boundary conditions of the casing are simpler as only one reference
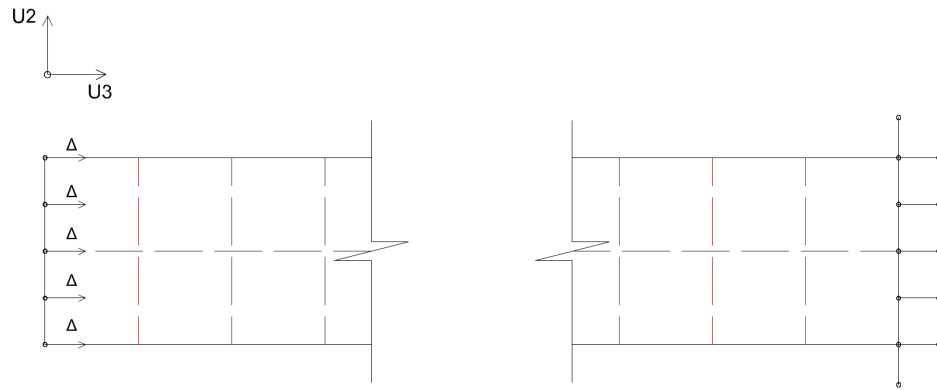
Figure 3.49: Boundary conditions and displacement applied to the core
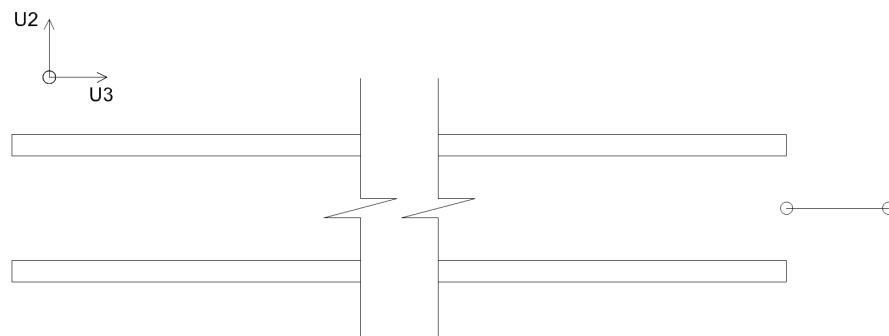
Figure 3.50: Boundary conditions of HSS

point was used so as to restrain the right tip of the Hollow Steel Section (HSS). Other reactions stabilising the casing are provided by the interaction with the grout which was modelled with a tie constraint. Figure 3.50 shows a diagram of the boundary condition used and the location of the reference point in the U3 direction. The grout is tied constrained to the HSS.

3.3.4 Results

Reverse loading on the bracing showed to evolve the distribution on the lateral thrust along time. Figure 3.51 shows key points to consider when analysing the evolution of effects of this loading on the casing. Based on the reasonable agreement found with the experimental data the lateral thrust was measured and associated with the points a-h where b represents the moment where failure occurs or maximum axial force. In this case Δ_1 and Δ_2 are larger than Δ_y being 12 and 24 mm the respective magnitudes of displacement.

From Figure 3.52 we can observe that after the first tensile peaking value (point a), compressive force values are reached before reaching displacement 0 and failure occurs (point b). This is due to a permanent deformation induced during the tensile amplitude, however
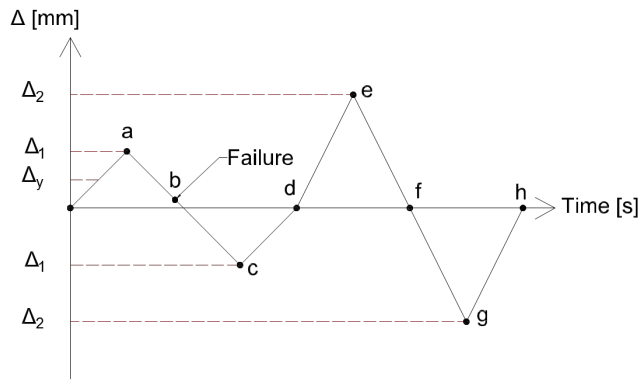
Figure 3.51: Loading applied and points of interest
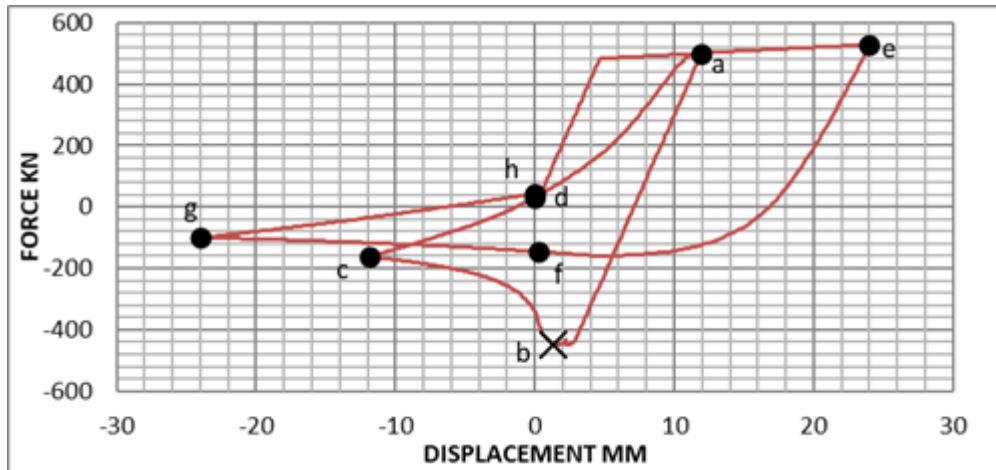
Figure 3.52: Key points of the behaviour in force-displacement curve

as it can be observed from Figure 3.53 the casing has not reach yield values at this stage.

Point c is the pair compressive displacement of the first cycle, the casing has reach yield in

the HSS and at this point it behaves similar to a simply supported beam. From point c to

point e, a nonlinear ascending segment is observed; such a segment indicates that the core

is in contact with the casing as tensile displacement is applied, this is due to yield values

have been reached in the HSS at point c. Point f indicates a decreased force response; the

reason is that tensile displacement in the core does not straighten the casing to its original

position. From Figure 3.53, it can be observed that the casing is presents stresses above the

yield stress (275 MPa), hence the transition from e to g is not abrupt as the transition from

a to c. Finally, the deformed shape in h shows the permanent deformation and the repetition

of the former behaviour.

Table 3.15 shows the values of lateral thrust and axial force; from this table we can observe

that the variation of the lateral thrust is not proportional to the axial force. Furthermore,

lateral thrust can be sometimes even greater than axial force.
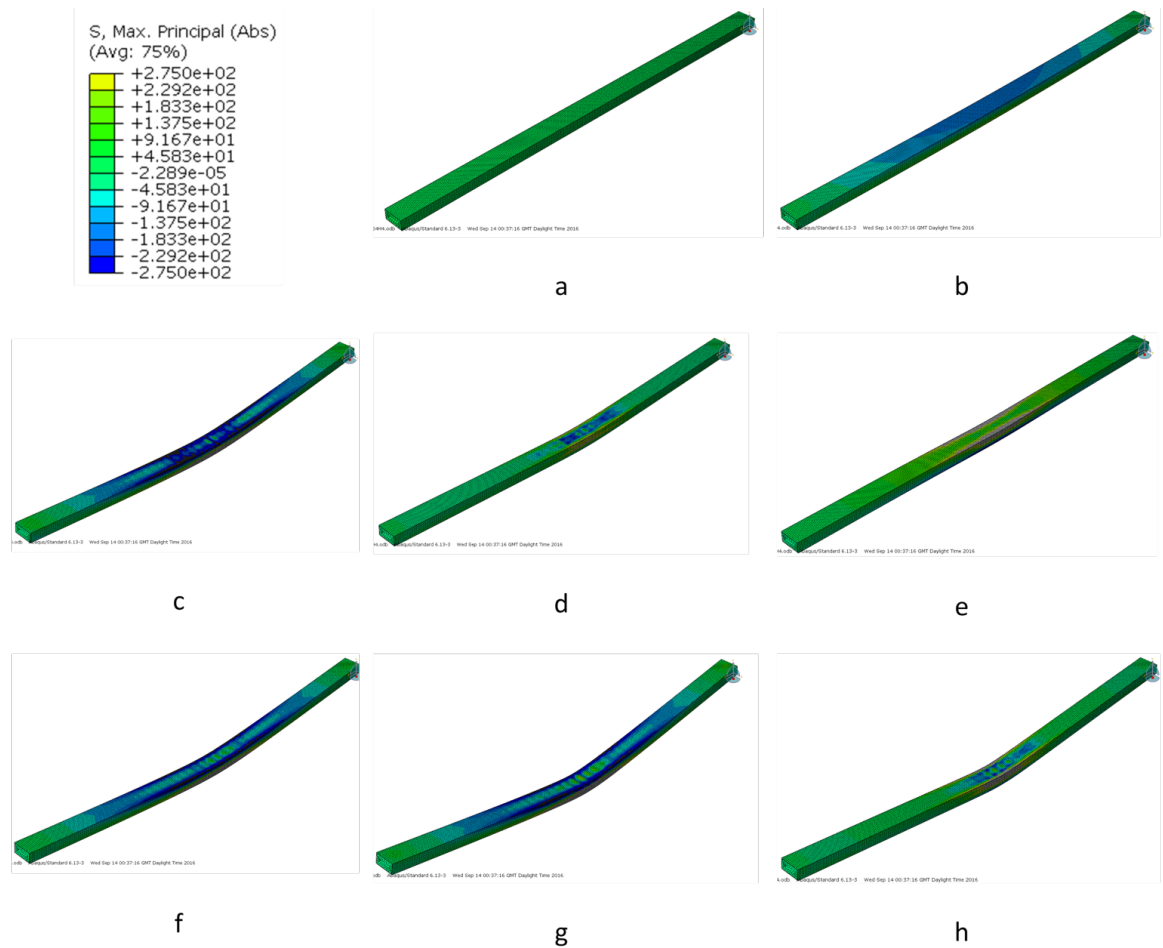
Figure 3.53: Evolution of deformation and principal stress distribution of casing (units in MPa)

Table 3.15: Values of axial force and lateral thrust for different stages of loading

Point	Axial force (KN)	Lateral thrust (KN)
a	499.79	-3.40E-07
b	-449.137	-82.1858
c	-163.013	-314.046
d	31.2795	-70.5729
e	527.958	-80.3126
f	-145.829	-213.188
g	-100.713	-394.04
h	42.3353	-85.2662

Figure 3.54 shows a sensitivity analysis on the strength of the grout in the force-displacement response. From this figure it can be observed that the model is not importantly sensitive to different grades of grout, hence the main contributing element to restrain buckling is the HSS.

From the former statement a comparison of the numerical and analytical solution was conducted. Since the casing behaves as a simply supported beam, lateral thrust value was assumed to be a point load acting at mid span. This force acting at the time of failure is compared with the magnitude of a concentrated force needed to make the section of the HSS
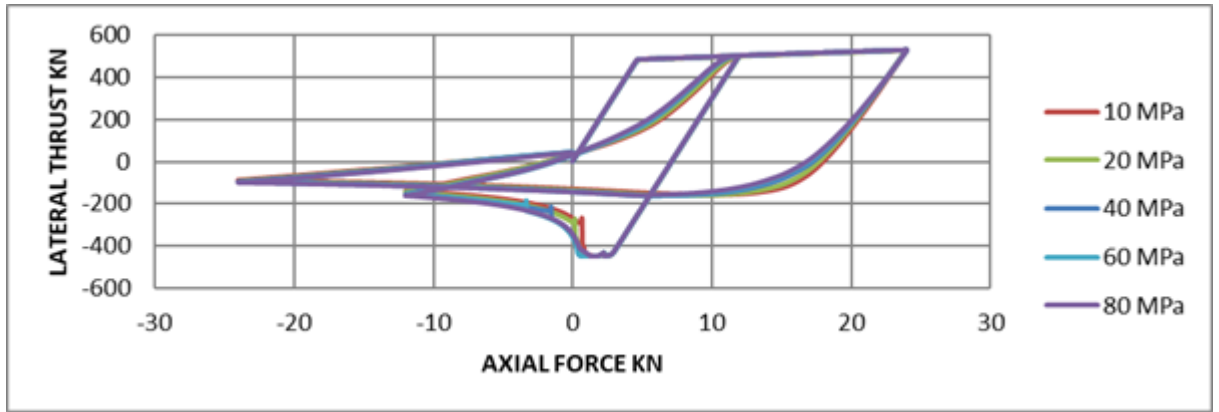
Figure 3.54: Effects of compressive strength of grout on Force-displacement response

yield in the case of a simply supported beam acting at the mid span which can be expressed as equation 3.1.

$$P_{eq} = \frac{4S_x f_y}{l} \tag{3.1}$$

Table 3.16: Section properties of the HSS

HSS	$I_x x (mm^4)$	$\bar{y}\,(mm)$	$S_x\,(mm^3)$	$f_y\,(MPa)$	$M_y\,(KN-mm)$	$P_{eq}\,(KN)$
150x75x4.5	1895360	75	50542.92	275	13899.3	16.8989

The comparison of the forces reveals that even though the casing is not sensitive at the strength of the steel, the grout is contributing in composite action, as the load required to make such a section yield is way lower than the maximum lateral thrust value obtained from the model. Composite action makes the casing more efficient however little information is known about the interface of these two components. Figure 3.55 shows the lateral thrust in function of the displacement; in this figure although failure patterns are not visible the behaviour shows that lateral thrust is proportional to the displacement. Likewise, the figure reveals that no lateral thrust is induced on the lateral sides, which prevents bulging on the casing.

3.3.5 Conclusions

In contrast to the case where the casing can restrain buckling, in this case global bending failure has important implications on the behaviour of the core. Firstly, due to the lack of sufficient flexural stiffness of the casing, lateral thrust magnitude is large enough to produce the formation of a plastic hinge at mid length of the HSS. The force was analysed and compared with the axial forced imposed, where the behaviour could be observed. In contrast

124
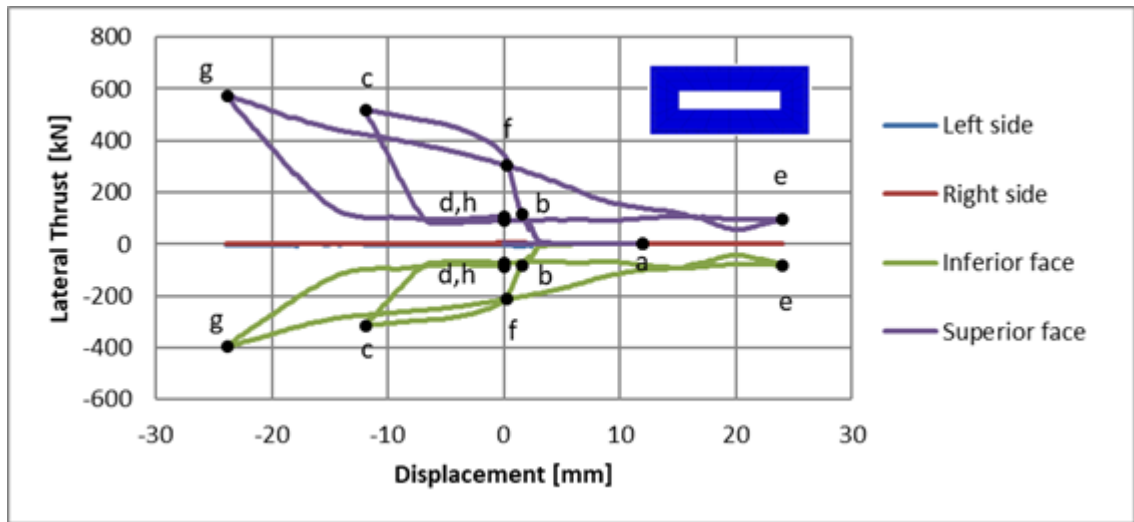
Figure 3.55: Lateral Thrust - displacement response

to section 5 where a non-failed casing was analysed, when bending failure occurs, lateral thrust magnitude is not proportional to the axial force; however displacement remains proportional to this value.

Secondly, failure occurs during the transition from mode 1 to mode 2 of buckling shape where the core buckles about the minor axis of the cross section. At this point, the problem can be simplified to an in-plane equivalent problem. Buckling does not occur in the perpendicular axis due to the sudden loss of axial force (bifurcation point).

It is proposed that the casing bending failure occurs similar to a simply supported beam subjected to a point load at mid span, where the load is correlated to the lateral thrust exerted by the core. In this idealised structure the position of the supports vary according to the displacement induced to the core as the core either lengthens or shortens, however, the effect of such displacement has been assumed as negligible in the proposed limit for flexural strength(Eq. 3.1) since the magnitude of the axial displacement (24mm) compared to the total length of the casing (3290mm) is less than 1%. Therefore the force has also been assumed to be acting at mid span in the proposed formulation.

Likewise the stress values were measured at the bottom and top of the section. It is to be remarked that at failure point, the casing does not reach yield value which implies that the existing methods for dimensioning the casing may be not be necessarily conservative.

3.4 Observations on the quasi-static behaviour of a Buckling Restrained Brace based on numerical analysis

A validated model is used in order to observe the behaviour of the BRB when axial compressive displacement is imposed; this behaviour corresponds to a slender bar (core) under reversed loading forming into a higher mode buckling shape as displacement increases. The evolution of the wave formation is highlighted and described based on two important assumptions: a) no friction and no penetration between core and grout, also b) no moment transfer to the casing from the connections is considered.

The three dimensional FEM reveals the behaviour of the core in terms of the magnitude and distribution of lateral thrust in two directions. Key particularities of bulging condition are explained.

In the previous section a model of a Buckling Restrained Brace was validated against numerical data. The objective of such a validation is to observe the evolution of the core and the force transfer to the casing when this latter can restrain buckling, therefore no failure pattern is involved, however the evolution of the core inside the casing subjected to a reverse loading aims at understanding the stages the core experience in order to transfer the loading to the casing during the compressive stage.

Previous research (Takeuchi et al. 2010;Takeuchi et al. 2012) has addressed the problem of bulging in the casing where the author highlights the relevance of studying this effect. Bulging is a consequence of the contact stress concentration in the major axis inner sides of the grout.

In this study, the evolution of these forces is analysed and quantified so as to understand key aspects on the behaviour and load transfer of the core when the casing is sufficient so as to maintain the core in its position.

Figure 3.56 shows the dimensions and layout of the BRB in study. The casing in contrast to the failed specimen studied in the previous section is sufficient to prevent bending failure. The maximum stress obtained at peaking loading can be seen in section 3.4 Contours in sections observed and deformed shapes
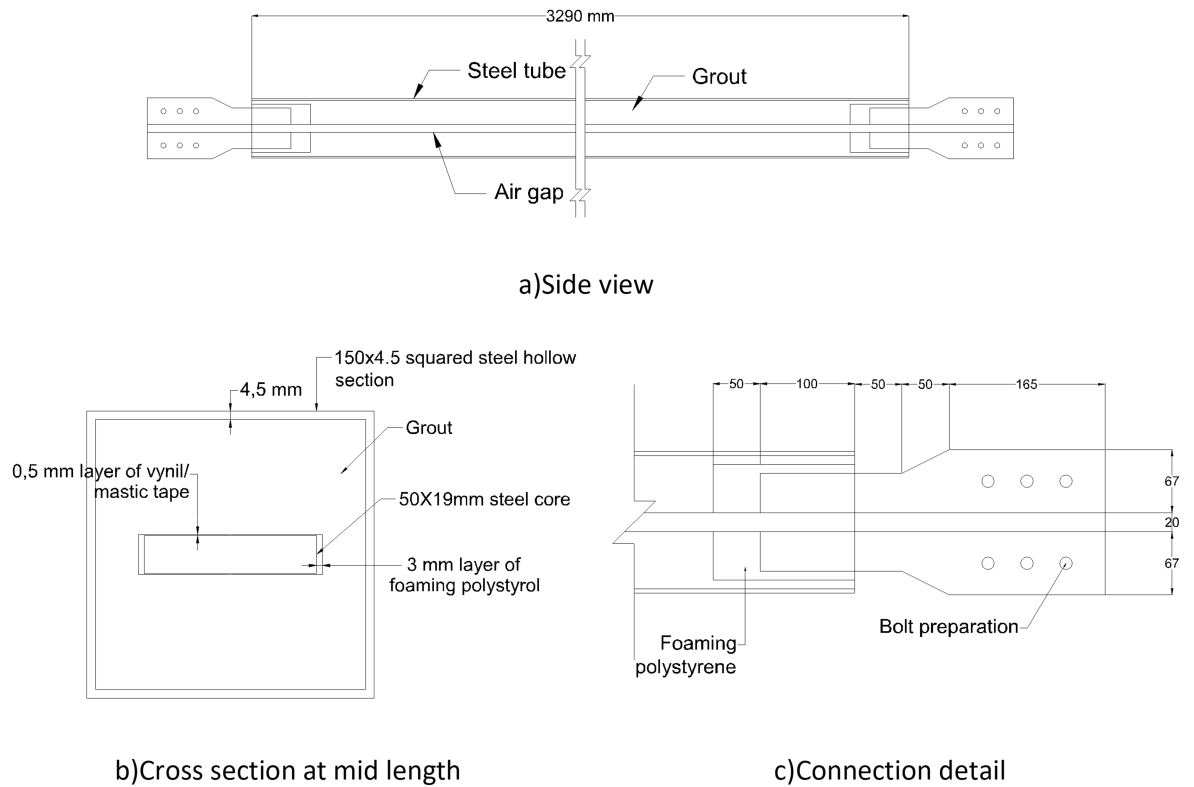
Figure 3.56: Specimen tested in Watanabe et al. (1988)

3.4.1 Core evolution into higher mode buckling shapes

Following the same methodology used in the sub section 4.3, lateral thrust was analysed under the application of reversed loading. Figure 3.58 shows a diagram of the loading applied which consists of 2 cycles of 24 and 48 mm of amplitude respectively. The segment a-c is of particular interest as this is the point where the load transfer begins the at the core-grout interface. From the analysis it could be observed that the core buckles in two directions and that this effect occurs at different times. Figure 3.58 shows the core fully yields in compression, as it can be noticed, a large displacement is to be induced in comparison with the yield displacement observed in tension. Figure 3.57 shows that maximum thrust values are concurrent with maximum axial load.

Table 3.17 summarises general key aspects of the core behaviour and qualitatively explains the evolution into higher buckling mode. It is important to remark buckling about the strong axis (major axis) is the cause of bulging however the parametric study showed that this phenomenon may depend on the proportion of the gap.
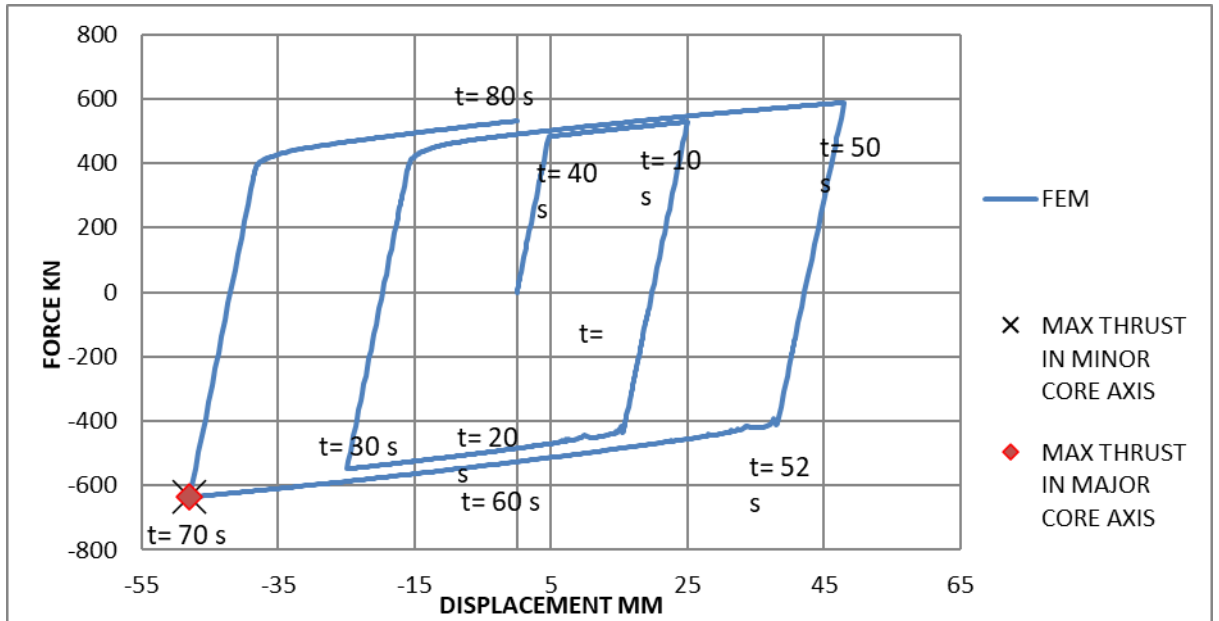
Figure 3.57: Maximum values for lateral trust in force displacement curve
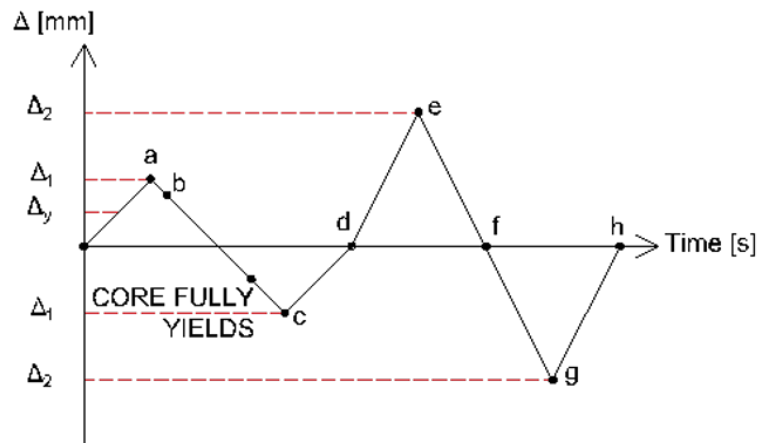
Figure 3.58: Axial displacement imposed and key points to highlight

3.4.2 Analysis of lateral thrust

Figure 3.59 shows the total magnitude of lateral thrust being applied at each face. This value was obtained by integrating the contact stress on each side, each increment of time. The figure shows that the lateral thrust in the upper and lower face (minor axis) are always larger however numerical error can be seen as the forces applied on opposite sides are not the same magnitude. The source of error possibly comes from the contact problem as the behaviour of the core is not symmetric; hard contact was considered and slip between the two surfaces is involved. It is likely that a more refined and compatible meshing on the surfaces is required. From these figures we can observe that even though the lateral thrust can reach values comparable to the axial force

Table 3.17: Evolution in higher buckling mode of core

Segment/point	Description
0-a	Yield starts at a stress of 282 MPa and strain of 0.00141
a	Tensile loading stops producing permanent deformation as the core is in beyond yield values
a-b	Elastic deformation is recovered and the bar starts working in compression. The first buckling mode triggers immediately about the minor axis and contact occurs
b-c	As load increases, the second mode is formed. The axial load increases due to strain hardening and wave formation as observed by Chai (1998)
b-c	After the 4th mode about the minor axis the first buckling mode is triggered in the perpendicular direction (major axis) and contact with grout occurs. Hence the lateral thrust is applied at one point contact
b-c	As load increases the former point contact becomes a line contact. Producing a shorter bar segment subjected to axial force and bending moment which will trigger the 3rd buckling mode
b-c	When the 3rd buckling mode is formed about the major axis yield valued are reached however yield only occurs in specific areas and this condition is not uniform along the core
b-c	Core fully yields when 17 waves are formed in the minor axis and no more waves were formed in the major axis. From this point changes in the buckling shape are minimal. Moreover, the contact points become lines of contact
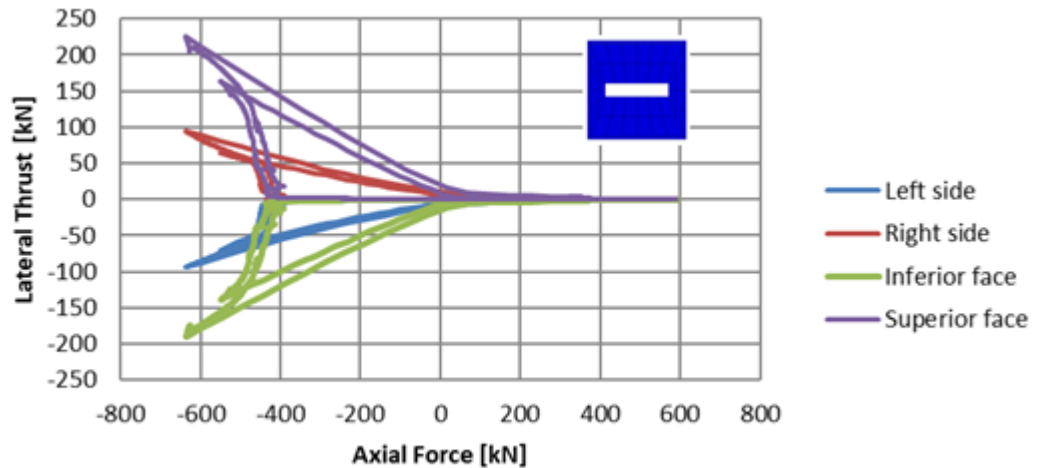
a)Lateral thrust-axial force curve
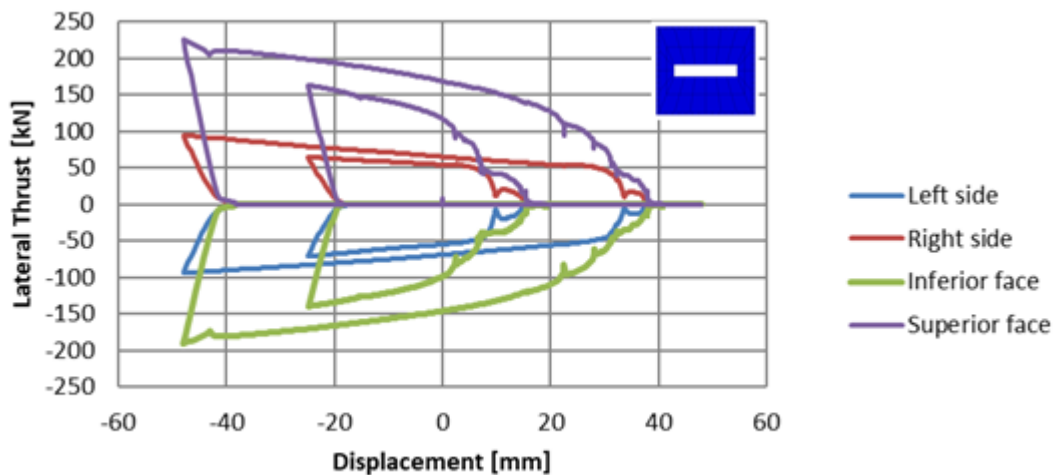
b)lateral thrust – axial displacement curve

Figure 3.59: Lateral thrust in function of a)axial force and b) displacement

Table 3.18: Distribution and total thrust along the core

| | Gap = 0.5 mm | | | | | | | |
| | Minor Axis | | | | Major Axis | | | |
| | Top | | Bottom | | Left | | Right | |
Number	F KN	x mm	F KN	x mm	F KN	x mm	F KN	x mm
1	-2.35	0	11.01	1.30E+02	12.16	1.40E+02	25.42	8.62E+02
2	-5.69	271	12.52	4.10E+02	20.26	1.60E+03	23.64	2.30E+03
3	-6.33	591	15.03	7.90E+02	12.52	3.00E+03		
4	-6.53	966	4.11	1.10E+03				
5	-5.97	1193	3.91	1.30E+03				
6	-13.02	1420	7.16	1.60E+03				
7	-15.17	1788	7.53	2.00E+03				
8	-16.55	2104	8.21	2.30E+03				
9	-18.12	2409	8.34	2.30E+03				
10	-8.27	2736	11.57	2.90E+03				
11	-6.63	3065	3.99	3.20E+03				
Total Thrust	-104.62		93.37		44.95		49.06	

Table 3.18 shows the distribution of lateral thrust exerted on the nodes of the inner faces of the casing. The total thrust shows that the summation of contact forces about the major axis (left and right faces) is less that the forces acting in the other direction (inferior and superior faces), however, the force magnitude is larger in that direction which is what makes the casing vulnerable to bulge. From this table we can also observe a numerical error since the summation of thrust nodal forces exerted on one surface is not the equal to the summation of thrust forces exerted on the opposite surface.

3.4.3 Parametric study and remarks on observed core behaviour

Once a good agreement with the experimental data was found, parameters were varied so as to measure the sensitivity of the device to these. In the case of friction (Figure 3.60), the force displacement response showed to be moderately sensitive however the analysis is incomplete as lateral thrust and other responses should have been addressed in order to provide a subjective statement. Nonetheless, the results show to increase the compressive force by approximately 10%

In the case of the size of the gap, the model showed to be highly sensitive as it can be seen from Figure 3.61 where the formation of the buckling modes can be seen in the compression branch of the force displacement curve. The net lateral thrust value rose to 10 times more than when a gap increase is not considered (0.5mm). Moreover, there is a noticeable discrepancy when increasing the gap by 0.5 mm (gap 1 mm, see Figure 3.62). Finally lat-
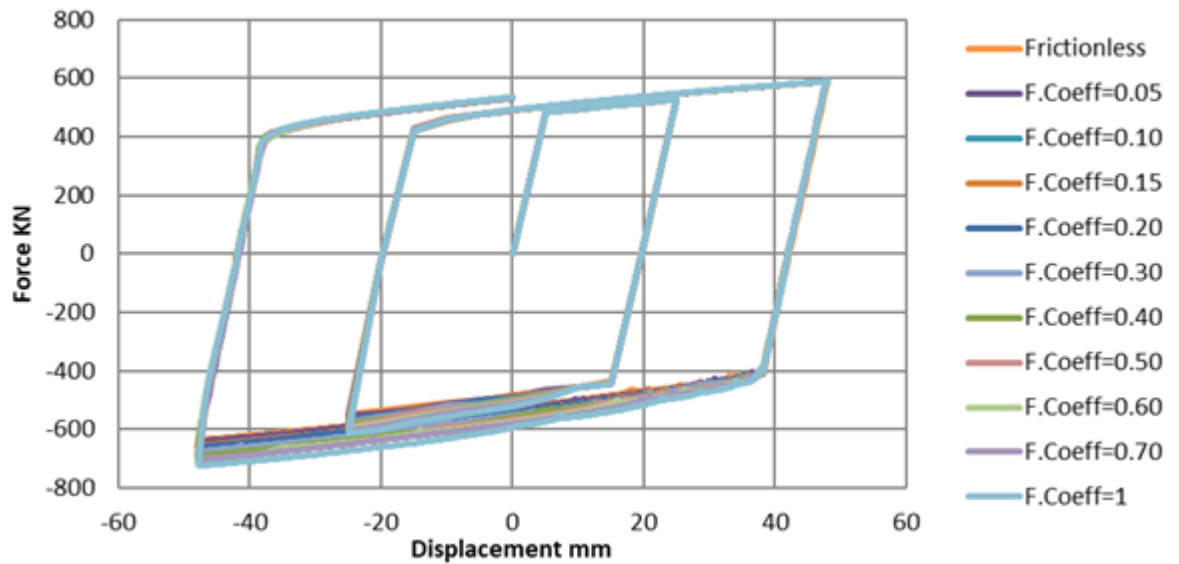
Figure 3.60: Effects of friction in terms of force and displacement
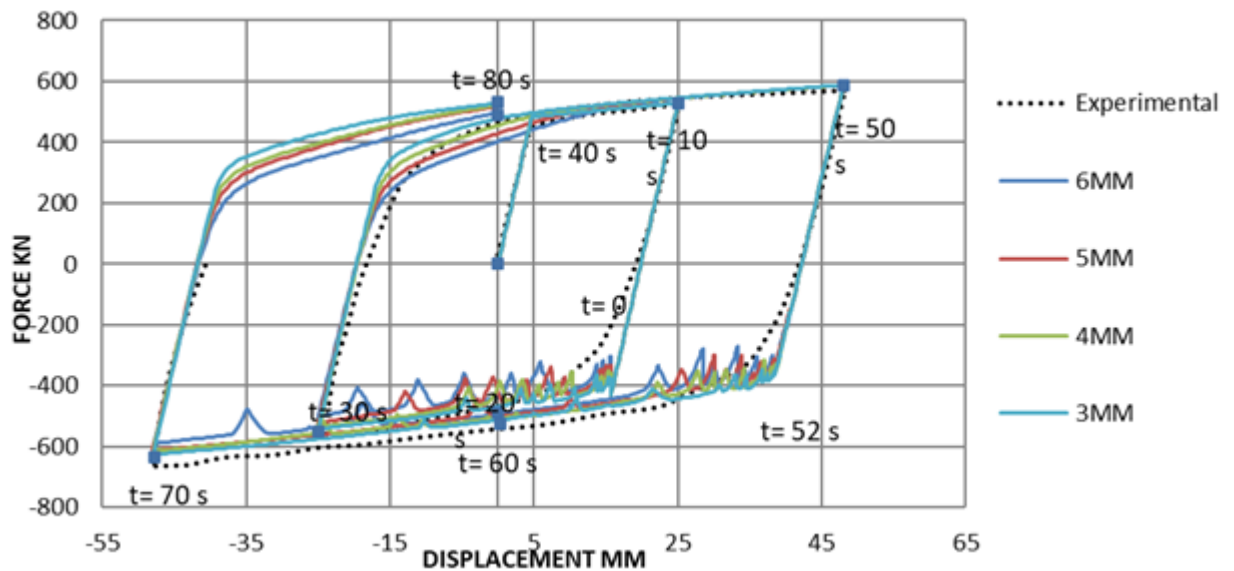
Figure 3.61: Effects of size of the gap

eral thrust about the strong axis seems to decrease when the gap is increased in 1 direction.

Observations on the behaviour were explained quantitatively; however general conclusions could be obtained in order to be applied in different BRBs.

The behaviour of the core can be described as follows:

As displacement increases the first buckling mode is triggered in the weak axis direction. Lateral displacement increases in a larger proportion until contact with the grout occurs at one point (pre contact) Once the core is in contact with the grout, the contact surface transits from a point to a surface, thus creating a reduced length column. If during this transition the stiffness of the casing is sufficient to provide a reaction so that the core remains in
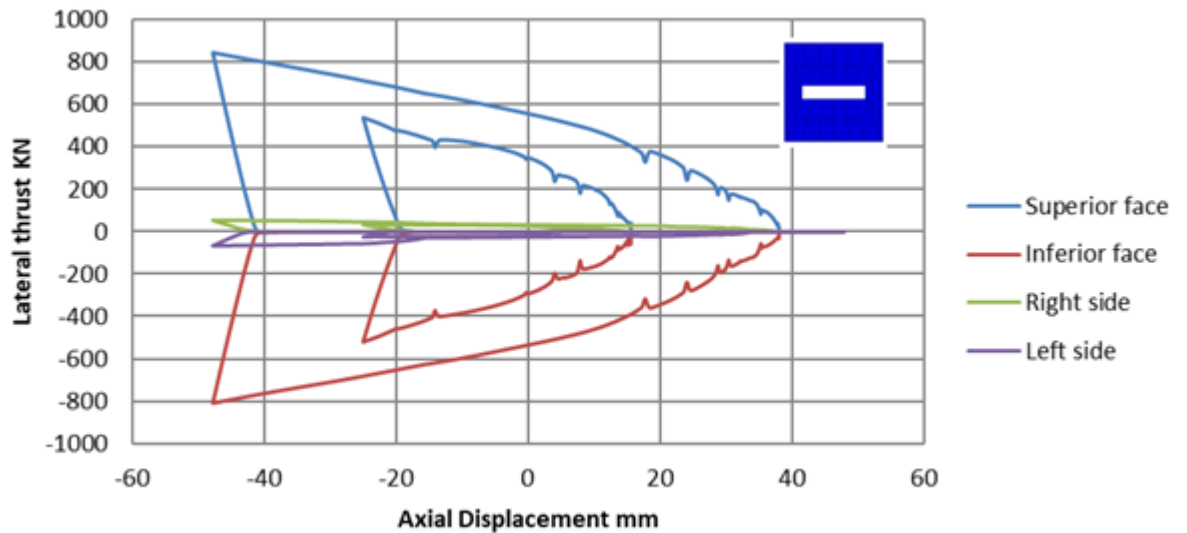
a) Gap 1 mm
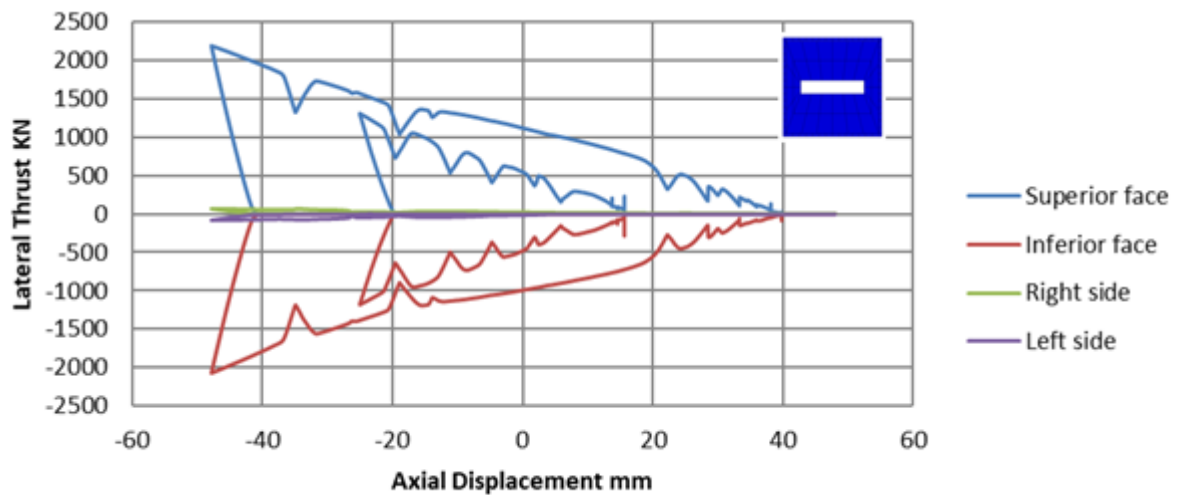
b)Gap 6 mm

Figure 3.62: Effects of size of gap in terms of lateral thrust

its initial position (within the gap), the core will increase the length of the contact surface until the load is sufficient to make the 'sub column' buckle, creating a higher mode formation and wave number increase. If the lateral displacement of the casing produced by this lateral thrust overpass the critical value, the system becomes unstable.

Once bending failure occurs, the casing is still able to dissipate energy having smooth ductile transitions from tension to compression and vice versa, however the dissipated energy is due to the ductility of the casing under bending conditions and the energy dissipation capacity is reduced importantly, however stability is recovered.

It is important to mention that axial force is not proportional to lateral thrust which suggests that axial force based criteria for stability of BRBs could be better treated by analysing the problem in terms of displacement in order to quantify the limits of the casing.

From the analysis the core behaves similar to the problem of a bi-laterally constrained column which has shown to be a highly non-linear problem. Buckling higher mode formation occurs in the 2 axes perpendicular to the application of the load where waves are formed as load increases, this occurs at different times for each axis. In this case, the casing shows to be stable in agreement with the experimental evidence.

In terms of lateral thrust, the magnitude of the force also increases in both directions at all stages of axial compressive displacement however the distribution varies depending on the second moment of area of the core. In the parametric investigation the lateral thrust is highly sensitive on the gap size. The lateral thrust for a gap size of 6mm was approximately 2.5 times more than in the case of a gap of 1 mm, likewise the influence of the friction requires further examination as even though the force displacement response does not appear sensitive.

The wave formation of the core starts with no yield stress values and the evolution shows that a high number of waves are required in order to make the core fully yield. Furthermore, minor changes in the lateral deformation are identified in the post- yield behaviour.

The model suggests that the lateral thrust about the strong axis is reduced when increasing the gap in the minor axis direction, this effect requires further study.

3.5 Equivalent Plane Stress FE Models for Grout-Filled Buckling Restrained Braces (Conference paper)

In chapter 3, one of the identified limitations of BRB research was the computational cost to analyse Grout-Filled BRB models by using a 3D model, this has a great impact in the effective investigation of GFBRBs which highly relies in Finite Element Models to estimate the performance, such models are normally conducted in 3 dimensions. Regardless the method of choice, whether implicit or explicit, the computational cost often poses a serious problem and raises the question whether BRB models require to be examined with such detail or excessive complexity is being used.

Genna and Gelfi (2012a) showed the feasibility of using a Plane Stress approach to model (Figure 3.65) an All-steel BRB pointing an improvement in terms of computational cost.
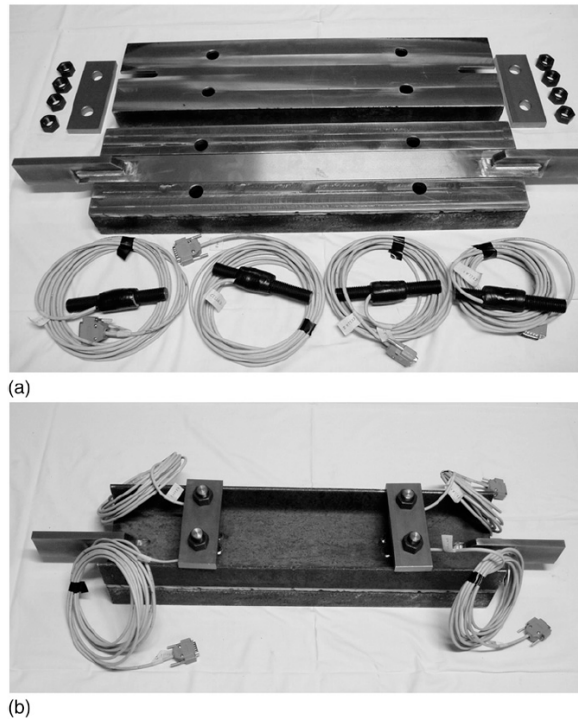
Figure 3.63: ABRB from Genna and Gelfi (2012a)
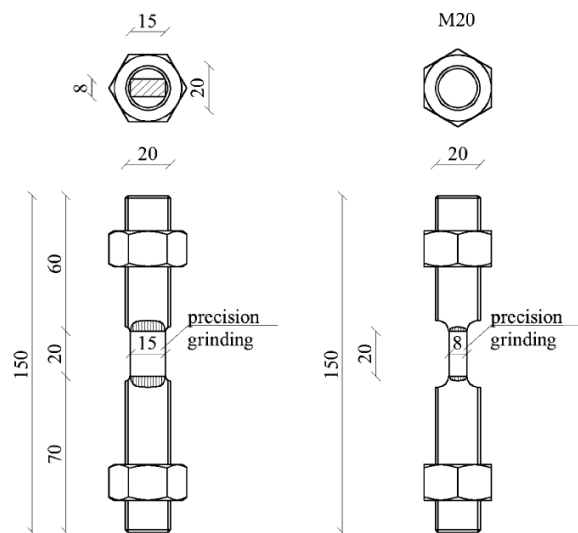
Figure 3.64: Instrumented bolts from specimen in Genna and Gelfi (2012a)

Although no comparison with a 3D model is used, the computing time was in the order of hours (42000s for cyclic and 7000s for monotonic) which is significantly less than in the models analysed in chapter 3 which were calculated in the order of days.

Although this innovative technique translates into an important contribution to the study of All-steel BRBs, it cannot be used directly in Grout-Filled BRBs since the specimen casing in Genna and Gelfi (2012a) is not a grout infilled tubular structure. The specimen comprised a core plate encased in a sandwich section formed with 2 bolted channels (Figure 3.63); the bolts of the specimen were instrumented with strain gauges(Figure 3.64), there-
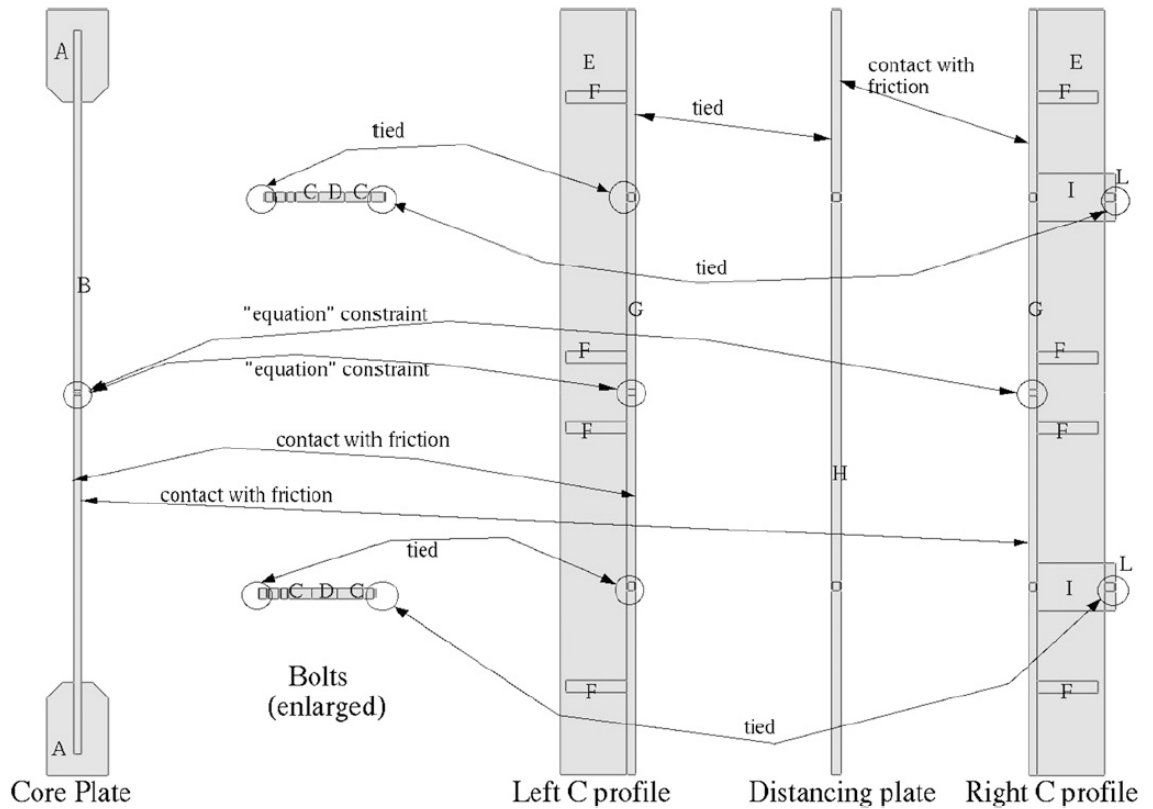
Figure 3.65: 2D FE model from Genna and Gelfi (2012a)

fore, the integration of the forces applied of the bolts equated to the lateral thrust.

The resent methodology proposes the use of the transformed section of a Grout- Filled Buckling Restrained Brace (GFBRB) casing to obtain 2 equivalent 2D problems with a significantly reduced number of elements similar to an All-steel equivalent sandwich structure which behaviour resembles that of the GFBRB casing within the elastic range. Therefore, the core behaviour such as higher-mode buckling shape formation and lateral thrust can be obtained with ease in both minor and major directions; also the Ultimate Limit state of the casing in the form of global buckling can be correctly captured by this technique. Although some limitations are identified, it is intended to pave the way to accelerate future research conducted on GFBRBs.

3.5.1 Introduction

Numerical analysis has been shown to be an important and economically effective tool to analyse both All-Steel Buckling Restrained Braces (ASBRBs) (Genna and Gelfi 2012a; Genna and Gelfi 2012b; Metelli, Bregoli, and Genna 2016) and Grout-Filled Buckling Restrained Braces (GFBRBs), however the analysis of the full device has usually only been

conducted with 3D Finite Element Models which in turn require a large amount of comput-
ing resources to extract results. Key output such as the force-displacement and lateral thrust
along the casing and the evolution of the core in higher buckling mode shapes (Wu and Mei
2015) are required in order to understand the behaviour of the system.

Existing available numerical studies of GFBRBs fail to analyse the forces exerted on the
inner surface of the casing due to the difficulty in quantifying this value experimentally, al-
though some data exists for ASBRBs. Coupled with the relative lack of experimental data,
the computationally expensive nature of 3D models remains one of the main obstacles in
exploring BRB behaviour. Hence use of more efficient, equivalent 2D models represents an
attractive alternative.

3.5.2 Methodology

Two experimental studies corresponding to an ASBRB and a GFBRB were used for vali-
dation purposes (Genna and Gelfi 2012a; Watanabe et al. 1988) where a rectangular area
equivalent to the flexural stiffness provided by the system's structural section was obtained
(Figure 3.66). In the case of the ASBRB, for the calculation of the second moment of area a
single channel section UPN160 was calculated equal to 8.5E+05 mm4 and transformed to a
rectangular section, while maintaining a constant Young's modulus. In the new section the
base of the rectangle is equal to the width of the core (50 mm) and h=59mm was calculated
with **Equation 3.2**.

$$h = \sqrt[3]{\frac{12I_{UPN160}}{b}} \tag{3.2}$$

Where h is the height of the equivalent rectangular cross section, b the core width and the
second moment of area of a single channel section (=850000mm4). For each case, 2 mod-
els were used (3D and 2D) in order to compare computational costs. In the case of the AS-
BRB 3D model, the curved corners/edges of the channel section were considered as right
angles which resulted in minor modification (1mm) of the height of the rectangular section.
The numerical results showed a good agreement with experimental data.

a)Cross section

b)Equivalent cross section
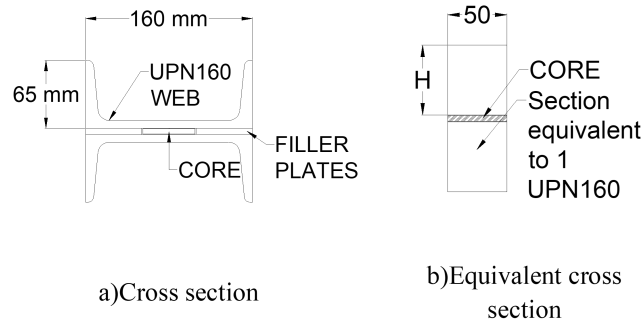
Figure 3.66: Specimen and equivalent cross section

a)effective cross section

b)transformed section
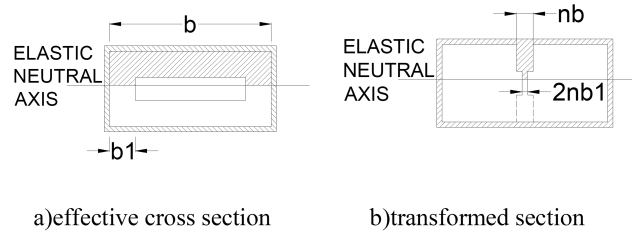
Figure 3.67: Effective cross section of GFBRB

In the case of the GFBRB the equivalent cross section was found by following a three step procedure: i) find the Elastic Neutral Axis and the transformed section with the factor $n = E_{concrete}/E_{steel}$ ii) determine a rectangular cross section equivalent to the second moment of area of the transformed section iii) define a linked double beam system with half of the second moment of area value for each beam. The Elastic neutral axis was found within the narrow grout section (gap) as shown in Figure 3.67a using the transformed section method, located at a distance of 34.38 mm measured from the top of the cross section.

Similar to the case of the ASBRB, equation 1 was used in order to determine a gross section with the same second moment of area with a width of 90mm (width of the core) and height of heq. The modelling method entails proposing a 2D linked beam system (see Figure 3.68) which avoids composite action in such a way that each beam provides half of the value of second moment of area with height $h_{I/2}$ using **Equation 3.3**.

$$h_{I/2} = \frac{1}{\sqrt[3]{2}} h_{eq} \tag{3.3}$$

It is assumed that the linked beam system is equivalent to 2 beams working together where composite action does not take place as there is slip between them and no shear restriction is provided since the link connections to the beams are pinned. Let us consider the internal

137

a)Cross section of   b)Cross section of casing in
equivalent casing (I)   2D model (I/2 each)
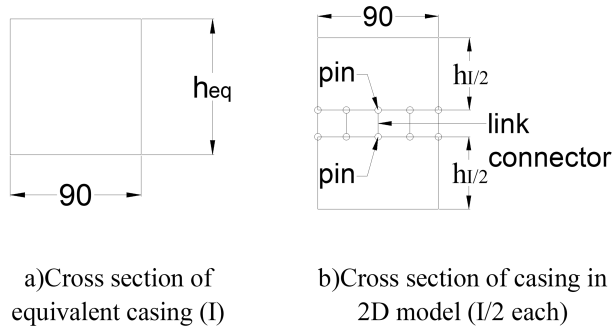
Figure 3.68: Proposed cross section for 2D FEM

a)Equivalent 2D beam

b)Linked beams with I/2 each
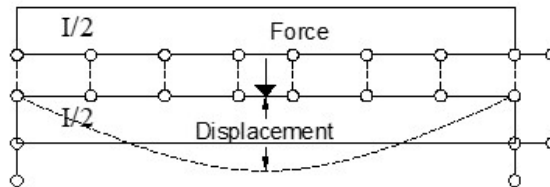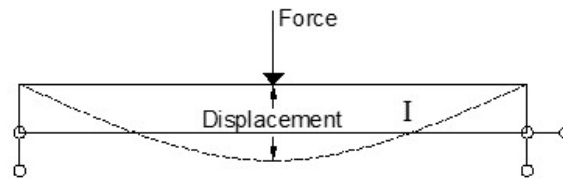
Figure 3.69: Idealisation of equivalent structure

forces of either beam in Figure 3.69b, the axial force is zero and therefore no pure moment is provided by the cross section; hence, the beams work in pure bending. Since the sections work separately, the flexural stiffness can be divided by 2 in order to keep the problem symmetric.

The flexural stiffness equivalence was verified by applying a vertical displacement at the mid length of the casing model as shown in Figure 3.69, correspondingly Figure 3.70 shows that the behaviour of both cross sections is the same in the elastic range, hence; the behaviour is equivalent before a vertical displacement of 55 mm where material nonlinearities appear.

Following generation of the equivalent 2 models, the results are used to compare axial force-displacement and lateral thrust against experimental data available. Also, computing time is compared with the 3D models.
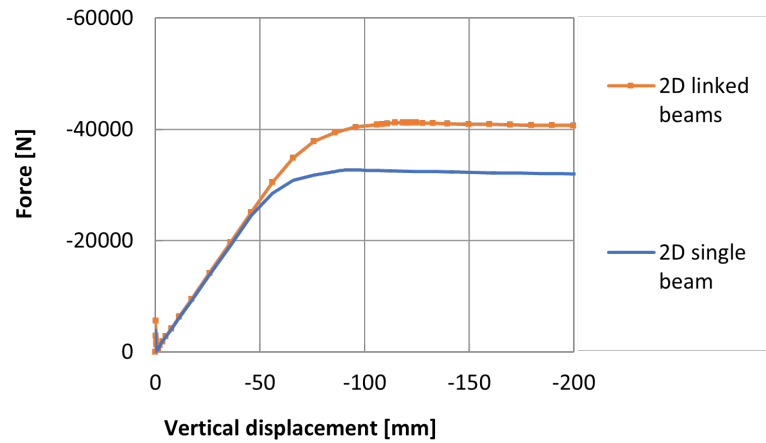
**Figure 3.70:** Force displacement curve for lateral point load

3.5.3 Results of Numerical Model

The numerical analysis was conducted using the software ABAQUS assuming plane stress conditions with a dynamic implicit solver. The 8-noded quadratic elements CPS8R were used for the analysis. The 2D models used only a fraction of the number of elements in the 3D models, 12.2% (1120 elements) and 15.4% (3960 elements) for ASBRB and GFBRB respectively.

The material properties used to model the steel of the core were set as nonlinear with kinematic hardening with σ_y= 250 MPa, C1=8000, γ1=50, C2=100000 and γ2=1000. The casing is assumed as a perfectly elasto-plastic material with σ_y= 282 MPa; in both cases the Young's modulus and Poisson's ratio are considered as 200000MPa and 0.3 respectively.

Figure 3.71 and Figure3.72 show the results of the validated model of ASBRB. The model shows an overall good agreement with both experimental data and the experimenters' own model; however some discrepancy between the experimental and numerical results can be observed. Clearly the idealisations of the equivalent 2D model, along with boundary condition and material simplifications all introduce a degree of inaccuracy. Some additional discrepancies may be introduced from the digitisation of the experimenters' data. Note backbone curves which outline the extents of the hysteresis are used here for visual clarity.

In the case of the GFBRB Figure 3.73 compares the results of the hysteretic axial behaviour of the device obtained from the 2D and 3D models. The 2D and 3D model exhibit similar failure conditions which take place during the first cycle in the compressive range. How-
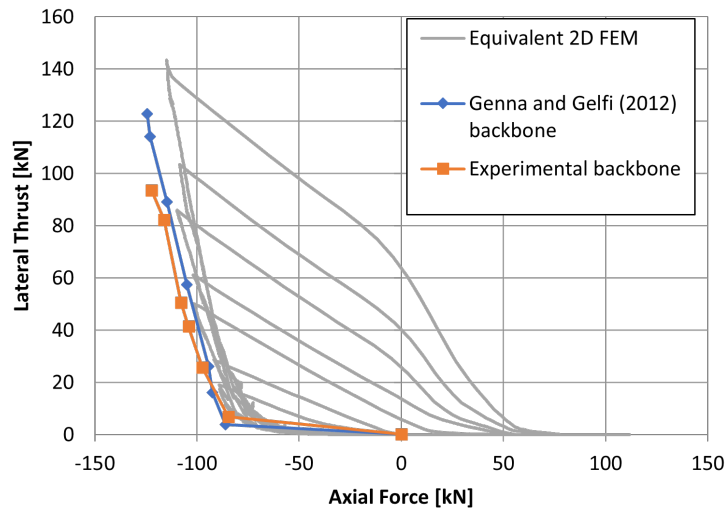
Figure 3.71: Validation of ASBRB in terms of lateral thrust
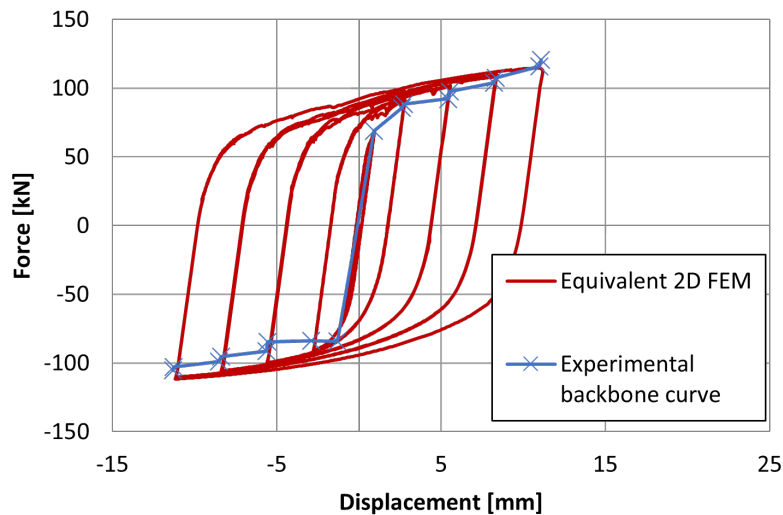
Figure 3.72: Validation of ASBRB in terms of force-displacement

ever, the behaviour differs in the post failure range due to the assumptions made in modifying the geometry to an equivalent rectangular section and the distance from the elastic neutral axis to the outermost fibre.

3.5.4 Conclusion

It is possible to study stability of GFBRBs by conducting 2D analysis, taking advantage of significant reduction in computational cost. Table 3.19 shows the effective reduction of computing time for the 2 studies presented here. The 2D models were analysed in less than 10% of the time used by a 3D analysis and successfully captured the global behaviour and estimation of the lateral thrust from the core. However, there are clear limitations of this method when modelling post failure effects as the casing transformed section is valid only
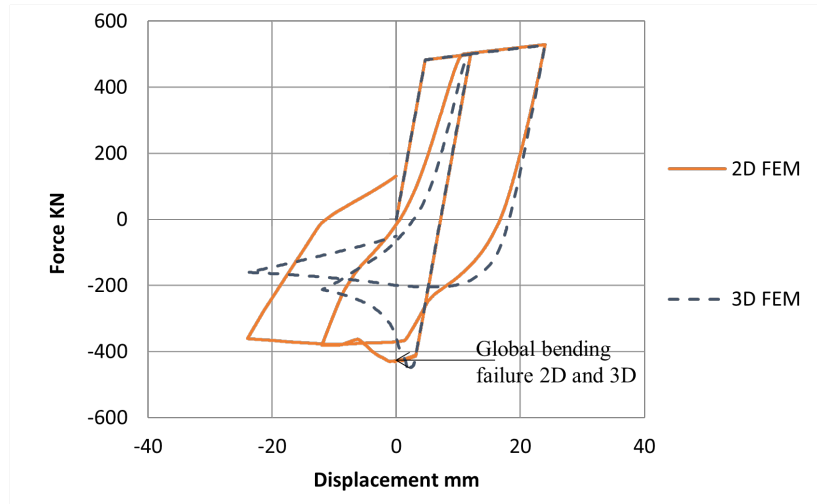
Figure 3.73: Numerical Results of 2D FEM of GFBRB hysteretic behaviour

for elastic conditions. Figure 3.73 reveals an important loss of accuracy in the post fail-
ure range. Although the model is valid for global stability checks, local buckling such as
bulging of the casing is unable to be captured. Improvement of these shortcomings will be
investigated as part of the authors' ongoing research.

Table 3.19: Reduction in computational time

BRB	Model	CPU time [hrs]	Reduction time
ASBRB	3D	153.36	–
	2D	2.61	98.30%
GFBRB	3D	89.01	–
	2D	5.14	94.20%

Bibliography

American Institute of Steel Construction (2005). "Seismic Provisions for Structural Steel Buildings". In: *Seismic Provisions for Structural Steel Buildings* 1, p. 402.

Chai, Herzl (1998). "The post-buckling response of a bi-laterally constrained column". In: *Journal of the Mechanics and Physics of Solids* 46.7, pp. 1155–1181. ISSN: 00225096. DOI: `10.1016/S0022-5096(98)00004-0`.

Genna, Francesco and Piero Gelfi (2012a). "Analysis of the Lateral Thrust in Bolted Steel Buckling-Restrained Braces. I: Experimental and Numerical Results". In: *Journal of Structural Engineering* 138.10, pp. 1244–1254. ISSN: 0733-9445. DOI: `10.1061/(ASCE)ST.1943-541X.0000564`.

– (2012b). "Analysis of the Lateral Thrust in Bolted Steel Buckling-Restrained Braces. II: Engineering Analytical Estimates". In: *Journal of Structural Engineering* 138.10, pp. 1244–1254. ISSN: 0733-9445. DOI: `10.1061/(ASCE)ST.1943-541X.0000564`.

Metelli, Giovanni, Guido Bregoli, and Francesco Genna (2016). "Experimental study on the lateral thrust generated by core buckling in bolted-BRBs". In: *Journal of Constructional Steel Research* 122, pp. 409–420. ISSN: 0143974X. DOI: `10.1016/j.jcsr.2016.04.004`.

MIT (2017). *Three-dimensional solid element library*.

Mughrabi, H (1987). "Johann Bauschinger, pioneer of modern materials testing". In: *Materials Forum*. Vol. 10. 1, pp. 5–10.

Razavi Tabatabaei, Seyyed Ali, Seyyed Rasoul Mirghaderi, and Abdollah Hosseini (2014). "Experimental and numerical developing of reduced length buckling-restrained braces".

In: *Engineering Structures* 77, pp. 143–160. ɪssɴ: 01410296. ᴅoɪ: `10.1016/j.engstruct.2014.07.034`.

Watanabe, Atsushi et al. (1988). "Properties of brace encased in buckling-restraining concrete and steel tube". In: *9th World Conference on Earthquake Engineering* IV, pp. 719–724.

Wu, Bin and Yang Mei (2015). "Buckling mechanism of steel core of buckling-restrained braces". In: *Journal of Constructional Steel Research* 107, pp. 61–69. ɪssɴ: 0143974X. ᴅoɪ: `10.1016/j.jcsr.2015.01.012`.

Chapter 4

Experimental and Numerical Investigation on the feasibility of PVC casings for Grout-Filled BRBs

Polyvinyl chloride (PVC) is a very popular material used mainly for drainage. PVC can be obtained with ease at a low cost and is highly versatile, making it possible to assembly pipelines of reduced length in a reduced time frame. PVC is one of the possible alternative materials that could form part of the BRB assembly comprising the tubular structure. Although PVC has not yet been explored for such a purpose, important attempts have been made using other types of materials such as Glass Fibre Reinforced Polymer (GFRP) (Sun et al. 2019), Carbon Fibre Reinforced Polymer (CFRP) (Jia et al. 2017) and bamboo (Jones 2011).

In the validation chapter, modelling techniques were deployed and compared against existing experimental data. Also, it was concluded that due to the extensive number of assumptions BRB models can only be validated against an experiment so all the assumed factors can be characterised reasonably. Therefore, one of the main challenges of investigating new casings is that experimental data needs to be obtained through the testing of coupon samples of the material in question, which in this case is PVC.

In this chapter a numerical and experimental investigation of Grout-Filled BRBs using PVC as a tubular structure is presented, in the study, coupon samples were obtained from the PVC and were tested in tension using a Universal Testing Machine. The PVC BRB speci-

Figure 4.1: Testing of PVC samples

Figure 4.2: Tested PVC coupon samples

mens were designed to the theoretical framework that is still used up to date.

Figure 4.3 shows the ductility of the samples which were tested by applying a displacement at a rate of 10 mm/min which was assumed as slow. In all cases, necking was observed, however, the PVC specimens failed to exhibit fracture as a form of failure under quasi-static tensile load. The testing was stopped at 50 mm which is the maximum displacement allowed by the Universal Testing Machine (UTM) used.

During testing, it was observed that the samples developed necking as shown in the coupon samples in Figure 4.2, this effect is due to the relaxation features of the material at constant load. Figure 4.4 shows the behaviour of the last sample when the displacement is stopped and kept constant for a few seconds to then be continued, this was done for illustrative purposes only. No relaxation effects were quantified or considered in the numerical analysis.

Figure 4.5 shows measurements taken from the wall thickness of the PVC casing in order to
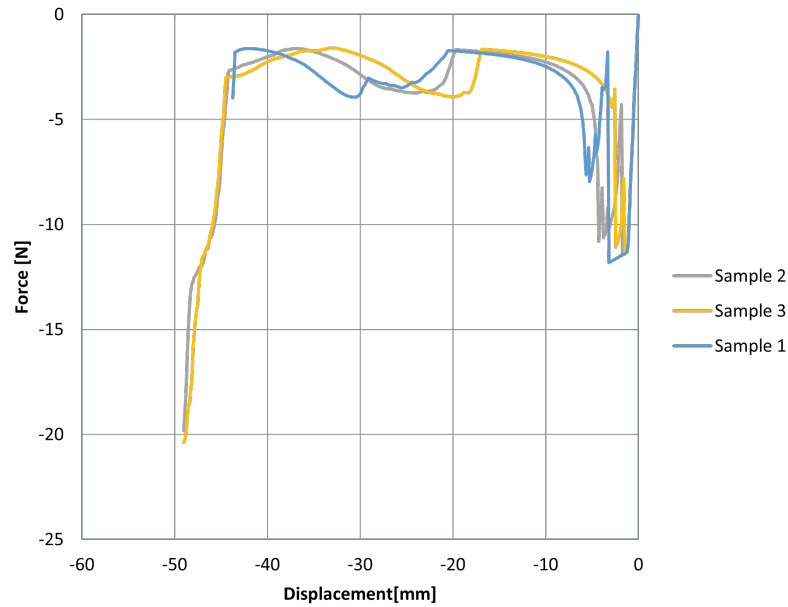
Figure 4.3: Ductility of PVC samples
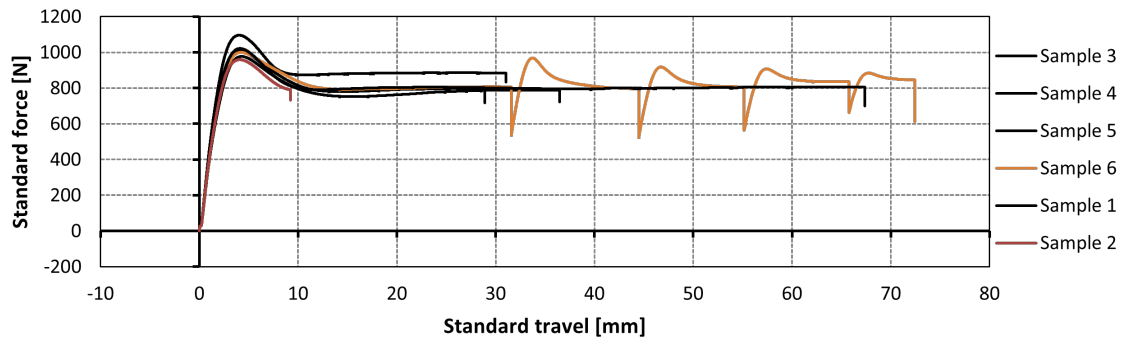
**Figure 4.4:** Relaxation spikes in PVC ductile zone

quantify how constant or smooth is the thickness in all the perimeter. Likewise, the value of average thickness was obtained for later use in the Finite Element Model. Figure 4.6 shows the stress-strain curve for the PVC, however, it only applies for the elastic range and, as mentioned earlier, only for PVC loaded at a slow rate.

4.1 Method Statement

The experimental design was based on the capacity and features of the equipment available in the lab, in this case, the equipment consisted mainly of a cyclic testing machine of the type INSTRON (see Figure 4.7 with a capacity of 500 KN. The main constraint in using this equipment was the size of specimens that could be tested, these can be up to 1-metre length and only a maximum diameter of 42 mm can be used to fit in the clamps using either
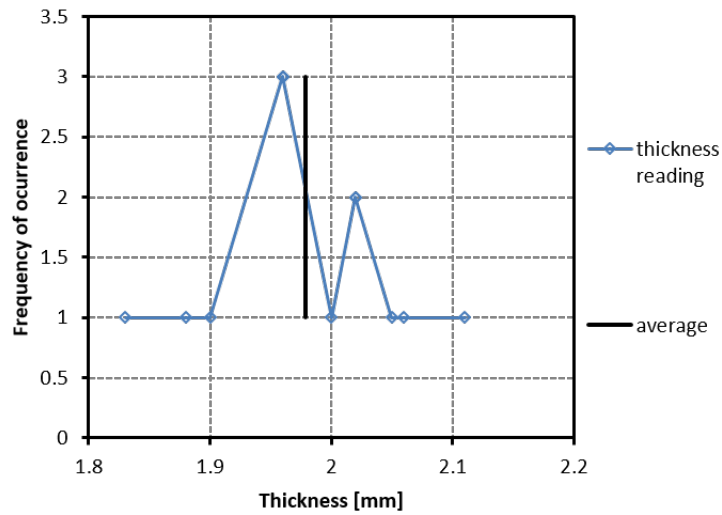
Figure 4.5: A sampling of the thickness of PVC casing
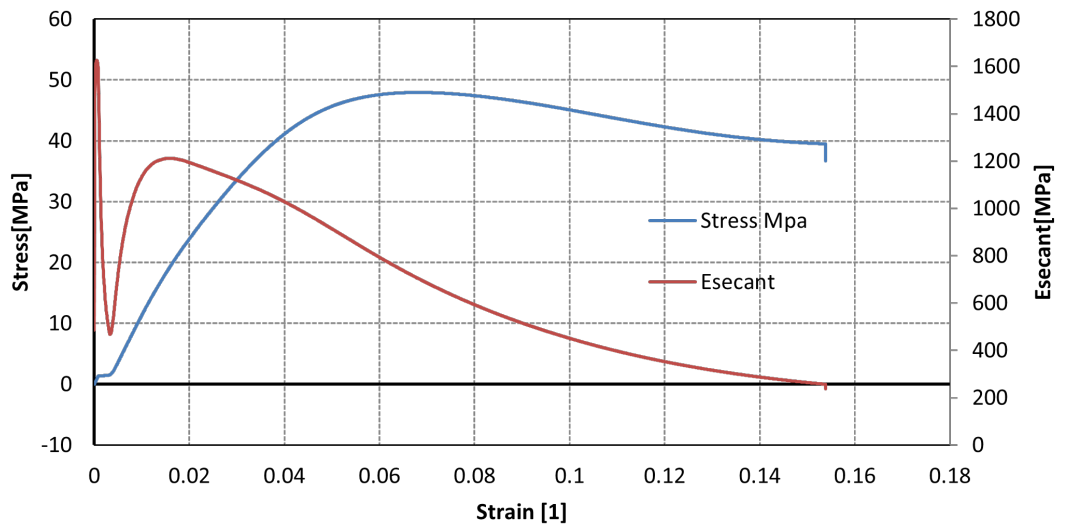
Figure 4.6: Stress-strain curve of PVC coupon and Secant modulus

squared or circular connections.

The dimensions constraints from the INSTRON governed the design of the specimens and defined and allowed to conduct the first iteration of specimen detailing. With the connection CHS of a maximum of 42mm, it was necessary to limit the width of the core plate that is bolted in the circular section.

For the PVC casing, a squared hollow core section was used, these sections are often used as downpipes. Although no specification for this material was obtained, it was possible to conduct a characterisation study by sampling the material geometry and tensile samples as shown in Figure 4.1 and Figure 4.2 to determine the Young's modulus and calculate the casing critical load P_e shown in Table 4.1. This result was later used for numerical analysis.

Figure 4.7: Instron equipment for cyclic uniaxial testing with a capacity of 500KN

Table 4.1: Core yielding lengths considered for pre-dimension

L [mm]	P_e casing [N]	P_e/P_y	Theoretical core area for $P_e/P_y = 1$ [mm2]	Core width (squared cross section) [mm]
1000.00	98814.08	5.99	359.32	18.96
950.00	109489.29	6.64	398.14	19.95
900.00	121992.70	7.39	443.61	21.06
850.00	136766.90	8.29	497.33	22.30
800.00	154397.01	9.36	561.44	23.69
750.00	175669.48	10.65	638.80	25.27
700.00	201661.40	12.22	733.31	27.08
650.00	233879.49	14.17	850.47	29.16

Figure 4.8 shows the theoretical buckling values for different core thicknesses with no lateral restriction under fixed boundary conditions for a varying length about the minor axis. These curves were used to select the length of the core yielding portion depending on the cross-sectional area used. Values greater than 1 fulfil the global stability criterion, in this case, a stability factor P_e/P_y of 5.99 is used.

A total of 4 specimens were fabricated with the characteristics shown in Table 4.2. Figure 4.9 shows the detailing of the PVC BRB Specimen that was fabricated, the specimen comprised a steel core of a rectangular section laser cut from a steel plate of 3mm of variable section. The steel core is wider in the connection zone due to the loss of cross-sectional area caused by the through-holes. The casing is comprised of a 65x65x2 PVC hollow core section casing.
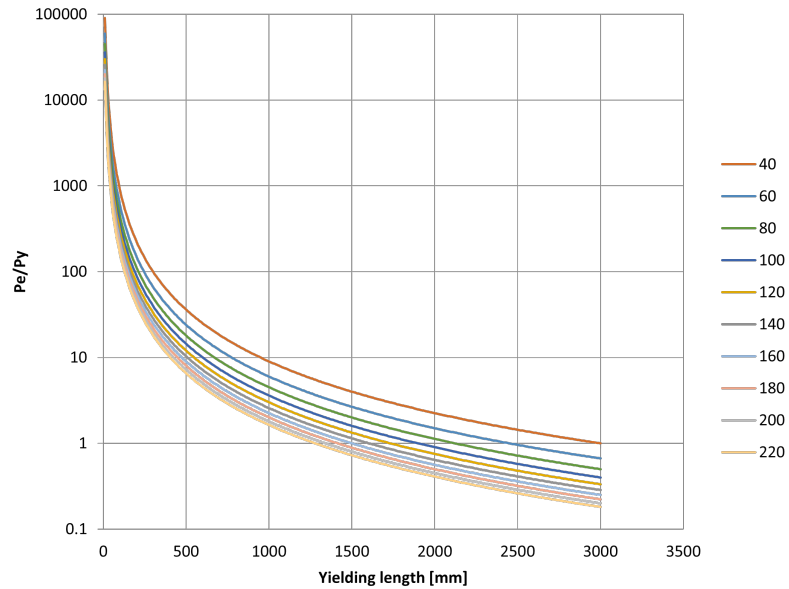
Figure 4.8: P_e/P_y-yielding length theoretical curves for different cross sectional areas

The debonding material was extruded polystyrene often used as underlay flooring and grout was used as filler material. The mix used for the grout was designed to achieve a 7 day cube strength of 30 MPa, 1:1.187 was used as a cement/sand ratio and a water/cement ratio of 0.549 was used. Finally, M10 bolts were used to assemble the components, however, during the assembly it became evident that not all aspects had been covered in the planning, one crucial aspect was the sealing of the gaps that needed to remain ungrouted to allow for large deformations in the axial direction.

Table 4.2: Specimen set

Specimen	Gap mm	Core cross section [mm2]	PVC Casing	Observation
C1	2	20	65X65X20	Successful
C2	4	20	65X65X20	Spoiled
C3	6	20	65X65X20	Spoiled
C4	8	20	65X65X20	Spoiled

Figure 4.10 shows the quality of the first mix used for specimen C1. Although some air bubbles could be seen when opening a sample PVC tube, this was not thought to be a major issue, however, as it is mentioned below in Figure 4.20 this created a problem when grouting the actual specimen since more parts were involved in the assembly.
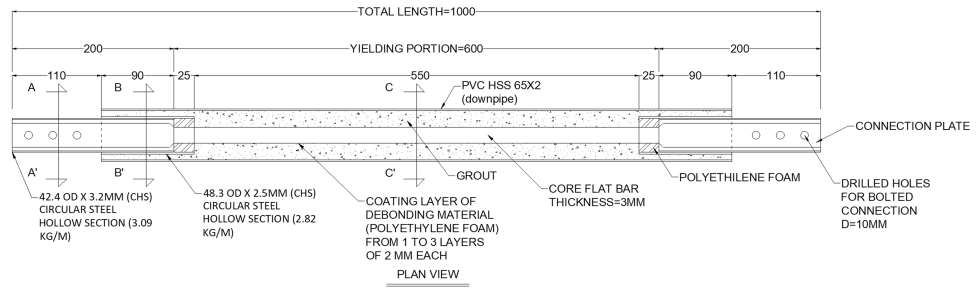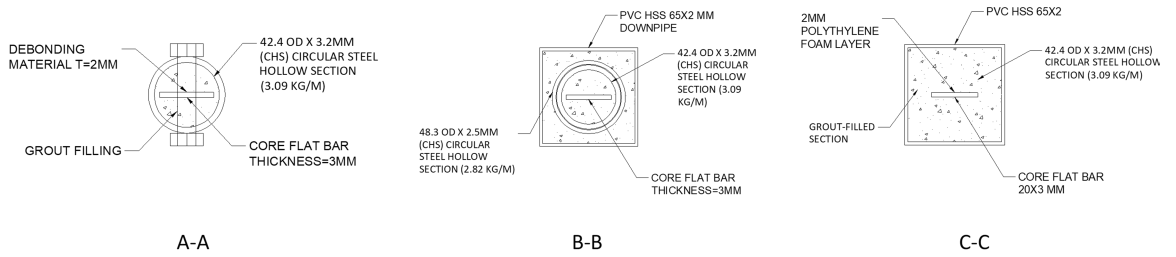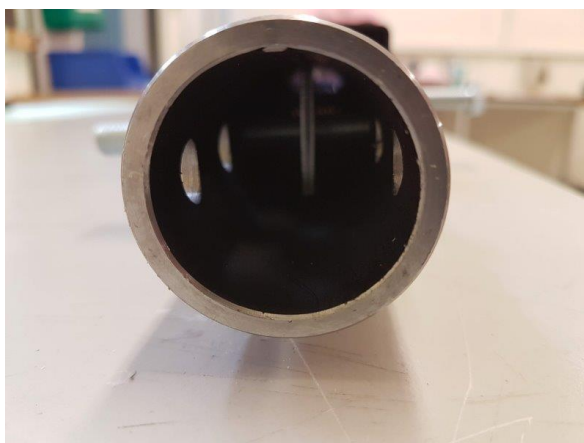
Specimens

Core 1,2 and 3

A-A

B-B

C-C
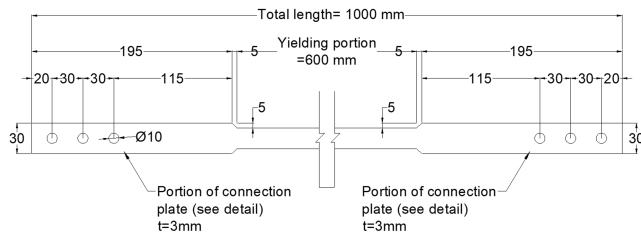
Figure 4.9: PVC BRB Specimen detailing

Figure 4.10: Bubbles observed in grout finish

Figure 4.11: Assembly of the manufactured parts. M10 bolts used to centre and position the parts in place

Figure 4.12: Bolted PVC connection

4.2 BRB Fabrication

The specimens were fabricated using the parts specified in the detailing plan. The CHS tubes that comprised the connection were ground to slide easily, these were provided with a series of through-holes to adjust the position with respect to the PVC casing. Likewise, the PVC tube was provided with holes to adjust the core in position for grouting. Figure 4.11 shows the assembly during calibration (adjusting the relative position of the components).Figure 4.12 shows the centred core respect the connection.

Figure 4.13 and Figure 4.14 show the application of the debonding material in layers of 2 mm each. These layers allowed to vary the gap for parametric study purposes. The debonding material used was extruded polystyrene which would provide a uniform layer as required, however, the installation of the material showed to be challenging as it is easily damaged, therefore, there is a risk of filtration of grout through gaps, as shown in Figure 4.14.

Figure 4.13: Debonding material (extruded polystyrene) applied around the core in layers of 2mm each

Figure 4.14: Gap openings in debonding layer

Figure 4.15 shows the two types of Circular hollow-core sections (CHS) to make the connection Figure 4.15a shows the CHS to be grouted inside to lock the core in one position, this part slides into the part shown in Figure 4.15b which is a CHS of larger diameter CHS and ground inner surface for ease of applying cyclic loading.

An air gap in the axial direction was provided by stacked polystyrene foam layers adding up to 50 mm as shown in Figure 4.16. This was a key part for the correct functioning of the BRB however, gaps in between the foam showed difficulty to seal appropriately (Figure 4.17), moreover, the reaction of the polystyrene embedded in wet grout was not tested and it is likely that some grout absorption occurs.

Figure 4.18 shows the ready core-connection assembly before the casing and outer CHS are installed, bolted and can be grouted.
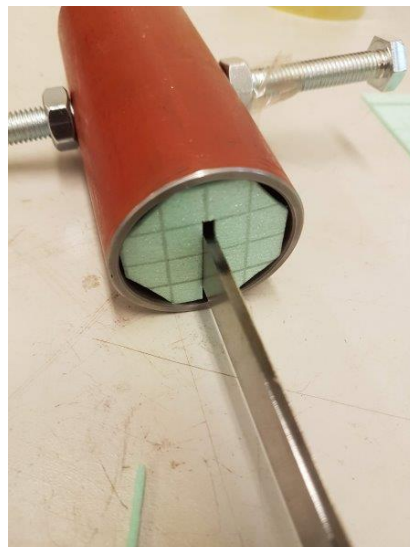
a

b

Figure 4.15: Circular hollow-core sections (CHS) used for the connection

Figure 4.16: Polystyrene gap

Figure 4.17: Polystyrene gap in the assembly

Figure 4.18: Ready parts before final assembly and preparation for grouting


**Figure 4.19:** Sealing of gaps to avoid grout infiltration

Figure 4.19 shows tape applied to the connection ends to stop the grout from infiltrating. This detail did not show to be effective in general, however, it is sufficient when the grout is slightly more viscous.

Figure 4.20 shows the grouting of specimen C1. It can be observed the mix was not sufficiently fluid to be cast effectively, moreover, an additional difficulty was to ensure the inner air gaps were filled. Due to the fragility of the calibrated assembly, it was not possible to vibrate the mix inside the tube, therefore some vibration was induced by tapping on the PVC surface with hand tools. The mix was later changed to highly fluid grout for specimens C2, C3 and C4, however, this would add unforeseen difficulties as discussed below in the testing results.

The CHS connecting to the INSTRON equipment was tested to ensure that the connections remain undamaged when applying the grasping force as the specimen shown in Figure 4.21. The grasping pressure of the equipment was reduced to 35 bar which was within the limits of the connection.
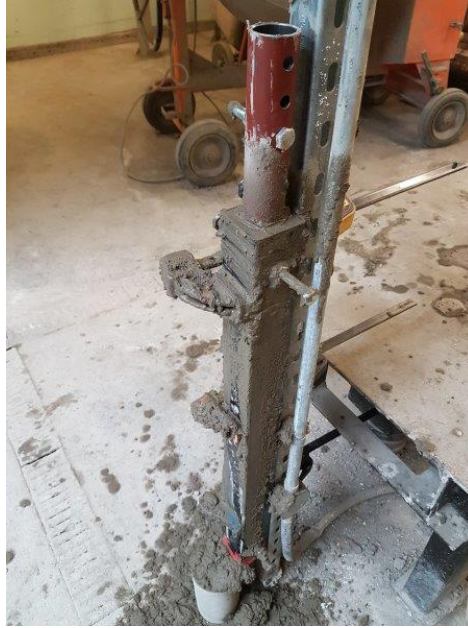
Figure 4.20: Grouting of specimen C1

a)

b)
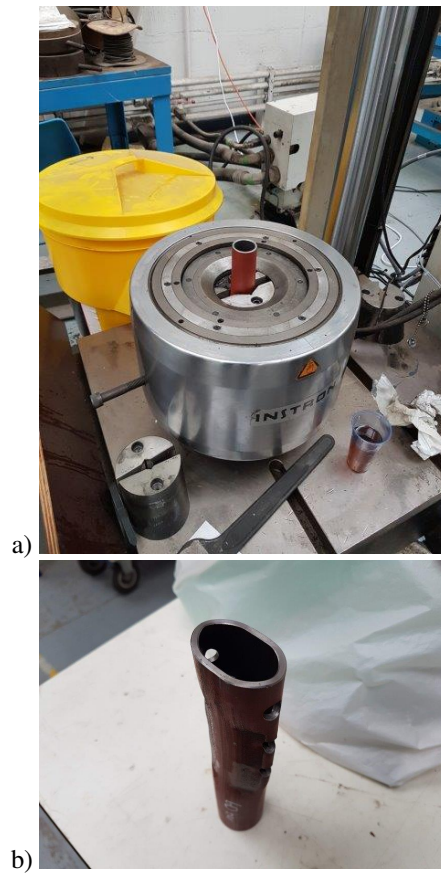
Figure 4.21: Testing of connection CHS tube subjected to a grasping force of 45 bar

**Figure 4.22:** Specimens C2, C3 and C4 assemblies

**Figure 4.23:** Modified grout mix for specimens C2, C3 and C4

Figure 4.22 shows specimens C2, C3 and C4 before being grouted, the specimens were clamped vertically, sealing the bottom of the PVC tube. Figure 4.23 shows the grout mix used, the mix correctly address the need that had been identified previously by being highly fluid, it managed to completely fill the BRB without the need for vibration. However, observed excessive bleeding was likely to get through the sealing tape applied for air gap protection.

4.3 Testing apparatus and loading protocol

Figure 4.24 shows the loading protocol used during testing. The load was applied in a cyclic manner with a period of 160 seconds and amplitude of 40 mm and the test was displacement-controlled. Although the loading applied was cyclic, the study objective of the study only concentrates on the first 40 seconds of compressive load since only the buckling phenomena is of relevance for the casing.
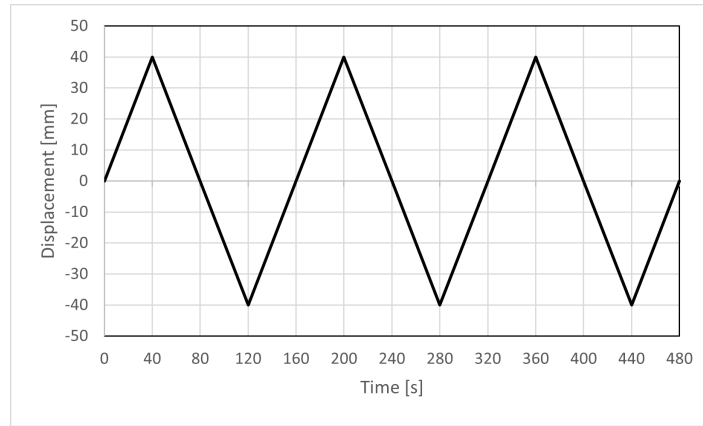
Figure 4.24: Load protocol for samples starting in compression
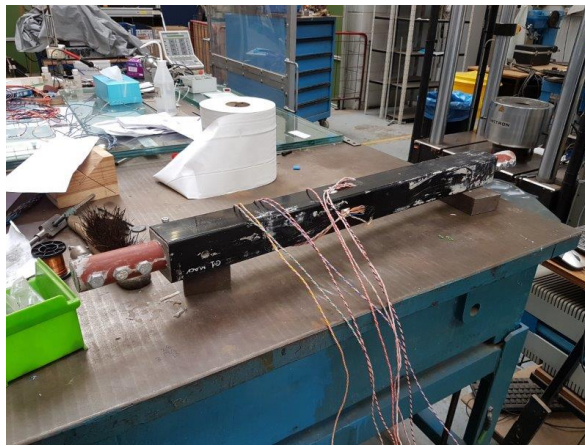
Figure 4.25: Instrumentation of specimen in core minor and major axis

The specimens were instrumented as shown in Figure 4.25 in orthogonal directions to measure the effects about the minor and major axis. The testing apparatus with the PVC BRB in the INSTRON can be observed in Figure 4.26, this was connected to a SOLARTRON recorder with 6 channels per specimen.

During testing of specimen C1, it could be observed that bulging developed (see Figure 4.27) in the casing, this was later confirmed when opening the casing. Likewise, the core failed to develop necking, however also higher-modes of buckling shape formation can be observed before failure. Figure 4.28 shows the final deformed shape in waves curling at failure.

Figure 4.29 shows grout punching causing bulging of the PVC casing in specimen C1. Figure 4.31 shows the instrumented remaining specimens to be tested C2, C3 and C4 which were fabricated with highly fluid grout. This change of mix eased the grouting of specimens, in addition, no vibration was needed. However, changing the mix signified unforeseen fundamental problems in how to stop the grout from infiltrating the connection CHS.

Figure 4.26: Testing apparatus
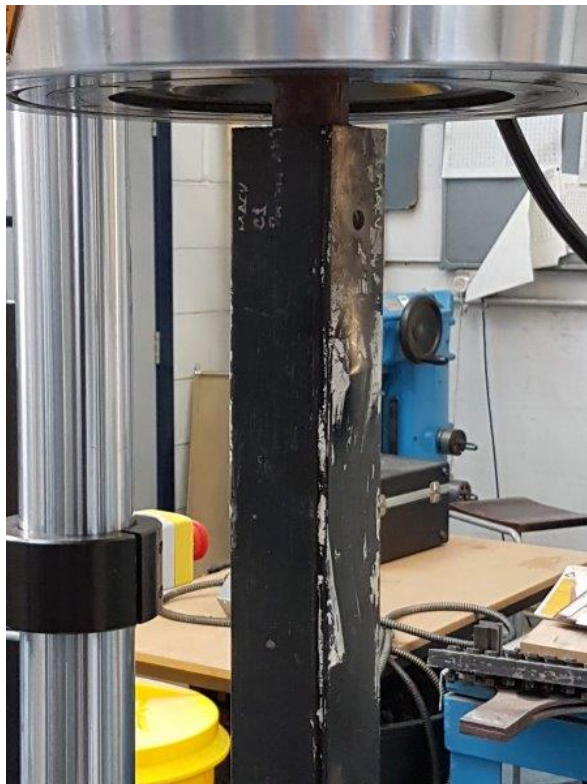
Figure 4.27: Bulging of casing

a)

b)
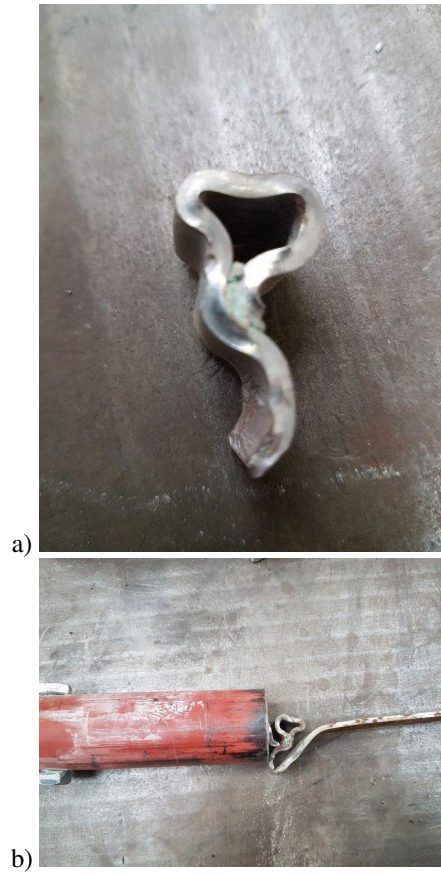
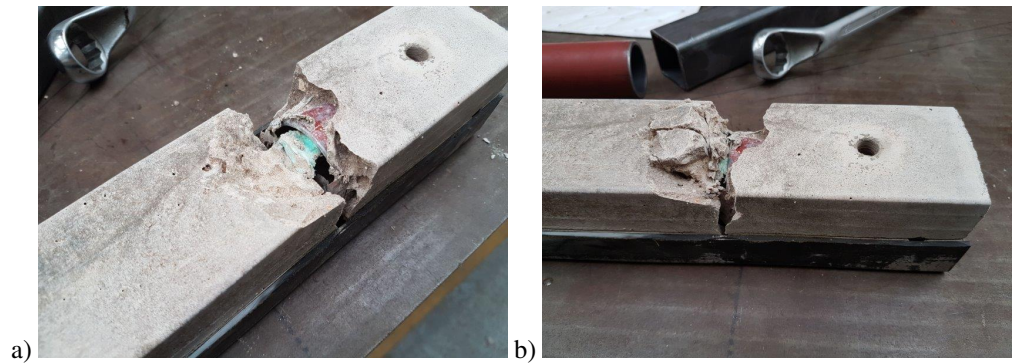**Figure 4.28:** Higher-buckling shape modes curling in grout punched pocket at core failure

a)   b)

Figure 4.29: Grout punching due to core lateral thrust

Figure 4.30: Final lateral core displacement in grout punched pocket

Figure 4.31: Instrumentation of remaining specimens C2, C3 and C4

Figure 4.32: Locking of CHS tubes and casing failure under compression

Testing of the samples revealed these flaws, therefore it was shown that the sealing method to stop the grout was not effective and resulted in spoiling the samples at different degrees.

Specimen C2 was a spoiled sample by not fitting in the testing equipment since the assembly was not aligned correctly. This BRB showed additional challenges in the fabrication of BRB which requires the constant quality control of the straightness of the connections. Only specimens C3 and C4 were tested, however, as mentioned above it was observed that not only did the grout infiltrate the parts that were supposed to be ungrouted but also grouting of the connection CHS tube spoiled the polystyrene by filling the material voids with the highly fluid mix.

Specimen C3 shown in Figure 4.32 failed in compression when the connection tubes locked due to the filler grout. Figure 4.33 shows the results of the testing, the surface of the grout

Figure 4.33: Failure of PVC casing of specimen C3

looks smooth as expected and no voids are appreciated in the mix, therefore continuity in the filler material can be assumed. Since the casing has been sized to restrain the thrust, the only explanation of failure remaining is the connection detailing. From Figure 4.31 it can be observed that one of the tubes that were supposed to be embedded in the grout was pulled out of the casing. Experimental results of specimen C3 and C4 are shown in Figure 4.35 and Figure 4.36 respectively, in the case of C4 it can be observed a rapid degradation from the initial loop which is highly correlated to damage.

4.4 Experimental Results

Figures 4.34, 4.35 and 4.36 show the experimental results of the specimens C1, C3 and C4 respectively, in the figures the convention for compressive force is negative.

- C1 - The specimen presented some challenges during fabrication concerning the mix used for the filler material, however, the hysteretic behaviour was overall stable up to the point of failure.

- C2 - The specimen was built with the same method used for the others however, the end connections did not line up with the clamps of the equipment. It is likely that initial imperfections of the core have been an important defect in the process which was unable to be avoided during assembly and testing.

- C3 - Similar to C2 this specimen testing was unsuccessful, the defect in this PVC BRB was found in the change of grout mix since excessive bleeding of the mix lead to the air gaps being filled with cementitious material, therefore it is important to seal the
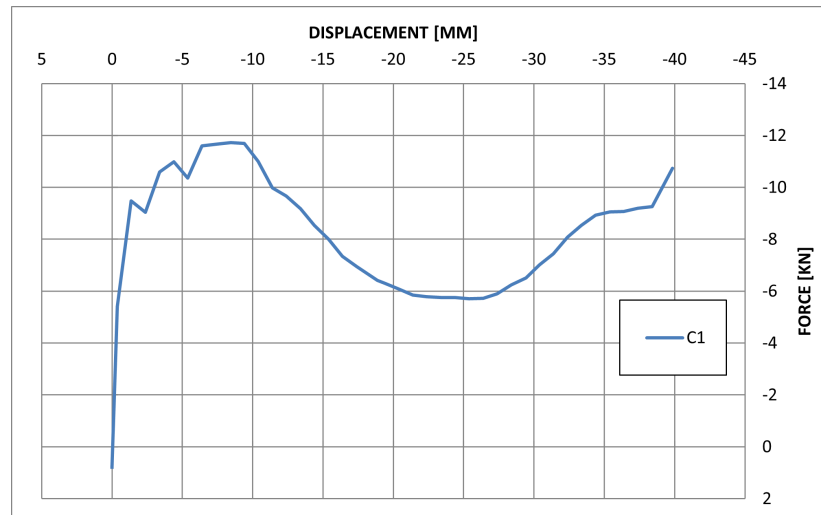
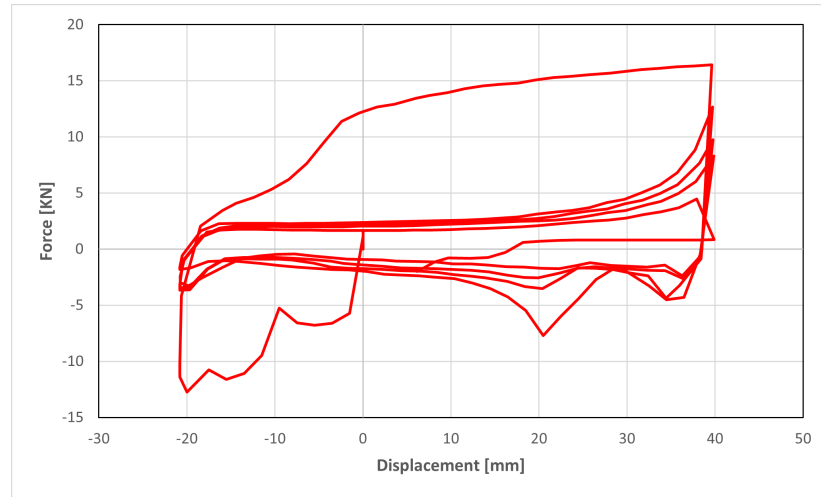**Figure 4.34:** Experimental result of PVC BRB C1
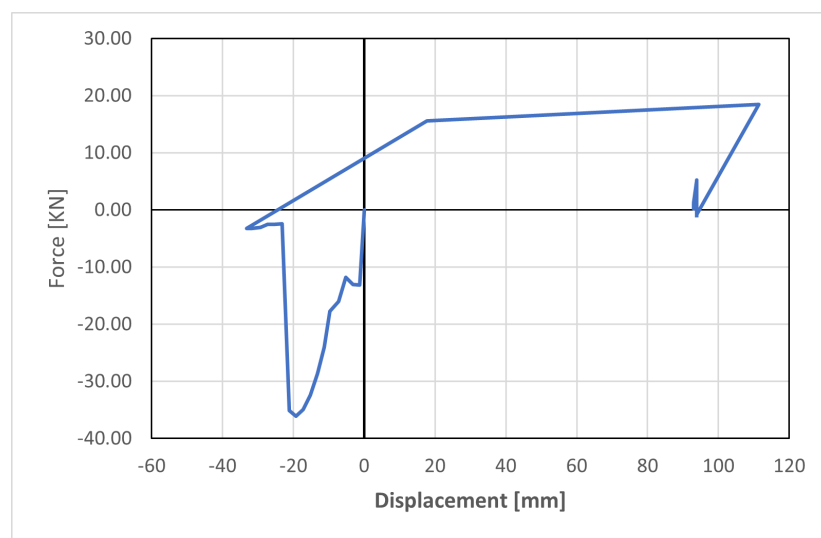
Figure 4.35: Hysteretic curve of PVC BRB C3

gaps with a more effective method. The specimen locked in compression to finally over stress the grout and break the casing.

- C4 - Although this specimen was also fabricated with the same grout, failure did not occur until some energy was dissipated. It is possible that this specimen has been also undermined with the gap sealing problem.

An immediate remark from these results is that sealing the gaps effectively has an important impact when using a highly fluid grout mix in BRBs with infilled tubular structures.

Figure 4.36: Hysteretic curve of PVC BRB C4

4.5 Numerical Analysis

A 3D Finite Element model was conducted after the PVC characterisation study and prior to the experimental testing with the objective of predicting the experimental result, the model used the material properties obtained from the PVC testing. However, although failure patterns have been observed in the experiment, the model does not account for damage models since this has not been included in the scope nor the validation chapter to ensure this is done correctly. Moreover, although modelling damage is a step to define the limit states, it is not regarded as needed to answer the question of whether PVC can restrain the buckling of the core as effectively as steel.

Table 4.3: Material Properties for steel

Steel		
P_y	11000	N
A_{core}	40	mm2
t	2	mm
b	20	mm
E	200000	MPa
f_y	275	MPa
PVC		
E	30000	MPa
I	333732	mm4
f_y	31	MPa

Figure 4.37 shows the full BRB assembly comprising 3 parts, core+connections, grout and PVC casing. Surface to surface interaction has been modelled between core and grout and a full bond between grout PVC casing and grout has been assumed. The core steel mechanical properties are $E = 200GPa$ and $f_y = 275MPa$ as shown with the rest of the input
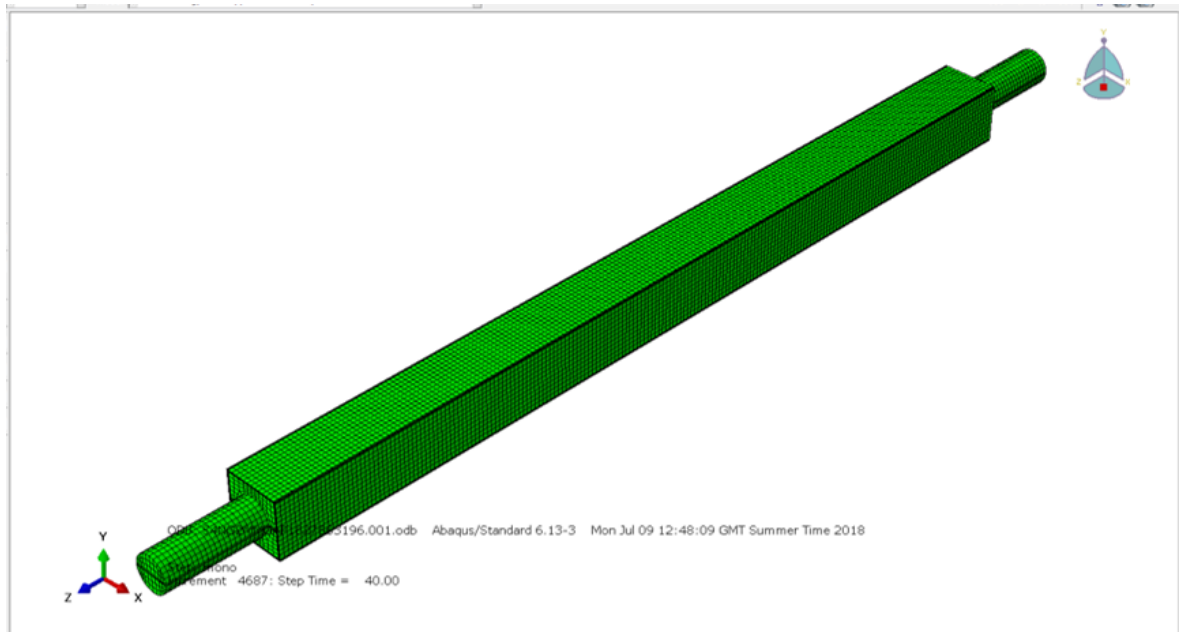
**Figure 4.37:** Assembly of parts of PVC BRB FE Model

Figure 4.38: Core mesh

parameters in Table 4.3, Figure4.38 shows the core with the connections as one part and Figure 4.39 shows the mesh detail in the connection. The full connection has been modelled as steel, the grout filling the connection CHS tube has not been considered.

Similarly, Figures 4.40 and 4.40 show the mesh of the PVC and the casing. Table 4.4 shows the number of elements used for each component, element type C3D20 was used for the core since it forms into higher-mode buckling shape in compression, therefore this element is more suitable for convergence, C3D8 was used in the remainder of elements since they remain in the elastic range unless damage is considered.
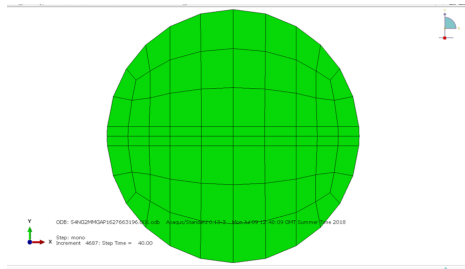
Figure 4.39: Connection mesh
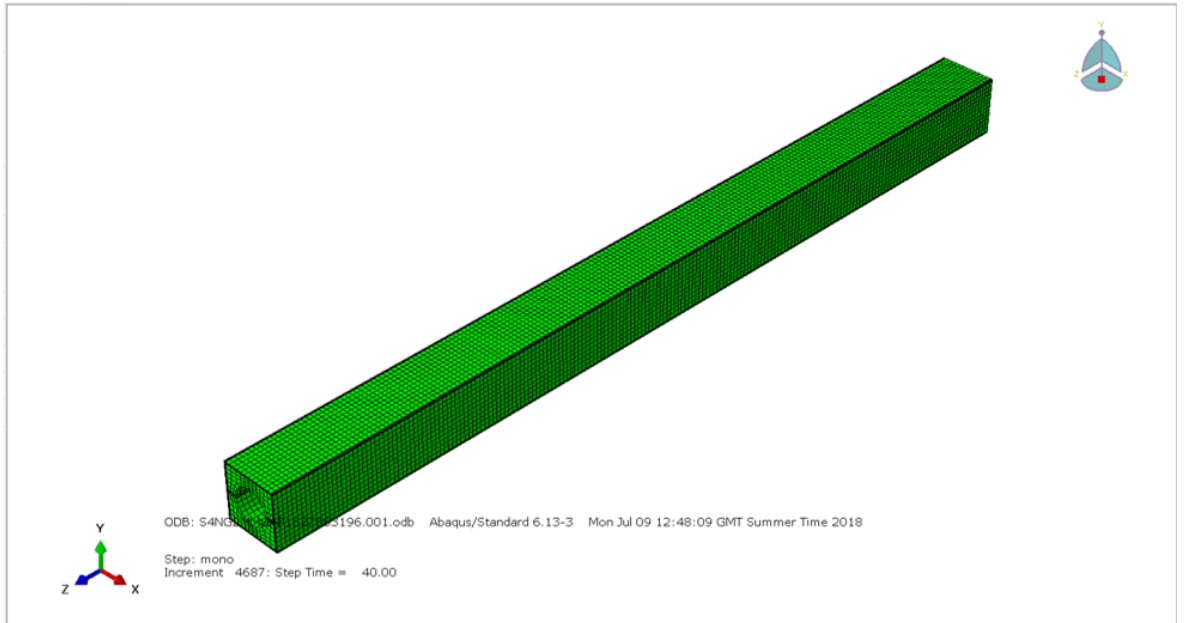
Figure 4.40: PVC casing mesh

Table 4.4: Number and type of elements used

Component	Number of elements	Type of element
Grout	36188	C3D8
Casing	21952	C3D8
Core	7360	C3D20
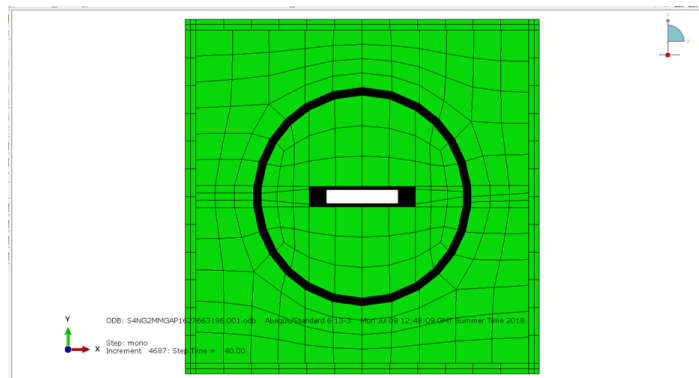
Figure 4.41: Grout mesh
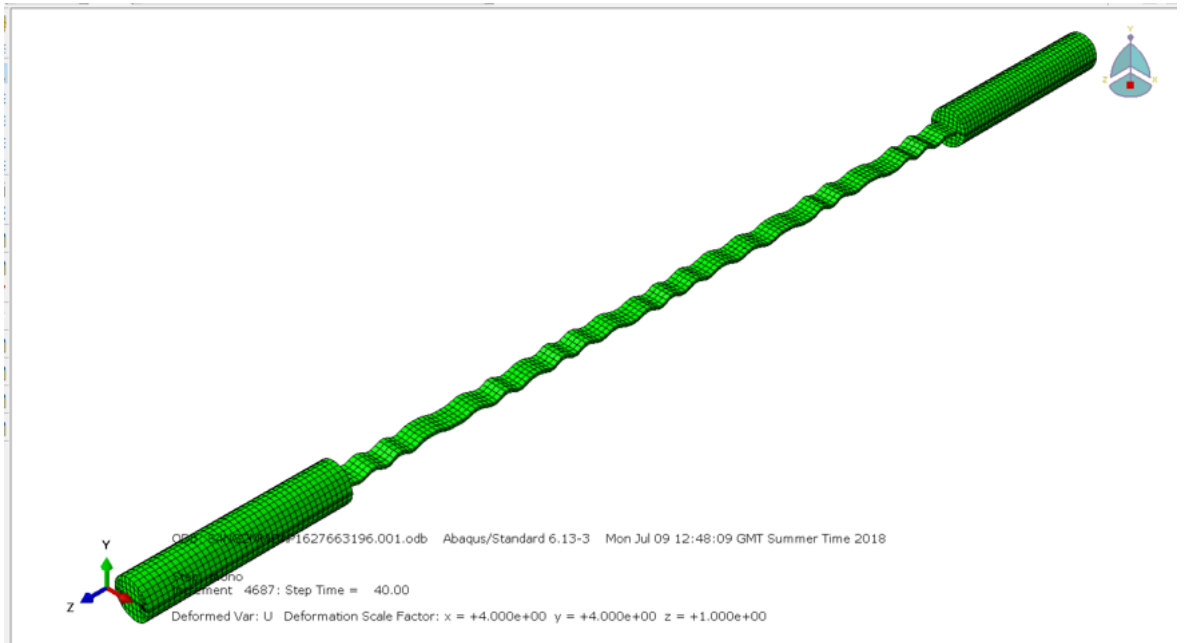
Figure 4.42: Core deformed shape magnified with a factor of 4
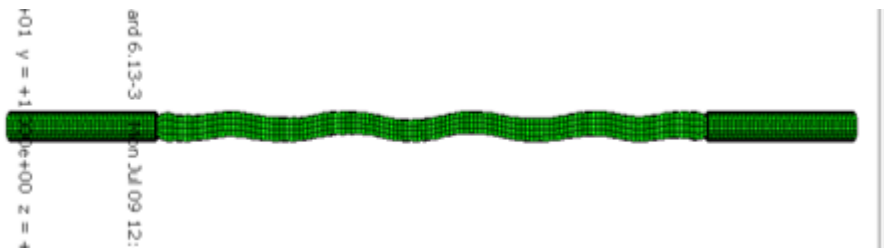
Figure 4.43: Core deformed shape magnified with a factor of 20

Figure 4.44: Principal stresses of steel core
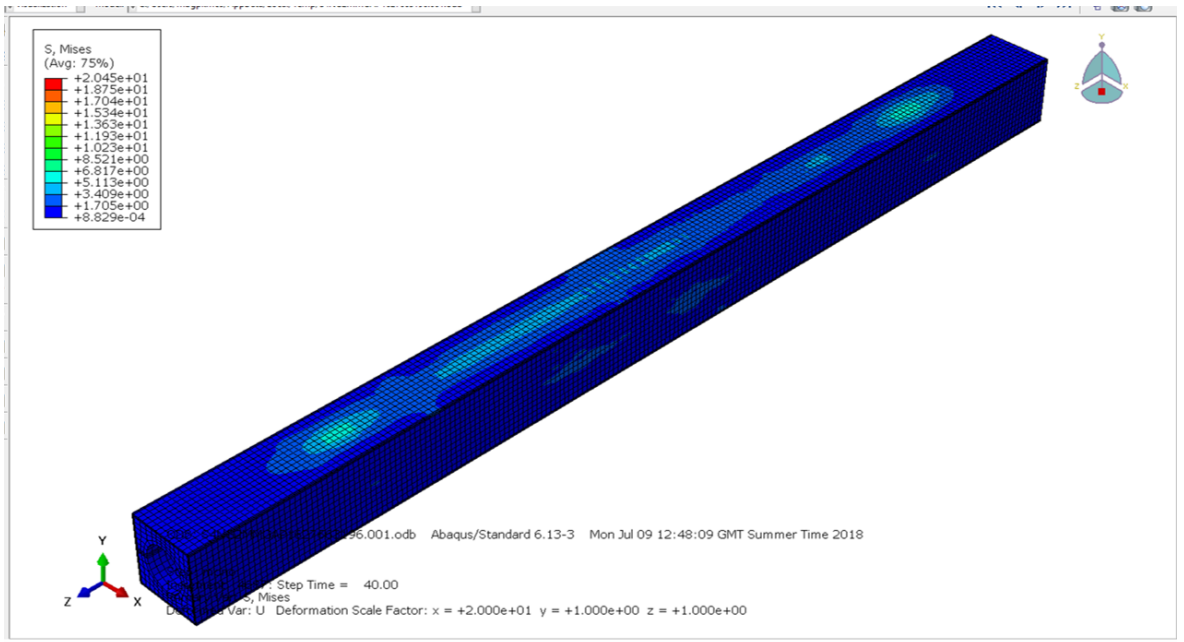
Figure 4.45: Principal Stresses on PVC casing
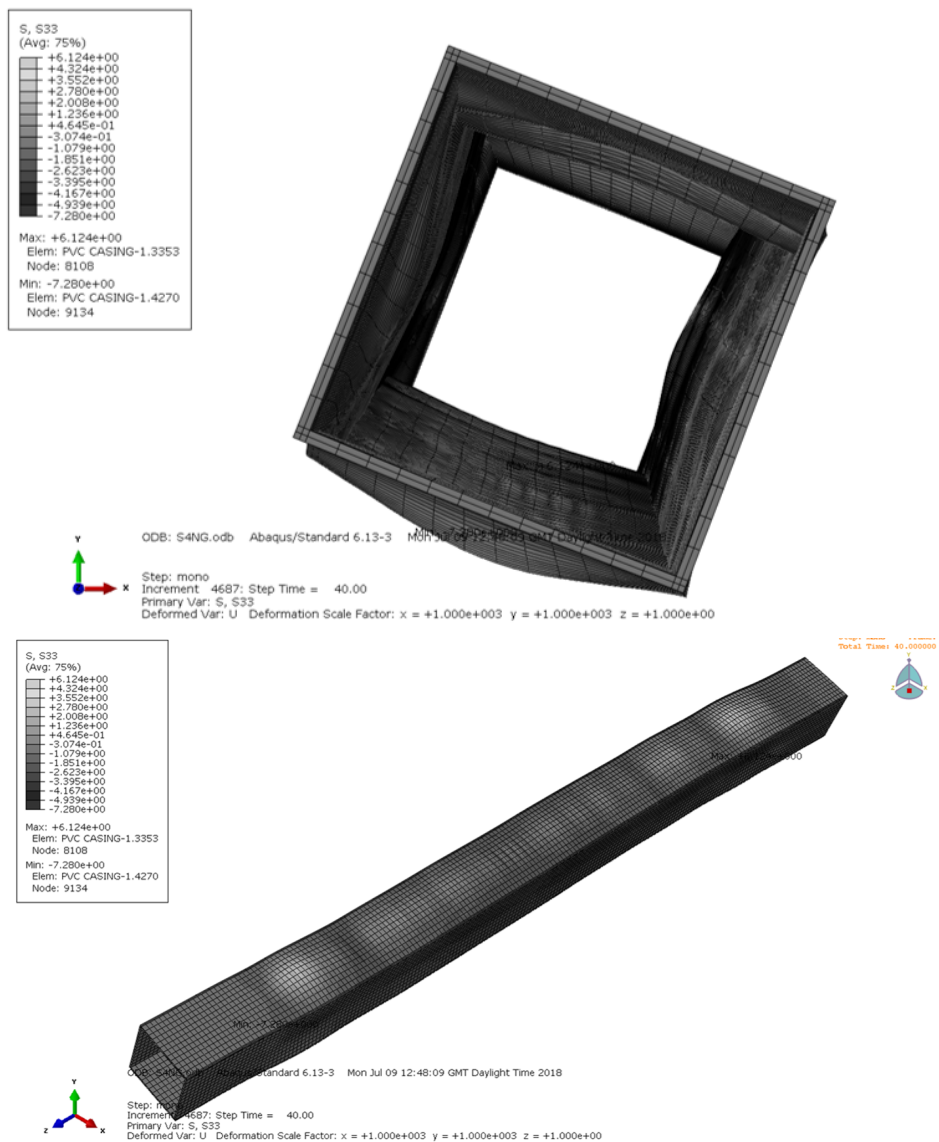
Figure 4.46: PVC Casing deformed shape
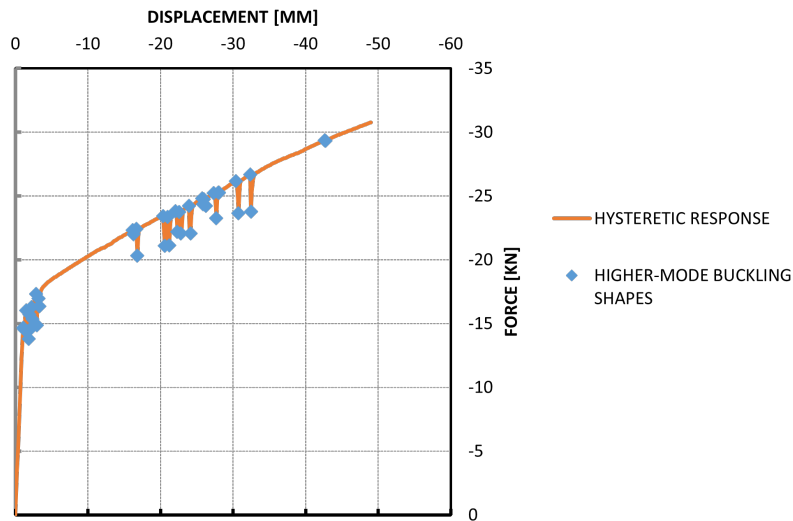
Figure 4.47: FEM result of specimen C1 and wave formation
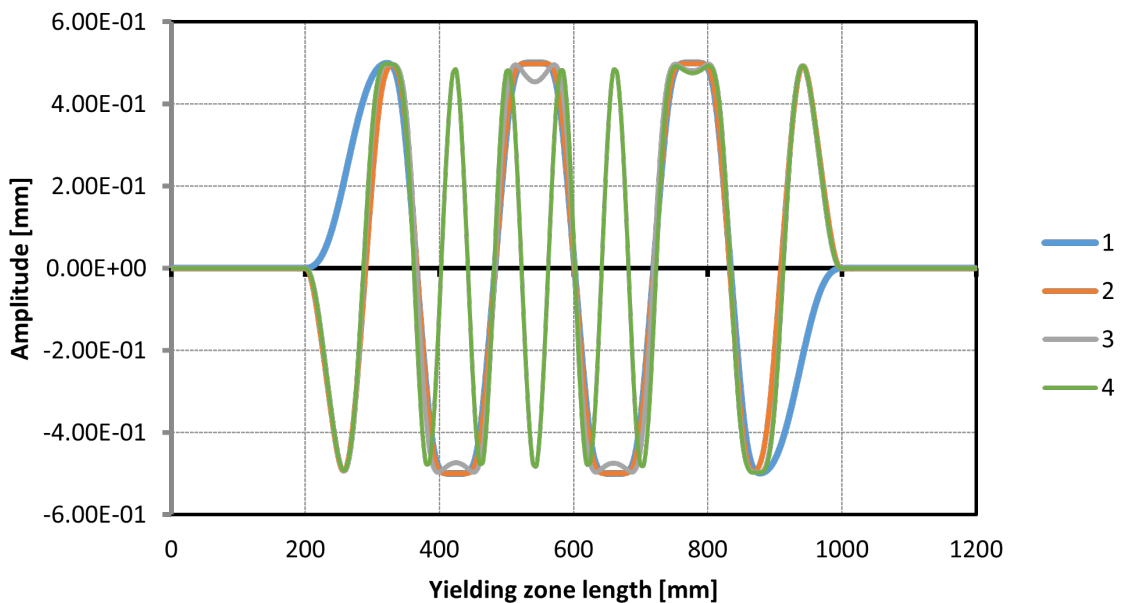
Figure 4.48: First core deformed higher buckling mode shapes

4.6 Results

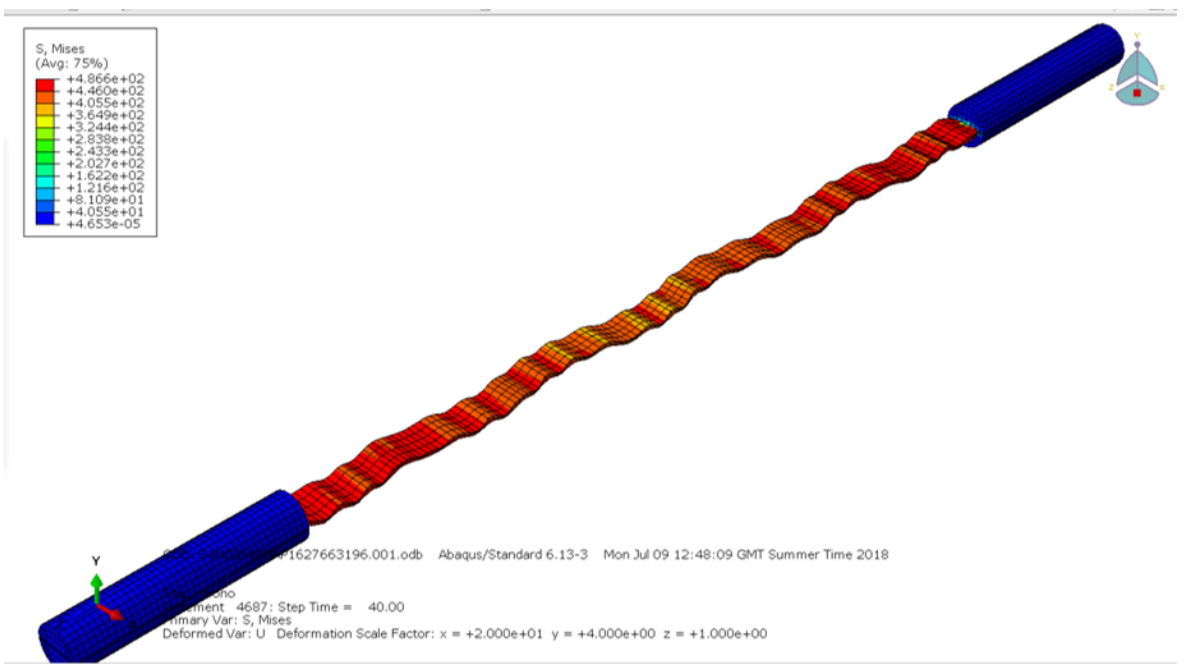Figures 4.47 show the response of the numerical analysis subjected to monotonic loading and the points where the formation of higher-buckling modes are formed, some deformed shapes corresponding to those points are shown in Figure 4.48. Figure 4.49 shows the full set of deformations corresponding to the blue points in Figures 4.47.

Figures 4.50, 4.51 and 4.52 show the comparison between numerical and experimental results, from the figures it can be seen that there is an important error from these two sets of data, one of the reasons why that can be the case is that the above-mentioned reasons on the
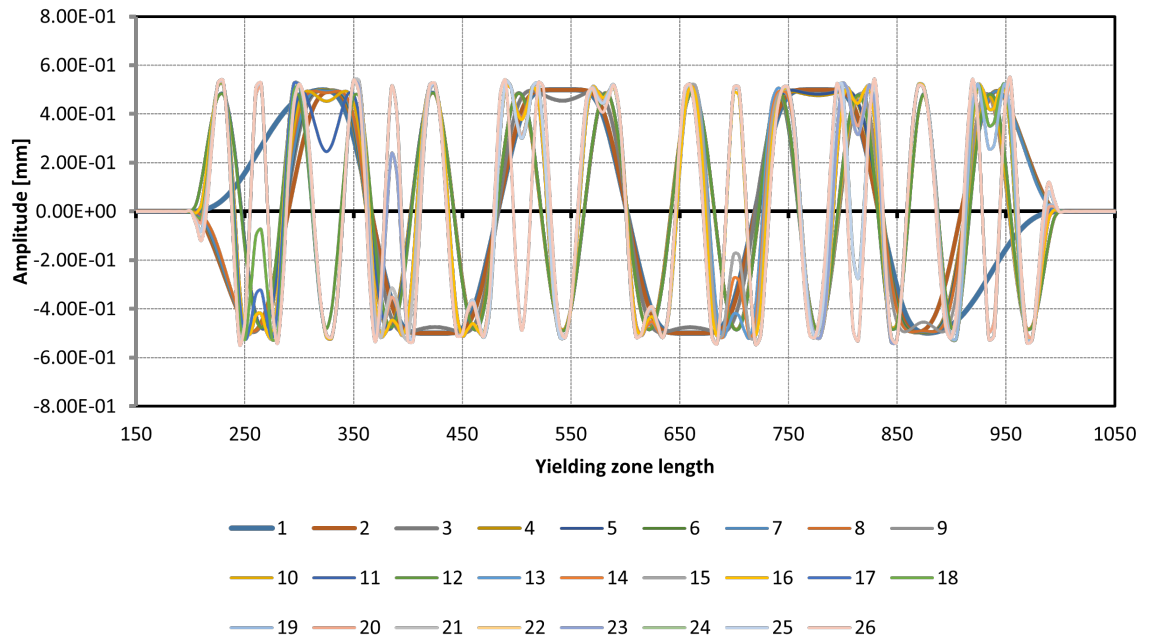
Figure 4.49: Complete core deformed higher buckling mode shapes
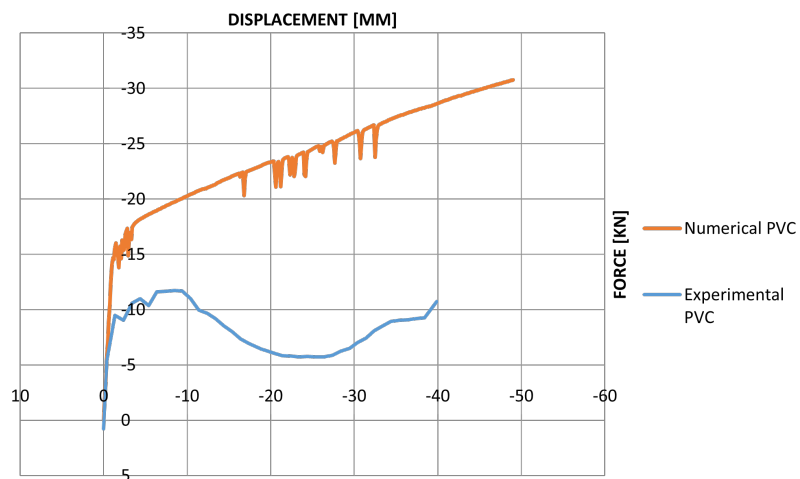
Figure 4.50: Comparison of Model and Experimental work for specimen C1

grout filling air gaps that are important for the functioning of the BRB, however that explanation would only be valid for the specimen C3 which failed due to grout crushing.

A possible explanation for the discrepancy in forces in compression could be that damage is being highly underestimated in the present work which leads to inaccurate predictions of the experimental setup. In addition, PVC failure highly contradicts the coupon testing conducted. This strongly suggests that PVC time dependant properties require to be examined in more depth
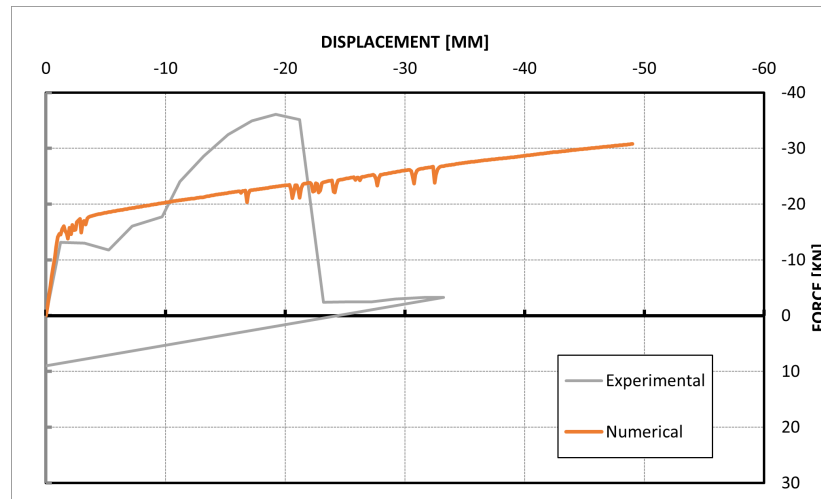
Figure 4.51: Comparison of Model and Experimental work for specimen C3
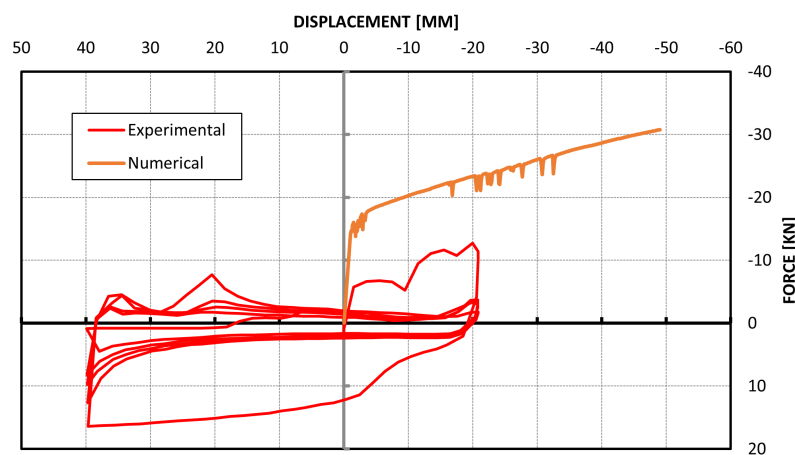
Figure 4.52: Comparison of Model and Experimental work for specimen C4

4.7 Conclusions

The present study shows experimental and numerical investigation conducted using PVC casings as tubular structures for Grout-Filled Buckling Restrained Braces to quantify the feasibility of PVC. The experimental results reveal that PVC can satisfactorily avoid Global Buckling as predicted by the theoretical stability criterion.

The conducted experiment revealed a few key fabrication challenges involved in future experimental research that required to take into account when designing an experimental set.

Although the experiment did not agree with the numerical analysis, this experimental data can be used to calibrate new models and modelling techniques that account for damage in the way that it was observed.

The PVC casing has shown similar failure patterns to its steel counterpart, therefore it would

be possible to adjust the current understanding of local failure conditions for PVC.

Although in the experiment, global stability was not observed due to using a stability factor of 6, it was unclear whether this condition would hold true for PVC closer to the stability factor limit of 1, testing for this would imply new challenges as a different experimental design would be required.

Bibliography

Jia, Mingming et al. (2017). "Experimental research of assembled buckling-restrained braces wrapped with carbon or basalt fiber". In: *Journal of Constructional Steel Research* 131, pp. 144–161. ISSN: 0143974X. DOI: 10.1016/j.jcsr.2017.01.004.

Jones, A S (2011). "Low Cost Lightweight Buckling Restrained Braces for Low Rise Buildings". In: *Proceedings of the Ninth Pacific Conference on Earthquake Engineering*. 130. Auckland, New Zealand, pp. 1–8.

Sun, Hongpeng et al. (2019). "Study of buckling-restrained braces with concrete infilled GFRP tubes". In: *Thin-Walled Structures* 136.December 2017, pp. 16–33. ISSN: 02638231. DOI: 10.1016/j.tws.2018.10.040.

Chapter 5

Final conclusions and Recommendations for Further Research

The Literature Review revealed the necessity of further study and testing of innovative casings that use materials different from steel since damage on the casing is often overlooked in FE models.

Based on the literature review, definition of research questions and focal points were introduced and explored. Within the present, the state of the art of Buckling Restrained Braces has been discussed, in addition, the feasibility of PVC casings for use in Grout-Filled Buckling Restrained Braces has been explored to a degree throughout testing.

In chapter 3, extensive numerical analysis was conducted and compared with past studies found in literature. The analysis revealed important features on the behaviour of the core when subjected to reversal axial loading.

The conducted numerical studies showed to successfully reproduce the limits of BRB global stability, moreover, the Finite Element analysis of surface to surface contact allowed to quantify the stress state of the casing resulting from the lateral thrust exerted by the core. In addition, other significant challenges concerning the computational time were discussed and a new method to conduct numerical analysis has been proposed, such method consists in converting a 3D problem into two equivalent 2D problems and it was shown that an important reduction of computational cost can be achieved and that Grout-Filled BRBs can be modelled at fraction of the computational cost.

Furthermore, experimental work in chapter 4 was conducted by designing a PVC BRB,

testing PVC coupons and conducting Numerical Analysis with the methods investigated in chapter 3. The results strongly suggested that load rate on PVC casings is an important factor to consider when conducting the characterisation of the material mechanical properties. Moreover, it has also been found that damage on PVC casings can be significant and therefore requires to be considered in the Numerical Analysis. . Therefore PVC time dependant mechanical properties require further examination.

5.1 Further work

Research on Grout-Filled BRBS can result in lighter, durable and versatile fuse structures i.e. with improved performance. In my view the following recommendations for further work would make significant improvements in the understanding and performance of BRBs.

5.1.1 Improving understanding of global failure

An active challenge in research of BRB casings is to understand how axial compressive displacements transfer lateral forces to the grout. Formulas to calculate total lateral thrust have been proposed by different authors (Chai 1998; Genna and Gelfi 2012), however improvement of accuracy has shown to be an opportunity of contribution in research.
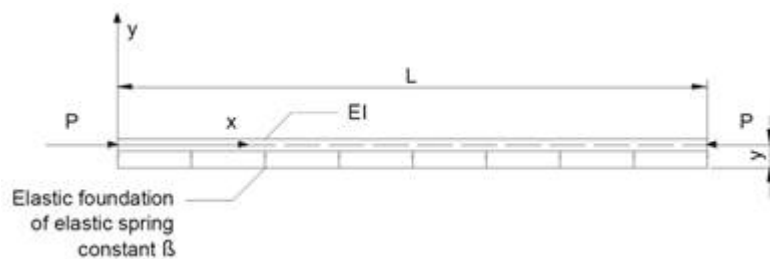
Figure 5.1: Beam column on an elastic foundation

The problem has been studied as a column on an elastic foundation where the elastic foundation is the flexural stiffness of the casing (Grout filled HSS system) shown in Figure 5.1. This criterion provides overall conditions for the BRB to be unstable however it cannot provide further information such as:

- Contact force

- Distribution of lateral force

- Core axial displacement (realistic deformed shape)

- Stress state of the casing during loading

The analysis requires a good understanding of the spring constant of the elastic foundation, therefore the system of the casing needs to be analysed under the application of lateral force in order to determine such a constant. From the literature, the flexural behaviour of a Concrete Filled Tubular Structure subjected to pure bending has been studied (Li et al. 2017), however no studies regarding a concrete filled tubular structure laterally loaded from inside were found. Figure 5.2 shows an experiment conducted to understand the flexural behaviour of a Concrete-Filled Steel Tubular Structure subjected to bending, the study revealed that the system works as a composite section and this should be considered to determine the spring constant. A strategy to conduct a more suitable study of the behaviour of the core is proposed and consists in 4 steps:

1. Analytical study of the spring constant of the elastic foundation

2. Analytical study of the final deformed shape based on the energy method Timoshenko and Gere (1961)

3. Analytical study of the lateral thrust

4. Experimental work

Distribution of lateral thrust has been studied partially by estimating the wavelength of the high-buckling mode deformed shape. The measurement of this parameter has only been experimentally obtained by extracting the core after testing a BRB; hence, only one value has been obtained for the wavelength. Understanding this parameter is important to quantify the distribution of the forces acting on the grout and this can be achieved analytically by considering that the elastic foundation is the addition of two elastic foundations as shown in.

The objective is to allow the core buckling within the gap value in the y direction until over closure is achieved (i.e. y=gap); at this stage the casing starts working. Hence the first elastic foundation accounts for the effect of formation of the core into higher buckling shape meanwhile the casing can work in parallel. The energy method will be used for this analysis. The method is described in the next section.

a)Test specimen

b)Instrumentation arrangement

c)Cross section
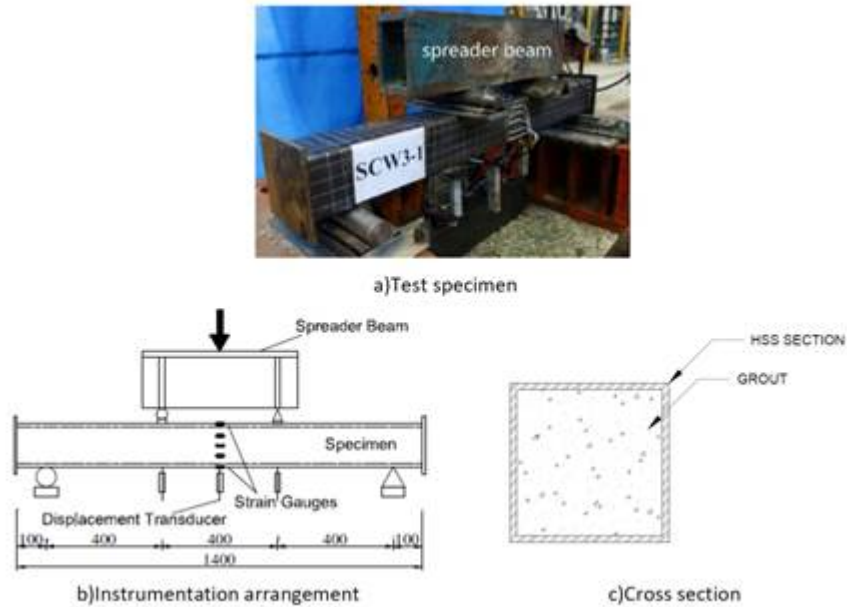
Figure 5.2: Experimental set up of Concrete-Filled Square Steel Tube from Li et al. (2017)
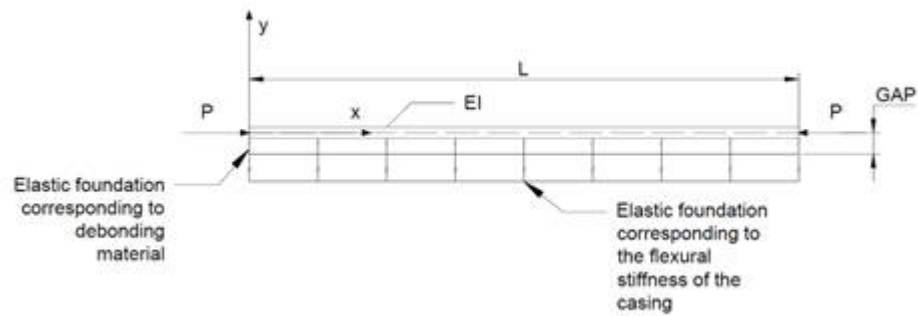
Figure 5.3: Elastic foundations considered for the study of lateral thrust

A new energy based approach stability criterion

It is recommended that further work in the investigation of BRB stability focus on the study of the mechanism of the yielding portion of the core and the load transfer to the casing. Figure 5.4 shows a basic composition of a core which comprises 3 parts being one of them a yielding portion.

Studies of the behaviour of the core have been conducted (Wu and Mei 2015) and formu-
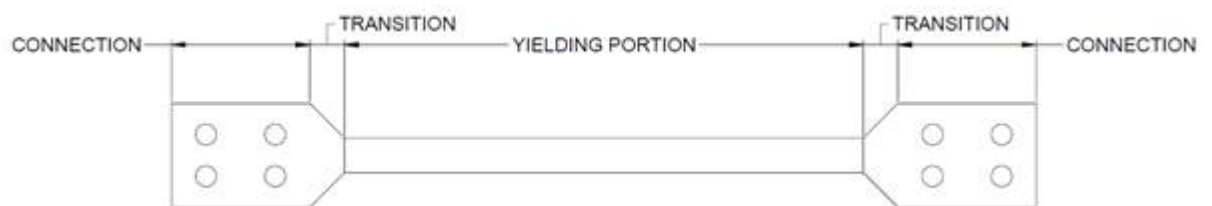
Figure 5.4: Typical core shape
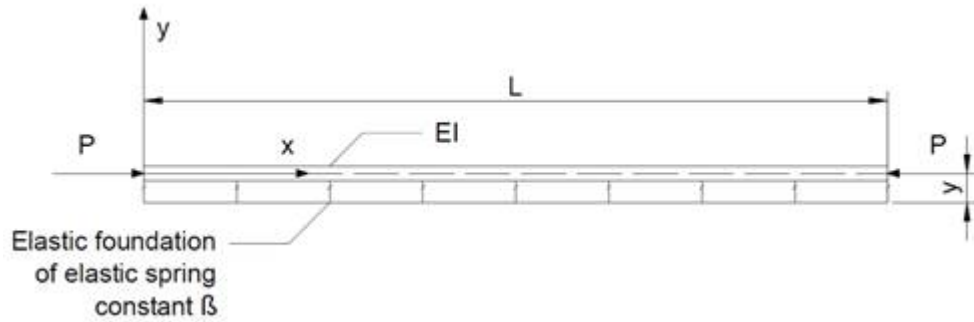
Figure 5.5: Common conceptualisation of core structure
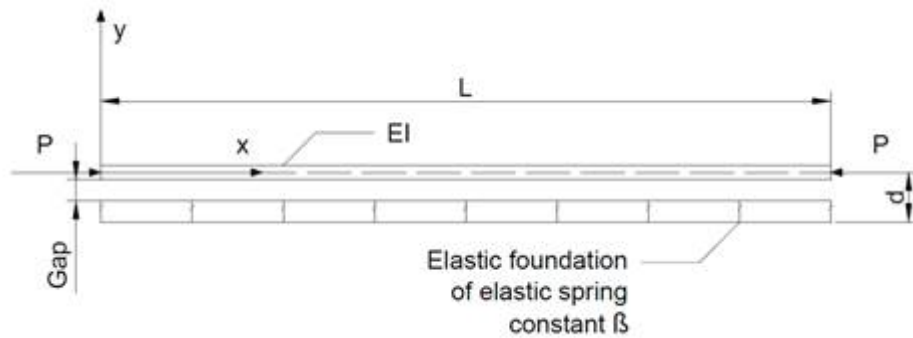
Figure 5.6: Column on an elastic foundation considering a gap

las to determine the stability conditions have been derived (C. Black, Makris, and I. Aiken 2002; Watanabe et al. 1988; Zhao, Wu, and Ou 2014) however the studies conducted to present are based on the solution of the general buckling differential equation of a column on an elastic foundation where elastic linear assumptions are made. A common conceptualisation of the system can be observed in Figure 5.5. The problem of this conceptualisation is that the higher buckling mode formation cannot be studied as no gap or second elastic foundation is considered as shown in Figure 5.6. Therefore, studies with a more appropriate method can be conducted.

From the theory of elastic stability, the problem can be studied from the point of view of energy (Timoshenko and Gere 1961) by assuming that the deformed shape can be expressed as the summation of sin series with amplitudes as follows:

$$y = a_1 \sin \frac{\pi x}{l} + a_2 \sin \frac{2\pi x}{l} + a_3 \sin \frac{3\pi x}{l} + ... \tag{5.1}$$

From this expression, the strain energy corresponding to the vertical displacement of the core and the deformation of the elastic foundation can be derived resulting in the following expressions:

$$\Delta U_1 = \frac{EI}{2} \int_0^l \left(\frac{d^2y}{dx^2} \right)^2 dx = \frac{\pi^4 EI}{4l^3} \sum_{n=1}^{\infty} n^4 a_n^2 \tag{5.2}$$

$$\Delta U_2 = \frac{\beta}{2} \int_0^l y^2 dx = \frac{\beta l}{4} \sum_{n=1}^{\infty} a_n^2 \tag{5.3}$$

On the other hand, the external work done is the force P times the axial displacement which can be derived from the difference between the arch and axial length of the column, resulting in:

$$\Delta T = \frac{P\pi^2}{4l} \sum_{n=1}^{\infty} n^2 a_n^2 \tag{5.4}$$

For an elastic system(not the case of a BRB), in equilibrium conditions, the internal energy should be equal to the external energy

$$\Delta U_1 + \Delta U_2 = \Delta T \tag{5.5}$$

Substituting equations 5.2-5.4 in 5.6 the following expression is obtained

$$\frac{\pi^4 EI}{4l^3} \sum_{n=1}^{\infty} n^4 a_n^2 + \frac{\beta l}{4} \sum_{n=1}^{\infty} a_n^2 = \frac{P\pi^2}{4l} \sum_{n=1}^{\infty} n^2 a_n^2 \tag{5.6}$$

Thus P can be obtained and the critical load can also be found by finding the minimum value for P

$$P = \frac{\pi^2 EI}{l^2} \left[\frac{\sum_{n=1}^{\infty} n^4 a_n^2 + \frac{\beta l^4}{\pi^2 EI} \sum_{n=1}^{\infty} a_n^2}{\sum_{n=1}^{\infty} n^2 a_n^2} \right] \tag{5.7}$$

For this problem, the force P can be expressed as follows

$$P = \frac{\pi^2 EI}{l^2} \left(m^2 + \frac{\beta l^4}{m^2 \pi^4 EI} \right) \tag{5.8}$$
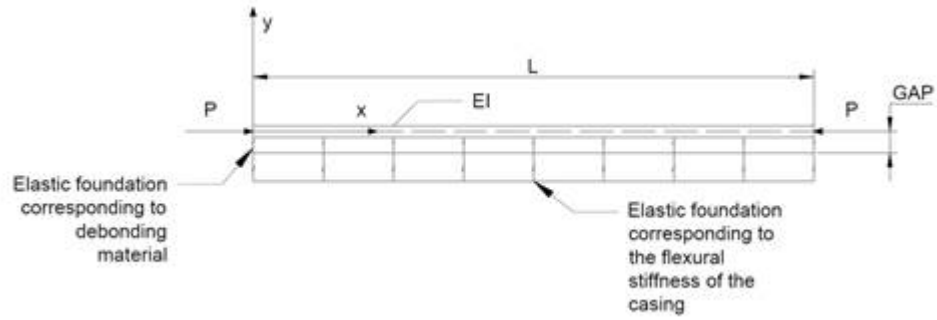
Figure 5.7: Idealisation of a beam on a elastic foundation with a gap spacing

From this formula, it can be seen that when the spring constant of the elastic foundation is zero, the minimum value is found when $m = 1$ (first buckling mode). From this equation, a loading condition for the transition from one mode to another can be derived as:

$$m^2 + \frac{\beta l^4}{m^2 \pi^4 EI} = (m+1)^2 + \frac{\beta l^4}{(m+1)^2 \pi^4 EI} \tag{5.9}$$

Where m is the current mode and $m + 1$ is the immediate higher mode. In general, the following equation must be satisfied

$$\frac{\beta l^4}{\pi^4 EI} = m^2(m+1)^2 \tag{5.10}$$

The former equation provides a direct correlation between the spring constant and the number of modes, however a gap and plastic deformation of the column are not considered. In the case of BRBs this method can be used to account for other nonlinearities such as gap and axial plastic deformation.

The energy equation to be satisfied is

$$\Delta U_1 + \Delta U_2 + \Delta U_3 = \Delta T \tag{5.11}$$

Where ΔU_1, is the strain energy due to bending of the core (assumed linear), ΔU_2 is the strain energy of the deformation of a non-linear spring Figure 5.8, ΔU_3 is the strain energy of the core due to axial force and ΔT is the external work considered non-linear.

Figure 5.8 shows the non-linear spring constant to be considered in the analysis which is
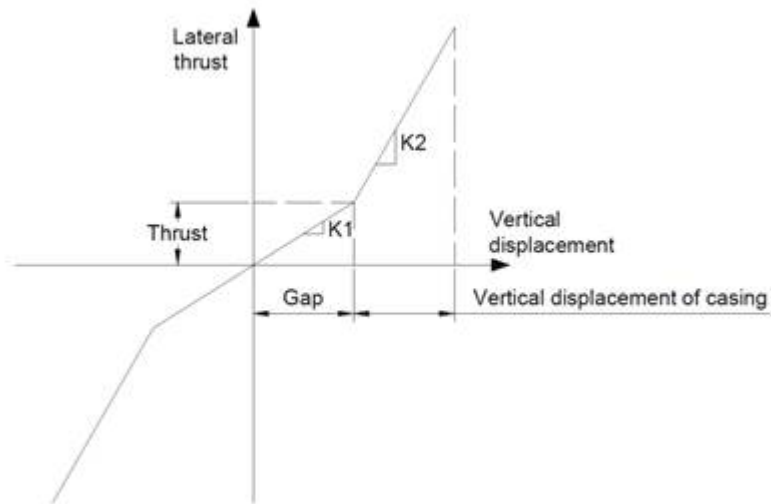
Figure 5.8: Superposition of nonlinear elastic foundations

the result of the superposition of the two elastic foundations. In this figure, K_1 indicates the constant for the debonding material and K_2 for lateral displacement of the casing which analysis will be approached as described in the question "How can we better understand BRB behaviour so that we can produce efficient, economic designs, using traditional or alternative materials?"

The objective of this new method is to obtain more realistic analytical model which can provide both a criterion for global instability and lateral trust under conservative axial loading which will allow having a better understanding in the load transfer from the core to the casing and an estimation of the distribution. Finally, important nonlinearities that cannot be considered in the general elastic approach can be included in this analysis.

5.1.2 Improving BRB performance

Buckling Restrained Braces have shown to be an effective solution for ductile demands where the damage induced by ground random vibrations is mainly concentrated on these devices working as a dual system with a frame. However, the device has limited use to low-rise edifications and although the life cycle cost is reduced by using structural fuses, the cost is still relatively high. The source of the cost comes from the expertise needed to design a ductile structure and the natural need to use only patented tested devices. Likewise, bracings are relatively heavy and as the weight increases, it represents a challenge for construction and design.

Going back to the basics of the mechanism of BRBs, lateral restriction is accomplished by the order of a steel casing resisting lateral thrust and moment transfer from the connection. If the BRB is of reduced length and the core has a small cross section, it is expected that the casing needed to restrain the core and resist the moments on the ends will be of no significant weight in comparison with a the weight of a comparable structural component or even the frame. However, as overall length and core cross section increases, any difference in weight, however small, represents a large demand on the connections and equivalent increase of mass on the structure.

Based on the structural concept of second moment of area, we can convey that the further away the area is from the centroid, the larger second moment of area is since the magnitude increases by the order of the centroid distance squared. Therefore, there is a critical value for the second moment of area already explained by Black and C. J. Black, Makris, and I. D. Aiken (2004) and (Watanabe et al. 1988) equivalent to the ratio of the casing Euler's load and core yielding force where no global failure is observed for values greater than 1. This has been demonstrated experimentally in (ibid.) and corroborated in (Wada and Nakashima 2004). The implication of using an increased second moment of area for the casing yields consequently that more filler material will be needed in order to transfer the lateral thrust to the casing, hence, the development of BRB requires the consideration of this mass increase.

As mentioned previously, current upward trend to use structural fuses can be observed in earthquake prone areas with a successful application of BRBs as retrofitting systems. Also, two different concepts have been addressed in order to justify the importance of utilising the correct size of casing and maintaining consideration of the subsequent increase of mass due to the filler material since this is the main weight component. It is therefore my recommendation that, should Buckling Restrained Braces be developed further, these two aspects are key to achieve further optimisation in both cost and weight. Along this thesis, the feasibility of PVC as a substitute material for the casing has been assessed, addressing only one of the above mentioned key factors that influence the design.

It is acknowledged that the present research would have been more relevant if a wider range of the following outlined studies had been explored, thus have a major impact in how structural fuses are used.

1. Establish the target performance for each component according to a selection of standards such as Eurocodes

2. Explore the feasibility of other materials that can be used for the outer casing

3. Explore alternative lightweight techniques to specify the filler material

4. Explore the durability aspect of BRBs

5. Derive new mathematical equations that can serve as stability criterion that consider plasticity

I am convinced that these aspects are reachable within current available tools, in addition a proposition for an improved filler material can be found in the next paragraphs.

Beyond exploring a filler material that can be made with light weight grout, it would be only natural to explore cellular structures using the concept of the honeycomb conjecture proved in Hales (2001) that states that a region that is discretised in patterns with a figure of the same area have at least the perimeter of the honeycomb hexagonal tiling. The honeycomb conjecture has been used in recent decades to produce lightweight durable products such as panels for furniture that use hexagonal cardboard fillings, also more recently has been applied to produce structural components using other materials such as **GFRP** and **CFRP**.

Honeycombs have been intuitively recognised as an optimal pattern by humans that mimics the shape in which bees build their natural habitat to store the maximum amount of honey using as little wax as possible, such intuition has been mathematically proven by Hales (ibid.). Similarly, in the case of BRBs filler material it is of particular interest to store the maximum amount of air for the minimum amount of structure. Feasible techniques to do so are yet to be explored, however, the extrapolation of the efficacy of honeycombs can potentially signify an improvement in terms of cost, weight and durability.

Bibliography

Black, Cameron, Nicos Makris, and Ian Aiken (2002). *Component testing, stability analysis and characterization of buckling-restrained Unbonded Braces*. Tech. rep. September. Berkeley, CA.: Pacific Earthquake Engineering Research Center, Univ. of California, p. 100.

Black, Cameron J., Nicos Makris, and Ian D. Aiken (June 2004). "Component Testing, Seismic Evaluation and Characterization of Buckling-Restrained Braces". In: *Journal of Structural Engineering* 130.6, pp. 880–894. DOI: 10.1061/(ASCE)0733-9445(2004)130:6(880).

Chai, Herzl (1998). "The post-buckling response of a bi-laterally constrained column". In: *Journal of the Mechanics and Physics of Solids* 46.7, pp. 1155–1181. ISSN: 00225096. DOI: 10.1016/S0022-5096(98)00004-0.

Genna, Francesco and Piero Gelfi (2012). "Analysis of the Lateral Thrust in Bolted Steel Buckling-Restrained Braces. I: Experimental and Numerical Results". In: *Journal of Structural Engineering* 138.10, pp. 1244–1254. ISSN: 0733-9445. DOI: 10.1061/(ASCE)ST.1943-541X.0000564.

Hales, T. C. (Jan. 2001). "The Honeycomb Conjecture". In: *Discrete & Computational Geometry* 25.1, pp. 1–22. ISSN: 0179-5376. DOI: 10.1007/s004540010071.

Li, Guochang et al. (2017). "Flexural behavior of high strength concrete filled high strength square steel tube". In: *Journal of Constructional Steel Research* 128, pp. 732–744. ISSN: 0143974X. DOI: 10.1016/j.jcsr.2016.10.007.

Timoshenko, Stephen and James Gere (1961). *Theory of Elastic Stability*. Ed. by McGraw-Hill. New York.

Wada, A and Masayoshi Nakashima (2004). "From infancy to maturity of buckling restrained braces research". In: *13th World Conference on Earthquake Engineering; Vancouver, B.C., Canada*.

Watanabe, Atsushi et al. (1988). "Properties of brace encased in buckling-restraining concrete and steel tube". In: *9th World Conference on Earthquake Engineering* IV, pp. 719–724.

Wu, Bin and Yang Mei (2015). "Buckling mechanism of steel core of buckling-restrained braces". In: *Journal of Constructional Steel Research* 107, pp. 61–69. ISSN: 0143974X. DOI: `10.1016/j.jcsr.2015.01.012`.

Zhao, Junxian, Bin Wu, and Jinping Ou (2014). "A practical and unified global stability design method of buckling-restrained braces: Discussion on pinned connections". In: *Journal of Constructional Steel Research* 95, pp. 106–115. ISSN: 0143974X. DOI: `10.1016/j.jcsr.2013.12.001`.